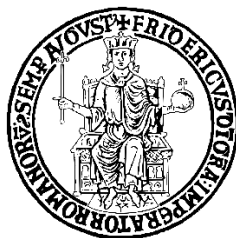# UNIVERSITÀ DEGLI STUDI DI NAPOLI "FEDERICO II"

SCUOLA POLITECNICA E DELLE SCIENZE DI BASE

Dipartimento di Ingegneria chimica, dei Materiali e della Produzione Industriale

CORSO DI LAUREA MAGISTRALE IN INGEGNERIA CHIMICA LM-22

TESI DI LAUREA

IN

FONDAMENTI DI CHIMICA INDUSTRIALE

Cyan H$_2$: un nuovo percorso per la produzione di idrogeno e la simultanea valorizzazione della CO$_2$

Cyan H$_2$: a new route for simultaneous hydrogen production and CO$_2$ valorisation

Relatore

Prof.ssa Almerinda Di Benedetto

Candidato

Vincenzo Ascione

Matricola:
M55001126

Correlatori

Prof.ssa Giuseppina Luciani

Ing. Alessandra Di Nardo

Ing. Maria Portarapillo

Ing. Danilo Russo

Anno Accademico 2021/2022

Table of Contents

INTRODUCTION

In the last few years, environmental problems such as climate change and air pollution have become increasingly important from a sustainability point of view because of their effects on humans and the planet's resources.

It is widely known and scientifically demonstrated that human activities contribute significantly to these problems, mainly due to the high-energy consumption that our lifestyle requires.

Energy is an essential commodity for increasing productivity in both agriculture and industry. At present, in fact, the production of energy is one of the main problems for climate change, due above all to the overuse of fossil fuels that implies the emission of CO_2 (the most responsible gas for the Greenhouse Effect) and, moreover, the use of low thermodynamic efficiency technologies such as internal combustion engines, typically used in transport.

The continuous increase in energy demand and the above issues require a new approach to satisfy global energy demands. Many proposals have been put forward by both the scientific world and politics but the main obstacle to their application essentially lies in the high cost of the new technologies. To overcome this problem, various solutions have been proposed over the years. Their aim is to reduce the emission of greenhouse gases by decreasing the use of fossil fuels and using more and more renewable energy sources, in order to be able to completely leave the production of energy from fossil fuels over time.

The established environmental impacts resulting from fossil fuel have stimulated urgent efforts to decarbonize our fuel sources, that is why hydrogen is considered as an excellent alternative to fossil fuels, and it has been suggested due to its abundance, high chemical energy, and pollution-free product. In fact, the most important property of alternative energy sources is their environmental compatibility and, in line with this characteristic, hydrogen likely will become one of the most attractive energy carriers in the near future.

The role of hydrogen energy will become increasingly important, and it is expected that world energy systems will undergo a transition to an era in which the main energy carriers are hydrogen and electricity [1].

The major problem in utilization of hydrogen gas as a fuel is its unavailability in nature, unlike fossil fuels, and the need for inexpensive production methods. It is an energy

carrier that can be produced from any primary energy source and then used as the fuel either for direct combustion in an internal combustion engine or in a fuel cell, producing virtually no greenhouse gas emissions when combusted with oxygen, but only water as a by-product.

A wide variety of processes are available for H_2 production which, according to the raw materials used, could be divided into two major categories, namely conventional and renewable technologies.

The first category processes fossil fuels and includes the methods of hydrocarbon reforming and pyrolysis. In hydrocarbon reforming process, the participating chemical techniques are steam reforming, partial oxidation, and auto-thermal steam reforming. The second one accommodates the methods, which produce hydrogen from renewable resources, either from biomass or from water.

Currently the annual production of hydrogen is about 0.1 GT, which is mainly consumed on-site, in refining and treating metals [2, 3]. A small fraction is already used to fuel driving cars while in the near future applications including power generation and heating in residential and industrial sectors are expected [2, 4, 5].

Therefore, to increase the penetration of hydrogen into energy markets, its production, storage, distribution, and economy must be considered seriously.

The aim of this thesis is to analyse and develop a new production process of high-purity hydrogen streams at low temperature starting from bio-alcohols and waste products, such as metaborate, and capturing all the carbon in high-value-added polymeric products.

After having made a comparison, through thermodynamic analysis, with the steam reforming of different fuels and alcohols and, having obtained promising results, the second target has been to optimize the process designed in terms of operating conditions.

Chapter 1

1. Hydrogen: the fuel for a more sustainable future

1.1. Hydrogen historical background

Hydrogen (H_2), often presented as the future source of energy due to its high energy potential and clean combustion, evokes both hope and fear due to its extremely flammable nature. In the minds of people, in fact, it is often synonymous with danger especially since the Hindenburg disaster on 6 May 1937 and the subsequent accidents as shown in Figure 1.1. On that day, the Zeppelin, inflated with 200,000 m^3 of H_2, ignited in less than a minute, resulting in the death of 35 out of the 97 passengers who jumped out of the airship in panic. Even though the origin of the ignition is unknown, the combined combustion of hydrogen and the coating of the shell (butyrate, iron and aluminium oxide) is the cause. This caused such a fear of hydrogen called the "Hindenburg syndrome" that ever since the gas supply to the town from coking plant made up of 96 % H_2 was called "water gas" to avoid any commercial repercussions [6].

Hydrogen appears in different forms in plants, animals, humans, fossil fuels, and other chemical compounds. It has been known for more than 200 years and many researchers have contributed to the historical development of hydrogen, as shown in Table 1.1.

Time period	Scientist	Contribution
16th Century	Paracelsus	Understanding of properties of hydrogen, including its flammability
16th Century	Van Helmot	Described hydrogen as a special kind of gas
17th Century	Robert Boyle	Produced hydrogen gas while experimenting with iron and acids
18th Century	Henry Cavendish	First recognized hydrogen as a distinct element
18th Century	Lavoisier	Hydrogen named
19th Century	Anonymous	Development of idea that hydrogen could be an energy carrier that facilitates use of renewable energy sources
19th Century	Carl Bosh	Hydrogen used in production of fertilizer
20th Century	Kordesch	Hydrogen used in vehicles
20th Century	T.N. Veziroglu	Organization of symposia on hydrogen energy, leading to expanded hydrogen energy study and utilization over the world

Table 1.1 - Historical developments related to hydrogen; Source: [7]

In the 20th century, hydrogen was extensively used in the manufacture of ammonia, methanol, gasoline and heating oil, as well as in such commodities as fertilizers, glass, refined metals, vitamins, cosmetics, semi-conductor circuits, lubricants and cleaners. After 1974, many studies were conducted to investigate the uses for hydrogen energy and

facilitate its penetration as an energy carrier. Subsequently, many industries worldwide began developing and producing hydrogen, hydrogen-powered vehicles, hydrogen fuel cells and other hydrogen-based technologies.
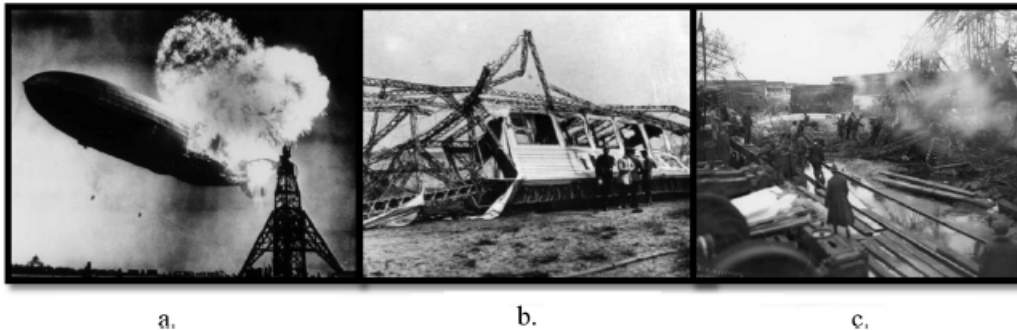
Figure 1.1 - Hydrogen historic accidents: a. Hindenburg, while on fire, b. Wreck of LZ-10 Schwaben at Düsseldorf, c. Airship Roma after ignition; Source: [8]

1.2. Hydrogen properties and safety

Hydrogen comes from the Greek words ''hydro'' and ''genes'' meaning ''water'' and ''generator'', referring to the fact that, when it burns, it generates only water.

It is the most abundant element in the universe, which is found on our planet Earth mainly in water and organic compounds. It is the lightest and simplest element, which consists of one electron and one proton, colourless, odourless, flammable gas. Hydrogen's atomic weight is 1,00794 atomic mass units rounded at 1,008. This atomic weight number (1,008) was considered in the USA as the 8th of October (10/08) as the National Hydrogen and Fuel Cell Day (see Figure 1.2) and this day is expected to be the International day of hydrogen energy.

Figure 1.2 - Hydrogen chemical element and USA National Hydrogen and Fuel Cell Day, picture modified from [9]

At ambient temperature and atmospheric pressure, atomic hydrogen does not occur and instead occurs as a highly stable hydrogen molecule (H_2). Under standard conditions, hydrogen has unique physical and chemical properties that play an important role in the

ways in which hydrogen is produced, stored and utilized. The key properties of hydrogen are summarized in Table 1.2:

Properties	SI Units
Discovery date/by/Chemical formula	1766/Henry Cavendish/H_2
Isotopes	^1H (99.98%), ^2H, ^3H, ($^4H-^7H$ Unstable)
Equivalences; Hydrogen solid, liquid and Gas at Pressure = 981 mbar and Temperature = 20 °C	1 kg = 14,104 l = 12,126 m^3
Molecular weight	1.00794
Vapor pressure at (−252.8 °C)	101.283 kPa
Density of the gas at boiling point and 1 atm	1.331 kg/m^3
Specific gravity of the gas at 0 °C and 1 atm (air = 1)	0.0696
Specific volume of the gas at 21.1 °C and 1 atm	11.99 m^3/kg
Specific gravity of the liquid at boiling point and 1 atm	0.0710
Density of the liquid at boiling point and 1 atm	67.76 kg/m^3
Boiling point at (101.283 kPa)	−252.8 °C
Freezing/Melting point at (101.283 kPa)	−259.2 °C
Critical temperature	−239.9 °C
Critical pressure	1296.212 kPa, abs
Critical density	30.12 kg/m^3
Triple point	−259.3 °C at 7.042 kPa, abs
Latent heat of fusion at the triple point	58.09 kJ/kg
Latent heat of vaporization at boiling point	445.6 kJ/kg
Solubility in water vol/vol at 15.6 °C	0.019
Dilute gas viscosity at 26 °C (299 K)	9×10^{-6} Pa s
Molecular diffusivity in air	6.1×10^{-5} m^2/s
Cp	14.34 kJ/(kg) (°C)
Cv	10.12 kJ/(kg) (°C)
Ratio of specific heats (C_p/C_v)	1.42
Lower heating value, weight basis	120 MJ/kg
Higher heating value, weight basis	141.8 MJ/kg
Lower heating value, volume basis at 1 atm	11 MJ/m^3
Higher heating value, volume basis at 1 atm	13 MJ/m^3
Stoichiometric air-to-fuel ratio at 27 °C and 1 atm	34.2 kg/kg
Flammable limits in air	4%−75%
Explosive (detonability) limits	18.2 to 58.9 vol% in air
Maximum combustion rate in air	2.7/3.46 (m s−1)
Maximum flame temperature	1526.85 °C
Autoignition temperature/in air	400 °C/571 °C

Table 1.2 – Hydrogen properties and specifications; Source: [10]

As shown in Table 1.2 and Figure 1.3, the temperature of transitions from gas to liquid is -252,76 °C (at atmospheric pressure) and the critical temperature is -239,96 °C, which means that above this temperature it cannot be liquefied, regardless of the pressure applied. Hydrogen's critical pressure is 13,1 bar and so above this pressure and the critical temperature, hydrogen can only exist as a supercritical fluid with characteristics of both liquid and gas. Due to these properties, liquefaction of hydrogen is accomplished by cooling rather than pressurization. The compressed storage of hydrogen (often at 350 or 700 bar) always takes place with hydrogen existing as a supercritical fluid. Hydrogen gaseous density is 0,089 g/L, which is approximately 14 times lower than the one of air (1,29 g/L). For this reason, hydrogen has high buoyancy in the atmosphere and it is highly volatile. Hydrogen liquefaction is extremely important for hydrogen storage and

5

transport. In the liquid state, at -253 °C and 1,013 bar, hydrogen has a density of 70,79 g/L, which is approximately 800 times its density as a gas.
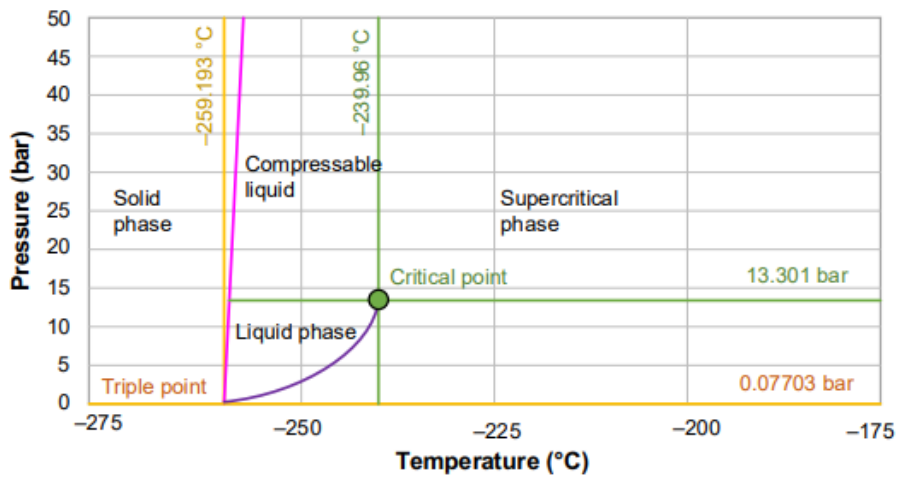
Figure 1.3 - Hydrogen phase diagram: Source: [11]

Hydrogen energy content at the higher heating value is 141,8 MJ/kg at 298 K and the lower heating value of the hydrogen is 120 MJ/kg at 298 K, which is much higher than that of most fuels (e.g., gasoline 44 MJ/kg at 298 K) [12, 13].

However, liquid hydrogen has less energy density by volume than hydrocarbon fuels such as gasoline by approximately a factor of four (i.e. density of 8 MJ/l whereas gasoline has a density of 32 MJ/l) [14, 15]. Since hydrogen gas has good energy density by weight but poor energy density by volume versus hydrocarbons, it requires a larger tank to store [14,16].

Hydrogen is flammable over a very wide range of concentrations in air (4% – 75%) and it is explosive over a wide range of concentrations (15% – 59%) at a standard atmospheric temperature. The flammability limits of the three component systems are shown in Figure 1.4; while the flammability and detonation limits of the three component systems are shown in Figure 1.5.

6
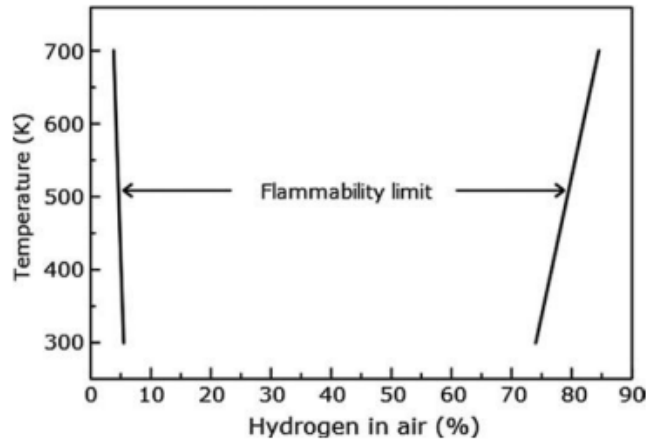
Figure 1.4 - Effect of temperature on flammability limits of hydrogen in air (pressure 100KPa); Source: [11]
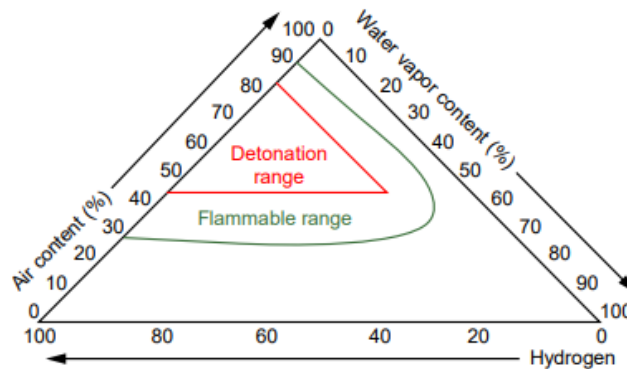
Figure 1.5 - Flammability and detonability limits of the three components system hydrogen-air-water vapor; Source: [11]

It is a flammable gas with low ignition temperature. In fact, its minimum ignition energy (MIE) is equal to 0,018 mJ in air at atmospheric pressure and room temperature [17]. This creates a large portion of the risk associated with its usage. Moreover, it has the ability to escape through materials due to its small molecule size and its destructive capability (hydrogen embrittlement) which can lead to mechanical degradation and failure to the point of leakage in certain materials [18, 19].

Hydrogen, as a fuel, has some degree of hazard; therefore, the safe use of any fuel focuses on preventing situations where the three combustion factors are present: ignition, oxidant and fuel [20]. Some properties of hydrogen require additional engineering controls to ensure its safe use. Its wide range of flammability concentration and its low MIE (only 1/10 as much energy to ignite as gasoline) means that it can ignite more easily. Consequently, adequate ventilation and leak detection are important elements in the

design of safe hydrogen systems. Since hydrogen burns with a nearly invisible flame, special flame detectors are required. In addition, some metals can become brittle when exposed to hydrogen, so selecting appropriate materials is important to the design of safe hydrogen systems. In addition to designing safety features into hydrogen systems, training in safe hydrogen handling practices is a key element for ensuring the safe use of hydrogen. In addition, testing of hydrogen systems, such as tank leak tests, garage leak simulations and hydrogen tank drop tests show that hydrogen can be produced, stored and dispensed safely. As more and more hydrogen demonstrations get underway, the safety results can grow and create confidence that hydrogen can be as safe as the fuels in widespread use today.

Some hydrogen properties make it safer to handle and use than the fuels commonly used today. For example, hydrogen is non-toxic. In addition, because hydrogen is much lighter than air, it dissipates rapidly upwards when it is released, allowing for rapid dispersal of the fuel in case of a leak. The primary safety concern is that if a leak goes undetected and the gas collects in a confined space, it can eventually ignite and cause an explosion. Especially in closed places it is easy to create flammable mixtures in the upper part of the room precisely because it tends to rise up [21].

1.3. Advantages and disadvantages of hydrogen energy

There are many advantages in the use of hydrogen but also some cons. Both are described in the Table 1.3-1.4:

Advantage	*Reference*
Non-toxic, clean energy carrier with a high specific energy on a mass basis (e.g., the energy content of 9.5 kg of hydrogen is equivalent to that of 25 kg of gasoline)	[22]
It can be produced through many production processes	[23]
It can be safely transported in pipelines	[7]
It can be used as a chemical feedstock in the petrochemical, food, microelectronics, ferrous and non-ferrous metal, chemical and polymer synthesis, and metallurgical process industries, and as an energy carrier in clean sustainable energy systems	[7]
When combusted, it produces non-toxic exhaust emissions, except at some equivalence ratios (where its high flame temperature can result in significant NO_x levels in the exhaust products)	[24, 25]
It can be utilized in all parts of the economy (e.g., as an automobile fuel and to generate electricity via fuel cells).	[7]
Compared to electricity, it can be stored over relatively long periods of time	[7]

Table 1.3 – Advantages of hydrogen energy

Disadvantage	*Reference*
It can burn in lower concentrations when mixed with air and this can cause safety concerns	[7]
Its storage in liquid form is difficult, as very low temperatures are required to liquefy hydrogen.	[7]

Table 1.4 - Disadvantages of hydrogen energy

1.4. Why hydrogen as an energy carrier?

Hydrogen has always been used for various industrial processes such as the production of methanol by hydrogenation of CO and CO_2 or the production of ammonia together with N_2.

Hence, hydrogen is expected in the future to replace to some degree fossil fuels and to become the preferred portable energy carrier for vehicles.

Currently 500 billions of cubic meters of hydrogen, equating to about 6,5 EJ of energy, are produced annually worldwide. Approximately, 99% is produced from fossil fuels, mainly by steam reforming of natural gas [26].

It is possible to produce hydrogen using other production techniques and different energy sources. Renewable energy sources such as hydraulic, solar, wind, geothermal, wave and solid waste energy can be used to generate hydrogen from hydrocarbons and/or water. For example, 108,7 kg of hydrogen can be produced from 1 m^3 of water by electrolysis using electricity and the energy of this amount of hydrogen is equivalent to that of 422 lt of gasoline [22, 27, 28].

The electricity for hydrogen production can come from fossil or renewable energy sources. Considering the energy density on a mass basis, the utilization efficiency factor, utilization safety (which is high for hydrogen), pollution and environmental effects (which can be low for hydrogen, depending on the energy source used to produce it, especially since CO_2 is not a necessary waste) of hydrogen fuel [28], hydrogen energy has many attractive features. The Figure 1.6 presents the importance, production techniques and application areas for hydrogen:
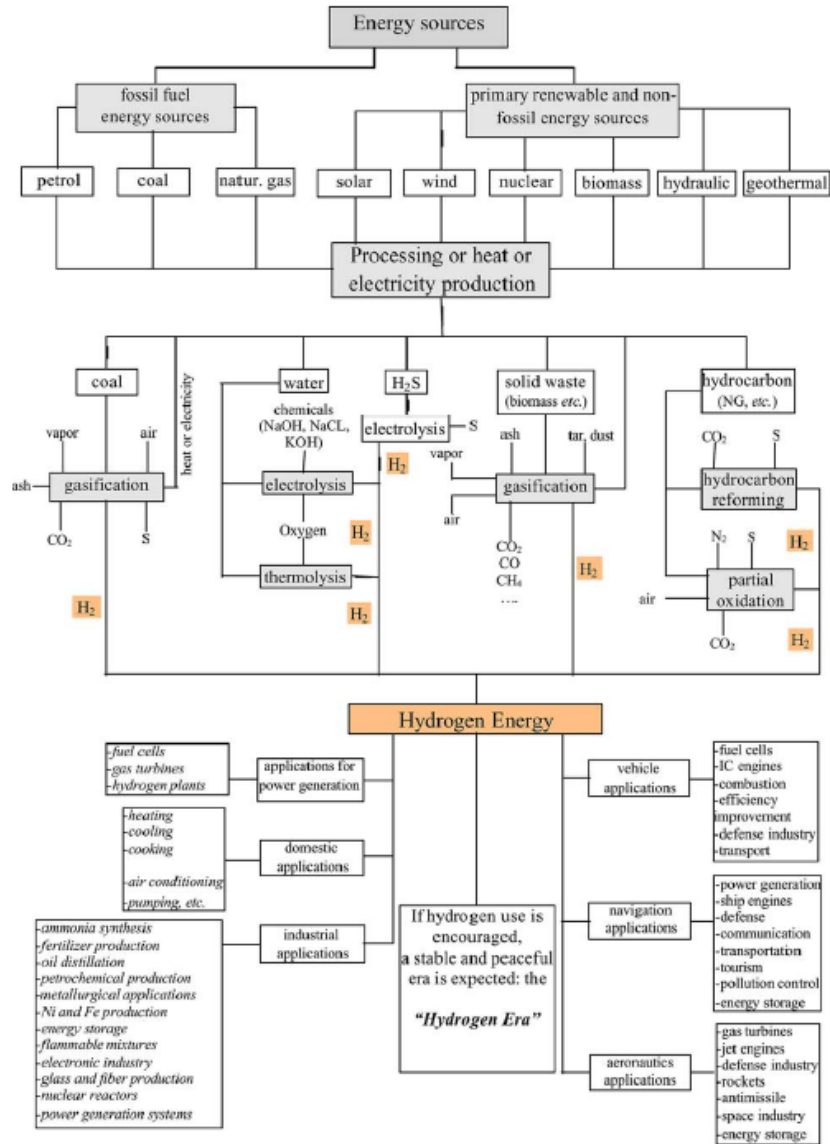
Figure 1.6 - Relationship of production techniques and types of utilization of hydrogen; Source: [7]

Hydrogen's attributes as an energy carrier relate to energy demand, production techniques and application fields, and include the following: clean, not harmful to the environment or life, renewable, securely storable and transportable, broadly utilizable in various applications, producible by different techniques and from various sources, and economically usable.

A comparison of hydrogen with other fuels is presented in Table 1.5:

Table 3
Comparison of key properties for hydrogen and other fuels

Fuel type	Energy per unit mass (J/kg)	Energy per unit volume (J/m^3)	Motivity factor	Specific carbon emission (kg C/kg fuel)
Liquid hydrogen	141.90	10.10	1.00	0.00
Gaseous hydrogen	141.90	0.013	1.00	0.00
Fuel oil	45.50	38.65	0.78	0.84
Gasoline	47.40	34.85	0.76	0.86
Jet fuel	46.50	35.30	0.75	–
LPG	48.80	24.40	0.62	–
LNG	50.00	23.00	0.61	–
Methanol	22.30	18.10	0.23	0.50
Ethanol	29.90	23.60	0.37	0.50
Bio diesel	37.00	33.00	–	0.50
Natural gas	50.00	0.04	0.75	0.46
Charcoal	30.00	–	–	0.50

Table 1.5 - Comparison of key properties for hydrogen and other fuels: Source: [7]

The above features of hydrogen suggest that it will be particularly advantageous as a transportation fuel because of its versatility, utilization efficiency factor and safety. The only waste from hydrogen oxidation is water, so only the engine lubricants from a hydrogen-fueled vehicle cause any pollutants.

1.5. Hydrogen colours in the energy transition

According to the relationship between its production and the relative emission of carbon dioxide, hydrogen is divided into different "colours" [29, 30]:

- *black and brown hydrogen*: the most polluting and impacting types of hydrogen are those produced by the gasification of coal (black hydrogen) and lignite (brown hydrogen): in special reactors and in the absence of oxygen, these substances are brought to high temperatures and react with water vapor to generate hydrogen, methane, monoxide and carbon dioxide. In this way the so-called "city gas" (composed of hydrogen, methane and carbon monoxide) and *syngas* (composed mainly of hydrogen and carbon monoxide) are produced. The production of these two types releases large quantities of CO_2;

- *grey hydrogen*: less polluting than the above types, it is hydrogen produced by hydrocarbons. The most common reaction is that between methane and water vapour, called steam methane reforming, from which carbon dioxide and

hydrogen are generated. However, this type of hydrogen also has the disadvantage of producing carbon dioxide;

- *blue hydrogen*: it is produced in the same way as grey hydrogen but also a CO_2 capture and sequestration process (CCS, Carbon Capture and Sequestration) is associated. Downstream of the hydrogen production process, the carbon dioxide generated is captured and stored instead of being released into the atmosphere. This type has the characteristic of being neutral with respect to the impacts on the climate;

- *turquoise hydrogen*: it is extracted from the pyrolysis of methane through a process that involves heating the gas in the absence of oxygen to thermally break the chemical bonds and obtain a flow of hydrogen and solid carbon. The latter could be used as a raw material (e.g. as carbon black in the production of tires). The process does not produce direct CO_2 emissions but, considering the entire life cycle, it is linked to significant levels of greenhouse gases;

- *purple hydrogen*: it is generated through the electrolysis of water and it is produced using electricity from nuclear sources and for this reason it is, in addition to green hydrogen, another type that does not emit carbon dioxide into the atmosphere, although there is the generation of radioactive waste;

- *yellow hydrogen*: it is generated by the electrolysis of water with electricity from the grid (i.e. supplied from mixed sources, including fossils);

- *green hydrogen*: it represents the "cleanest" type of hydrogen: in fact, it is hydrogen produced with electricity from renewable sources such as wind, solar, photovoltaic and marine in the absence of CO_2 or other pollutants emissions. Moreover, this type of hydrogen favours the penetration of these non-programmable sources in the energy landscape by using it to balance the grid based on energy production.

In Figure 1.7 the hydrogen colour spectrum and indications for carbon emissions (GHG: *Greenhouse Gases*) are shown:

	Terminology	Technology	Feedstock/Electricity source	GHG footprint*
PRODUCTION VIA ELECTRICITY	Green Hydrogen	Electrolysis	Wind | Solar | Hydro Geothermal | Tidal	Minimal
	Purple/Pink Hydrogen		Nuclear	
	Yellow Hydrogen		Mixed-origin grid energy	Medium
PRODUCTION VIA FOSSIL FUELS	Blue Hydrogen	Natural gas reforming + CCUS Gasification + CCUS	Natural gas | coal	Low
	Turquoise Hydrogen	Pyrolysis	Natural gas	Solid carbon (by-product)
	Grey Hydrogen	Natural gas reforming		Medium
	Brown Hydrogen	Gasification	Brown coal (lignite)	High
	Black Hydrogen		Black coal	

*GHG footprint given as a general guide but it is accepted that each category can be higher in some cases.

Figure 1.7 – Hydrogen colours; Source: [31]

At the moment, however, 99% of the hydrogen produced is black or grey: on an annual basis 70 million tons of hydrogen (about 76% of world demand) are produced using 250 billion cubic meters of natural gas and another 23% is produced by coal gasification. Only less than 1% is produced by electricity. The main cause is the high cost of green hydrogen compared to grey hydrogen [29]. To date, as can be seen in Figure 1.8 (graphic developed by SNAM) the cost of green hydrogen is still about double that grey; parity is expected to be achieved by 2030, thanks to the increase in installed renewable power in conjunction with the increase in the price of carbon dioxide produced.
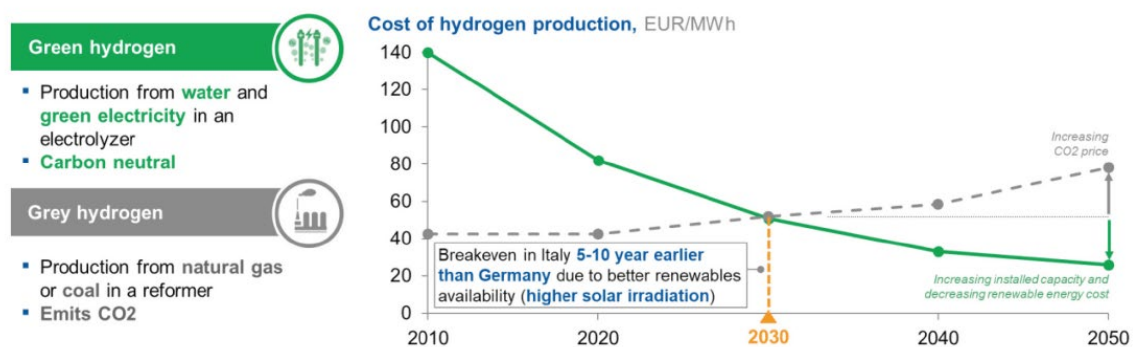
Figure 1.8 - Production costs evolution of green and grey hydrogen in Italy; Source: [29]

Hence, the primary challenge for the development of a clean hydrogen economy remains not only the scaling-up of hydrogen production but above all the transition from carbon-intensive to low carbon intensity hydrogen production. To get a clearer idea, looking at

the Figure 1.9, to reach the levels of low-carbon hydrogen production, needed to satisfy the Sustainable Development Scenario, the road is still long, but not impossible.
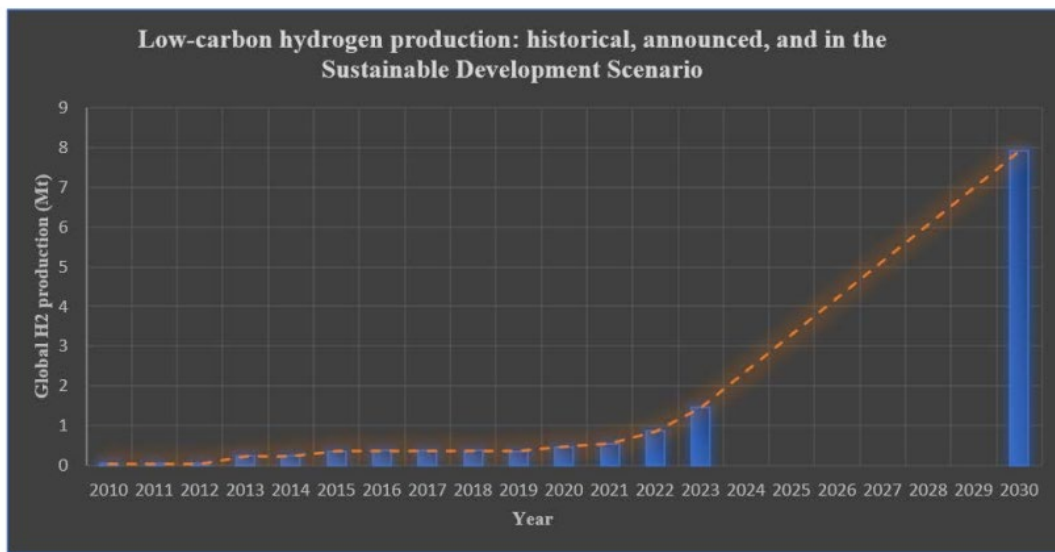
Figure 1.9 – Low carbon hydrogen production history, 2010-2030; Source: [32]

1.6. Hydrogen costs and prices

Regarding to the costs of hydrogen, estimates can be made, which are very sensitive to places and conditions of production. According to the article published by Stefano Agnoli on the *Corriere della Sera* on December 2020 [33], grey hydrogen production cost is strongly correlated to the price of methane. Looking at the price of pre-pandemic European methane, the producing cost was around 1 €/kg. Due to the increase in the price of methane during the Covid-19 emergency (25 €/MWh), the cost of grey hydrogen, to date, is around 1,5 €/kg.

Moving from grey to blue hydrogen, costs for carbon dioxide capture and sequestration must be taken into account which inevitably lead to an increase in the overall cost of the plant. Evaluating the current plant costs, the cost of production of blue hydrogen is equal to that of grey hydrogen plus 0,5€/kg (about 2,0 €/kg). In the long-term, the plus of blue hydrogen could drop to 0,25 €/kg, considering the increase in economies of scale in this sector.

15

The calculation of the cost of producing green hydrogen is clearly more complex, which mainly depends on the cost of renewable electricity and on the cost of electrolysers, which are still handcrafted today, and not on an industrial scale.

In Italy, for example, assuming that the plant is powered by solar energy in an area characterized by massive irradiation, green hydrogen would cost between 6 to 8,7 €/kg today, depending on the size of the electrolyser. By 2030, it is estimated that green hydrogen could cost between 3,7 and 5,9 €/kg and in the future between 2,1 and 4,4 €/kg.

To understand the fluctuations in hydrogen prices based on the source of production and the cost of energy, it is compared with the case in which the electrolyser is powered by an offshore wind farm, as is the case today in the North Sea. In the latter case, in fact, hydrogen could cost between 4 and 5,2 €/kg; within 2030 from 3 to 3,9 €/kg and in the long term between 2 and 2,8 €/kg [33].

In the Figure 1.10 the fluctuation of hydrogen prices in the world based on the source of production is shown:
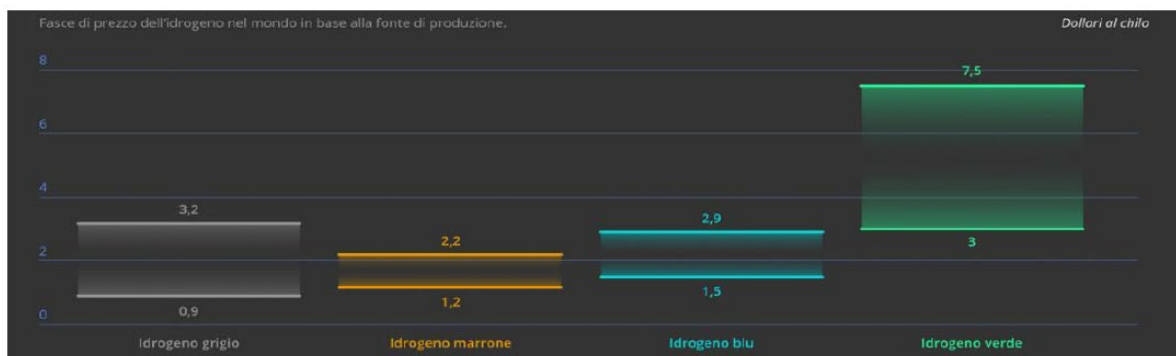
Figure 1.10 – Price ranges of hydrogen in the world based on the source of production; Source: [34]

1.7. Hydrogen sectors and application

The exploitation of hydrogen is still strongly anchored to a type of production aimed at being used as a chemical product in industrial applications (for example in the refining of oil or the production of ammonia and nitrogen fertilizers). The prospect, however, is that hydrogen could replace fossil fuels for various applications, including buildings, electricity, industry and transportation. The advantage of hydrogen is found in its potential to reduce emissions from sectors that are difficult to decarbonise. Hydrogen can also be used in the production of fuels produced by synthesizing (or combining) different

types of gas (such as carbon monoxide and carbon dioxide). Since hydrogen produces no harmful emissions at the point of use of fuel cell, it contributes to improving air quality in regions where it replaces the more polluting fossil fuels, such as natural gas, petrol or diesel, which emit various levels of air contaminants that have negative effects on health and the environment (e.g., smog, acid rain). Green hydrogen and blue hydrogen can also be mixed with fossil fuels (for example natural gas) to reduce the carbon intensity of the fuel. Table 1.6 describes the main final uses of hydrogen that are currently under development or available on the market, in four primary sectors:

Sector	Hydrogen In fuel cells: Hydrogen is directly converted into electricity Through combustion: This typically requires switching to different engines or turbines.	Blended hydrogen Blended with existing gas and liquid fuels to lower their carbon intensity.
Buildings	Can be used to: • power household appliances, such as hydrogen fuel cell heat pumps • generate home electricity using a fuel cell • produce combined heat and power (e.g. district heating systems)	Blended with natural gas used to heat, cool and power buildings (including combined heat and power) Can be used in existing appliances (like furnaces and stoves) if blended into the natural gas grid.
Electricity	Can be used for: • electricity generation (in some turbines) • electricity storage: using electrolysis to convert excess electricity generation (e.g. from renewable sources) to hydrogen, in a process called "power-to-gas"	Blended with natural gas for electricity generation (in some turbines)
Industry	Theoretically feasible for use in high-temperature heat processes but technical challenges remain[22]	Blended with fossil fuels used to generate high-temperature heat in industry
Transport: Light-duty passenger vehicles	Can be used in fuel cell vehicles	Not being pursued commercially
Transport: Heavy-duty freight and mass transit	Can be used in fuel cell vehicles that carry heavy loads over long routes (i.e. heavy-duty vehicles (trucks, buses, rail, marine)) Fuel cell vehicles have higher energy storage density and shorter refuelling times, and are lower in weight than battery electric vehicles	Blended with diesel for use in retrofitted diesel engines[23]

Table 1.6 - Possible end uses of hydrogen across various sectors: Source: [35]

Certainly, the most interesting sector for which hydrogen can really make a difference is heavy transport; we refer to buses, trucks, trains, sectors in which it is possible to implement the use of green hydrogen without excessive additional costs. It is clear that the non-negligible costs of a new infrastructure must be considered along with the costs of new vehicles equipped with electric motors with fuel cells that produce electricity by using hydrogen as a source. Therefore, the efficiency of these new vehicles would be much greater than that of the current combustion engines, which would lead to a compensation of the extra cost given by the new equipment that can be easily amortized over the life of the vehicle.

Other important sectors to remain in the heavy transport area are those of ships and airplanes. In the long run, there is no better alternative than hydrogen to start the decarbonisation procedure. In the naval sector, hydrogen is exploited in the form of ammonia; for the aviation sector, we find hydrogen in the form of synthetic kerosene for long-distance flights, while for short-medium distance flights, 500-800 km, hydrogen in fuel cells could be congenial.

The challenge in these sectors is very ambitious as it is necessary to generate green hydrogen to react with the other elements mentioned above (carbon dioxide from the combustion of bio-methane or air capture for kerosene synthetic and nitrogen with ammonia) [36].

In any case, according to Bloomberg NEF estimates, the market prospects in the various hydrogen sectors are very encouraging and the demand is expected to grow exponentially in the coming years. In the Figure 1.11, the graph of the forecasts of growth in demand for hydrogen in the various sectors by 2050 is reported:
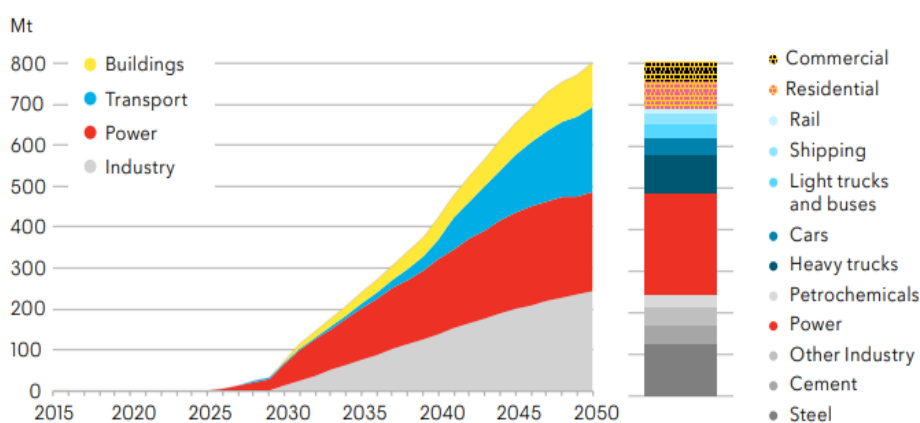
Figure 1.11 – Forecasts of growth in hydrogen demand in the NCS-CEHP by 2050; Source: [37]

1.8. Hydrogen-economy: future prospects

One of the most pressing problems is the need for an energy carrier; in this regard, chemistry can help us to find new means and technologies for the storage of energy obtained from renewable sources. Chemistry must also aim at improving the technologies for the transformation of biomass, aimed both at the direct production of biofuels and at the choice of the best energy carrier.

The most studied solution to store the energy produced is the use of hydrogen as an energy vector, this by virtue of various reasons. First, it is widely available; secondly, the devices for the use of H_2 as a fuel are well known and developed: the fuel cells. Obviously, from a sustainability perspective, the production of "clean" hydrogen implies the use of renewable sources, both for energy and for raw materials; precisely, for this reason, the production of hydrogen from water is one of the biggest challenges to be faced.

Currently, the production of H_2 is totally based on the use of methane as a source; this does not lead to nullifying the environmental problems mentioned above and makes new developments necessary.

However, it is necessary to point out that the use of hydrogen produced from methane, both as regards raw materials and energy, is already a step forward with respect to the problems of air pollution and the greenhouse effect. In fact, most of the atmospheric pollution derives from the use of fossil fuels in small engines, such as in cars or homes; concentrating the production of energy in large plants increases the efficiency of these transformations, reducing the energy demand. In large energy production plants, it would also be possible to introduce CO_2 capture systems to reduce greenhouse gas emissions (CCS technology). To achieve these goals, it will be necessary to change the behaviour of the large energy producing companies, of the entire economic system as well as the distribution infrastructures in the perspective of a hydrogen economy.

Another important consideration concerns technology: fuel cells are considered the best device for the efficient use of hydrogen but their cost is still high. To overcome this problem, systems have been studied to use H_2 in traditional systems (internal combustion engines, boilers); in this case, the purpose of reducing energy consumption would not be achieved but it would still be a first step towards reducing the environmental impact.

Hydrogen, as we have seen, is a particularly interesting chemical element. With it, once the problems of storage and transport have been solved, as well as those related to the sustainability of its production, it could really become the form of energy that will accompany humanity in the future. A future, clearly, of sustainability.

Chapter 2

2. State of art

2.1. Hydrogen production processes

At present, hydrogen is mainly used in the chemical industry but, in the near future, it will become a significant fuel. There are many processes for hydrogen production. In this chapter, the technologies related to hydrogen production from both fossil and renewable biomass resources will be treated.

In Figure 2.1 the hydrogen production routes are shown. In particular, in the paragraphs 2.2 and 2.3 reforming processes (from hydrocarbons) will be discussed, while in the paragraph 2.4 non-reforming processes (from biomass and water) will be covered.

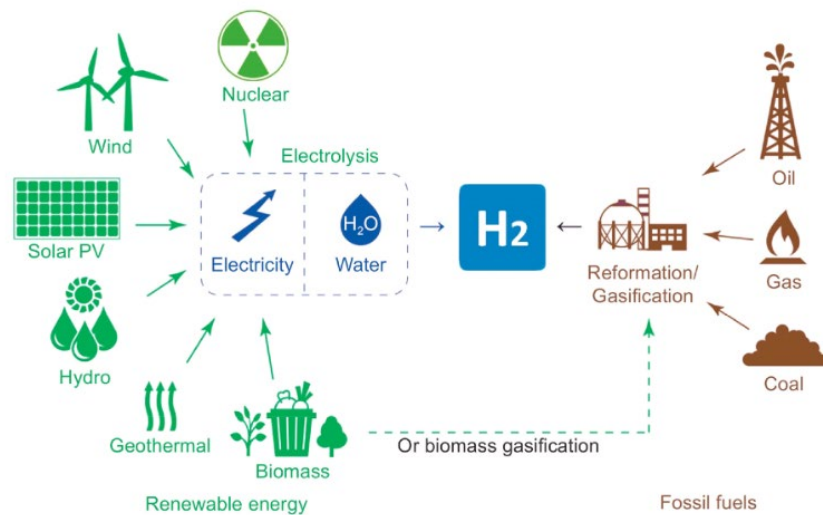*Figure 2.1 - Hydrogen production routes; Source: [38]*

2.2. Hydrogen production processes by hydrocarbons reforming

Many technologies are accessible for hydrogen generation by fossil fuels but the mains are hydrocarbon reforming and most advanced methods. The three primary techniques used to produce hydrogen from hydrocarbon fuels are steam reforming, partial oxidation (PO_x) and autothermal reforming (ATR).

Various kinds of feedstock are available for H_2 production on industrial bases but the ideal feedstock as input material is natural gas due to the availability of huge amount and its favourable price. There are also some light alcohols such as ethanol and methanol, which are easy handling and globally distributed. Nowadays, steam reforming of methane is the most common hydrogen production method in commercial use. Most hydrocarbon fuels contain at least some amount of sulphur, which poisons the fuel processing catalyst, and this represents the biggest challenge for the reforming.

The reforming process produces a gas stream composed mainly of hydrogen, carbon monoxide and carbon dioxide. Endothermic steam reforming of hydrocarbons requires an external heat source.

Steam reforming does not require oxygen, has a lower operating temperature than PO_x and ATR, and produces a stream with a high H_2/CO ratio (~3:1). However, it has the highest emissions of the three processes.

Partial oxidation converts hydrocarbons into hydrogen by partially oxidizing (combusting) the hydrocarbon with oxygen. The heat is provided by the ''controlled'' combustion. It does not require a catalyst to operate and is more sulphur tolerant than the other processes. The process occurs at high temperatures with some soot formation and the H_2/CO ratio varies from 1:1 to 2:1.

Auto-thermal reforming uses the partial oxidation to provide the heat and steam reforming to increase the hydrogen production resulting in a thermally neutral process. It is conducted at a lower pressure than PO_x reforming. Since PO_x is exothermic and ATR incorporates PO_x, these processes do not need an external heat source for the reactor. However, either they require an expensive and complex oxygen separation unit to supply with pure oxygen the reactor or the produced gas is diluted with nitrogen [39].

Since all three processes produce large amounts of carbon monoxide, one or more water-gas-shift (WGS) reactors – typically a high temperature reactor and low temperature reactor – are used. The high temperature (>350 °C) reaction has fast kinetics but is limited by thermodynamics to the amount of carbon monoxide that can be shifted. Therefore, a lower temperature reaction (210÷330 °C) is used to convert the carbon monoxide to a lower level. High temperature WGS process commonly use an iron catalyst and lower temperature WGS often use a copper catalyst [40]. In the Table 2.1 are summarized the advantages and challenges of each of these processes.

Technology	Advantages	Disadvantages
Steam reforming	Most extensive industrial experience Oxygen not required Lowest process temperature Best H_2/CO ratio for H_2 production	Highest air emissions
Autothermal reforming	Lower process temperature than POX Low methane slip	Limited commercial experience Requires air or oxygen
Partial oxidaiton	Decreased desulfurization requirement No catalyst required Low methane slip	Low H_2/CO ratio Very high processing temperatures Soot formation/handling adds process complexity

Table 2.1 - Comparison of reforming technologies; Source: [39]

2.2.1. Steam methane reforming (SMR)

Steam reforming is a kind of technique to produce hydrogen through different feedstock like (higher hydrocarbon, acetone, ethanol, methanol, ethane and methane) with different catalysts. Methane is a more favourable feedstock to others because of better by-product formation [41]. This technique can produce hydrogen in multiple stages, as shown in Figure 2.2:
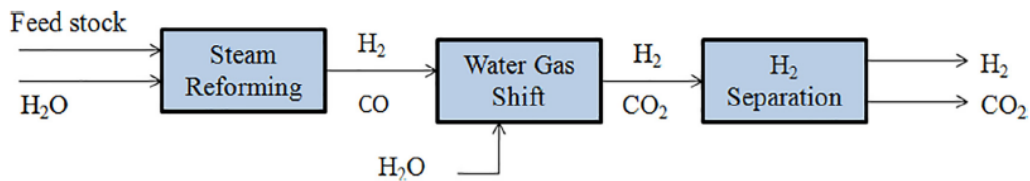

Figure 2.2 - Flow process of multistage for production of hydrogen

Steam methane reforming of natural gas is a well-established technology that is used to generate hydrogen with the presence of steam through the conversion of hydrocarbon. The steam methane reforming process involves catalytically reforming or (syn-gas) production, gas purification or methanation and water gas shift. It is usually operated at a higher temperature range 700÷900°C due to the highly endothermic nature of the process.

Conventional SR catalysts are nickel on oxide supports, which are typically aluminium or magnesium, but these catalysts often have problems with carbon deposition [42, 43]. They normally involve steps after the steam reforming reaction to remove CO [44]. Typical steam reforming reactions over nickel catalysts are performed at high temperatures between 750 and 1450 °C and 5 and 25 atm due to the endothermic nature of the reaction [45, 46].

The chemical reactions involved in steam reforming of CH_4 are represented as follows:

$$Reformer\ Equation: CH_4 + H_2O \leftrightarrow 3H_2 + CO \quad \Delta H = 206,2\ \frac{kJ}{mol}\ at\ 298\ K \quad (2.1)$$

$$\textit{Water gas shift reaction}: CO + H_2O \leftrightarrow H_2 + CO_2 \quad \Delta H = -41{,}1\frac{kJ}{mol} \; at \; 298 \, K \quad (2.2)$$

$$\textit{Methanation reaction}: CH_4 + 2H_2O \leftrightarrow 4H_2 + CO_2 \quad \Delta H = -164{,}9\frac{kJ}{mol} \; at \; 298 \, K \quad (2.3)$$
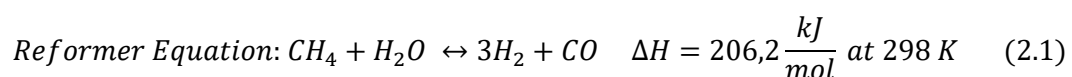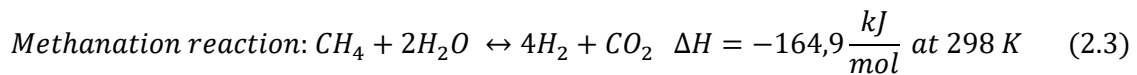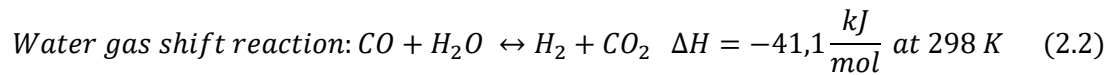
The reaction of water gas shift and reverse methanation are involved in a reaction of steam reforming over a catalyst at a higher temperature of more than 700 °C [45].

However, the reverse methanation reaction is thermodynamically a resultant from CH_4 steam reforming and water–gas shift reactions but it is determined to be kinetically independent.

The catalysts can be divided into two types: non-precious metal (typically nickel) and precious metals from Group VIII elements (typically platinum or rhodium based). Due to severe mass and heat transfer limitations, conventional steam reformers are limited to an effectiveness factor for the catalyst which is typically less than 5% [46]. Therefore, kinetics and thus the activity of the catalyst are rarely the limiting factors with conventional steam reformer reactors [47], so less expensive nickel catalysts are used almost universally in industry.
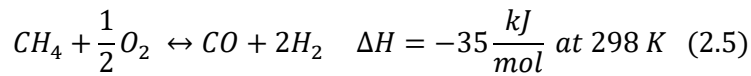
Coke formation is much less over the noble Group VIII metals. Promoters, such as magnesia or potassium or other alkaline components, are added to the catalyst support to minimize the coke formation [48]. Steam reforming is commonly used in industry for hydrogen production from methane where high thermal efficiencies of up to approximately 85%, based on the higher heating values, have been achieved [49].

The reforming process produces a product gas mixture with significant amounts of carbon monoxide, often 5% or more. To increase the amount of hydrogen, the product gas is passed through a water gas shift reactor to decrease the carbon monoxide content while increasing the hydrogen content. Typically, a high temperature is desired in order to achieve fast kinetics, but results in high equilibrium carbon monoxide selectivity and decreased hydrogen production. Therefore, the high temperature WGS reactor is often followed by a low temperature reactor to decrease CO content to 1% or less. The most common catalyst for WGS is Cu based.

2.2.2. Partial oxidation (PO_x)

PO_x is another standard route to H_2 production which uses oxygen and hydrocarbon or methane fuel. The syngas ($H_2 + CO$) and a mixture of CO_2, N_2, H_2O, and a small amount

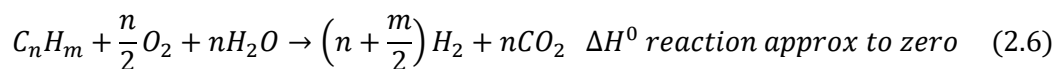of products such as methane are produced through partial oxidation. In a general way, oxidizing fuel is a requirement of energy balance in the presence of air. If sufficient air is not added, the fuel will oxidize incompletely, yielding mainly CO and H_2. However, it provides the sufficient air yielding, mainly CO_2 and H_2O as well. However, if the air present becomes half, at that time the chemical equilibrium will predict the mixture of CO and H_2, along with small traces of CO_2 and H_2O. The general equations are partial oxidation [50]:

$$C_nH_m + \frac{n}{2}O_2 \rightarrow nCO + \frac{m}{2}H_2 \quad (2.4)$$

$$CH_4 + \frac{1}{2}O_2 \leftrightarrow CO + 2H_2 \quad \Delta H = -35\frac{kJ}{mol} \ at \ 298 \ K \quad (2.5)$$
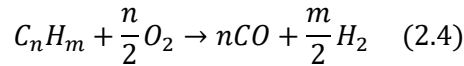
Two-step reactions consist of partial oxidation of methane. In the first step reaction, total methane combustion in the presence of O_2 to get CO_2 and H_2O. This is followed by steam reforming of un-reacted methane and CO_2 to receive syngas. The reaction accumulates with the reaction of water gas shift to obtain CO_2 and H_2O. The reactions of reforming are endothermic, instead total oxidation methane is an exothermic process ($\Delta H = - 803$ KJ /mol at 298K) [51]. The non-catalytic partial oxidation of hydrocarbons in the presence of oxygen typically occurs with flame temperatures of 1300÷1500 °C to ensure complete conversion and to reduce carbon or, in this case, soot formation [47]. Catalysts can be added to the partial oxidation system to lower the operating temperatures. For natural gas conversion, the catalysts are typically based on Ni or Rh; however, nickel has a strong tendency to coke and Rh cost has increased significantly [49].

2.2.3. Auto thermal reforming (ATR)

This approach is combined with steam reforming and POx methods in an adiabatic reactor. This technique also provides the neutral reaction of pairing the endothermic as steam reforming and exothermic as partial oxidation. H_2 yield is low than steam reforming, a better alternative option for fuel reforming due to neutral reaction in thermodynamically [52]. The general equation is the following:

$$C_nH_m + \frac{n}{2}O_2 + nH_2O \rightarrow \left(n + \frac{m}{2}\right)H_2 + nCO_2 \quad \Delta H^0 \ reaction \ approx \ to \ zero \quad (2.6)$$

Natural gas converted into a gas (H_2 + CO) in the furnace of catalytic and then produced CO_2 and H_2 in catalytic shift reaction along with the water when CO reacts. CO_2 can be captured through an absorption process by amines [53].

2.2.4. Steam iron process

This process is the old technique for H_2 generation. This method is started in the 20th century and mainly for balloons and airships. This is also known as a conventional method in which produces the hydrogen from iron oxide and performed the temperature nearly 540°C÷900°C [43]. It is a repeated process for H_2O split by which oil and coal are utilized. This process is done to produce reducing gas by coal gasified and containing H_2 and CO. This type of gas reacts by iron oxides like magnetite (Fe_3O_4), hematite (Fe_2O_3), and wuestite (FeO) to generate an iron oxide with reduced form [43]. The regenerated iron utilized in the reactor of the steam iron, consist of oxidized through steam to generate high abundant gas of H_2 and Fe_3O_4 and touch the temperature nearly (1088 K÷1143 K), represented by a chemical reaction:

$$3FeO + H_2O \rightarrow Fe_3O_4 + H_2 \quad (2.7)$$
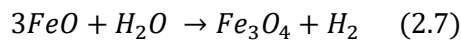
2.2.5. Pyrolysis

Pyrolysis is another hydrogen-producing technology where the hydrocarbon is decomposed (without water or oxygen present) into hydrogen and carbon. Pyrolysis can be done with any organic material [54] and is used for the production of hydrocarbons [55] and carbon nanotubes and spheres [56, 57].

Since no water or air is present, no carbon oxides (e.g., CO or CO_2) are formed, eliminating the need for secondary reactors (WGS, PrOx, etc.). Consequently, this process offers significant emissions reduction. However, if air or water is present, the materials have not been dried, and then significant CO_2 and CO emissions will be produced. Among the advantages of this process are fuel flexibility, relative simplicity and compactness, clean carbon by-product and reduction in CO_2 and CO emissions. The reactions can be written in the following form [58]:

$$C_nH_m \rightarrow nC + \frac{1}{2}mH_2 \quad \Delta H = hydrocarbon\ dependent \quad (2.8)$$
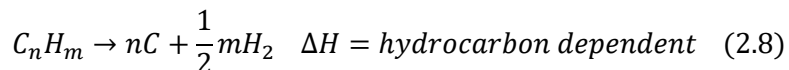
One of the challenges with this approach is the potential for fouling by the carbon formed, but proponents claim this can be minimized by appropriate design [59]. Since it has the potential for lower CO and CO_2 emissions and it can be operated in such a way as to recover a significant amount of the solid carbon which is easily sequestered [54, 58], pyrolysis may play a significant role in the future.

2.3. Steam reforming of other fuels

2.3.1. Methanol

Methanol or methyl alcohol is the simplest member of alcohols family with the formula of CH_3OH and the molecular structure given in Figure 2.3. It is a colourless, flammable liquid and miscible with water in all proportions. It is volatile and poisonous for human consumption, unlike ethanol. It is mainly used to produce chemicals and create fuels, antifreeze and solvents. Some of methanol properties and its safety data sheet based on National Fire Protection Association (U.S.A) are shown in Table 2.2.

The modern way to produce methanol is the catalysed direct combination of syngas, gaseous mixture of hydrogen and carbon monoxide. The required syngas can be obtained from several sources such as natural gas, coal, oil, and biomass. Utilization of biomass-derived syngas is highly increasing; thus, it is a renewable energy source.
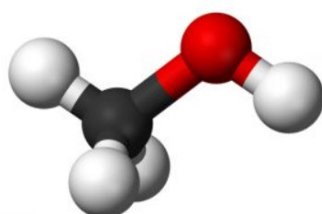
Figure 2.3 – Methanol molecular structure: black: Carbonium, grey: Hydrogen, red: Oxygen; Source: [60]

Property	Value	Property	Value
Molecular weight (g/mol)	32.042	Heat of combustion* (kJ/mol)	726.1
Melting point* (°C)	-97.8	Heat of vaporization* (kJ/mol)	37.34
Boiling point* (°C)	64.7	Vapor pressure* (kPa)	12.3
Density § (kg/m³)	0.81	Flash point* (°C)	15.6
Viscosity* (pa.s)	5.44×10^{-4}	Auto ignition temp. (in air) (°C)	464
CAS number	67-56-1	Health 2 / Fire 3 / Reactivity 0 / Personal Protection H	

* measured at normal temperature and pressure; 20 °C and 1 atm
§measured at 0 °C

Table 2.2 - Properties of methanol; Source: [61]

Methanol steam reforming (MSR) can be operated at atmospheric pressure. Due to absence of strong carbon-carbon bonds in methanol structure, less energy is required to break the molecule; consequently, the reforming temperature is low (200÷300 °C). This reforming temperature range is much lower compared to that of the other common hydrocarbons such as ethanol (400 °C) and methane (500 °C) [62]. Consequently, the risk of coke formation and catalyst fouling is lower. The generated carbon monoxide is low, whereas, the high hydrogen to carbon ratio of methanol leads to high H_2 production. Additionally, less efforts and cost will be expected to change the current refueling systems from gasoline and diesel to methanol. Furthermore, the study of L. R. Borup's group [63] compared the needed start-up energy of the various fuels utilized in the on-board H_2 production system. The start-up energy is the required energy to increase the system temperature from ambient temperature to the temperature that system can produce the fuel cell quality hydrogen. The results, presented in Figure 2.4, show the low start-up energy requirement of methanol:
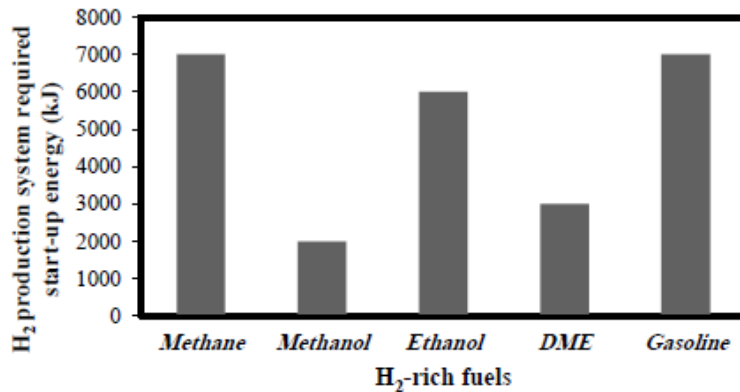
Figure 2.4 - Required start-up energy of various feedstocks; Source: [63]

The overall reaction network of methanol steam reforming process can be described as follows:

$$CH_3OH + H_2O \leftrightarrow CO_2 + 3H_2 \quad \Delta H = 49{,}7 \frac{kJ}{mol} \quad (2.9)$$

$$CH_3OH \leftrightarrow CO + 2H_2 \quad \Delta H = 90{,}2 \frac{kJ}{mol} \quad (2.10)$$

$$CO + H_2O \leftrightarrow CO_2 + H_2 \quad \Delta H = -41{,}2 \frac{kJ}{mol} \quad (2.11)$$
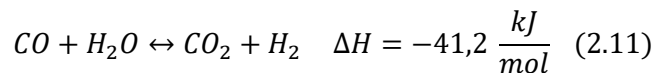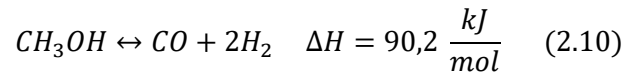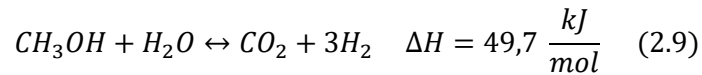
The general operating conditions of this process are reported in Table 2.3:

Pressure	*1 bar*
Temperature	*250-300 ˚C*
Reactants molar ratio (MeOH/H₂O)	*1:1-1:1.3*

Table 2.3 - General operative conditions of the MSR reaction

Methanol steam reforming reaction (2.9) comprises the combination of methanol decomposition (2.10) and water-gas shift (2.11) reactions. The main products of the process are hydrogen and carbon dioxide. However, trace amount of carbon monoxide is produced by the reverse water-gas shift reaction at high temperature, since the reaction is exothermic. The methanol decomposition reaction rate is much 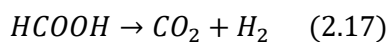lower than that of the steam reforming reaction. It is stated that adding water to the feed decreases the temperature that methanol decomposition begins [64, 65]. Moreover, it is also expressed that the absence of steam in the feed leads to coke formation [66]. Another study showed that there is no CO formation at low contact times [67]. However, the reaction mechanism is still a controversial issue due to the reaction complexity and two other reaction mechanisms, rather than methanol decomposition followed by water-gas shift reaction, have been postulated too. They are described as follows:

$(A)\ via\ methyl\ formate$:

$$2CH_3OH \rightarrow HCOOCH_3 + 2H_2 \quad (2.12)$$

$$HCOOCH_3 + H_2O \rightarrow CH_3OH + HCOOH \quad (2.13)$$

$$HCOOH \rightarrow CO_2 + H_2 \quad (2.14)$$

$(B)\ via\ formaldehyde$:

$$CH_3OH \rightarrow HCHO + H_2 \quad (2.15)$$

$$HCHO + H_2O \rightarrow HCOOH + H_2 \quad (2.16)$$

$$HCOOH \rightarrow CO_2 + H_2 \quad (2.17)$$
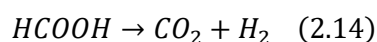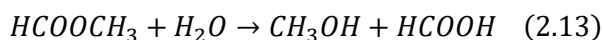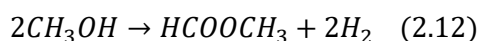
Jiang et. al [68] suggested that the mechanisms *(A)* and *(B)* are the main reaction routes over copper-based catalysts. R. Thattarathody et al. [66] expressed that the side reactions of (2.12) and (2.15) and the corresponding mechanisms occur with high MeOH/steam ratio [48]. The mechanism study of MSR reaction over the group 8-10 catalysts was done by a few research groups as well. Those studies showed that the reaction mechanism is similar to the mechanism *(B)* [40]. To the extent of our knowledge, a detailed MSR

mechanism study has not been done yet. Consequently, the controversy still remains on the mechanism of this process.

MSR is a heterogeneously catalysed reaction. Copper-based and group 8-10 catalysts are two common types of catalysts used in this process. However, in order to enhance the activity of copper-based catalysts and prevent the copper from sintering, the copper catalysts are promoted with various types of metal oxides. The copper-based catalysts are the most conventional type of catalysts used in MSR process because of their high activity, high selectivity and low cost. However, some disadvantages are attributed to them, such as pyrophoricity, change in oxidation state, deactivation due to sintering, and coke deposition. The copper-based catalysts are highly prone to sintering at a temperature higher than 300 °C. Nevertheless, it is proved that the process temperature in MSR should not exceed 260 °C [69].

2.3.2. Bio-ethanol

Hydrogen production from bio-ethanol has been considered as a promising opportunity since bio-ethanol is the most available bio-fuel in the world. Ethanol, whose molecular structure is shown in Figure 2.5, has many advantages that are described below:

- Ethanol possesses very high hydrogen content (103 g H_2/ litre of ethanol) [70];
- Storage and transportation of ethanol is safe;
- It can be produced from cellulosic biomass which is abundant in nature by fermentation;
- Produced ethanol contains significant amount of water which can be directly used in steam reforming reaction;
- It possess no sulphur derivatives that would be poisonous to the catalyst;
- Using bio-ethanol for hydrogen production completes the carbon balance since carbon dioxide produced from the production of hydrogen is reabsorbed during the growth of biomass [71].
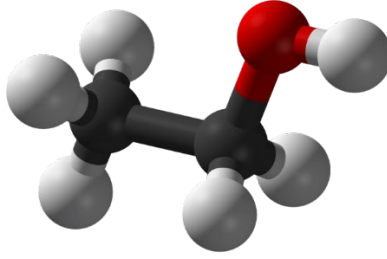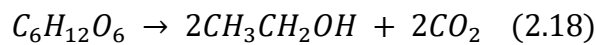
Figure 2.5 - Ethanol molecular structure: black: Carbonium, grey: Hydrogen, red: Oxygen; Source: [72]

Bio-ethanol is the product of anaerobic respiration done by yeasts converting glucose into ethanol and carbon dioxide and generally called biomass fermentation [73]. It is represented by the following reaction:

$$C_6H_{12}O_6 \rightarrow 2CH_3CH_2OH + 2CO_2 \quad (2.18)$$

Bio-ethanol can be produced by fermentation of biomass sources, like energy plants, agro-industrial wastes, forestry residue materials and organic fraction of municipal solid waste. While using starch-rich materials such as sugar cane, switch grass, corns as feedstock is efficient, it is not preferred due to high cost of feedstock plantation. Production of ethanol using lignocellulosic biomass as the feedstock has many advantages such as lower production price and abundance of lignocellulosic biomass, which corresponds to 50% of the biomass in the world. However, due to its more complex molecular structure, process is more challenging compared to process using starch-rich materials as feedstock.

Bio-ethanol is preferred to be used for hydrogen production instead of a fuel directly in internal combustion engines. The reason is the costly separation processes required for separating water from ethanol produced from biomass, which contains $13 \frac{mol\ of\ water}{mol\ of\ ethanol}$ [71]. Hydrogen can be produced from ethanol generally by three different routes, which are steam reforming, partial oxidation and oxidative steam reforming. Between these three processes, steam reforming of ethanol requires less total energy demand compared to partial oxidation and auto-thermal reforming processes and has higher hydrogen yield. In this thesis, we will focus only on steam reforming to compare the steam reforming of ethanol with the steam reforming of the other fuels. A possible pathway of reactions of SRE is shown in Table 2.4:

REACTION NO.	REACTION FORMULA	REACTION TYPE
R1	$C_2H_5OH + 3H_2O \leftrightarrow 2CO_2 + 6H_2$	Sufficient steam supply reaction
R2	$C_2H_5OH + H_2O \leftrightarrow 2CO + 4H_2$	Insufficient steam supply reaction
R3	$C_2H_5OH + 2H_2 \leftrightarrow 2CH_4 + H_2O$	Insufficient steam supply reaction
R4	$C_2H_5OH + H_2O \leftrightarrow CH_3COOH + 2H_2$	Insufficient steam supply reaction
R5	$C_2H_5OH \leftrightarrow CH_3CHO + H_2$	Ethanol dehydrogenation
R6	$CH_3CHO \leftrightarrow CH_4 + CO$	Acetaldehyde decomposition
R7	$CH_3CHO + H_2O \leftrightarrow 3H_2 + 2CO$	Acetaldehyde decomposition
R8	$C_2H_5OH \leftrightarrow C_2H_4 + H_2O$	Ethanol dehydration
R9	$C_2H_5OH \leftrightarrow {}^1\!/_2\, C_2H_5OC_2H_5 + {}^1\!/_2\, H_2O$	Ethanol dehydration
R10	$C_2H_4 \leftrightarrow polymers \leftrightarrow 2C + 2H_2$	Ethylene polymerization
R11	$C_2H_5OH \leftrightarrow CO + CH_4 + H_2$	Ethanol decomposition
R12	$C_2H_5OH \leftrightarrow \frac{1}{2}CO_2 + \frac{3}{2}CH_4$	Ethanol decomposition
R13	$C_2H_5OH \leftrightarrow \frac{1}{2}CH_3COCH_3 + \frac{1}{2}CO + \frac{3}{2}H_2$	Ethanol decomposition
R14	$CO + 3H_2 \leftrightarrow CH_4 + H_2O$	CO methanation
R15	$CO_2 + 4H_2 \leftrightarrow CH_4 + 2H_2O$	CO_2 methanation
R16	$CH_4 \leftrightarrow 2H_2 + C$	Methane cracking
R17	$CO \leftrightarrow \frac{1}{2}CO_2 + \frac{1}{2}C$	Boudouard reaction
R18	$CO + H_2O \leftrightarrow CO_2 + H_2$	Water-gas-shift
R19	$CO + H_2 \leftrightarrow C + H_2O$	CO reduction
R20	$CO_2 + 2H_2 \leftrightarrow C + 2H_2O$	CO_2 reduction

Table 2.4 - Main reactions take place in the steam reforming of ethanol process; Source: [74]

Steam reforming of ethanol is an endothermic process as shown by (R2). When combined with water gas shift reaction (R18), 6 mol of hydrogen can be obtained from one mol of ethanol via the ideal pathway which is overall steam reforming of ethanol (R1). Hydrogen production rate can be changed significantly by adjusting steam supply and operating temperature. Major disadvantage of this process is coke formation.

Operating conditions of steam reforming of ethanol does not only favour R1, there are also other reactions, which could reduce the hydrogen production, depending on the temperature, supplied steam amount and catalyst properties. Many authors have studied thermodynamics of this process and reaction pathways extensively and a detailed thermodynamic analysis is also carried out in this thesis and whose results are provided in the *Chapter 5*.

Ideal reaction pathway for maximum hydrogen production is overall steam reforming reaction (R1), as mentioned before. For this reaction to be dominant, sufficient steam should be supplied and side reaction should be minimized. If steam supply is insufficient or reaction environment is not suitable for water gas shift reaction (R18), only the ethanol steam reforming reaction (R2) takes place instead of overall reaction, reducing the maximum allowable hydrogen yield from 6 to 4. Besides water gas shift reaction, insufficient steam could also lead to the occurrence of R3. The occurrence of R3, R14 and R15 reduces the hydrogen productivity by using hydrogen as reactant and forming methane, which is the main by-product of this process. Methane could also be formed mainly from ethanol decomposition (R12). Acetaldehyde and ethylene are accepted to be important intermediates formed through ethanol dehydrogenation (R5) and ethanol dehydration (R8) reactions, respectively. Decomposition of acetaldehyde (R6) and ethylene (R10) leads to formation of main undesired by-products methane, carbon and carbon monoxide. In addition to ethylene decomposition (R10), carbon depositions also occur via Boudouard reaction (R17) and methane decomposition reaction (R16) [74].

Besides thermodynamic limitations that affect the hydrogen productivity, the most important factor in this process is the catalyst selection, which could alter the pathway of reaction network. The selected catalyst should maximize hydrogen selectivity via activating ethanol steam reforming reaction, while minimizing side product formation by inhibiting cracking reactions and coke formation. The catalyst properties, which are specified by the metals selected, their proportions and synthesis method used, has an important impact on the activity of the catalyst. While active metal generally is used for

the cleavage of C-C bonds in steam reforming of ethanol, the catalyst support has also effects on the cleavage and activation of the bonds. For ethanol steam reforming reaction, generally noble metal catalysts such as Rh, Ru, Pd and Pt and non-noble metal catalysts such as Ni and Co have been extensively investigated [73].

Hydrogen productivity and ethanol conversion in ethanol steam reforming reaction depend on many factors, such as the type of active metal used, the type of catalyst support, the catalyst synthesis route, the presence of additional metals and the operating conditions. Among the active metals investigated by many researchers, Ni has emerged as the most promising catalyst for high purity hydrogen production. However, Ni-based catalysts suffer from deactivation due to coke formation, limiting the usage of nickel-based catalysts in long term applications. Deposited coke could rupture catalyst structure and reduce surface area leading to deactivation of the catalyst [73]. Coke formation can be minimized by optimization of operating conditions such as operating temperature, steam-to-ethanol ratio and formulation of the catalyst [75]. Low temperatures are preferred for ethanol steam reforming reaction to achieve energy conservation. Unfortunately, coking is generally observed near temperatures of 500°C due to insufficient gasification by steam. Minimization of coke formation can be achieved by using feedstock having high steam-to-ethanol ratios. Increasing of partial pressure of steam in the reaction medium increases the chemisorbed water on the catalyst, leading to higher gasification of coke deposited on the surface [76, 77].

2.3.3. Glycerol

Glycerol (1,2,3 - propantriol) is a colourless, odourless product with a sweet taste and appears as a viscous liquid. The glycerol molecule is completely soluble in water and methanol, slightly soluble in other polar solvents and insoluble in non-polar solvents such as diethyl ether and hydrocarbons. Table 2.5 lists the physico-chemical characteristics of glycerol.

Pure and anhydrous glycerol has a density of 1,261 g / mL, a melting point of 17,9 ° C and a boiling point of 290 °C with simultaneous decomposition of the molecule. It is non-toxic and edible, therefore it lends itself to being added in the formulations of pharmaceutical products for therapeutic use, personal hygiene products and in the food sector. In addition, glycerol maintains chemical stability during storage; it is not irritating

in its applications and is not dangerous for the environment as it is completely biodegradable [78, 79].

Glycerol contains three hydroxyl groups, which are responsible for its high solubility in water and its hygroscopic character. His molecular structure is shown in Figure 2.6:
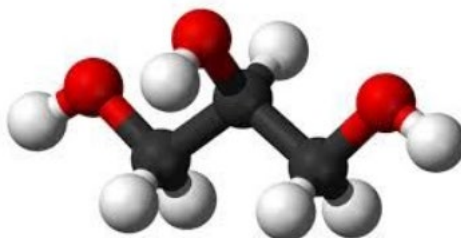

Figure 2.6 - Glycerol molecular structure: black: Carbonium, grey: Hydrogen, red: Oxygen; Source: [80]

Properties	Values
Chemical formula	$CH_2OH-CHOH-CH_2OH$
Formula weight	92.09
Form and color	Colorless and liquid
Specific gravity	$1.260^{50/4}$
Melting point	17.9°C
Boiling point	290°C
Solubility in 100 parts	
Water	Infinitely
Alcohol	Infinitely
Ether	Insoluble
Vapor pressure in 760 mmHg	290°C
Heat of fusion at 18.07°C	47.49 cal/g
Viscosity liquid glycerol 100%	10 cP
50%	25 cP
Diffusivity in	$(DL \times 10^5 \text{ sq.cm/s})$
i-Amyl alcohol	0.12
Ethanol	0.56
Water	0.94

Table 2.5 – Physico-chemical properties of glycerol at 20 °C; Source: [81]

The use of biofuels for hydrogen production emits low carbon dioxide, as the CO_2 produced is consumed for biomass growth, which provides significant environmental benefits. Bio-glycerol is produced as a by-product of biodiesel synthesis from transesterification of vegetable oils or animal fats, allowing it to be used as a low-cost raw material in a large supply of renewable materials. Glycerol offers advantages such as its natural availability such as low toxicity, safe storage and handling [82, 83]. Hydrogen can be produced from glycerol through several processes, such as steam reforming, partial oxidation and autothermal reforming but the first one is the most efficient and widely

used. Steam reforming is the most widely used method for hydrogen production because this process is economically viable, environmentally friendly, and allows easy scaling of the process in industrial applications. In this process, glycerol reacts with water vapour in the presence of a catalyst, produces mainly hydrogen, carbon dioxide and carbon monoxide. Even though the presence of water increases the hydrogen yield, a large amount of water is necessary to prevent coke deposition on the catalyst. In addition, glycerol steam reforming is an endothermic reaction; therefore, it requires high operating temperature that increases energy consumption and inherently operating cost. In addition, due to the high operating temperature, more heat resistant reactors are required and thereby higher capital cost is involved. In particular, at lower temperatures, in addition to the main products, CH_4 is formed decreasing the selectivity of H_2. In glycerol steam reforming reaction, 7 moles of hydrogen is produced by one mole of glycerol. So, it may be viewed as the combination of glycerol decomposition and water-gas shift reactions. However, these reactions may also be accompanied by methanation, methane dry reforming, methane steam reforming and a series of carbon formation reactions [84, 85], as reported in the Table 2.6:

REACTION NO.	REACTION FORMULA	REACTION TYPE
R1	$C_3H_8O_3 + 3H_2O \leftrightarrow 3CO_2 + 7H_2$	Glycerol Steam Reforming
R2	$C_3H_8O_3 \rightarrow 3CO + 4H_2$	Glycerol Decomposition
R3	$CO + H_2O \leftrightarrow CO_2 + H_2$	Water Gas Shift
R4	$CO_2 + 4H_2 \leftrightarrow CH_4 + 2H_2O$	CO_2 Methanation
R5	$CH_4 + CO_2 \leftrightarrow 2CO + 2H_2$	Methane Dry Reforming
R6	$CH_4 + H_2O \leftrightarrow CO + 3H_2$	Methane Steam Reforming
R7	$2CO \leftrightarrow CO_2 + C$	Boudouard reaction
R8	$CH_4 \leftrightarrow C + 2H_2$	Methane cracking
R9	$CO + H_2 \leftrightarrow H_2O + C$	Carbon monoxide reduction
R10	$CO_2 + 2H_2 \leftrightarrow C + 2H_2O$	Carbon dioxide reduction

Table 2.6 - A possible pathway of reactions of Glycerol Steam Reforming; Source: [84], [85]

Considering the above-stated reactions, glycerol steam reforming reaction occurs at temperatures in the 300÷900 °C range; however, according to studies, the maximum H_2 yield is obtained between 525÷725 °C [86]. Although the operating pressure is generally atmospheric pressure, vacuum pressure is better not only to achieve higher H_2 yield, but also to reduce energy consumption by lowering operating temperatures [82, 87, 88]. Similar to glycerol steam reforming reaction, glycerol decomposition reaction occurs over a wide temperature range (400÷900 °C), but its yield increases between 650÷750 °C at atmospheric pressure [89, 90]. In addition, water gas shift reaction favours the product side up to 450 °C; this reaction may also occurs at high temperatures, depending on the amount of water in the feed [91, 92]. Exothermic methanation reaction generally takes place between 200÷550 °C at atmospheric pressure [93]. Aside from these reactions, both methane dry reforming and methane steam reforming reactions operate at high temperature (700÷1000 °C) and at high pressure (3÷20 bar) [94]. Moreover, while carbon formation reactions may occur at the temperature higher than 400 °C, reverse carbon formation reactions (carbon gasification reactions) may occur, particularly at high water/glycerol ratios [95].

2.3.4. Biogas

Biogas is a product obtained from the anaerobic digestion of organic material such as manure, sewage sludge and the organic fraction of domestic and industrial waste. All types of biomass can be used as substrates for biogas production, as long as they contain carbohydrates, proteins, fats, cellulose and hemicellulose as main components. Only woody organic substances are unsuitable due to the extreme slowness of their decomposition process.

Biogas is a gaseous mixture composed of CH_4 (40÷75%) and CO_2 (15÷60%), with small fractions of other compounds such as N_2 (0÷2%), CO (<0.5%), H_2S (0.005÷2%), O_2 (0÷1%), NH_3 (<1%); occasionally other trace compounds may be present, such as aromatic hydrocarbons, alkanes, alkenes, etc. The whole is saturated with water vapour. The biogas yield and its composition directly depend on the type of biomass from which it derives and on the quantity of organic fraction present [96] (see Figure 2.7).
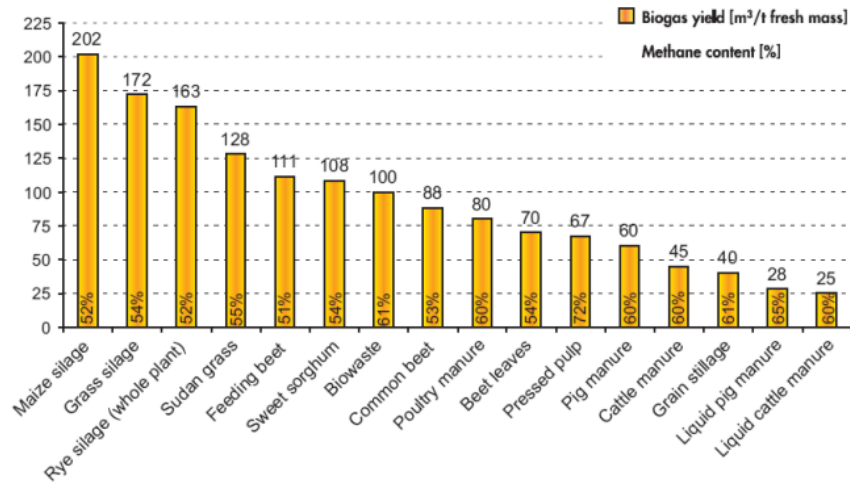
Figure 2.7 - Biogas yield and methane content by type of biomass; Source: [97]

The different raw materials have different degradation rates: for example, lipids give the highest yield in biogas, but their decomposition is slow; while carbohydrates and proteins are in the opposite situation. The efficiency of the anaerobic digestion process is determined by some operational parameters that affect the growth and activity of microorganisms: absence of oxygen, temperature, pH, nutrients, humidity, and the presence of inhibitors [97].

Most of the biogas produced in Europe is used in internal combustion engines or turbines to produce electricity, while the heat produced is recovered and redistributed through district heating networks [97]. Another solution is combustion in boilers for the production of hot water and steam.

The disadvantages of using biogas as an energy source are essentially two [96]:

- The presence of impurities that do not allow the use of biogas as it is. In particular the fuel cells suffer from the presence of sulphides that deactivate the catalyst, while in engines and turbines they can instead give rise to corrosion phenomena;
- The large concentration of CO_2 which, being inert, dilutes the fuel, lowering the efficiency of the process.

The biogas must therefore be purified in order to obtain "clean biogas"; choosing to eliminate CO_2, bio-methane (> 95% methane) would be obtained, which can be fed into the traditional distribution network of methane of fossil origin. CO_2 can even represent 50% of the biogas, eliminating it would mean losing a substantial portion of the power supply, increasing the cost of the plant due to the separation process. It is therefore

possible to try to valorise clean biogas by converting it into syngas through reforming processes from which to produce hydrogen, methanol or hydrocarbons from Fischer-Tropsch processes [96].

All fossil methane reforming processes can be used to produce hydrogen from bio-methane. The reaction produces syngas with a different H_2 / CO ratio, which can later be corrected by the WGS reaction to remove the CO and maximize the hydrogen yield. Compared to the use of fossil methane, the reforming of biogas to produce hydrogen theoretically allows a zero balance on CO_2 emissions. With this type of approach, however, it is not possible to efficiently exploit the biogas [96].

The most suitable process for the full utilisation of this gaseous mixture is the reforming of CH_4 with CO_2 or Dry Reforming (DR). The DR reaction has the advantage of fully exploiting the biogas stream by converting CO_2, which in other processes is only an inert to be separated (with associated costs). However, this reaction also has significant disadvantages such as the strong tendency to form coke, the high operating temperatures required, but above all the very low H_2 / CO ratio, which makes the syngas produced not directly suitable for use in subsequent upgrading processes (methanol production, F-T, etc).

$$Dry\ Reforming: CH_4 + CO_2 \leftrightarrow 2CO + 2H_2 \quad (2.19)$$
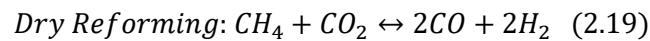
The reaction is strongly endothermic, it is favoured at low pressures, producing a syngas with theoretical ratio H_2 / CO = 1.

A series of parallel reactions take place in the process, in particular the Water Gas Shift Inverse (RWGS) reaction, which further lowers this ratio and makes it less than 1 [98, 99]:

$$WGS\ inverse: CO_2 + H_2 \leftrightarrow CO + H_2O \quad (2.20)$$
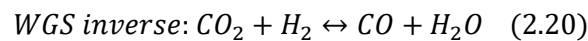
Other secondary reactions are the decomposition of methane and the disproportionation of CO or Boudouard reaction: these reactions cause the production of coke, which deactivates the catalyst and, if produced in high quantities, can lead to the breakage of the pellets with consequent blockage of the reactor [99]:

$$Decomposition\ of\ methane: CH_4 \rightarrow C + 2H_2 \quad (2.21)$$

$$Boudouard\ reaction: 2CO \rightarrow C + CO_2 \quad (2.22)$$
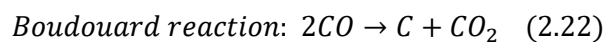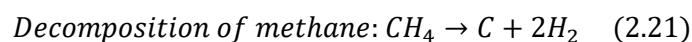
Thermodynamic studies on the DR reaction have revealed that at 1 atm this is spontaneous above 640 °C, the RWGS reaction is spontaneous above 820 °C, while the decomposition of methane and Boudouard reaction occur respectively above 577 °C and up to 700 °C. Therefore, the greatest production of coke occurs within this temperature range [98, 100].

At high temperatures the supported metal catalysts are subject to deactivation phenomena by sintering. For this reason, it is necessary to develop catalysts that are extremely thermally stable and resistant to coke deposition. The overall activity of the catalyst in the DR depends on the type of metal used, the nature and surface of the support, the size of the metal particles and the interaction between metal and support. Noble metals such as Pt, Pd, Ir, Ru and Rh are very active catalysts in DR, resistant to coke formation, even if they are very expensive [101]. Among the "non-noble" metals, the most active are Ni, Fe and Co [102]. Even if the type of support plays a fundamental role in the activity of the catalyst, it is still possible to draw up a general reactivity scale on the active phases. Among the noble metals, the sequence applies both to the catalytic activity, to the DR reaction, and to the resistance to the formation of coke and is as follows:

$$Rh, Ru > Ir > Pt, Pd$$
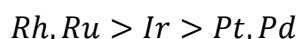
Among the transition metals the best is clearly Ni [102]:

$$Ni > Co > Fe$$

Obviously, the amount of metal present on the catalyst also determines its activity, but while a small weight fraction (1÷5% w/w) is sufficient for noble metals, higher percentages are needed for Ni to have good conversions. The greater cost-effectiveness makes Ni the most used element in this type of reactions at an industrial level, although it does not have the same performance in terms of thermal stability and resistance to coke as noble metals. To overcome these defects, bi- or tri-metal catalysts have been studied in which noble metals (or even other elements) are present in small quantities together with nickel [103].

An evolution of the DR process makes it possible to correct the H_2 / CO ratio by adding steam to the biogas, so as to combine Dry Reforming and Steam Reforming (S / DR or bi-reforming).

Bi-reforming is the combination of reactions of Dry Reforming and Steam Reforming:

$$3CH_4 + CO_2 + 2H_2O \leftrightarrow 4CO + 8H_2 \quad (2.23)$$
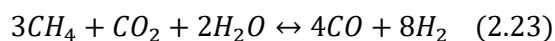
The main advantage of this process is the possibility to vary the H_2 / CO output ratio based on the steam / methane ratio used [104]. By increasing the amount of steam, the behaviour of the system approaches that of pure SR, the conversion of CO_2 is lowered and the H_2 / CO ratio approaches 3; if, on the other hand, the quantity of steam decreases, the process approaches a DR, the CO_2 conversion increases and the H_2 / CO ratio approaches 1.

A further advantage due to the addition of steam to the feed is that the production of coke can be suppressed thanks to the gasification reaction:

$$C + H_2O \rightarrow CO + H_2 \quad (2.24)$$

The operating conditions of the process are similar to those already seen for the SR and the DR [105]. Bi-reforming is also endothermic and must be carried out at high temperatures (800÷1000 °C), at pressures between 5 and 30 atm [104].

2.3.5. Propane

Propane is a saturated aliphatic hydrocarbon with three carbon atoms of the brute formula C_3H_8. Its molecular structure is shown in Figure 2.8.
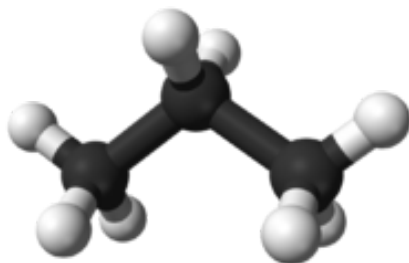

Figure 2.8 - Propane molecular structure: black: Carbonium, grey: Hydrogen; Source: [106]

It is a colourless, odourless and easily liquefiable gas through compression. It has a molecular mass of 44.09 g / mol, a melting point of -187.6 °C, a boiling point of -42.1 °C and, under standard conditions, it has a density of 0.49 g / cm^3 [106]. It is an easily flammable substance and, although non-toxic, it is classified among the asphyxiating gases that is among those gases which, if present in high concentration in the air, prevent the cellular respiration process [107]. Slightly soluble in water, acetone and partially in ethanol due to its non-polar nature, it is instead well miscible with diethyl ether, chloroform and benzene. Propane occurs in nature as a component of natural gas and crude oil, from which it is extracted by fractional distillation, and is also the main

constituent of liquefied petroleum gas (LPG), a hydrocarbon mixture commonly obtained from petroleum widely used as a fuel.

Steam reforming of propane was studied to investigate a feedstock other than natural gas for production of pure hydrogen. Irreversible propane steam reforming is limited by the reversibility of the steam reforming of the methane that is formed. A possible pathway of reactions of Propane Steam Reforming is shown in Table 2.7:

REACTION NO.	REACTION FORMULA	REACTION TYPE
R1	$C_3H_8 + 3H_2O \rightarrow 3CO + 7H_2$	Propane Steam Reforming
R2	$C_3H_8 + 3CO_2 \leftrightarrow 6CO + 4H_2$	Propane CO_2 Reforming
R3	$C_3H_8 + \frac{3}{2}O_2 \rightarrow 3CO + 4H_2$	Propane partial oxidation
R4	$C_3H_8 \rightarrow 3C + 4H_2$	Propane decomposition
R5	$CO + 3H_2 \leftrightarrow CH_4 + H_2O$	CO Methanation
R6	$CO + H_2O \leftrightarrow CO_2 + H_2$	Water Gas Shift
R7	$CH_4 + 2H_2O \leftrightarrow CO_2 + 4H_2$	Methane Overall Steam Reforming
R8	$C_3H_8 + 6H_2O \leftrightarrow 3CO_2 + 10H_2$	Propane Overall Steam Reforming
R9	$CH_4 \leftrightarrow C + 2H_2$	Methane cracking
R10	$2CO \leftrightarrow CO_2 + C$	Boudouard reaction
R11	$CO + H_2 \leftrightarrow H_2O + C$	Carbon monoxide reduction
R12	$CO_2 + 2H_2 \leftrightarrow C + 2H_2O$	Carbon dioxide reduction

Table 2.7 - A possible pathway of reactions of Propane Steam Reforming; Source: [108]

There are various methods to generate hydrogen from propane (see R1-R4). Among these, propane CO_2 reforming [109] is relatively slow and un-economical compared to steam reforming [110]. The decomposition pathway is attractive since the hydrogen produced is free of CO and no additional greenhouse gases, like CO_2 or CH_4, are produced.

Partial oxidation [111] is preferred when a carbon-monoxide-rich syngas is desired or if inexpensive oxygen is available. Steam reforming is the most economical pathway in terms of hydrogen yield, since hydrogen is produced from steam as well as propane.

Several other reactions take place following the main steam reforming process (R5-R7). Summing R1 and 3 times R6 propane overall steam reforming (R8) is obtained.

Since industrial operations always use excess steam to minimize catalyst deactivation, the maximum yield of hydrogen per mole of propane fed can be 10. The carbon formation processes (R9-R12) can also take place as unwanted side reactions.

Steam reforming of hydrocarbons can be catalysed by several transition metals. The specific activities of metals supported on alumina or magnesia have been found to be in rank order Rh, Ru > Ni, Pd, Pt > Re > Co [112]. Catalyst selection is mainly an economic consideration followed by considerations regarding catalyst activity and stability. In terms of activity and stability, both ruthenium and rhodium are more effective catalysts than nickel [113, 114], on which carbon formation appears to occur via a different mechanism [115]. In addition to its lower activity, more coking arises with nickel because of formation, diffusion and dissolution of carbon in the metal, whereas dissolution of carbon in ruthenium and rhodium is considerably less. Despite their advantages, the cost and availability of Rh and Ru are such that these catalysts are not used widely in industrial applications. The most widely used catalysts for large scale industrial reformers are Al_2O_3-supported nickel.

Especially for higher hydrocarbon feedstocks, these catalysts are frequently modified by promoters such as earth alkaline metals like Mg and Ca to improve their stability and selectivity, by reducing the acidity of the support, there by suppressing cracking and polymerization reactions. Commercial steam reforming catalysts are usually designed for operation at 850÷900 °C and above [112].

2.4. Hydrogen production from renewable sources

2.4.1. Hydrogen production from biomass

In the near term, biomass is the most likely renewable organic substitute to petroleum. It is a renewable source of primary energy derived from plant and animal material, such as animal wastes, municipal solid wastes, crop residues, short rotation woody crops,

agricultural wastes, sawdust, aquatic plants, short rotation herbaceous species (i.e., switch grass), corn, and so on.

Biomass, that comes from plants, is organic matter in which the energy of sun light is stored in chemical bonds via photosynthesis. Although CO_2 is released when biomass is utilized for energy production, this amount of gaseous emission is equal to the amount that absorbed by organisms when they were still living.

Thermochemical and biological methods are the two modes for hydrogen production from biomass.

Thermochemical processes involve two processes: pyrolysis and gasification.

Biomass pyrolysis is the thermochemical process of generating liquid oils, solid char coal and gaseous compounds by heating the biomass. It takes place in the total absence of oxygen except in cases where partial combustion is allowed to provide the thermal energy needed for the process [116].

Biomass gasification is the thermochemical conversion of biomass into a gaseous fuel (syngas) in a gasification medium such as air, oxygen and/or steam [117].

Biological processes utilized for hydrogen production are: direct and indirect bio-photolysis, photo and dark fermentations and sequential dark and photo-fermentation. The feeds for bio-hydrogen are water (for photolysis) and biomass (for fermentative processes).

Bio-photolysis is a biological process where hydrogen is produced by some bacteria or algae directly through their hydrogenase or nitrogenase enzyme system. It uses the same principles found in plants and algal photosynthesis but adapts them for the generation of hydrogen gas. Green algae and blue-green algae are able to split water molecules into hydrogen ion and oxygen via direct and indirect bio-photolysis, respectively.

Fermentations are biochemical processes where the carbohydrate containing materials are converted to organic acids and then to hydrogen as by using bio-processing technologies. It takes place with or without oxygen. They perform microbial transformations of organic feed materials producing alcohols, acetone and H_2 in minimal amounts as well as CO_2.

These include: photo-fermentation, dark fermentation and the combination of both.

Photo-fermentation, instead, is realized in deficient nitrogen conditions using solar energy and organic acids (acetic, lactic and butyric). Increasing light intensity has a stimulatory

effect on H_2 yield and production rate, but an adverse effect on the light conversion efficiency [118].

Dark fermentation uses primarily anaerobic bacteria on carbohydrate rich substrates under anoxic (no oxygen present) dark conditions [119].

The combination of dark and photo-fermentation is called sequential dark/photo-fermentation. Using hybrid systems, higher hydrogen production yields and reduced light energy demand can be obtained [120].

2.4.2. Hydrogen production from water

Water is one of the most abundant and inexhaustible raw materials in Earth and can be used for H_2 production through water-splitting processes such as electrolysis, thermolysis and photo-electrolysis. If the required energy input is provided from renewable energy sources, the hydrogen produced will be the cleanest energy carrier that could be used by mankind.

Electrolysis is an established and well-known method, constituting the most effective technique for water splitting. The reaction is very endothermic and the required energy input is provided by electricity. A typical electrolysis unit or electrolyser consists of a cathode and an anode immersed in an electrolyte and generally, when electrical current is applied, water splits and hydrogen is produced at the cathode while oxygen is evolved on the anode side [68].

Thermolysis or thermochemical water splitting is the process at which water is heated to a high temperature until decomposed to hydrogen and oxygen. The decomposition of water is not effected until the temperature is very high (generally over 2500 °C) in order to separate hydrogen from the equilibrium mixture in a feasible way. Since these expenditures of primary energy could not be achieved by sustainable heat sources, several thermochemical water-splitting cycles have been proposed to reduce the temperature and improve the overall efficiency [121]. The energy efficiencies and rates of hydrogen produced increase with rise in solar light intensity [122].

Photolysis, in general, is effected when the energy of visible light is absorbed with the help of some photo-catalysts and is then utilized to decompose water into H_2 and O_2. In photo-electrolysis, the sunlight is absorbed through some semiconducting materials and the process of water splitting is similar to electrolysis [120].

44

In the Table 2.8 are summarized the various advantages and disadvantages of each process described:

Process	Efficiency (%)	Major advantages	Major disadvantages
SR	74–85	Most developed technology, existing infrastructure.	CO_2 byproduct, dependence on fossil fuels.
POX	60–75	Proven technology, existing infrastructure.	CO_2 byproduct, dependence on fossil fuels.
ATR	60–75	Proven technology, existing infrastructure.	CO_2 byproduct, dependence on fossil fuels.
CHs pyrolysis	–	Emission-free, reduced-step procedure.	Carbon byproduct, dependence on fossil fuels.
Biomass pyrolysis	35–50	CO_2-neutral, abundant and cheap feedstock.	Tar formation, varying H_2 content due to seasonal availability and feedstock impurities.
Biomass gasification	–	CO_2-neutral, abundant and cheap feedstock.	Tar formation, varying H_2 content due to seasonal availability and feedstock impurities.
Bio-photolysis	10	CO_2-consumed, O_2 is the only byproduct, operation under mild conditions.	Requires sunlight, low H_2 rates and yields, requirement of large reactor volume, O_2 sensitivity, high raw material cost.
Dark fermentation	60–80	CO_2-neutral, simple, can produce H_2 without light, contributes to waste recycling, no O_2 limitation.	Fatty acids removal, low H_2 rates and yields, low conversion efficiency, requirement of large reactor volume.
Photofermentation	0.1	CO_2-neutral, contributes to waste recycling, can use different organic wastes and wastewaters.	Requires sunlight, low H_2 rates and yields, low conversion efficiency, requirement of large reactor volume, O_2 sensitivity.
Electrolysis	40–60	No pollution with renewable sources, proven technology, existing infrastructure, abundant feedstock, O_2 is the only byproduct, contributes to RES integration as an electricity storage option.	Low overall efficiency, high capital costs.
Thermolysis	20–45	Clean and sustainable, abundant feedstock, O_2 is the only byproduct.	Elements toxicity, corrosive problems, high capital costs.
Photo-electrolysis	0.06	Emission-free, abundant feedstock, O_2 is the only byproduct.	Requires sunlight, low conversion efficiency, non-effective photocatalytic material.

Table 2.8 - Comparison of the different hydrogen production processes; Source: [120]

2.5. Hydrogen storage technologies

Hydrogen storage is a key element in hydrogen energy systems, especially when it comes to large scale utilization of hydrogen. To address the current and potential future demands of hydrogen energy market, having a robust and reliable storage solution for each application is vital. The applications of hydrogen storage can be divided in two groups: stationary and mobile applications. Stationary storage methods are mainly for on-site storage at either point of production or use, and for stationary power generation. Mobile applications are either for the purpose of transporting the stored hydrogen to point of storage or use, or use of hydrogen in a vehicle [123]. Hydrogen has a low energy density by volume equal to 9,9 MJ/m^3 (LHV: Lower Heating Value). It could result in extremely large storage vessels [124]. To avoid that, at least one of the three following features are required to store sufficient quantity of hydrogen: high storage pressure, low storage temperature or using a material that attracts large amount of hydrogen molecules. The hydrogen storage technologies can be divided into two main groups: physical-based and material-based, as demonstrated in Figure 2.9. The first group includes storing hydrogen as compressed gas, cold/cryo-compressed, and liquid hydrogen storage. Material-based storage has two main sub-groups of chemical sorption/chemisorption and physical sorption/physisorption [125].
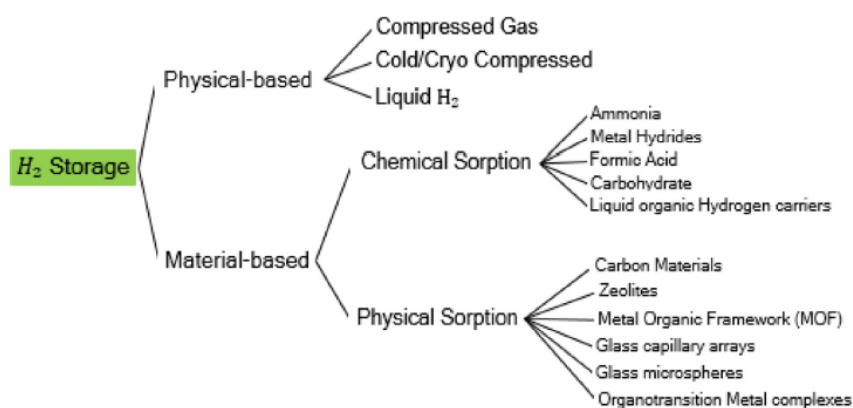
45

Figure 2.9 - Different approaches for hydrogen storage; Source: [124]

In the Table 2.9 the characteristics of the hydrogen storage methods are summarized:

Hydrogen storage technologies	Main group	Features
Compressed gas	Physical-based	- high pressure
Cryo-compressed	Physical-based	- gaseous hydrogen compressed at -233°C - high storage density - quick and efficient refueling - high safety level
Liquid H_2	Physical-based	- very low temperatures (-250°C)
Chemical sorption	Material-based	- more energy is needed to release the chemically bonded hydrogen - stored at high density even at ambient conditions
Physical sorption	Material-based	- high capacity - reliable storage units - low hydrogen binding energy - low cost of the materials - requirement of low temperature and high pressure - low gravimetric and volumetric hydrogen density

Table 2.9 - Characteristics of the various hydrogen storage methods

46

Regarding the storage of compressed hydrogen, there are four types of pressure vessels that can be used for storing hydrogen, namely: fully metallic pressure vessels (Type I), steel pressure vessel with a glass fiber composite overwrap (Type II), full composite wrap with metal liner (Type III) and fully composite (Type IV) [126].

Instead, liquifying hydrogen is done at very low temperatures (- 250°C). Maintaining hydrogen at such a low temperature is probably the main challenge of cryogenic hydrogen storage [126].

Cryo-compressed hydrogen is a super critical cryogenic gas. Liquefaction does not happen, and gaseous hydrogen will be compressed at about -233°C. It has proven promising with respect to storage and safety level. Cryo-compressed storage provides high storage density (80 g/L, which is about 10 g/L more than cryogenic storage), quick and efficient refueling, and high safety level due to the existence of a vacuum enclosure [127].

In physical sorption, porous material-based storage systems are potentially a mean to achieve high capacity and reliable storage units. Among all porous materials, Metal Organic Frameworks (MOFs) and porous carbon materials are known to be most promising [128, 129]. The use of this method will provide high surface area, low hydrogen binding energy, faster kinetics in charge and discharge processes and low cost of the materials. Plus, potentially physical absorption can mitigate thermal management issues during charge and discharge of the storage unit. On the other hand, the issues involved with this method are weight of the carrier materials, requirement of low temperature and high pressure, and still low gravimetric and volumetric hydrogen density [130].

In chemical sorption, hydrogen molecules are split into atoms and integrated with the chemical structure of the material. Among all, metal hydrides are probably the most famous group of materials that can be used for chemical sorption. Detailed information and a comprehensive list of related references about metal hydrides can be found in Reference [131]. Hydrogen is chemically bonded in the metal hydrides. These bonds are much stronger than the physical bonds involved in the adsorption of hydrogen. Consequently, more energy is needed to release the chemically bonded hydrogen.

On the other hand, the stronger bonding allows hydrogen to best stored at high density even at ambient conditions. Hydrogen release from metal hydrides can be achieved in two

main ways: via heating (thermolysis) or reaction with water (hydrolysis). These approaches are radically different. Thermolysis is endothermic, reversible in some cases and occurs in the solid phase requiring elevated temperatures; while hydrolysis is exothermic, irreversible, generally occurs in solution and may be spontaneous at room temperature.

A vast array of metal hydrides have been developed and investigated for thermolysis-based storage, relatively few have been applied for hydrolysis with any significant success.

The most well-investigated metal hydride for the release of hydrogen via hydrolysis is sodium borohydride ($NaBH_4$) [132]. In hydrolysis, $NaBH_4$ is typically dissolved in an alkaline solution, often sodium hydroxide (NaOH), which is then sent to a catalytic bed reactor to induce hydrogen release. Catalysts for the hydrolysis of $NaBH_4$ are most commonly based on cobalt (Co), mainly due to their relatively low cost; catalysts based on Ru are generally more active, but also expensive. The advantages of hydrolysis-based dehydrogenation are compelling: fast kinetics at room temperature, high exothermicity (240 kJ/mol), straight-forward control of hydrogen release, and cold start possibilities. Unfortunately, the widespread use of $NaBH_4$ hydrolysis is being held back by several problems. Most critically, the products of the hydrolysis reaction, hydrated borates, are very stable, rendering regeneration to $NaBH_4$ challenging [133].

2.6. Sodium metaborate tetrahydrate ($NaBO_2 \cdot 4\ H_2O$)

2.6.1. Role of $NaBO_2 . y H_2O$ in H_2 release from $NaBH_4$

Sodium metaborate constitute the by-product of the following hydrolysis reaction of $NaBH_4$:

$$NaBH_4 + (2 + \alpha)H_2O \rightarrow NaBO_2 \cdot \alpha H_2O + 4H_2 + heat$$
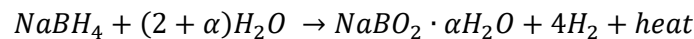
where α is the excess hydration factor and represent the unutilized H_2O in the H_2 release reaction. Therefore, the solid by-product can exist in varying degrees of hydration.

In an ideal way, the quantity of water just required to evolve $H_2(g)$ is only considered, i.e. α = 0. This implies that the hydrogen storage capacity of $NaBH_4 \cdot H_2O$ system would be 10,8 wt% hydrogen. The hydrogen storage capacity is calculated according to [134]:

$$\frac{m(H_2)}{m(reactants)} \times 100$$

In practical systems, the low solubility of metaborate by-products reduces the storage capacities. For example, in the case of $NaBO_2$ by-product, where only 28 g could be dissolved in 100 g H_2O at 25°C, the above reaction would give only 2.9 wt% hydrogen to keep the system in solution. Consequently, as water enters in the reagents, the amount of hydrogen provided by the reaction decreases when α increase. Therefore, minimizing α is the key to improve the hydrogen storage capacity of $NaBH_4$-H_2O system [135].

2.6.2. Borates and sodium metaborate compounds

Boron is usually coordinated to oxygen in three- or four-fold coordination forming trigonal planar $(BO3)^{3-}$ and tetrahedral $(BO4)^{5-}$ primary units, respectively. These fundamental units often polymerize by oxygen-sharing atoms yielding complex varieties of borate anions [136]. Hydration of borates is referred to the presence of crystalline H_2O molecules and/or structural water in the form of hydroxyls –OH groups. The representation $ABO_2 \cdot yH_2O$ (with A being the alkali metal) is commonly used to represent the hydration degree y of the borate including H_2O and –OH groups.

The thermal dehydration of synthetic and mineral borates produces anhydrous borates. It is a complex process, which involves multiple steps including generally the release of crystal water, the removal of –OH groups (dehydroxylation), amorphization and re-crystallization of the anhydrous remains of the precursor solid structure [137].

Sodium metaborates $NaBO_2.yH_2O$ are derivatives of BO_2^-. Five principal different degrees of hydration have been reported until now, with y = 4, 2, 2/3, 1/3 and 0. Crystallographic data and molecular structure of the corresponding borate anions are outlined in Table 2.10.

Tetrahydrate and dihydrate sodium metaborate, $NaBO_2 \cdot 4H_2O$ and $NaBO_2 \cdot 2H_2O$ respectively, contain the tetrahedral tetrahydroxoborate anion $B(OH)_4^-$. The unit cells of the tetrahydrate and the dihydrate are shown in Figure 2.10. The tetrahydrate contains in addition to $B(OH)_4^-$ anions two crystallographically distinct molecules of water.

NaB(OH)₄.2H₂O (y = 4)   NaB(OH)₄ (y = 2)

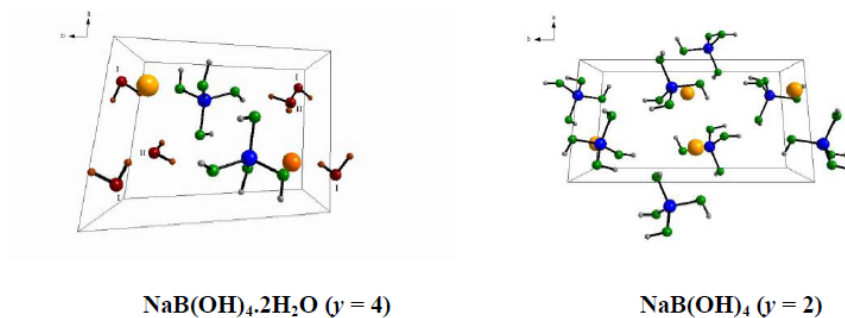*Figure 2.10 - Crystal structures of sodium metaborate tetrahydrate and dihydrate (projection along c-axis). I and II denote the two distinct crystallographic molecules of water of the tetrahydrate (Na: orange, B: blue, O: green, H of B(OH)₄⁻: grey and H₂O molecules; Source: [138]*

The borate anion in the two-third $NaBO_2 \cdot 2/3H_2O$, the one-third $NaBO_2 \cdot 1/3H_2O$ and the anhydrous $NaBO_2$ phases consists of 6-membered ring formed by oxygen corner sharing between three boron entities, called triborate anion. The anhydrous sodium metaborate has the structure formula $Na_3B_3O_6$ and contains $(B_3O_6)^{3-}$ anion built of three $(BO_3)^{3-}$ moieties which consist of a boron atom B three-fold coordinated to three oxygen O atoms [137].
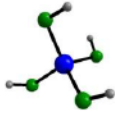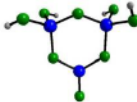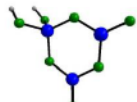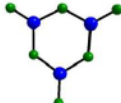
NaBO₂.yH₂O	Crystallographic data	Borate anion
y = 4 NaB(OH)₄.2H₂O	P-1 (triclinic) a= 6.126 Å b= 8.18 Å c= 6.068 Å α= 67.92° Å β= 110.58° γ= 101.85°	 B(OH)₄⁻
y = 2 NaB(OH)₄	P2₁/a (monoclinic) a= 5.886 Å b= 10.566 Å c= 6.146 Å β= 111.60°	
y = 2/3 Na₃[B₃O₄(OH)₄]	C1c1 a= 12.8274 Å b= 7.7276 Å c= 6.969 Å β= 98.161°	 [B₃O₄(OH)₄]⁴⁻
y = 1/3 Na₃[B₃O₃(OH)₂]	Pnma a= 8.923 Å b= 7.152 Å c= 9.548 Å	 [B₃O₅(OH)₂]³⁻
y = 0 Na₃B₃O₆	R-3c a= 11.925 Å c= 6.439 Å	 (B₃O₆)³⁻

Table 2.10 - Crystallographic data of $NaBO_2 \cdot yH_2O$ compounds and molecular structure of the borate anion (B: blue, O: green, H: grey); Source: [138]

50

2.6.3. Chemical and physical properties of $NaBO_2 \cdot 4\ H_2O$

The molar mass of $NaBO_2$ is 137.86 g/mol. This compound is odourless and it appears as a white crystalline solid with a trigonal crystalline structure. It has a melting point of 966 °C and a boiling point of 1434 °C. The solubility of $NaBO_2$ in water is strictly dependent on the temperature and grows linearly as the temperature increases. It is insoluble in ether and ethanol [139]. The infrared spectrum (FT-IR) of $NaBO_2 \cdot 4H_2O$, obtained from the literature [140], is shown in Figure 2.11.
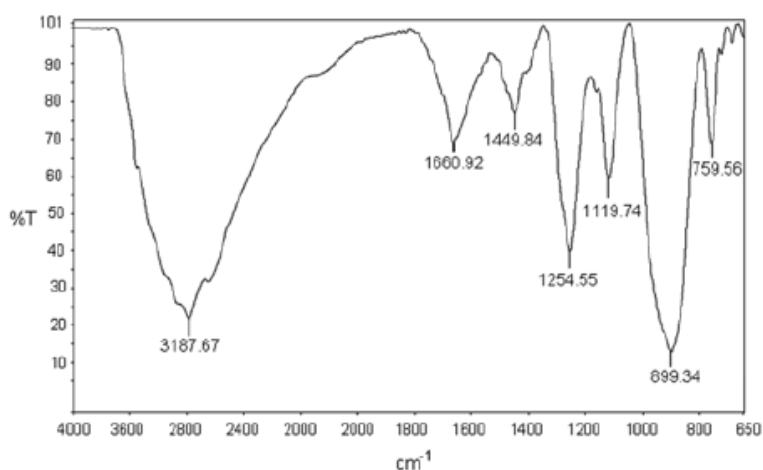
Figure 2.11 - The FT-IR spectrum of $NaBO_2 \cdot 4H_2O$; Source: [140]

The IR spectrum was recorded in the spectral range of 4000 to 650 cm^{-1} at ambient temperature and the resolution used was 8 cm^{-1}. The assignment of the bands to the various functional groups is reported in the Table 2.11:

Band (cm^{-1})	Assignment
3186	Stretching mode of O-H
1661	Bending mode of H-O-H
1450	Asymmetric stretching of B-O
1255	In-plane bending band of (OH)$^{-1}$
1120	Asymmetric stretching of B-O
899	Symmetric stretching of B-O
760	Out-of-plane bending of (OH)$^{-}$ and symmetric stretching band of B-O

Table 2.11 - Assignment of the absorption bands of the $NaBO_2 \cdot 4H_2O$; Source: [141]

The thermal dehydration of $NaBO_2 \cdot yH_2O$ is carried out using thermogravimetric analyses. Kanturk et al. [140] reported five mass loss steps for $NaBO_2 \cdot 4H_2O$. The two first were assigned to the release of crystal molecular water yielding $NaB(OH)_4$ below 100°C and the last three steps to the removal of –OH groups yielding the anhydrous phase near 300°C (see Figure 2.12).
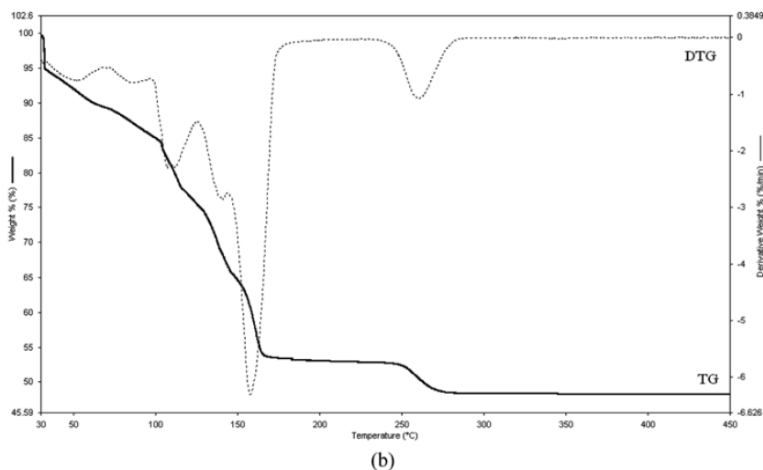

Figure 2.12 - TG/DTG curve of $NaBO_2 \cdot 4H_2O$ obtained at a heating rate of 5 °C/min under non-isothermal conditions in N_2 atmosphere; Source [140]

For a heating rate of 5 °C/min, the first two steps showed total weight loss of 24,37% that was observed in the temperature ranges 30,97÷103,85 °C and 103,85÷127,76 °C. It was attributed to the release of 1,86 moles of crystalline water and can be compared with the theoretical value of 2 for 5 °C/min. In the third step (127,76÷148,76 °C), in fourth step (148,76÷242,10 °C) and in fifth step (250,85÷296,93 °C), weight losses of 0,79 mole, 0,88 mole and 0,30 mole were observed, respectively. This corresponds to the loss of 1,97 moles of structural water and can be compared with theoretical value of 2. Consequently, total weight loss was calculated as approximately 4 moles of water at 25÷310 °C temperature range.

2.6.4. $NaBO_2 \cdot 4 H_2O$ uses and application

The borates of sodium and their derivatives are the main materials for chemical and metallurgy industries and also the medical sector. Especially, sodium metaborate ($NaBO_2$) is commonly used in the commercial production of sodium perborate tetrahydrate (a photochemical used as an ingredient of photographic developers and replenishers), as a stabilizer in textile processing, in adhesives due to the high degree of alkalinity, as a corrosion inhibitor in protecting central heating systems and cooling

towers and in detergents and cleaners [142]. Moreover, as mentioned above, sodium metaborate is used also in the production of $NaBH_4$, which is a hydrogen storage medium [143].

2.6.5. The reasons for the choice of $NaBO_2 \cdot 4\ H_2O$ for H_2 production

The main topics of hydrogen energy and economy concern mainly his production, storage, and transportation. Among them, storage of hydrogen is commonly elaborated in the literature. Main storage types of hydrogen can be listed as pressurized gas, cryogenic liquid, adsorption by porous materials and metal/chemical hydrides. Sodium borohydride ($NaBH_4$) is a chemical hydride that has high hydrogen storage potential. When the theoretical hydrogen content (10,6%) of sodium borohydride ($NaBH_4$) [144] and its more controllable hydrolysis reaction are considered [145], it is accepted as a good storage material. By hydrolysis reaction, mentioned above, $NaBH_4$ can release its theoretical hydrogen content and two moles of hydrogen is gained from water.

In order to support the hydrogen economy, $NaBH_4$ is needed to be regenerate because the current cost of $NaBH_4$ is around 46 €/kg and, considering the production of four moles of hydrogen from the reaction, the cost of hydrogen from $NaBH_4$ is approximately 218 €/kg. This is not a promising source of hydrogen considering its current price [146].

Therefore, in previous thesis works [146, 147], the main aim was to regenerate $NaBH_4$ using the corresponding by-product $NaBO_2 \cdot 4H_2O$ in addition to promising reducing agents.

$NaBO_2 \cdot 4H_2O$ reacts with the reducing agent to form, by reaction in an atmosphere of N_2, trialchylborate ($B(OR)_3$) and hydroxyl anions that can rehydrolyze. The reaction evolves in isothermal mode at 300 ° C with an excess of reducing agent. To force the equilibrium to the right, it is necessary to add water to the reaction mixture. It is advantageous to start with the water of crystallization from the metaborate, which shows an effect of considerable importance for the evolution of the reaction between metaborate and reducing agent. For this reason sodium metaborate tetrahydrate is used instead of sodium metaborate anhydrous [146].

Since a considerable production of H_2 has been seen from GC analysis, it was possible to deduce that the reducing agent exploits the co-catalytic effect of $NaBO_2$ in order to release

hydrogen at a low temperature compared to the many methods developed. This is the starting point, for this thesis, to develop a system for the production of hydrogen based on double cycles of liquid reducing agents and water, added to $NaBO_2$, trying to optimize the operating conditions.

Furthermore, in addition to the hydrogen-rich stream in the outlet stream, there has been evidence of the presence of polymer in the solid residue at the end of each test. This led to investigate the nature of the polymer through analytical techniques which, however, have not yet given any certainty about this nature of the species formed. Given that, again in these previous works, the presence and subsequent disappearance of CO_2 during intermediate sampling was noted [147], the formation of the polymer chain in the final solid residue could be attributed precisely to the capture of CO_2 in it.

In other words, to be more accurate, the fact that CO_2 disappears from the gas phase is certain, as it is not found in the analysis of the gas sampling bags. This CO_2 is captured in-situ in the liquid and / or solid. Evidence from previous works [146, 147] suggests that a high molecular weight organic phase (a polymer) appears in the solid in which carbon (C) but also oxygen (O) may have been captured.

Therefore, in the next paragraphs it was chosen to report a state of the art about the formation of polymers from CO_2 to understand, through literature articles, what are the possible polymeric species that can be formed by consuming CO_2 and also about the formation of polymers from alcohols, therefore also non-oxygenated polymers such as polyethylene and polypropylene etc., since it is actually not known whether C and O of CO_2 are in the solid.

2.7. Polymers from CO_2

Day after day, polymers have become increasingly irreplaceable due to their properties and their versatility. They constitute the basis of modern life and greatly contribute to improving the quality of life itself. They are an integral part of almost all existing objects and technologies: from the materials used to make clothes, houses, cars, airplanes up to the most sophisticated applications in the medical, electronic and diagnostic fields. They are also used as materials for water purification or as polymeric compounds in order to reduce fuel consumption in aerospace applications. According to the latest estimates made by the consulting firm AMI (Applied Market Information), in 2015 the world

consumption of polymers reached the record of 300 million tons (thirty years ago it was just 45 million tons). Currently, most plastics of synthetic origin, such as polypropylene (PP), polyethylene (PE), polystyrene (PS) and polyvinyl chloride (PVC), are 100% petroleum-derived with a carbon footprint of 4,50 – 6,75 tons of CO_2 per ton of plastic [148, 149]. It is therefore imperative to replace conventional plastics with CO_2-based ones as soon as possible in order to limit the consumption of petrochemical resources. In fact, about 6% of the oil produced worldwide is used in the production of polymers, raising strong concerns, in particular of an environmental nature. Therefore, the development of "sustainable" polymers is strongly encouraged in the political sphere and by international agreements, including the negotiations that took place in the 2015 at United Nations Conference on climate change (COP21) in Paris on the reduction of CO_2 emissions [149]. The first big challenge that eco-sustainable polymers have to face is the transforming of renewable resources and production, which must be highly efficient in order to reduce costs. The other big challenge concerns the properties of eco-sustainable polymers, properties that must be complementary or better than the traditional polymers available. Although the commercial application of bio-derived polymers offers great advantages and potential, their large-scale diffusion still requires improvements, especially in terms of performance. Currently, in fact, only some sustainable polymers possess properties equivalent to those of conventional polymers. In the next paragraphs a state of the art on polymers produced using CO_2 will be presented.

2.7.1. The use of CO_2 for the polymers production

Carbon dioxide (CO_2) is produced by several anthropogenic activities and it is considered as the major contributor to global warming because of its greenhouse properties. Current emission rate of CO_2 is about 35 billion tonnes per year, which main sources are combustion of fossil fuel, utilization of biomass for energy and decomposition of carbonates [149]. While carbon dioxide is indispensable for the existence of all living organisms via photosynthesis of green plants, the utilization of carbon dioxide as a feedstock for industrial products is rather limited. More recently, the capture and utilization of CO_2 has attracted the attention of the scientific community. The possibility of being able to use it as a carbon building block to produce basic chemicals, plastics, inert solvents, fuels and other high value products is desirable not only to limit its emission into the atmosphere but also to partially replace fossil derived resources to

produce chemicals and materials [150]. Possible applications of CO_2 for value-added applications are shown in Figure 2.13:
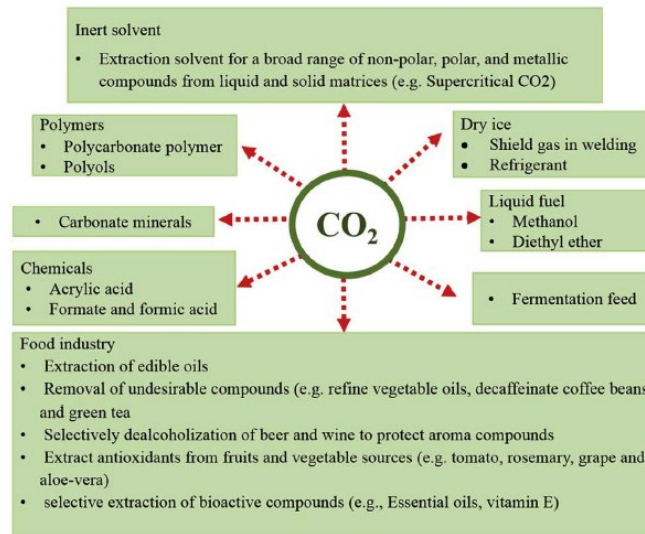

Figure 2.13 - CO₂ as a renewable feedstock in common applications; Source: [150]

CO_2 is an attractive feedstock because it is abundant, inexpensive, safe, non-flammable, non-oxidant, FDA approved for food use, with a balanced geographic distribution and renewable. However, being a very stable molecule from the thermodynamic point of view, it requires a considerable amount of energy; consequently, it is necessary to use a catalyst to reduce the energy barrier [150]. The report, published by Nova Institute in 2021 (Figure 2.14), is optimistic about the growth in the production of carbon dioxide capture based polymers and assumes that on 1,200 Mt (million tonnes) of plastic materials over 315 Mt will be CO_2-based and another 135 Mt bio-based [151].
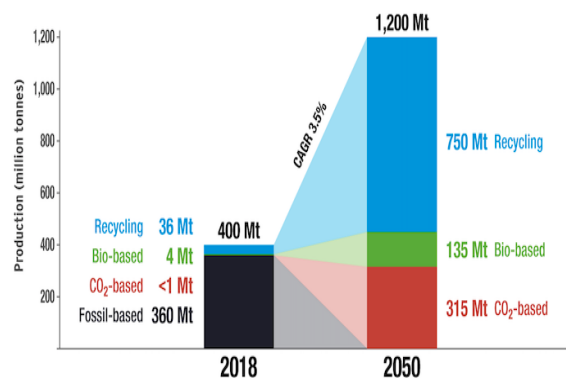
Figure 2.14 - World Plastic Production and Carbon Feedstock in 2018 and Scenario for 2050 (in Million Tonnes): Source: [152]

Renewable Carbon, in a post of January 2021 [153], provides a picture of the state of applied research (Figure 2.15) explained below.

56

CO_2-based polycarbonates are already commercially available from various suppliers. One of the largest volumes available are aromatic polycarbonates but several players worldwide are also offering aliphatic polycarbonates such as polypropylene carbonate (PPC) or polyethylene carbonate (PEC) for a large range of applications. The amount of CO_2 incorporated can reach up to 50 % by weight for these types of aliphatic polymer.

Different pathways for the chemical conversion of CO_2 into various polymers, such as polyureas, are being studied, even if still at an academic level. In some of these, CO_2 is used as a co-monomer and participates directly in the polymerization process; while, in others, it is used for the synthesis of building blocks that can be subsequently involved in a polymerization process. In addition to the chemical conversion of CO_2, the electrochemical conversion has also progressed. In recent years, in fact, many improvements have been made to electrocatalysts for the conversion of CO_2 into chemicals and chemical building blocks.

The electrosynthesis of chemicals such as ethylene or monoethylene glycol has been of particular interest due to its potential for the production of polyethylene or polyethylene terephthalate, two main conventional plastics used in high volumes. Chemicals such as methanol, formic acid and other chemical components also have great potential to be produced via this technology. Thanks to the use of various microorganisms or cyanobacteria and improvements in microbial engineering, biotechnological conversion of CO_2 to polymers has seen tremendous growth in recent years.

Lastly, companies working on the Fischer Tropsch conversion of syngas to hydrocarbons are already operating with pilot plants for the production of diesel, kerosene, wax and naphtha. CO_2-based Naphtha can be used in the already established cracking process to produce olefins, which are needed for most plastics currently in use.
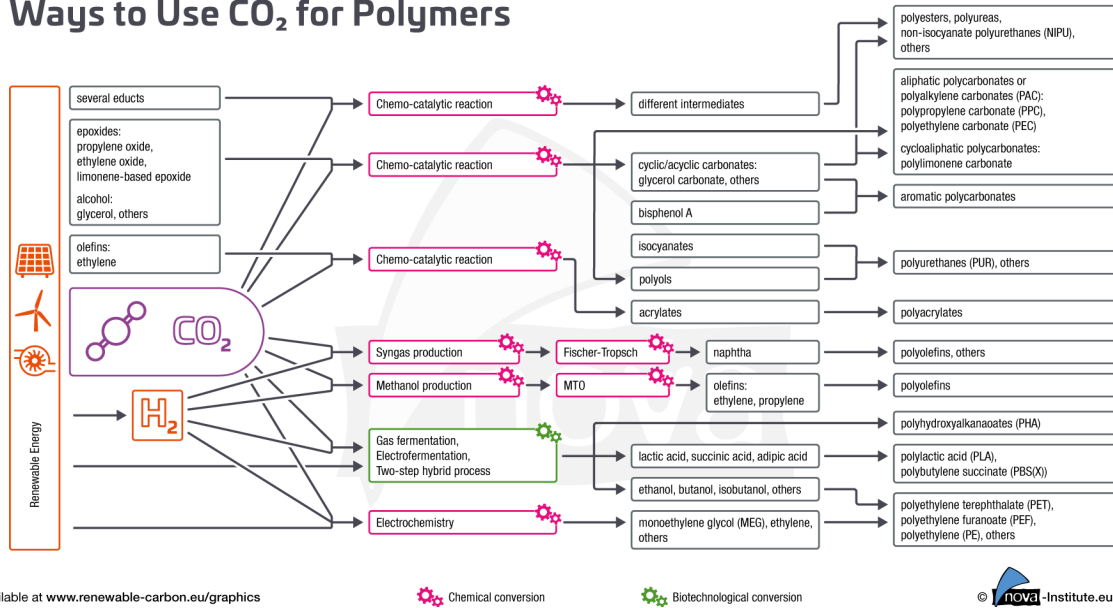
Ways to Use CO₂ for Polymers

Figure 2.15 - Ways to use CO_2 for polymers; Source: [152]

Some typical examples of synthetic fuels ("e-fuels"), chemical feedstocks and polymers, that are produced from CO_2, are shown in Figure 2.16:
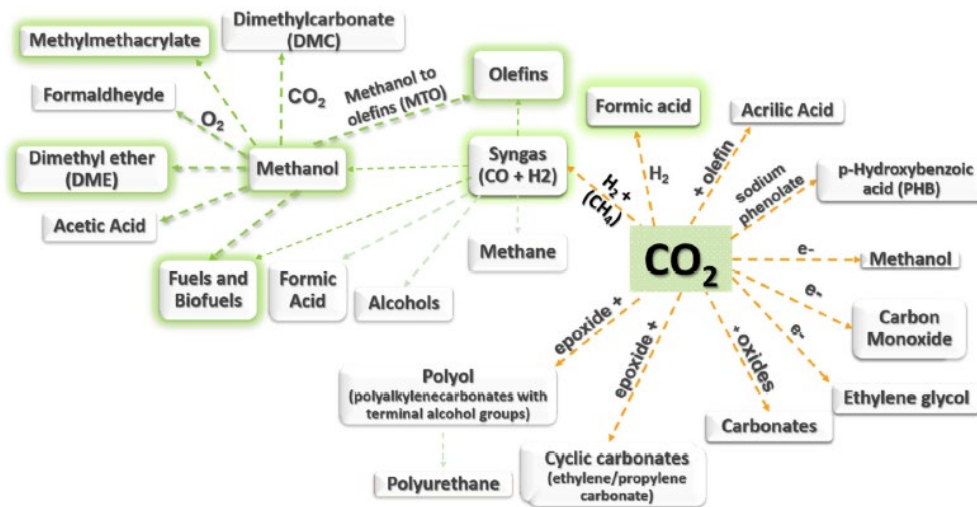

Figure 2.16 - Products that can be currently manufactured using CO_2 as a building block; Source: [154]

2.7.2. Polycarbonates from CO_2

Polycarbonates (PCs) are polymers with –(OCO_2R)– repeat units within their main backbone. Aromatic PCs have high impact resistance, stiffness, toughness, good thermal stability and transparency and are used as engineering plastic in automotive, electrical and electronic devices and in construction; while aliphatic PCs exhibit poor mechanical

58

properties which restricts their use in packaging, as a binder in ceramics or as polyols for the formulation of polyurethane foams. Industrially, these materials are largely produced from bisphenol A (BPA; cf., aromatic PCs) or diols (cf., aliphatic PCs) and phosgene or diphenyl carbonate (DPC; Asahi process) by melt polycondensation (Scheme 2.1) [155]:
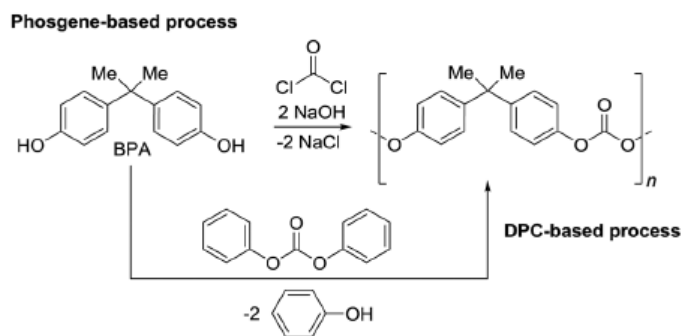

Scheme 2.1 - Synthesis of aromatic PCs by a phosgene- or a DPC-based process; Source: [155]

Scheme 2.2 illustrates the most relevant alternative pathways to the industrial route that valorises CO_2-sourced building blocks or CO_2 as monomers for PC synthesis. These strategies include the ring-opening polymerisation (ROP) of cyclic carbonates, the ring-opening copolymerisation (ROCOP) of CO_2 with oxiranes and various step-growth approaches (i.e. the polycondensation through transesterification of acyclic carbonates) with diols, the direct copolymerisation of CO_2 with diols or mixtures of diols and dihalides and the polyaddition of activated bis-a-alkylidene five-membered cyclic carbonates and diols [155].
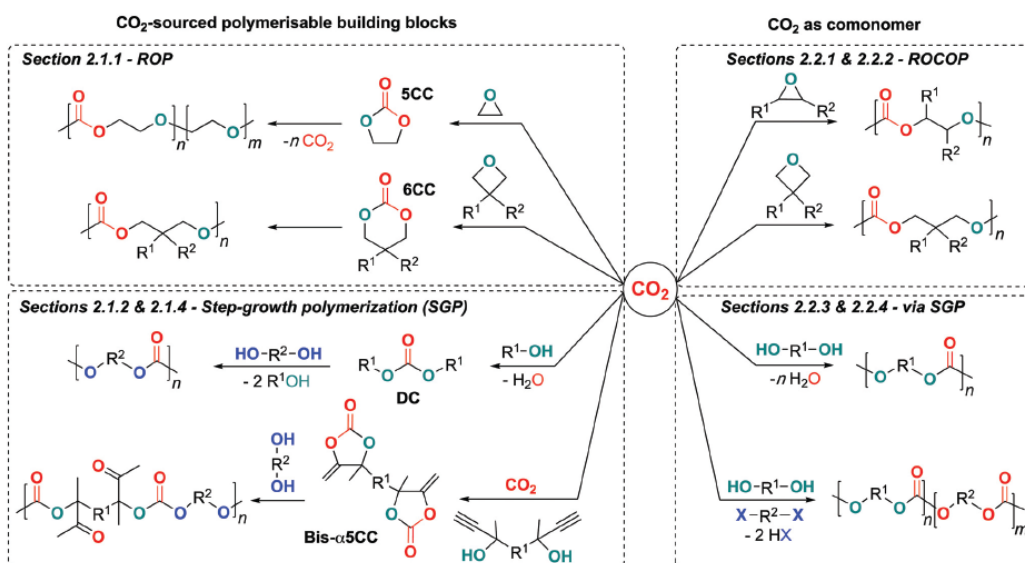
Scheme 2.2 - Pathways for the synthesis of PCs from CO_2-sourced building blocks or from CO_2 directly; Source: [155]

Referring to the ROCOP strategy reported in Scheme 2.2, a promising CO_2 utilization in the copolymerization of CO_2 and epoxide to afford polycarbonates pioneered by Inoue in 1969 [156]. Depending on the type of catalyst and the reaction conditions, the reaction can be steered to produce alternating polycarbonate (Scheme 2.3-A, top) or polyethercarbonate containing carbonate as well as ether linkages (Scheme 2.3-B, bottom, m > 1). Aliphatic polycarbonates have potential applications as packaging materials, whereas polyethercarbonates are promising raw materials for new structure polyurethanes [157].
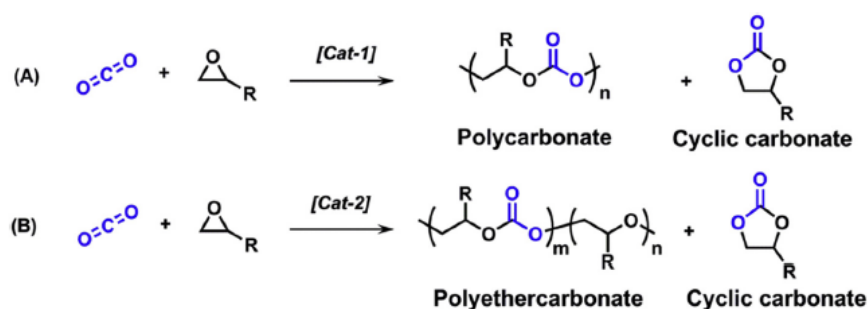
Scheme 2.3 - Copolymerization of CO_2 and epoxides to alternating polycarbonates (A) and polyethercarbonates (B); Source:[157]

The use of complexes of Co (III) and Cr (III) or selected Lewis acidic compounds as catalysts (Cat-1) leads to alternating polycarbonates ($\geq$ 99% carbonate linkages). Catalyst mixtures and chain transfer agents have been used to optimize the product properties. Alternating polycarbonates with high molecular weight are materials with interesting properties such as biodegradability. Nevertheless, their broad implementation as mass products is currently restricted by technical limitations such as the low glass transition temperature (T_g). Instead, polyethercarbonates are obtained when double metal cyanides (DMC), dinuclear Zn-complexes or Cr-bishydroxychinoline complexes are employed as a catalyst (Cat-2) [158]. As already mentioned above, polycarbonates are produced by a phosgenation process which used toxic phosgene ($COCl_2$)[1] and bisphenol A as starting materials (Figure 2.17, Column 2) [159].

---

[1] **Phosgene ($COCl_2$)**: a colourless gas. Phosgene is formed from carbon monoxide (CO) produced by incomplete combustion of coal, and chlorine (Cl_2) produced by electrolysis of salt (sodium chloride, NaCl). It has asphyxiating properties and is extremely toxic, and was used as poison gas during World War I. Furthermore, it is highly reactive and is used as a synthetic starting material for polyurethane and dye.
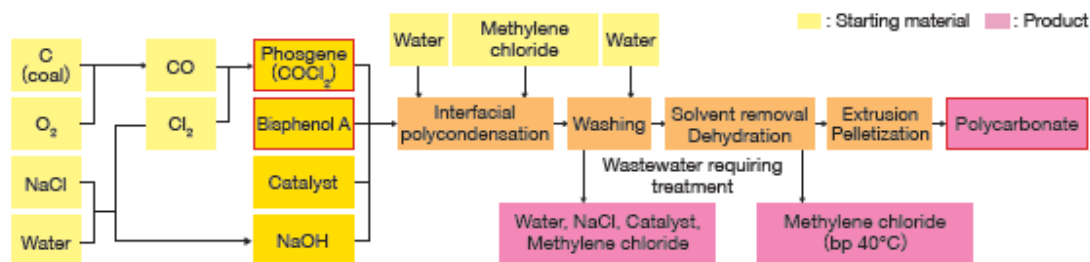
Figure 2.17 - Polycarbonate production process by phosgenation process; Source: [159]

The expected increase in the demand for polycarbonates prompted many companies to start to develop a polycarbonate production process without using toxic phosgene. For the first time in the world, a polycarbonate production process in which carbon dioxide and ethylene oxide replaced phosgene and were reacted with bisphenol A was developed by ASAHI KASEI (Figure 2.18).

In this process, ethylene carbonate is formed from carbon dioxide and ethylene oxide, which is then converted to diphenyl carbonate and polymerized with bisphenol A to produce polycarbonate. The by-product ethylene glycol is used as a starting material for plastic and synthetic fibres. This process does not use toxic phosgene and the carbon dioxide that is discharged from the production of ethylene oxide is used as a starting material.
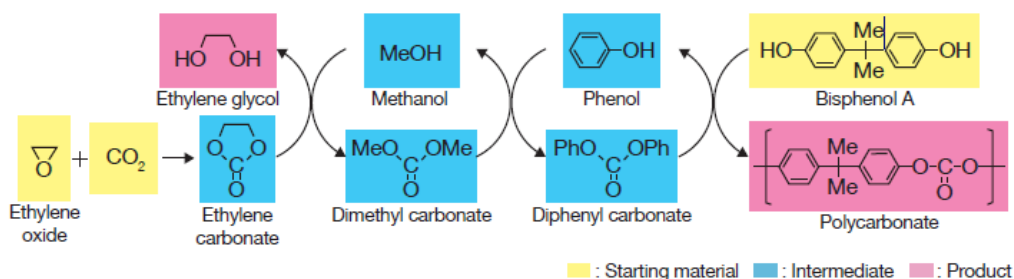
Figure 2.18 - Non-phosgene polycarbonate production process by ASAHI KASEI; Source: [159]

2.7.3. Polyurethanes from CO_2

Discovered by Otto Bayer in 1937, polyurethanes (PUs) have become one of the most important polymers finding everyday life applications such as in coatings, adhesives, sealants, elastomers and foams, heart valves, and cardiovascular catheters, among others [160, 161].

Polyurethane (PU) indicates a large family of polymers in which the polymer chain is made up of urethane bonds, whose chemical formula is NH-(CO)-O-.

Industrially, PUs are produced by polyaddition between diisocyanates and di- or polyols (Scheme 2.4).

Isocyanate-based process

$$O=C=N-R^1-N=C=O \ + \ HO-R^2-OH \longrightarrow$$
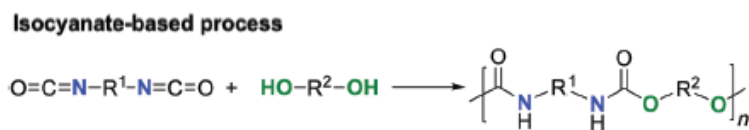
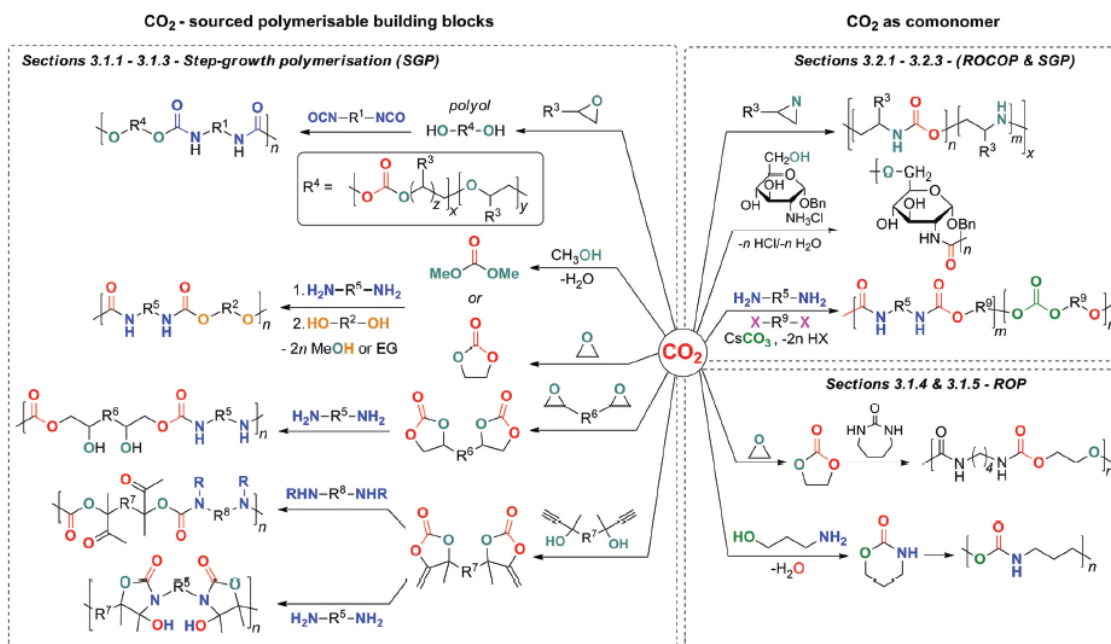*Scheme 2.4 - Industrial synthesis of polyurethanes from isocyanates; Source: [155]*

With the decreasing price of isocyanate in recent years, the originally cheap polyols become the key barrier to cut PU cost. One promising route is the introduction of extremely low-cost feedstock, such as CO_2, into the backbone of polyether polyols, yielding polyethercarbonates polyols, or so-called CO_2-polyols. Life cycle assessment indicates that oligoethercarbonates with 20 wt % CO_2 reduces greenhouse gas emissions by 11-19% and saves fossil resource by 13-16% [162].

As shown in Scheme 2.5, CO_2-polyols are generally obtained from copolymerization of CO_2/PO under Zn-Co-DMC catalyst in the presence of proton-containing starter. Zn-Co-DMC, a heterogeneous catalyst with good prospect for industrialization, is quite active for the random copolymerization of CO_2/PO [163]. In addition to catalyst, starter is another important variable to determine the feature of CO_2-polyols. If oligomeric alcohol starters are used, longer copolymerization time will be necessary [164].
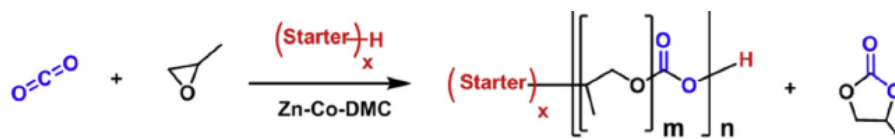
Scheme 2.5 - Schematic synthesis of CO_2-polyols from copolymerization of CO_2 and PO; Source: [157]

Recent focus in the field of PUs has been on establishing isocyanate-free routes for their production; carbon dioxide can play a crucial role in this important transition (see Scheme 2.6).

Scheme 2.6 - Synthetic pathways for the synthesis of polyurethanes from CO_2 and/or from CO_2-sourced building blocks; Source: [155]
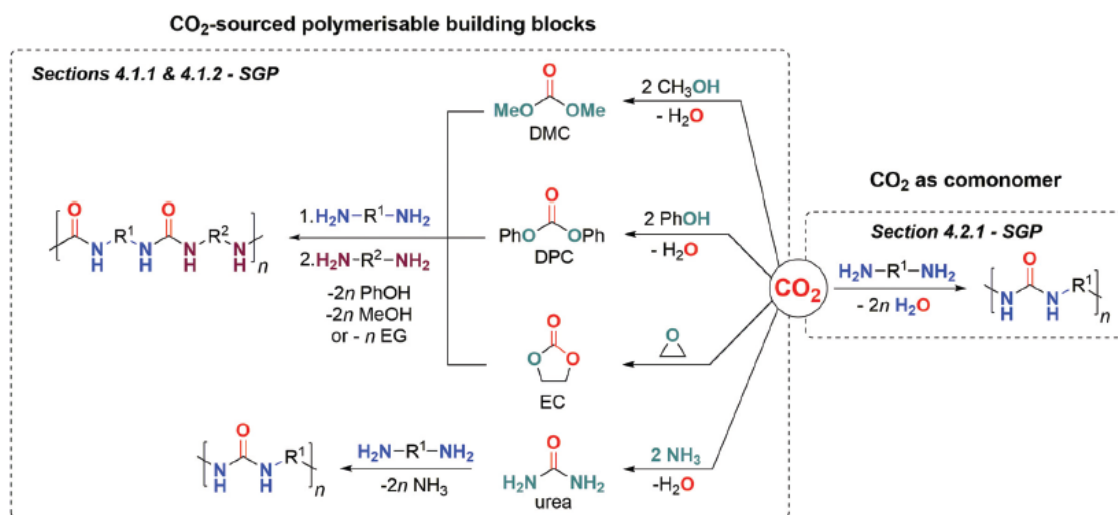
2.7.4. Polyureas from CO_2

Polyureas (PUA)s are polymers containing urea linkages (i.e., having –NH–C(O)–NH– groups) within the polymer backbone. They find applications as linings, joint sealants and microcapsules, among others, in numerous sectors such as in the automotive industry, construction, household products.

Industrially, PUAs are prepared by polyaddition using diisocyanate and diamine reagents (Scheme 2.7).
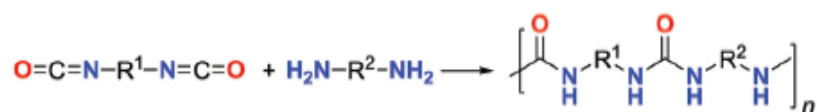
*Scheme 2.7 - Industrial synthesis of PUAs by polyaddition of isocyanates and diamines; Source: [155]*

As for the conventional synthesis of PUs, non-isocyanate routes have been engineered to synthesize these polymers from CO_2-sourced cyclic carbonates or urea or via direct copolymerisation of CO_2 with diamines (Scheme 2.8).

63

Scheme 2.8 - Synthetic pathways towards CO_2-sourced polyureas; Source: [155]

2.7.5. Polyesters from CO_2

Poly(ester)s are polymers containing –C(=O)–O– linkages within the polymer backbone. They are widely used in packaging, fabrics and in surgery/therapeutic applications due to their excellent (bio)degradability and biocompatibility features. Their industrial production is based on the ROP of lactones/lactides, the dehydrative polycondensation of dicarboxylic acids with diols or the self-polycondensation of a-hydroxyacids. The synthesis of this important class of polymers from CO_2 remained long elusive but new conceptual routes for their production are now emerging as illustrated in Scheme 2.9.
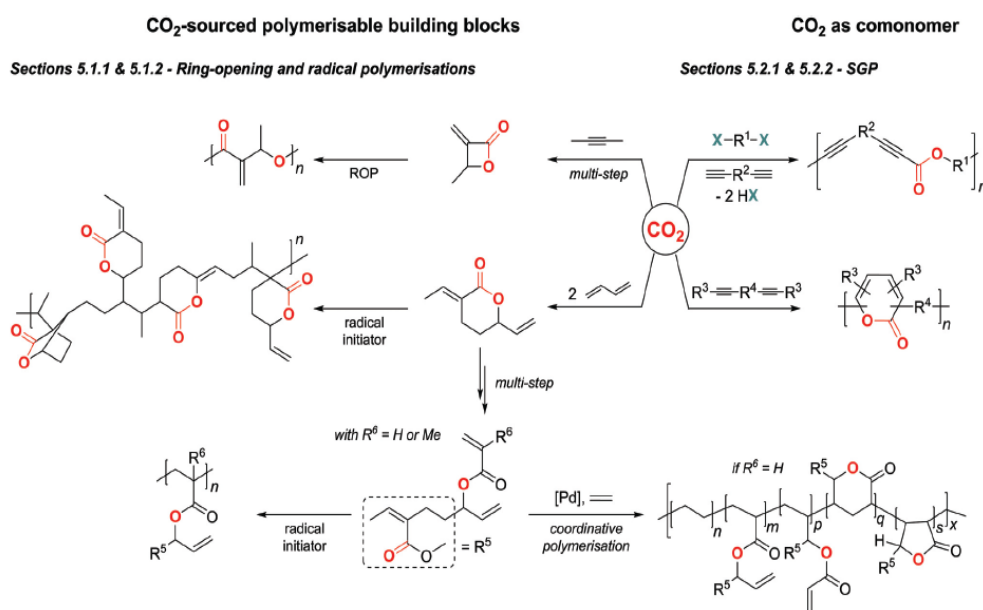

Scheme 2.9 - Synthetic pathways towards CO_2-sourced polyesters; Source: [155]

2.8. (Poly) ethylene glycol (PEG)

Since, from our experiments, it has been seen that the possible polymer that is created at the end of the process could be polyethylene glycol, it seems necessary to rationalize, in the state of the art, what this polymer is and how it could be formed using CO_2.

2.8.1. Chemical and physical properties of PEG

Polyethylene glycol is one of the most important polyether. Also known as PEG, is a linear or branched, neutral polyether soluble in water and most organic solvent. The chemical formula of this molecule is:

$$HO - (CH_2 - CH_2O)_n - CH_2CH_2OH$$
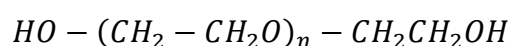
where n is the number of ethylene oxide groups.

It is a polymer prepared by polymerization of ethylene oxide. PEGs are also sometimes referred to as poly (ethylene oxide) (PEO) or poly (oxy-ethylene) (POE) depending on the molecular weight.

Historically these acronyms are used to refer to polymeric mixtures of polyethylene glycol having different average molecular weights [165]:

- POE: average molecular weight less than 20,000 g / mol;

- PEG: average molecular weight of 20,000 g / mol;

- PEO: average molecular weight greater than 20,000 g / mol.

Their chemical properties are the same due to the presence of same functional groups, but physical properties like viscosity, colour, etc. are different because of different chain length of ethylene glycol. This difference also affects their utility in different areas of industries [166].

Ethylene glycol is the simplest diol and possesses numerous unique properties owing to its characteristic structure (i.e., two hydroxyl (OH) groups at adjacent positions along a hydrocarbon chain). It is an odourless, colourless, relatively non-volatile and hygroscopic liquid with low viscosity. It is completely miscible with many polar solvents such as water, alcohols, glycol ethers and acetone and only slightly soluble in non-polar solvents such as benzene, toluene, dichloroethane, and chloroform. It is difficult to crystallize [167, 168].

65

PEG is a polyether composed of repeated ethylene glycol units [$(CH_2CH_2O)_n$]. It is formed by the inter linkage of ethylene oxide with H_2O, ethylene glycol and its oligomers. PEGs that have a molecular weight between 100 to 700 are liquids at room temperature; those between 1000 and 2000 are soft solids and PEGs with molecular weight greater than 2000 are hard crystalline solids with melting points of around 63 °C [169].

The physical properties of polyethylene glycol (such as viscosity for example) vary according to the average length of the macromolecules, that is to the average number n of repetitive units; while the chemical properties remain almost unchanged. At molecular weight less than 1000 (low n values), PEGs are viscous, colourless liquids; while higher molecular weight PEGs are waxy, white solids (with a relatively low melting point) [170, 171].

The melting point of the solid is proportional to molecular weight and it approaches a plateau at about 67 °C. PEGs possess a variety of properties pertinent to biomedical and biotechnical applications such as [172]:

- Soluble in water, toluene, and many organic solvents such as methanol);
- Insoluble in ethyl ether and hexane;
- Insoluble in water at high temperature;
- Forms complexes with metal cations;
- Highly mobile: large exclusion volume in water;
- Forms two-phase systems with aqueous solutions of other polymers;
- Non-toxic;
- Hospitable to biological materials;
- Causes cell fusion in high concentration;
- Weakly immunogenic.

2.8.2. Production of PEG

The path that leads to the formation of PEG starting from ethanol and using CO_2 is shown in the Figure 2.19:

$$I\ step:\ C_2H_5OH \rightarrow C_2H_4 + H_2O$$

$$II\ step:\ C_2H_4 + CO_2 \rightarrow C_2H_4O + CO$$

$$III\ step:\ C_2H_4O + H_2O \rightarrow HOCH_2-CH_2\ OH$$

$$IV\ step:\ n\ C_2H_4O + HOCH_2-CH_2\ OH \rightarrow HO-(CH_2-CH_2-O)_n\ CH_2-CH_2-OH$$
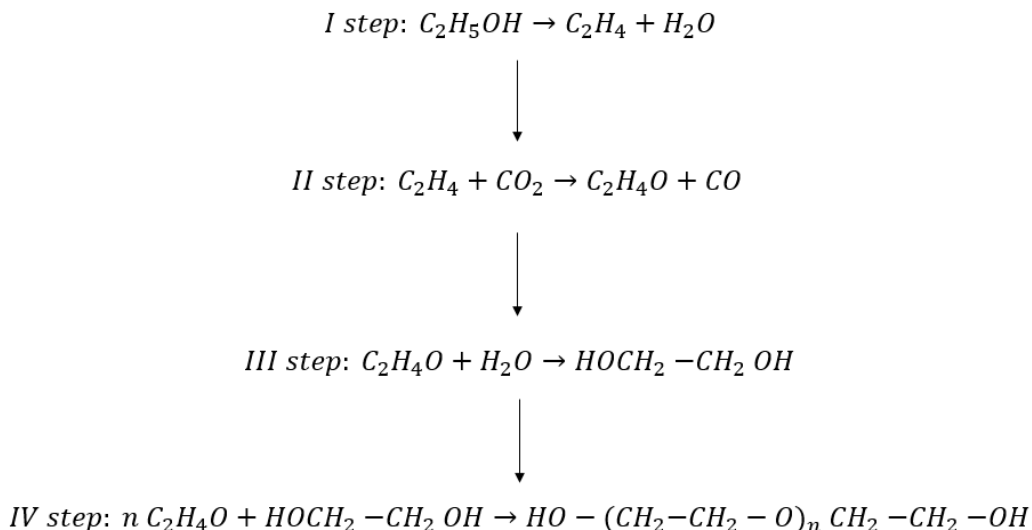
Figure 2.19 - Pathway for PEG formation starting from ethanol and using CO_2

In the I step there is the dehydration of ethanol to ethylene. The bio-ethanol is the main product obtained from biomass fermentation process, i.e., agricultural products rich in sugar (carbohydrates) such as cereals, sugar crops and starch. The ethanol to ethylene reaction occurs through ethanol dehydration under the condition of appropriate temperature and the effect of the catalyst. In the catalytic dehydration of ethanol to form ethylene, an acid catalyst first protonates the hydroxyl group, which leaves as a water molecule. The conjugate base of the catalyst then deprotonates the methyl group, and the hydrocarbon rearranges into ethylene. This mechanism is depicted in Figure 2.20. [173].
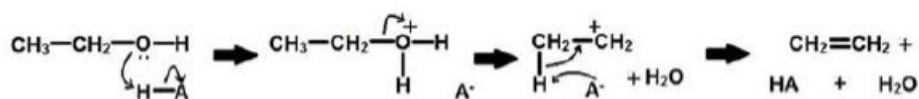

Figure 2.20 - Mechanism for the dehydration of ethanol to ethylene; Source:[173]

The reaction of ethanol dehydration to ethylene is an endothermic reaction and it requires relatively more heat, with higher reaction temperature, ranging from 180 °C to 500 °C; meanwhile, reaction temperature plays a key role in the selectivity of the target product, ethylene. The main by-product generated is ether when the temperature is below 573 K, while the main product, ethylene, is only generated when the temperature is over 573 K. In addition to the main product and the main by-product, the reaction of ethanol dehydration may also generate a small amount of other by-products, such as acetaldehyde, hydrocarbons (methane, ethane, propylene, butylene) and light base-groups (CO_2, CO, H_2, etc.) and so on. As the amount of other by-products is small, most research on the

ethanol dehydration reaction mechanisms considers mainly the generation of ethylene and ether, which can be summarized as three kinds of routes: (1) parallel reactions, (2) a series of reactions, and (3) a parallel series reaction [174]. The main controversy lies in whether ethylene is directly generated from ethanol or indirectly generated from ether, or both routes coexist, as shown in the Figure 2.21:
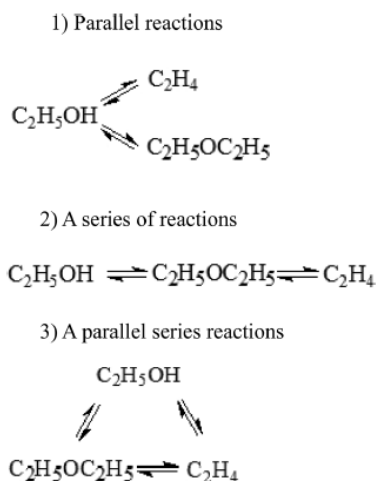

Figure 2.21 - Three kinds of routes for ethanol dehydration; Source: [174]

In Figure 2.22, the endothermic dehydration process to convert bio-ethanol to ethylene involves heterogeneous catalysts, such as zeolites (HZSM-5) or mesoporous silica (Ni-MCM-41). Depending on the reaction temperature for a particular catalyst, diethyl ether may be an intermediate in the formation of ethylene. The formation of diethyl ether is exothermic and would be favoured at lower temperatures [175].
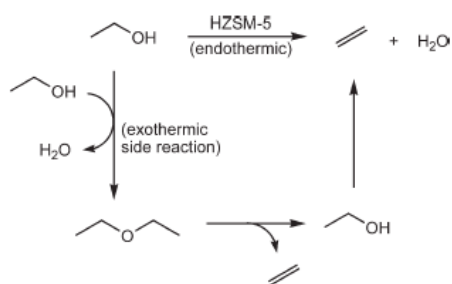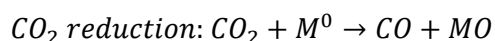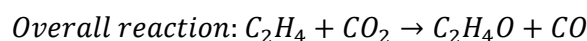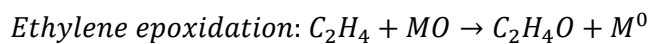

Figure 2.22 - Synthesis of ethylene via the dehydration of bio-ethanol obtained from fermenting biomass; Source: [175]

In II step ethylene oxide (EtO) production by reaction between CO_2 and ethylene occurs, following the general scheme of reactions present in the equations below:

$$CO_2\ reduction\colon CO_2 + M^0 \rightarrow CO + MO$$

$$Ethylene\ epoxidation: C_2H_4 + MO \rightarrow C_2H_4O + M^0$$

$$Overall\ reaction: C_2H_4 + CO_2 \rightarrow C_2H_4O + CO$$

$$M^0 = Reduced\ metal; MO = Metal\ oxide$$

This general reaction scheme uses the mixed-metal oxide as an oxygen carrier [176].

In fact, the chemical methodology by which EtO is currently produced is the partial oxidation of ethylene with oxygen (O_2) using a catalyst but several mixed-metal oxides have been developed. This can be used for ethylene epoxidation using CO_2 instead of O_2. The mixed-metal oxides react with CO_2 and remove an oxygen atom to produce EtO and carbon monoxide (CO).

In the III step, there is the ethylene glycol production starting from ethylene oxide through direct, noncatalytic, liquid-phase hydration (Figure 2.23).
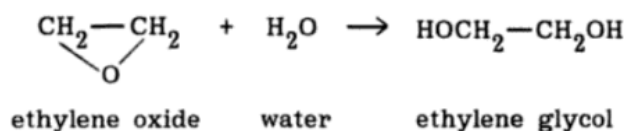

Figure 2.23 – Ethylene oxide hydration for ethylene glycol production

Through hydrolysis of ethylene oxide (EtO), mono-ethylene glycol (MEG) can be formed simultaneously also to di-ethylene glycol (DEG) and tri-ethylene glycol (TEG). The selectivity of MEG is determined only by the ratio of ethylene oxide to water. Although the use of excess water increases the MEG produced, it lowers its concentration [176, 177].

Finally, in the IV step, polyethylene glycol is produced by the interaction of ethylene oxide with water, ethylene glycol, or ethylene glycol oligomers (Figure 2.24).
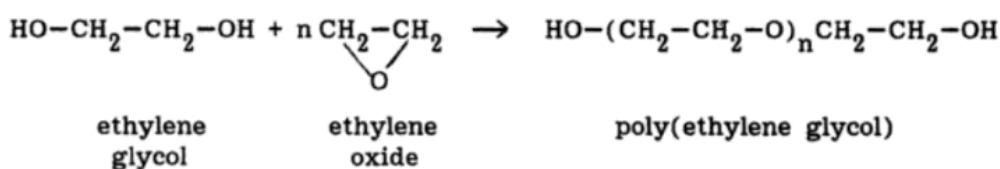

Figure 2.24 - Polymerization reaction of ethylene glycol

This reaction is catalysed by acidic or basic catalysts. Ethylene glycol and its oligomers are preferable as a starting material instead of water because they allow the creation of

polymers with a low polydispersity (narrow molecular weight distribution). The length of the polymer chain depends on the ratio of the reactants [178].

Depending on the type of catalyst, the polymerization mechanism can be cationic or anionic. The anionic mechanism is preferable because it allows to obtain PEG with a low poly-dispersion. Polymerization of ethylene oxide is an exothermic process. Overheating or contamination of ethylene oxide with catalysts such as alkali or metal oxides can lead to uncontrolled polymerization, which can result in an explosion after a few hours.

High molecular weight polyethylene glycol is synthesized by suspension polymerization. The reaction is catalysed by organic compounds of magnesium, aluminium or calcium; instead, alkaline catalysts such as sodium hydroxide (NaOH), potassium hydroxide (KOH) or sodium carbonate (Na_2CO_3) are used to prepare low molecular weight polyethylene glycol [178].

2.8.3. Uses and applications of PEG

Thanks to its properties, such as non-toxicity, non-immunogenicity and high water solubility, PEG has been approved by the Food and Drug Administration (FDA), for various biomedical uses [179].

It has many applications, mainly in the biotechnical and biomedical fields because PEG is unusually effective at excluding other polymers from its presence when it is in an aqueous environment. This property results into protein rejection, formation of two-phase systems with other polymers, non-immunogenicity and non-antigenicity. Moreover, this polymer is also non-toxic and does not harm active proteins or cells although it interacts with cell membranes. When it is attached to other molecules, it has little effect on their chemistry but controls their solubility and increase their size [172].

PEG in medicine is called macrogol. It is used in the treatment of adult and child constipation and in bowel preparations prior to a diagnostic colonoscopy [180].

The non-toxicity of PEG allows its use in the pharmaceutical field and in particular for parenteral, topical, ophthalmic, oral and rectal pharmaceutical formulations which are briefly described below [165]:

- ointments: they are used as hydrophilic bases for ointments due to their stability, hydrophilicity and lack of irritating effects on the skin;

- emulsions: aqueous solutions of PEGs are used as suspending agents or as viscosifiers in the preparation of emulsions;

- parenteral formulations: they are used in concentrations up to 30% v/v (liquid PEGs are used, therefore PEG300/400) for the preparation of vehicles for parenteral formulations;

- thermoplastic granulations: when used for this type of formulation, the mixture to be granulated is pulverized and mixed hot (75 °C) with PEG 6000 at 15% v / v. After mixing, the mass becomes similar to a paste and after stirring and cooling at the same time, granulation is obtained;

- pills: they are used for this purpose due to their plasticising properties. In fact, combined with the polymers used for the production of film for pills, they can increase the plastic properties of the film coating of the pill. However, the presence of liquid PEGs in the film reduces the gastro-resistant properties of the film itself.

In cosmetics, it is used in many formulations as a humectant. In fact, they maintain the right degree of humidity in the product, preventing the surface from drying out or can also boast a slight antimicrobial activity, thus helping the preservation of the product itself.

In addition, polyethylene glycol is used to obtain non-ionic surfactants to produce, together with other substances, the foaming effect in a cleaning product [181].

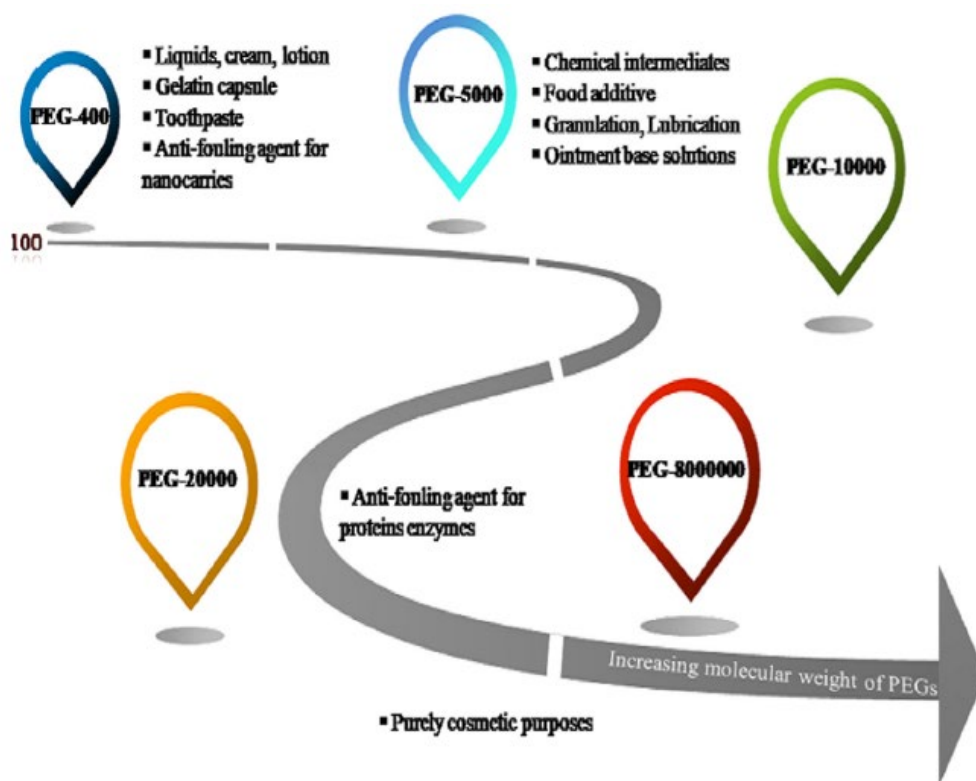The miscellaneous applications of PEG have been illustrated in Figure 2.25.

Figure 2.25 - Miscellaneous applications of PEG; Source: [166]

2.9. Polymers from alcohols

In this paragraph the synthesis processes of polymers starting from some alcohols such as ethanol, propanol, glycerol etc. will be described.

2.9.1. Polyethylene from ethanol

Ethylene can be produced in plants and microorganisms or via synthetic methods such as pyrolysis of naphtha or ethane and catalytic dehydration of ethanol [182]. A scheme is reported in Figure 2.26:
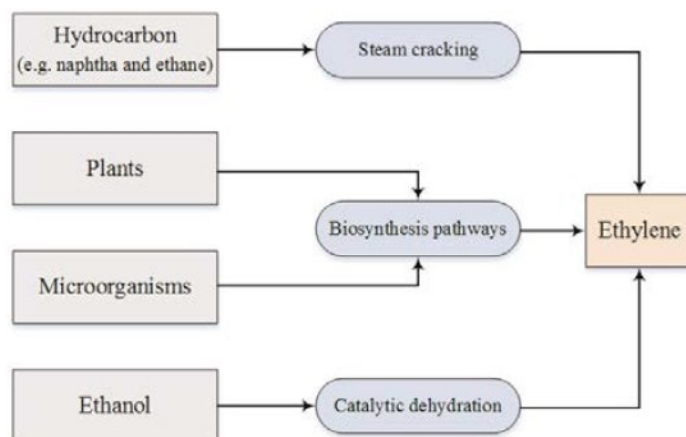
Figure 2.26 – Schematic diagram of different methods for producing ethylene; Source: [182]

In this paragraph, we will focus only on the production of ethylene from ethanol through catalytic dehydration of ethanol.

The ethanol dehydration is an endothermic reaction (requiring 1632 J g^{-1} of ethylene formed). Therefore, the reaction temperature affects the yield of ethylene. The highest selectivity towards ethylene is obtained at 300÷500°C (Eq. (1)). Higher temperatures shift the reaction towards acetaldehyde production (Eq. (2)), while lower temperatures result in production of diethyl ether (Eq. (3)). Isothermal and adiabatic modes of operations have been suggested for the dehydration of ethanol to ethylene, while the latter is more economically feasible [174, 183]. In Figure 2.27 the three reactions mentioned above are shown:
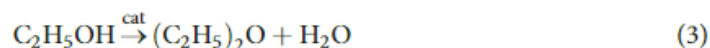
$$C_2H_5OH \xrightarrow{\text{cat}} C_2H_4 + H_2O \qquad\qquad (1)$$

$$C_2H_5OH \xrightarrow{\text{cat}} C_2H_4O + H_2 \qquad\qquad (2)$$

$$C_2H_5OH \xrightarrow{\text{cat}} (C_2H_5)_2O + H_2O \qquad\qquad (3)$$

Figure 2.27 – Ethanol dehydration (1), Acetaldehyde production (2), Diethyl ether production (3);
Source: [182]

The dehydration reaction occurs in the vapour phase inside fixed or fluidized-bed reactors with catalyst. The process in the fixed-bed reactor can be either isothermal or adiabatic, while it is usually adiabatic in the fluidized bed reactor.

The dehydration of ethanol is an acid-catalyzed reaction. There are four main categories that can be used as catalyst in such a process including phosphoric acid, oxides, molecular sieves, and heteropoly acid catalysts [174].

Ethylene ($CH_2=CH_2$) is the first member of the alkenes. It is a colourless gas with a normal boiling point of –103.7°C and is slightly soluble in water and alcohol. This compound is highly active and reacts easily when added to many chemical reagents. It is also the raw material for the production of different grades of polyethylene and other bulk and base chemicals [184, 185].

Therefore, starting from ethylene, it is possible to produce one of the most used polymers in the world: polyethylene.

Polyethylene is the simplest of the synthetic polymers and is also the most widely used plastic material in the world. Polyethylene is a thermoplastic resin with formula $(C_2H_4)_n$ and it appears as a transparent (amorphous form) or white (crystalline form) solid with excellent insulating properties and chemical stability. It is a very versatile and economical material. Its molecular structure is shown in Figure 2.28:
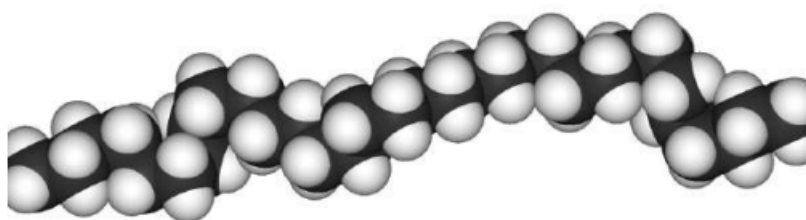

Figure 2.28 - 3D linear stroke model of polyethylene; Source: [186]

Polyethylene is classified according to the molecular weight and the quantity of branches, parameters that define its final physical characteristics (Table 2.12).

Type of polyethylene	Features and uses
UHMWPE	*Very high molecular weight polyethylene*: it is a type of polyethylene whose molecular weight varies from 3 · 106 to 6 · 106 uma. Its crystalline structure is characterized by excellent packaging, which makes it very resistant. The uses are very particular and specific, such as medical prostheses or bulletproof vests
HDPE	*High-density polyethylene*: it is a low-branched polyethylene characterized by large intermolecular forces and high stiffness.
LDPE	*Low density polyethylene*: it is very branched, therefore not very dense. It is ductile and less rigid than HPDE.
MDPE	*Medium density polyethylene*: it is a cross between HDPE and LPDE as regards the percentage of branches. Physical characteristics are also intermediate between the two.
LLDPE	*Linear low-density polyethylene*: it is a substantially linear polyethylene with a significant number of short branches
Expanded PE	*Expanded polyethylene*: it is a polyethylene that is made porous, light and soft through physical and chemical processes.

Table 2.12 - Classification of polyethylene as a function of density; Source: [186]

Polyethylene is produced by several methods by polymerization of ethylene.

The process for the production of LDPE is carried out at very high pressure (1000÷3000 atm) at moderate temperatures (250÷300 ° C). The reaction equation is as follows (Figure 2.29):

$$\text{n } C_2H_4 \longrightarrow \left[CH_2 - CH_2 \right]_n \qquad \Delta H^0 \ = \ -92 \ kJ \ mol^{-1}$$
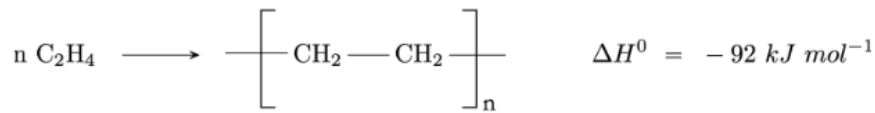
Figure 2.29 – LDPE production from ethylene; Source: [187]

This is a radical polymerization process conducted in the presence of an initiator, such as a small amount of an organic peroxide.

Two types of ballasts can be used [187]:

- Autoclave type reactor: it works as a CSTR adiabatic reactor in which the heat is removed by adding fresh monomer. The temperature is controlled by regulating the amount of radical initiator in the feed;
- Tubular reactor: it is made up of jacketed pipes hundreds of meters long. The temperature is controlled both by regulating the power supply of the initiators and by removing the excess heat through the cooling fluid that flows in the jacket. The use of this reactor allows to achieve higher conversions than the autoclave process but at the expense of a higher cost for the compression of the monomer.

Ethylene (purity greater than 99.9%) is compressed and passed into the reactor together with the initiator. The polyethylene obtained is removed, extruded and cut into granules. The unreacted ethylene is recycled. On average, the obtained polymeric macromolecule contains 4000÷40000 carbon atoms, with many short branches. There are about 20 branches for 1000 carbon atoms. The relative molecular mass and branching affect the physical properties of LDPE. Branching affects the degree of crystallinity which in turn affects the density of the material. LDPE is generally amorphous and very transparent, with about 50% crystallinity. In fact, the ramifications prevent the molecules from packing tightly together and therefore the resulting material has a low density.

For the production of HDPE, instead, two types of catalysts are mainly used [187]:

- The Ziegler-Natta organometallic catalyst (based on compounds of titanium and an aluminium alkyl);
- An inorganic compound known as a Phillips-type catalyst. A well-known example is chromium (VI) oxide on silica, which is prepared by roasting a chromium (III) compound at about 750 °C in oxygen and then stored under nitrogen before use.

HDPE is produced by three types of process that are: suspension process (using a CSTR or a "loop" reactor), process in solution and gas phase process. All operate at relatively

low pressures in the presence of a Ziegler-Natta or inorganic catalyst. In all three processes, hydrogen is mixed with ethylene to control the length of the polymer chain [187].

2.9.2. Polypropylene from propanol

The term propanol (propyl alcohol) can indicate the following chemical compounds [188]:

- 1-propanol (or n-propyl alcohol);
- 2-propanol (or isopropyl alcohol).

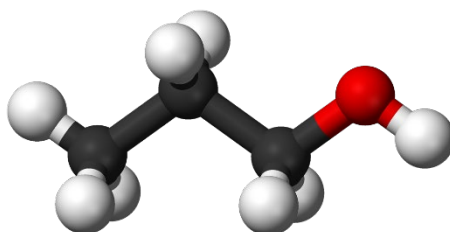In Figure 2.30-2.31 their molecular structure is shown:

Figure 2.30 – 1-propanol molecular structure; Source: [189]
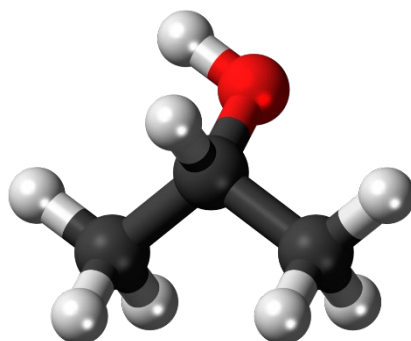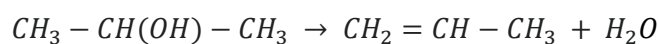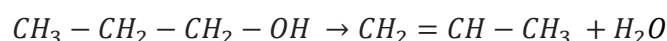

Figure 2.31 - 2-propanol molecular structure; Source: [190]

Through dehydration of propanol or isopropanol, propylene can be formed. The reaction involves the hot treatment of the alcohol, with consecutive removal of water and formation of the double bond [191]:

$$CH_3 - CH_2 - CH_2 - OH \rightarrow CH_2 = CH - CH_3 + H_2O$$

$$CH_3 - CH(OH) - CH_3 \rightarrow CH_2 = CH - CH_3 + H_2O$$

Propylene is an unsaturated aliphatic hydrocarbon belonging to the family of alkenes with chemical formula CH_2=CH-CH_3 (its molecular structure is shown in Figure 2.32):
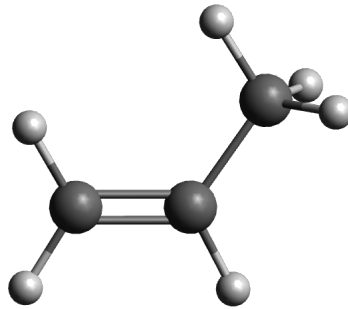
Figure 2.32 - Propylene molecular structure; Source: [191]

It has a molar mass of 42.08 g / mol, a melting point of -185.25 ° C and a boiling point of -48 ° C. At room temperature it appears as a colourless and odourless gas, not very soluble in water but soluble in organic solvents. It is not toxic but is considered an asphyxiating gas [192].

Not being a component of fossil gas or crude, and being relatively rare in nature, to obtain propylene it is necessary to resort to chemical synthesis processes.

Propylene, together with many other low molecular weight compounds, is produced spontaneously following the cracking of hydrocarbon mixtures, with a yield ranging from 3% to 20% depending on the type of mixture, pressure and temperature used in the process. Propylene is then easily purified by exploiting its different boiling temperature compared to the other components of the mixture obtained from cracking [191].

The most used industrial production methods are: steam cracking of propane and butane, steam cracking of naphtha and catalytic cracking of diesel and propane.

Subsequently, propylene is subjected to polymerization to obtain polypropylene (PP), one of the most versatile thermoplastic polymers available on the market. Its molecular structure is reported in Figure 2.33:
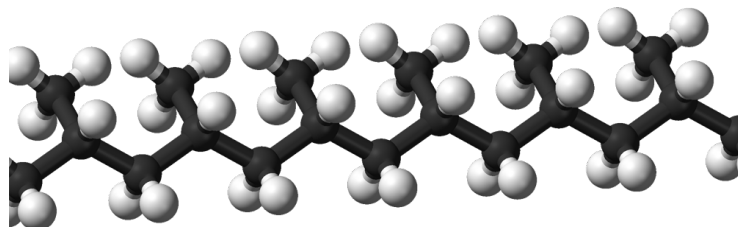

Figure 2.33 - Polypropylene molecular structure; Source: [193]

Polypropylene has several properties that make it suitable for replacing glass, metals, cardboard and other polymers. These properties include low density (weight saving), high

rigidity, heat resistance, chemical inertness, easy to weld, recyclability etc. It is one of the lightest thermoplastics (density 0,905 g / cm^3). It has a melting point of 170 °C and a crystallinity of about 50÷60% [194].

Polypropylene is made from propylene, which is obtained in large quantities from diesel, naphtha, ethane and propane. In parallel, various methods for producing bio-propylene are being developed.

Industrially, polypropylene was obtained for the first time in Italy in 1954 by Giulio Natta at the Politecnico di Milano [195]. To produce stereoregular PP, the key to success is the availability of stereospecific catalysts, that can provide polymer chains with high structural regularity. The various research works over the years have provided different types of catalysts, such as to be classified into different generations (first, second, third, etc.).

The first catalytic system used by Natta in 1954 was the one obtained by combining $TiCl_4$ and AlR_3 (where R represents ethyl or isobutyl), previously used by Ziegler for the polymerization of ethylene [195]. Subsequently it was modified using $TiCl_3$ which allowed to have greater stereoregularity. These first catalysts are called first generation. Later, Solvay patented a catalytic system always based on $TiCl_3$ but with better performance in terms of yield, stereospecificity and ability to control the morphology of the polymer which was called second generation. In the catalysts of subsequent generations, systems containing magnesium chloride ($MgCl_2$) have been developed [194, 195].

There are various types of processes to produce polypropylene but those that have found the greatest industrial development operate in suspension of a hydrocarbon diluent, in bulk or in the gaseous phase.

The process in suspension in a hydrocarbon diluent was used by the main PP producers until 1976 using first generation catalysts. It was progressively abandoned since it is characterized by a low polymerization yield. The most used hydrocarbon diluents were n-hexane or n-heptane and the monomer that had not reacted after polymerization was recycled [194, 196].

In the bulk process, the polymerization takes place in liquid propylene, in the absence of solvent, at a temperature of 70÷90 °C and pressures of 30÷40 atm (to keep the propylene in the liquid state). After polymerization, the solid polymer particles are separated from

the liquid propylene, which is then recycled. The high concentration of the monomer in the absence of solvent allows high productivity for unit volume of the reactor. Furthermore, the catalytic residues are soluble in small quantities of solvent and are easily removable. In this way it is avoided that the polymer is subject to post-treatment at the end of the process. The use of liquid propylene as a solvent means that it is not necessary to use hydrocarbons such as C_4-C_8 alkanes which are used as solvents in the similar production of polyethylene [194].

In the gas phase process, the gas phase propylene is polymerized in the presence of a Ziegler-Natta catalyst, in fluidized or stirred bed reactors. Operating conditions typically consist of temperatures of 50÷90 ° C and pressures of 8÷35 atm. The polymer is separated from the gaseous propylene by cyclones and the unreacted gas is recycled. No post-treatments are required for the removal of the catalyst [194].

2.9.3. Polymers from glycerol

Glycerol-based polymers exhibit excellent biocompatibility; hence polymers such as poly (glycerol ether), poly (glycerol carbonate)s and dendritic hyperbranched glycerol-based polymers have been extensively studied for pharmaceutical applications such as drug delivery, tissue implants and as an anti-bacterial agent [197].

To date, much attention has been paid to glycerol-based hyper-branched and dendritic polymers or block copolymers for bio-medical applications due to their excellent water solubility and biocompatibility [198, 199]. In Figure 2.34 various synthesis routes for polymers obtained from glycerol are shown:
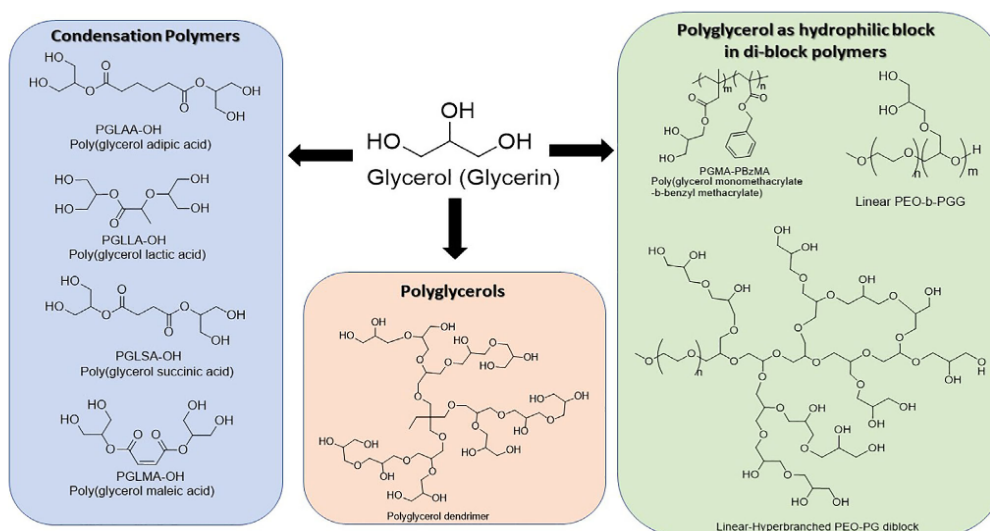

Figure 2.34 – Various synthesis routes for glycerol polymers; Source: [200]

Chapter 3

3. Aim of the thesis

Hydrogen is an important energy carrier due to its high energy density by weight, high abundance and environmental friendliness. Among the various processes for the production of hydrogen, the most consolidated is steam reforming of fossil fuels (e.g. methane, propane) and biofuels (bio-ethanol, methanol, biogas). In general, the main issue of steam reforming processes are the emissions of carbon-based substances (mainly CO_2 in the case of fossil fuels and of CH_4 in the case of alcohols) and the high energy required for sustaining the reactions. The H_2 gaseous stream is not a pure hydrogen and needs separation and CO_2 capture steps to obtain pure hydrogen. As previously discussed, a novel process (cyan H_2) has been recently developed and patented (n. 102021000030875) which allows overcoming all these issues.

The aim of the thesis activity is to optimise the processes by focusing on the role of the operating conditions (water content; feedstock…).

To this end, ethanol, glycerol and methanol are tested as bio-fuel in the presence of sodium metaborate tetrahydrate as a solid catalyst / reagent material. All the (gas, liquid and solid) products are analysed with advanced techniques (IR, TGA, XRD, GC…).

Furthermore, the process yield are compared to the H_2 yield obtained by conventional steam reforming. To this end, the thermodynamic steam reforming H_2 yield is computed at varying the feed, the temperature and the pressure.

Chapter 4

4. Materials and methods

This section describes the materials and methods applied in experimental studies of the hydrogen production from sodium metaborate tetrahydrate and the software used to carry out the thermodynamic analysis.

4.1. Materials

The reagents used for experimental tests were the following:

-   sodium metaborate tetra-hydrate ($NaBO_2 \cdot 4H_2O$, 99,95 % in mass fraction) purchased from the company Sigma-Aldrich. The reagent was found in a solid state and was characterized by a white colour;
-   ethanol (C_2H_5OH, $\geq$ 99,8 % in mass fraction) provided by Sigma-Aldrich. It is in a liquid state, and it is colourless;
-   methanol (CH_3OH, $\geq$ 99,9 % in mass fraction) provided by Sigma-Aldrich. It is a colourless liquid;
-   glycerol ($C_3H_8O_3$, $\geq$ 99,5 % in mass fraction) provided by Sigma-Aldrich. It is a viscous liquid, and it is odourless and colourless.

All raw materials were purchased from Sigma-Aldrich and used as received. The Table 4.1 shows the main characteristics of the raw materials used in experimental tests.

Substance	Formula	Company	Molecular weight (g/mol)	Assay
Sodium metaborate tetrahydrate	$NaBO_2 \cdot 4H_2O$	Sigma-Aldrich	137,86	99,95%
Ethanol	C_2H_5OH	Sigma-Aldrich	46,07	99,8%
Methanol	CH_3OH	Sigma-Aldrich	32,04	99,9 %
Glycerol	$C_3H_8O_3$	Sigma-Aldrich	92,09	99,5%

Table 4.1 - Material used in the experimental texts

4.2. Experimental tests

4.2.1. Reactor

The experimental tests present in this work were carried out in a model Parr 4567 reactor. It is a tri-phases batch reactor and its volume is 450 mL, suitable to carry out activity tests in batch mode. The reactor is equipped with a controller (Parr 4848) to monitor the temperature, pressure and stirring rate. The Parr 4848 Reactor Controller brings digital communications to all the functions of these modular reactor controllers. The 4848 offers all the features expected in a Parr general purpose reactor controller, namely:

- PID programming with auto-tuning capability for precise temperature control and minimum overshoot;
- Ramp and soak programming;
- Separate heating and cooling control loops;
- Optional solenoid valve module for cooling control;
- Motor speed control;
- High or low power heater switch;
- Lockout relay and reset for over temperature protection;
- Optional expansion modules for tachometer, pressure, and high temperature alarm.

With the 4848 Controller, all the expansion modules as well as the primary temperature control module are equipped with bidirectional digital communications [RS-485] that enable the user to not only log all current readings to a PC, but also to send set points, stirrer speeds, and alarm values from the PC to the 4848 Controller. It utilizes a feedback control system. Therefore, the desired value for the temperature, for example, is entered as a set-point in the controller by the operator. The signal from a thermocouple placed into the reactor is compared with the set-point value. In this way the controller can adjust the heat rate to maintain the set-point. In the Figure 4.1 the controller is shown:

Figure 4.1 - Reactor controller

The operating limits of the system are reported in the Table 4.2:

Parameters	Operating limit	u.o.m.
Temperature	350	°C
Pressure	160	bar
Stirring rate	1500	RPM

Table 4.2 - Operating limit of Parr 4567 reactor

Available accessories of reactor include a vessel, a pressure gauge, an internal stirring system, a thermocouple, a liquid sampling valve, a gas release valve, a gas inlet valve, a safety rupture disk, an electric heater and control system. Some of these are schematized in the Figure 4.2. Moreover, the control system is connected to a computer for the storage of the collected data.
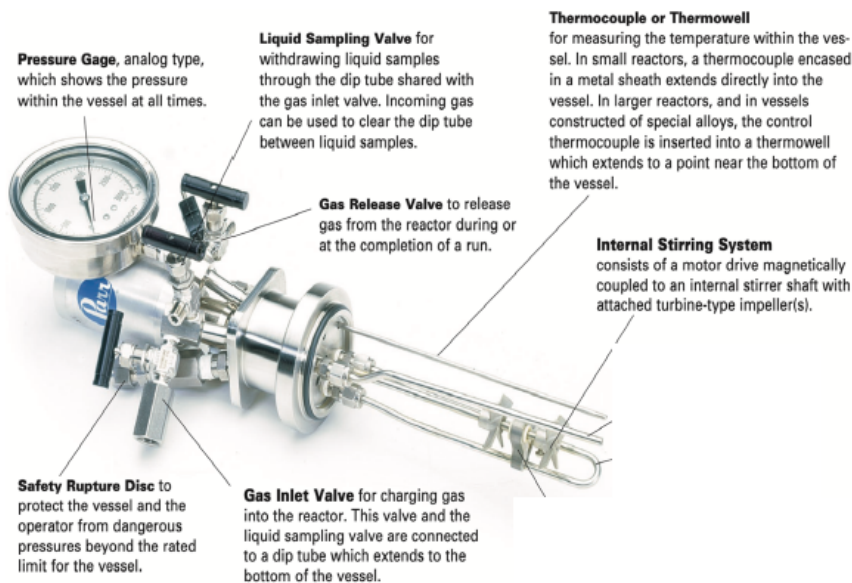
Figure 4.2 - Reactor accessories

The entire apparatus of the reactor is shown in Figure 4.3:

Figure 4.3 - Reactor apparatus

4.2.2. Experimental test procedure

The experimental tests took place according to a procedure whose purpose is to have reproducibility of the tests and above all to avoid the formation of explosive hydrogen-oxygen mixtures that have a flammability field in air at atmospheric pressure in the range 4% - 74.5%. The reactive system consists of three phases: gas, solid and liquid.

All the tests were characterized by five main steps:

- Loading of the reagents into the vessel and reactor inertization (pressure purging);
- Temperature and stirring speed setting and test start;

85

- Test run;
- End of the test and cooling at 60°C with gas sampling;
- Cooling at room-temperature and solid-liquid sampling;

More in detail, the first step involved a preliminary phase in which the solid and liquid reagents were weighted and loaded appropriately into the vessel. Subsequently, the reagent system was blanketed by Nitrogen. The number of inerting cycles has been calculated with the following formula:

$$ j = \frac{\ln\left(\frac{y_j}{y_0}\right)}{\ln\left(\frac{P_l}{P_h}\right)} $$

where:

- y_j: initial concentration;

- y_0: final concentration;

- P_l: pressure prior to inerting;

- P_h: pressure following the inerting.

For the system considered, six inerting cycles were required (5 - 0,3 barg), in order to avoid the presence of oxygen inside the reactor.

The initial operating pressure was fixed at 0,3 barg. Later, the set-point temperature value and the desired stirring rate value were manually set. Once the previous operations had been completed, the test could start. During the test, it was possible to monitor the time dependent evolution of pressure and of temperature. An increase in pressure allows us to identify the evaporation of the alcohol and then the formation of products in the gas phase. The test was interrupted after about 6 h, i.e., when the pressure-time curve plateau was reached. The system was cooled down to 60°C.

At this temperature, the gas was sampled by using a GC sampling bag. The sampling bag was connected to the gas release valve, shown in Figure 4.2 in the previous paragraph, and the valve remained open until the pressure inside the reactor became 0 barg, so all the gas was removed.

As regards the gas sampling temperature, for almost all the tests it was 60 ° C, since the boiling temperature of ethanol is about 78 ° C. Therefore, 60 ° C is a good compromise

temperature to avoid that a lot of ethanol can condense inside the sampling bag. All the more reason, it is even better when using glycerol, which instead has a much higher boiling temperature (290 °C). Only when methanol was used in the tests, it was decided to carry out the gas sampling at 50 ° C since the boiling temperature of the methanol is about 64.7 °C. Hence, 60 °C would have been too close and consequently there would have been a lot of condensed methanol in the bag.

Lastly, at room temperature, the reactor was opened, and a residue sample (solid+liquid) was taken.

For subsequent steps in the process, the addition of other reagents is required. These are loaded into the vessel through the liquid inlet valve and then the same experimental procedure as for the first step, described above, is carried out.

After the various tests, the residue present in the reactor was usually characterized by a solid phase (small particles) dispersed in the liquid phase. For this reason, the treatment of the final residue was carried out according to an accurate and structured procedure.

This procedure includes the following steps:

- the residue was taken from the reactor and stored in a 50 mL polypropylene centrifuge tube;
- this Falcon tube is subjected to a centrifuge (12500 RPM) for 10 minutes at a temperature of 10 °C. In this way the solid phase was separated from the liquid;
- the liquid was stored in another Falcon tube;
- the solid sample was dried in a tubular oven (Figure 4.4) in nitrogen stream at 50°C for five hours. It is not exceeded 50 °C to avoid losing organic substance.

Finally, all the products (gas, liquid and solid) were analysed through advanced techniques: FT-IR (Fourier Transform Infrared Spectroscopy), TGA (Thermogravimetric Analysis) and XRD (X-ray diffraction analysis) for solid analysis and GC (Gas Chromatography) for the gas analysis.

4.2.3. Thermo Scientific Lindberg/Blue M Tube Furnaces

This tubular oven has been used to dry the solid residue. It presents the following performance features:

- three zones, each of which is set using three programmable controllers (one for each zone);
- a microprocessor-based self-tuning PID control (proportional, integral, derivative) that provides optimum thermal process without overshoot;
- a single program with multiple segments for ramp (up/down) and dwell (timed hold) temperature control;
- an adjustable high-limit over-temperature protection;
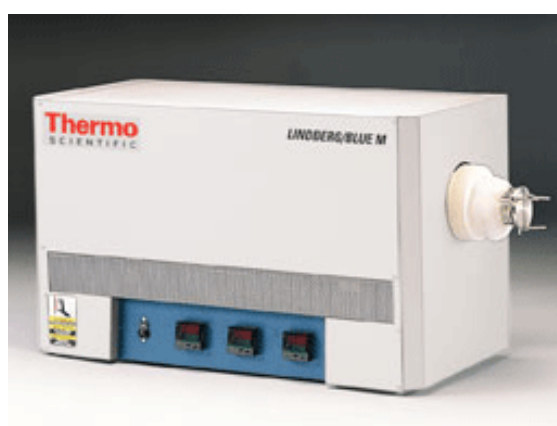- a simultaneous LED display of temperature and set-point in °C or °F.

In the Figure 4.4 this tube furnace is shown:

Figure 4.4 - Thermo Scientific Lindberg/Blue M Tube Furnaces

Specifications are given in the Table 4.3:

Specifications	
Controller	Three-zone programmable controllers - single program w/16 segments
Temperature Range	100° to 1100°C (212° to 2012°F)
Display	LED; temperature and setpoint in °C or °F
Volts	208/240
Hertz	50/60
Includes	Two tube adapters

Table 4.3 - Specifications of the tubular oven

4.3. Material characterization

4.3.1. FTIR Analysis

Fourier Transform Infrared Spectroscopy, also known as FTIR Analysis or FTIR Spectroscopy, is an analytical technique used to identify organic, polymeric, and, in some cases, inorganic materials.

This method uses infrared light to scan test samples and it is concerned with the vibration of molecules. Each functional group has its own discrete vibrational energy, which can be used to identify a molecule through the combination of all the functional groups. This makes FTIR microscopy ideal for sample ID, multilayer film characterization, and particle analysis.

Infrared spectroscopy works on principle that the molecules vibrate at specific frequencies. These frequencies ($\sim$ 4000 to $\sim$ 200 cm^{-1}) fall in IR portion of electromagnetic spectrum. When IR radiation is incident on a sample, it absorbs radiation at frequencies similar to its molecular vibration frequencies and transmits other frequencies. Frequencies of absorbed radiation are detected by infrared spectrometer and a plot of absorbed energy against frequency, called 'infrared spectrum', can be obtained. Since dissimilar materials possess dissimilar vibrations and give distinct infrared spectra, a particular molecule can be identified.

Light (radiation) can be thought of both as traveling particles (photons) and as waves. The waves consist of magnetic and electric fields, which oscillate perpendicular to each other. A wave can be described by its wavelength and frequency. The wavelength is the distance between two crests (one complete oscillation) (Figure 4.5-A); light of different wavelengths can be categorized into regions of the electromagnetic spectrum (Figure 4.5-B).
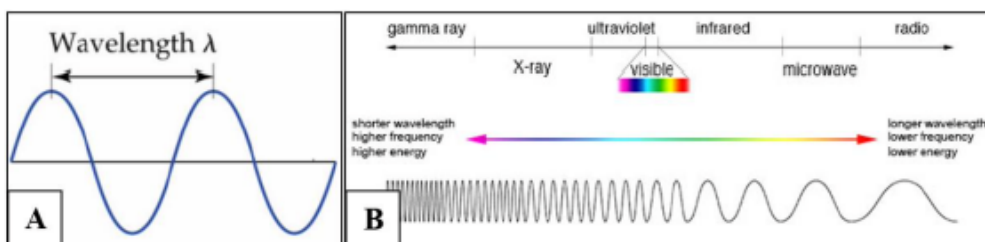

Figure 4.5 - A) Wavelength; B) electromagnetic spectrum

The frequency is defined as the number of finished oscillations per second. One hertz (Hz) is defined as one oscillation per second. The relationship between wavelength and frequency is given below:

$$\nu = \frac{c}{\lambda}$$

where:

- ν: frequency;

- c: speed of light ($2,998 \times 108$ m/s in vacuum);

- λ: wavelength.

As equation states, the frequency increases with decreased wavelength. The number of oscillations for a defined distance is called the wavenumber and is often given in cm^{-1} (number of oscillations per cm). The relationship between wavenumber and wavelength is given below:

$$\tilde{\nu} = \frac{1}{\lambda}$$

where:

- $\tilde{\nu}$: wavenumber.

The energy of a photon can be described by the equation:

$$E = h\,\nu$$

where:

- h: Planck's constant ($6,626 \times 10^{-34}$ J·s).

By combining these equations, it is obtained:

$$E = h\frac{c}{\lambda} = hc\tilde{\nu}$$

The previous equations illustrate that the energy of a wave will increase with decreased wavelength, increased frequency or increased wavenumber.

When radiation strikes a molecule, the molecule can absorb a photon and thereby get excited from the ground energy state to a higher energy level. The absorbance (also called optical density) can be expressed by the following equation:

$$A = \log\left(\frac{I_0}{I}\right)$$

where:

- I_0: intensity of the radiation that strikes the sample;

- I: transmitted light (the remaining part of the light that leaves the sample).

Thus, absorption of 90 % of the light will give an absorbance of 1; while absorption of 99 % will give an absorbance of 2.

Regarding the precision of the spectrophotometer, it is preferable to achieve an absorbance approximately between 0,3 and 2.

Different types of radiation affect the molecules in different ways. For example, when visible and ultraviolet radiations are absorbed, electrons will jump to a higher energy orbital, while absorption of microwave radiation will stimulate rotation of the molecule.

Infrared light, which is used in this project, will stimulate vibrations in the molecule. The atoms naturally vibrate in different directions in the ground energy state of a molecule. The most interesting vibrations are symmetric and asymmetric stretching, and different types of bending movements.

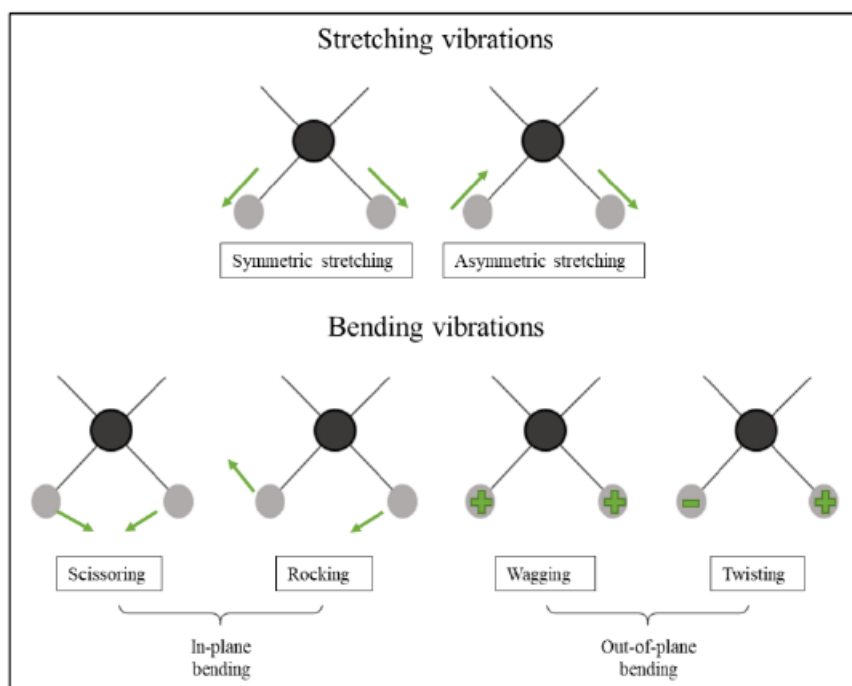These vibrations are presented in Figure 4.6:

Figure 4.6 - Different types of vibrations

The amplitude of the oscillations, and the energy of the molecule, will increase when infrared radiation is absorbed. When the molecule goes back to its ground state, it converts the energy from the photon to heat.

The wavelength of the absorbed light depends on the type of vibration and the atoms involved. In other words, different amounts of energy are required to increase the amplitude of the oscillation for different types of chemical bonds and vibrations. Functional groups will therefore absorb infrared light at characteristic frequency ranges. Due to this, it is possible to identify the functional groups in a molecule by use of infrared spectrophotometry.

The most useful infrared region is from 4000 to 625 cm^{-1} since many functional groups vibrate with frequencies within this range.

FTIR analysis is absolutely an excellent technique to recognize the bonds present within a substance, but it is not a quantitative technique and often does not allow you to uniquely recognize a substance (as in our case). In addition, the intensity of the signal of a certain vibration is strongly dependent on the quantity of substance characterized by that type of bond in the analysed sample.

In this work, Nexus FTIR spectrometer equipped with a DTGS KBr (deuterated triglycine sulfate with potassium bromide windows) detector was used to perform Fourier transform infrared (FTIR) spectroscopy (Figure 4.7). FTIR absorption spectra of all sample were recorded in the 4000÷500 cm^{-1} range at a 2 cm^{-1} spectral resolution.

Samples were prepared by mixing 200 mg of KBr and 1 mg of dried samples powders and pressing into pellets 13 nm in diameter. The spectrum of each sample was corrected for that of blank KBr.

Figure 4.7 - Nexus FTIR spectrometer

4.3.2. GC Analysis

Gas chromatography (GC) is a separation technique capable of separating highly complex mixtures based primarily upon differences of boiling point.

Common gas chromatographic equipment consists of a carrier gas system, injector, gas chromatographic column, detector and data processing unit.

The carrier gas is generally a permanent gas with low or negligible adsorption capacity, i.e., hydrogen, helium or nitrogen.

The nature of the carrier gas may influence the separation characteristics of the GC system and can modify the sensitivity of the detection. As the stability and reproducibility of the carrier gas flow-rate is a prerequisite of a successful gas chromatographic analysis, they considerably influence both the efficacy of separation and the quantification of results. Injectors deliver the sample to the head of the GC column. They can be classified into two major groups: vaporization and on-column injectors.

Vaporisation injectors utilise high temperatures (100÷300°C) to vaporise a liquid sample rapidly. Usually, a syringe is used to introduce the sample into the thermostated injector. In this case the sample rapidly vaporises, mixes with the carrier gas, and is transported into the column. On-column injectors deposit the sample directly into the column without relying upon vaporization of the sample and its subsequent transport into the column. Separation of volatile compounds of the injected sample is performed in the GC column.

Columns for gas chromatography can be divided into two distinct groups: packed and capillary columns of various dimensions. The length, diameter and inner lining of the columns may vary. Each column is specially made to be used with different compounds. The purpose of the column and furnace is to break down the injected sample into individual compounds as it passes through the column.

The separation and identification of the components of a mixture by the GC is divided into three main phases (Figure 4.8):

1. Injection of a sample into the GC (injector).

2. Separation of the sample into individual components (in the furnace column).

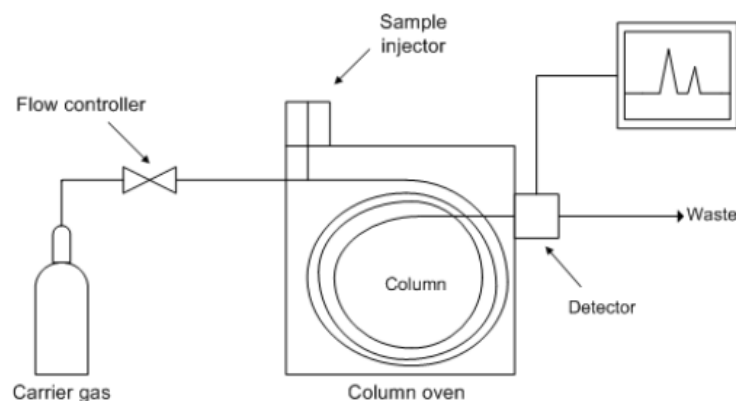3. Identification of the compounds in the sample (in the detector).

Figure 4.8 - Physical components of a typical GC system.

The columns of the GC are placed in a temperature-controlled furnace.

In the present case, the GC was used to evaluate hydrogen production. The detectors identify the presence of the compounds at the exit from the column. When the compounds enter the detector, an electrical signal proportional to the amount of compound detected is generated. The signal is usually sent to a data analysis system, for example Agilent Chem Station, where it is represented as a peak in the chromatogram.

The output of the chromatographic analysis is the chromatogram, which is characterized by the succession of the various peaks, as each substance leaving the column generates a signal that is recorded in the form of a 'peak'.

The chromatogram looks like a diagram (Figure 4.9), in which the response of the detector is reported on the ordinate axis and the detention times of the various substances on the abscissa axis (in this work, the elution time of hydrogen is about 2 minutes and depends on the created method, it is not absolute time).

Each peak is characterized by:

- *Peak height*: the distance between the peak maximum and its base, measured perpendicular to the time axis;
- *Peak amplitude*: is the segment bounded based on the peak by the intersection points of the tangents drawn at the inflection points of both sides;
- *Retention time*: this is the time taken between the injection of the sample and the recording of the maximum peak. It depends on the nature of the substance, the column and the operating conditions. The recognition of the gaseous components takes place by comparing the retention time of the various peaks with the retention time of the standard reference substances;

94

- *Peak area*: this is the surface bounded by the contour of the peak and the baseline. It depends on the amount of substance output and the characteristics of the detector. It is fundamental for quantitative analysis, as the concentration of the detected substances takes place based on the comparison of the peak areas with the calibration curve of the standard substances.
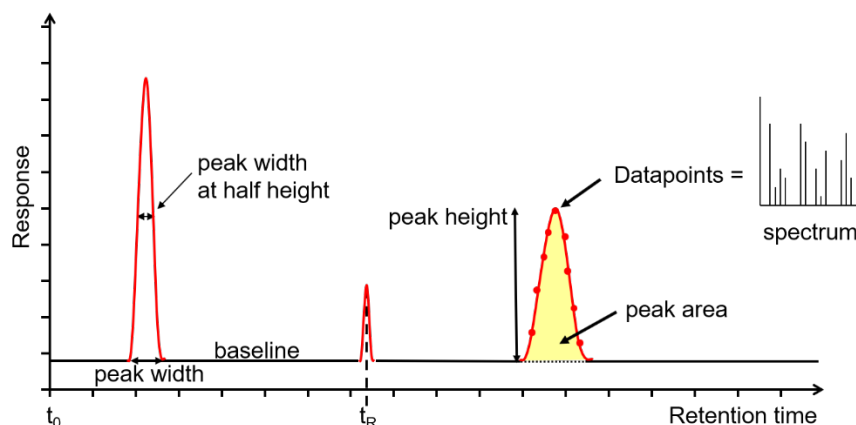

Figure 4.9 - Example of a chromatogram

In this thesis, Agilent Technologies 3000A 4-Channel Micro GC G2802A has been used (Figure 4.10). The injection temperature is set at 70 °C for each module, while a specific analysis temperature is set for each column. The column temperature is 65 °C, 90 °C, 80 °C and 100 °C for OV-1, Alumina, PLOT U and MS5A column (Agilent columns), respectively. In particular, the column OV-1 detects hydrocarbon species as isoC$_4$, methyl3butene1, pentene, hexene, etc.; the column Alumina detects species as C$_4$H$_{10}$, C$_2$H$_2$ and propylene; the column PLOT U is used to identify mainly CO$_2$ and ethylene; finally, the column MS5A detects the presence or not of H$_2$, O$_2$, N$_2$, CH$_4$ and CO in the gas sample. The detector used is a TCD (*thermal conductivity detector*). It is a non-specific and non-destructive detector and is based on the principle of thermal conductivity which depends upon the composition of the gas. The difference in thermal conductivity between the column effluent flow (sample components in carrier gas) and the reference flow of carrier gas alone, produces a voltage signal proportional to this difference. The signal is proportional to the concentration of the sample components. As for any GCs the carrier gas must be inert and may not be adsorbed by the column material. Helium is typically used as the carrier gas for the TCD because of its high thermal conductivity.

Figure 4.10 - Agilent Technologies 3000A 4-Channel Micro GC G2802A

Starting from the chromatogram, the software *Soprane* connected to the instrument carried out an integration of the areas underlying the detected peaks. To obtain the volumetric compositions of the gases present in the gas pockets, for each detected species the value of the area obtained was multiplied by a response factor. The response factor is a different number for each species and was determined through calibration lines. In Table 4.4 are shown all the response factor used:

Species	*Response factors*
Butane C_4H_{10} e isoC4	9,39088E-06
C_2H_2	1,68685E-05
butene, methyl3butene1 e isoC5	8,4637E-06
CO_2	0,000138126
ethylene	0,000145866
C_2H_6	0,000133786
C_3H_8	5,83095E-05
H_2	0,000125028
O_2	0,001291855
N_2	0,001250105
CH_4	0,000581611
CO	0,001458263

Table 4.4 - Response factors of each species for the conversion from area to volumetric composition

Then, the sum of the volumetric compositions of all species was calculated. The volumetric compositions of N_2 (since it is the one inserted before the start of each test to inert the reactor) and of O_2 were then subtracted. In this way, the normalized sum was obtained, i.e. without N_2 and O_2. Then, to obtain the normalized volumetric compositions, for each species its own volumetric composition was divided by the normalized sum. This procedure for the calculation of the normalized compositions was used, exactly as it is, for all the tests reported in the *Chapter 5*.

4.3.3. TG Analysis

Thermogravimetric analysis (TGA) is an analytical technique used to determine the thermal stability of a material and its fraction of volatile components by monitoring the weight change that occurs as a sample is heated at a constant rate. This technique allows a quantitative thermal analysis of a sample, without however identifying the nature of the components, but only by measuring how much weight is lost from the sample at a certain temperature. From this analysis graphs of weight loss as a function of temperature are obtained. They are known as thermogravimetric curves (see Figure 4.11).
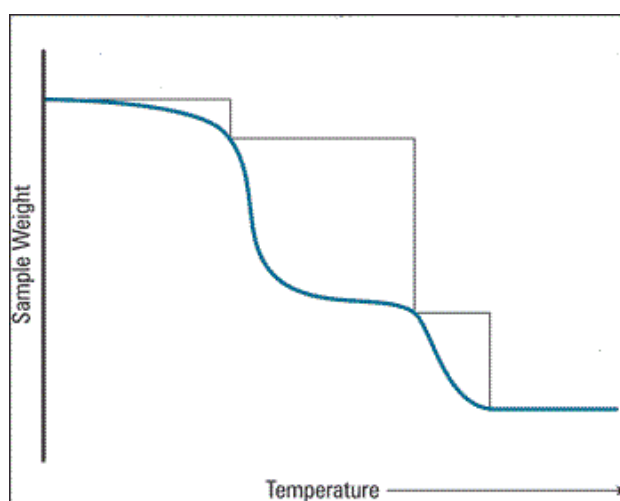
Figure 4.11 - Example of a Thermogravimetric curve

The main components are the following:

- Sensitive analytical balance (range between 5 and 20 mg);
- Furnace (temperature from 25 to 1500 °C);
- Purge gas system that ensures an inert atmosphere and the diffusion of heat at every point;
- Processor for instrument control, data acquisition and display.

TGA is one of the other routine methods for polymer characterizations. It is known how the thermal degradation mechanism of polymers can be significantly influenced by the experimental conditions in which the heating is performed. Hence, the reproducibility of the thermogravimetry data of the polymers requires the control as detailed as possible of the operating conditions of the experiment, such as size and shape of the sample, rate of heating, type of atmosphere in which the sample is heated. Anyway, the identification of the complex reactions that occur as a result of heating cannot be carried out only on the basis of the weight variations that they cause (complementary use of thermoanalytical techniques, e.g. DSC).

Thermogravimetric analysis was carried out with the TGA/DSC TA instrument Q600SDT, shown in Figure 4.12:

Figure 4.12 - TGA/DSC TA instrument Q600SDT

The Q600 features a highly reliable horizontal dual-balance mechanism that supports precise TGA and DSC measurements. It provides simultaneous measurement of weight change (TGA) and differential heat flow (DSC) on the same sample from ambient temperature to 1500 ˚C with heating rates from 0.1 to 100 °C/min.

In Figure 4.13 there is a schematization of the main components of the instrument:
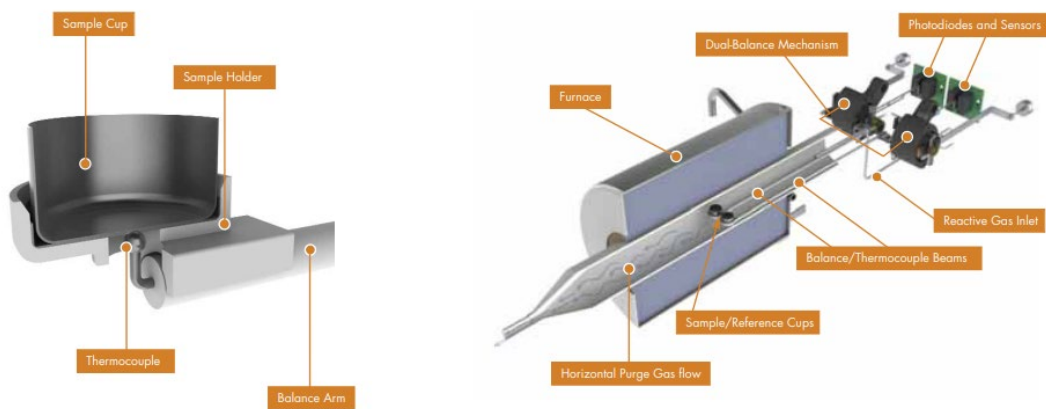
Figure 4.13 - Schematization of the main components

Platinum pans (40 and 110 µL) and ceramic cups (40 and 90 µL) are available for use with the Q600 (Figure 4.14). The platinum cups are recommended for operation to 1000 ˚C, and for their general inertness and ease of cleaning. The ceramic cups are advised for operation to 1,500 ˚C, and for samples that react with platinum.

Figure 4.14 - Q600 Sample Pans (platinum pans on the left, ceramic cups on the right)

The specifications of this instrument are given in the following Table 4.5:

System Design	Horizontal Balance & Furnace
Balance Design	Dual Beam (growth compensated)
Sample Capacity	200 mg (350 mg including sample holder)
Balance Sensitivity	0.1 µg
Furnace Type	Bifilar Wound
Temperature Range	Ambient to 1500 ˚C
Heating Rate – Ambient to 1000 ˚C	0.1 to 100 ˚C/min
Heating Rate – Ambient to 1500 ˚C	0.1 to 25 ˚C/min
Furnace Cooling	Forced Air (1500 to 50 ˚C in < 30 min, 1000 ˚C in 50 ˚C in < 20 min)
Thermocouples	Platinum/Platinum-Rhodium (Type R)
Temperature Calibration	Curie Point or Metal Standards (1 to 5 Points)
DTA Sensitivity	0.001 ˚C
Calorimetric Accuracy/Precision	± 2% (based on metal standards)
Mass Flow Controller with Automatic Gas Switching	Included
Vacuum	to 7 Pa (0.05 torr)
Reactive Gas Capability	Included – separate gas tube
Dual Sample TGA	Included
Auto-Stepwise TGA	Included
Sample Pans	Platinum: 40 µL, 110 µL Alumina: 40 µL, 90 µL

Table 4.5 - Specifications of this instrument

In this thesis, TG analysis was carried out in N_2 stream at a rate of 10 ºC/min to 1000 ºC using a mass sample of about 8 mg and platinum pans.

4.3.4. X-ray diffraction (XRD)

X-ray diffraction (XRD) is a technique used to study the crystalline structure of solids through the interaction of atoms with electromagnetic radiation of a wavelength comparable to atomic size.

When an X-ray beam is directed on the solid sample, which can be crystalline or amorphous, the affected atoms re-emit part of the X-rays, causing the radiation to be scattered in all directions (spherical waves). If the wavelength of the scattered radiation is equal to that of the incident radiation scattering is elastic; while if the wavelength of the scattered radiation is greater than that of the incident radiation it is inelastic. In the first case, the atoms maintain their kinetic energy, in the second the atoms absorb part of the energy (Compton Effect). In some directions, the elastically scattered waves are in phase and give constructive interference (coherent elastic scattering); while in others, the waves are not in phase and give destructive interference.

Bragg's law considers the reflection of waves (Figure 4.15) and provides the refraction conditions, i.e. the ratio between the incident wavelength and the distance between the scattering objects (reticular planes in the case of solids crystalline) for which the reflected rays are in phase and give constructive interference:

$$2d \sin \theta = n \cdot \lambda$$

where:

- d: the interplanar distance;
- θ: the angle of incidence whose amplitude is equal to half the diffraction angle;
- 2θ: the angle between the transmitted and reflected ray;
- n: a whole number (1, 2, ...);
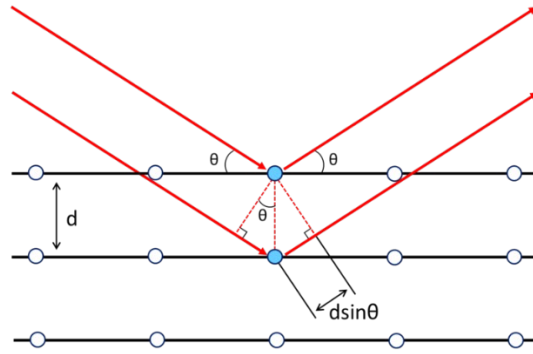- λ: the wavelength of the incident ray.

Figure 4.15 - Radiation diffraction by a family of reticular planes

X-ray diffraction can be used for the analysis of single crystals, polymer fibres, films or powders with different methods. A polycrystalline powder sample is ideally an isotropic system with crystals, and therefore reticular planes, randomly oriented in all directions. The incident radiation is monochromatic and the angle of incidence varies over a specific range. For each value of θ, some floor families are in diffraction conditions. The diffracted rays are collected by a mobile detector or by a cylindrical photographic film as in the traditional Debye-Scherrer method.

A diffractogram gives the diffraction intensity (relative to the base peak, i.e. the most intense peak) as a function of the angle 2θ, which is inversely proportional to the interplanar distance, as evidenced by Bragg's law.

The most relevant information obtainable from this analysis are:

- nature and relative quantity of the crystalline phases present;
- properties of the matrix;
- degree of crystallinity and amorphous phase content;
- preferred crystal sizes, distortion and orientations;
- study of the formation of solid solutions, reactions and phase transformation.

The identification of the crystalline phase of a sample is carried out by comparing its experimental diffractogram (Figure 4.16-b) with the PDF (Powder Diffraction File) sheets of the International Center for Diffraction Data. It is a database that contains all the diffraction profiles of known materials and contains approximately 800,000 datasets. The comparison is based on the distance values on the relative intensities of the peaks. The scheme of the structure of a diffractometer is shown in Figure 4.16-a:
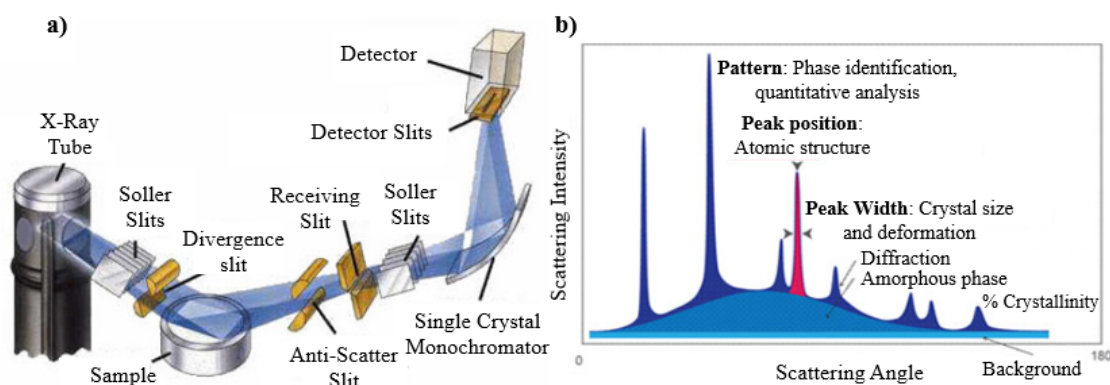
Figure 4.16 - a) Bragg-Brentano focusing geometry; b) Acquired diffractometric spectrum.

In this work, XRD analysis (X-Ray Diffraction) was carried out through XRD diffractometer PANalytical X'Pert Pro using Cu Kα radiation (1.5406 Å). The scanning range of 2θ is [5°; 100°] with a step size of 0.013° and a scan step time of 18.87 s.

It was chosen to use this analysis to see if in the solid residue there was the presence of an amorphous phase which would indicate the formation of polymer chains and therefore a further confirmation of the presence of the polymer in the solid.

4.4. Modeling and simulation methodology

4.4.1. Software description for thermodynamic analysis

In this paragraph, the software used for the thermodynamic study will be described. To compare experimental and thermodynamic results, the thermodynamic model was created using Aspen Plus V10, a software provided by Aspen Technology.

The yield, selectivity and conversion degree, together to the mole fractions of the products, has been calculated under equilibrium conditions in the outlet flow, using Gibbs energy minimisation.

The simulations are carried out using essentially the following features contained in the Aspen Plus package:

-    Type of reactor: RGibbs;
-    Property method: Peng-Robinson

As regards the RGibbs reactor, it allows the determination of the thermodynamic equilibrium conditions through the minimization of Gibbs free energy; this model can be used for the following types of equilibria:

- Single phases (liquid or vapour);
- Vapour phase with several liquid phases;
- Solid phases in solution;
- Conventional solid components in fluid phases.

The property method chosen for the model, Peng-Robinson, is commonly used for the thermodynamic analysis of polar and non-polar mixtures and in particular for hydrocarbons and light gases.

The Figure 4.17 shows an image of the Aspen Plus program interface with the RGibbs reactor used.
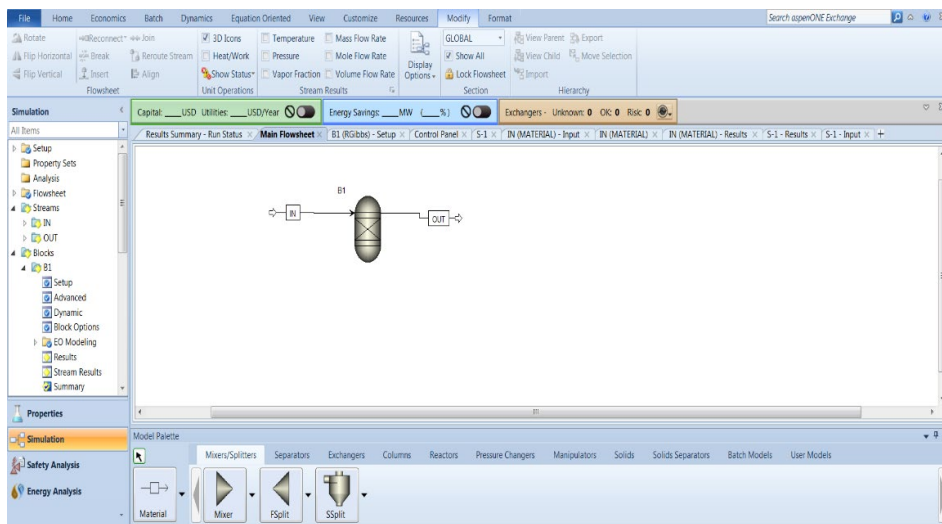
Figure 4.17 - Aspen Plus V10 program interface

The components that were considered to be always present at thermodynamic equilibrium were: CH_4, CO_2, CO, H_2, H_2O and C.

Moreover, other species have been added to the equilibrium according to the reaction pathways found in the literature and mentioned in the *Chapter 2* for each fuel. However, it was noted that, for the operating conditions we have chosen, their presence at equilibrium is almost negligible.

4.4.2. Minimization of Gibbs free energy

The minimization of total Gibbs free energy is a suitable method to calculate the equilibrium compositions of any reacting system. The total Gibbs free energy of a system is given by the sum of ith species:

$$G^t = \sum_{i=1}^{N} n_i G_i = \sum_{i=1}^{N} n_i \mu_i = \sum n_i G_i^0 + RT \sum n_i \ln \frac{f_i}{f_i^0} \quad (1)$$

where:

- G^t: total Gibbs free energy;

- G_i: partial molar Gibbs free energy of species i;

- $G_i^0 = \Delta G_{f_i}^0$: standard Gibbs free energy for reaction equilibria in gas phase;

- μ_i: chemical potential;

- R: molar gas constant;

- T: temperature of system;

- P: pressure of system;

- $f_i = y_i \varphi_i P$: fugacity in system (for reaction equilibria in gas phase);

- $f_i^0 = P^0$: standard-state fugacity (for reaction equilibria in gas phase);

- n_i: mole of species i.

By using the Lagrange multiplier method, the minimum Gibbs free energy of each gaseous species and that of the total system can be expressed as the following two Equations, respectively:

$$\Delta G_{f_i}^0 + RT \ln \frac{y_i \varphi_i P}{P^0} + \sum_k \lambda_k a_{ik} = 0 \quad (2)$$

$$\sum_{i=1}^{N} n_i \left(\Delta G_{f_i}^0 + RT \ln \frac{y_i \varphi_i P}{P^0} + \sum_k \lambda_k a_{ik} \right) = 0 \quad (3)$$

with the constraining equation:

$$\sum_i n_i a_{ik} = A_k \quad (4)$$

where:

104

- $\Delta G^0_{f\,C(s)}$: standard Gibbs function of formation of species i;

- P^0: standard-state pressure of 101.3 kPa;

- y_i: gas phase mole fraction;

- φ_i: fugacity coefficient of species i;

- λ_k: Lagrange multiplier;

- a_{ik}: number of atoms of the kth element present in each molecule of species i;

- A_k: total mass of kth element in the feed.

When solid carbon (graphite) is involved in the system, exploiting the vapor–solid phase equilibrium is applied to the Gibbs energy of carbon as shown below:

$$G_{C(g)} = G_{C(s)} \cong \Delta G^0_{f\,C(s)} = 0 \quad (5)$$

Substituting Equation (1) into Equation (2) for gaseous species and into Equation (5) for solid species gives the minimization function of Gibbs energy as follows:

$$\sum_{i=1}^{N-1} n_i \left(\Delta G^0_{f_i} + RT \ln \frac{y_i \varphi_i P}{P^0} + \sum_k \lambda_k a_{ik} \right) + n_C \Delta G^0_{f\,C(s)} = 0 \quad (6)$$

where $G_{C(g)}, G_{C(s)}, \Delta G^0_{f\,C(s)}$ and n_C are the partial molar Gibbs free energy of gas carbon, that of solid carbon, the molar Gibbs free energy of solid carbon, the standard Gibbs function of formation of solid carbon and mole of carbon, respectively.

4.4.3. Operating conditions of simulation

As mentioned above, the equilibrium calculations employing the Gibbs energy minimization were done with Aspen Plus V10 software package. To evaluate the thermodynamics properties, it was used the "PENG ROB" method; while it was chosen "RGIBBS" as reactor to perform the thermodynamics analysis.

In "RGIBBS", phase equilibrium and chemical equilibrium were chosen as calculation options, and a pressure of 30 bar and a temperature of 850°C were chosen as operating conditions. Then, through a sensitivity, it was decided to vary the temperature between 25 °C and 1000 °C and the pressure in the range 1÷40 bar. Moreover, the water-to-fuel ratio was varied in the range of 1÷10.

The equilibrium conversions of the various fuels and their hydrogen yield are defined as follows:

$$X_{fuel} = \frac{F_{fuel,in} - F_{fuel,out}}{F_{fuel,in}}$$

$$Y_H = \frac{F_{H,out}}{v_{H_2} \cdot F_{fuel,in}}$$

where:

- X_{fuel}: equilibrium conversion of the fuel;

- Y_H: yield of hydrogen;

- $F_{fuel,in}$: molar flow rates of the fuel at inlet;

- $F_{fuel,out}$: molar flow rates of the fuel at outlet;

- $F_{H,out}$: molar flow rate of hydrogen at outlet;

- v_{H_2}: stoichiometric coefficient of hydrogen in the overall steam reforming reaction of the fuel (it is: 4 for methane and biogas, 10 for propane, 3 for methanol, 6 for ethanol, 7 for glycerol);

- $v_{H_2} \cdot F_{fuel,in}$: theoretical mole ratio of fuel feed and hydrogen produced.

Furthermore, selectivity has also been defined as follows but only for methane and biogas because for all the other fuels selectivity was equal to the yield as the degree of conversion was unitary:

$$\chi_H = \frac{F_{H,out}}{v_{H_2} \cdot (F_{fuel,in} - F_{fuel,out})}$$

where:

- χ_H: selectivity of hydrogen.

The operating conditions that have been examined are summarized in the Table 4.6:

Parameters	Values	u.o.m.
Pressure	1÷40	bar
Temperature	25÷1000	°C
Feed ratio H₂O/fuel	1÷10	/

Table 4.6 - Ranges of investigated parameters

However, in *Chapter 5*, only the hydrogen yield will be represented since it will be used for the final comparison between experimental and simulation results. In fact, the selectivity, except for methane and biogas, has always been equal to the yield.

Chapter 5

5. Results and discussion

5.1. Thermodynamic analysis

For a chemical process to take place, two aspects must be examined:

- Kinetic;

- Thermodynamic.

Thermodynamics describes the overall properties, behaviour and equilibrium composition of a system; while kinetics studies the reaction rate and the factors that influence it, describing the mechanisms involved in the formation of the final products. In this paragraph, the thermodynamic aspect will be described because it is fundamental to explore the limits of operability of a chemical process.

In real reactive systems, there is often a quite complex network of chemical reactions. It is difficult for a reagent system to provide a single chemical reaction during operation, but it is possible to ensure that the desired reactions - i.e. those that generate the product of interest - are accelerated with respect to the others, leading overall to a mixture of a very precise composition. To design and operate an industrial process, it is always advisable to start from an analysis of the thermodynamics of the process itself. The latter, thanks to the methodological tools available and to the models developed to describe the behaviour of the substances, allows to establish the limit values for some quantities of interest (degree of conversion of the fuel, yield to hydrogen, etc.), as a function of manipulable operative variables of the process, such as pressure, temperature and feed ratio.

5.2. Thermodynamic analysis of SRE

In this paragraph, thermodynamic analysis of SRE is analysed in more detail, because ethanol is the fuel used largely in our laboratory experiments.
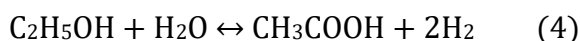
5.2.1. Reaction pathways of SRE

Thermodynamic aspects of ethanol steam reforming (SRE) have been extensively analysed in the literature. The reaction pathways and thermodynamics of SRE have been studied recently [201, 202, 203]. The possible reaction pathways of SRE can be described by Equations (1) ÷ (20).

The reaction with sufficient steam supply, Equation (1), is strongly endothermic and produces only hydrogen and carbon dioxide if ethanol reacts in the most desirable way. It is an ideal pathway by which the highest hydrogen is produced:

$$C_2H_5OH + 3H_2O \leftrightarrow 2CO_2 + 6H_2 \qquad (1)$$
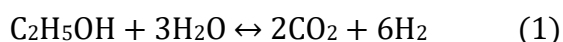
Lower hydrogen production and undesirable products, such as carbon monoxide and methane, are formed during insufficient steam supply reactions:

$$C_2H_5OH + H_2O \leftrightarrow 2CO + 4H_2 \qquad (2)$$
$$C_2H_5OH + 2H_2 \leftrightarrow 2CH_4 + H_2O \qquad (3)$$
$$C_2H_5OH + H_2O \leftrightarrow CH_3COOH + 2H_2 \qquad (4)$$

Ethanol can dehydrogenize to acetaldehyde through the following equation:

$$C_2H_5OH \leftrightarrow CH_3CHO + H_2 \qquad (5)$$

Acetaldehyde can decompose to methane and carbon monoxide or transform into hydrogen and carbon monoxide through Equation (6) or Equation (7), respectively:

$$CH_3CHO \leftrightarrow CH_4 + CO \qquad (6)$$
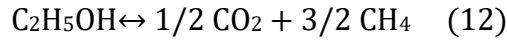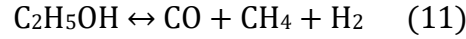$$CH_3CHO + H_2O \leftrightarrow 3H_2 + 2CO \qquad (7)$$
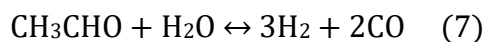
Ethanol can dehydrate to ethylene or ether according to Equation (8) or Equation (9), respectively:

$$C_2H_5OH \leftrightarrow C_2H_4 + H_2O \qquad (8)$$
$$C_2H_5OH \leftrightarrow 1/2\ C_2H_5OC_2H_5 + 1/2\ H_2O \qquad (9)$$
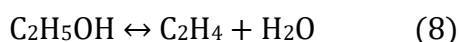
A possible route for the formation of carbon is ethylene polymerization (Equation (10)):

$$C_2H_4 \leftrightarrow \text{polymers} \leftrightarrow 2C + 2H_2 \quad (10)$$
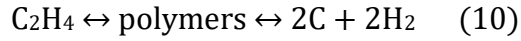
Ethanol can decompose into carbon monoxide, methane, carbon dioxide, hydrogen, and acetone through Equations (11) ÷ (13):

$$C_2H_5OH \leftrightarrow CO + CH_4 + H_2 \quad (11)$$
$$C_2H_5OH \leftrightarrow 1/2\ CO_2 + 3/2\ CH_4 \quad (12)$$
$$C_2H_5OH \leftrightarrow 1/2\ CH_3COCH_3 + 1/2\ CO + 3/2\ H_2 \quad (13)$$
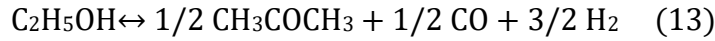
Carbon monoxide and carbon dioxide could transform into methane through methanation reactions (Equations (14) and (15)):

$$CO + 3H_2 \leftrightarrow CH_4 + H_2O \quad (14)$$
$$CO_2 + 4H_2 \leftrightarrow CH_4 + 2H_2O \quad (15)$$
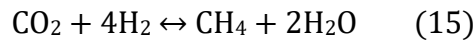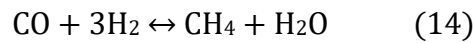
Coke formation may occur through methane decomposition reaction (Equation (16)) and Boudouard reaction (Equation (17)):

$$CH_4 \leftrightarrow 2H_2 + C \quad (16)$$
$$CO \leftrightarrow 1/2\ CO_2 + 1/2\ C \quad (17)$$
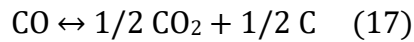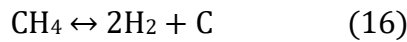
Water gas shift reaction (WGSR), Equation (18), is exothermic and reversible and hence the equilibrium shifts to the right and favours the formation of H_2 and CO_2 at lower temperatures:

$$CO + H_2O \leftrightarrow CO_2 + H_2 \quad (18)$$

Reduction of carbon oxides may also lead to carbon formation through the following equations:

$$CO + H_2 \leftrightarrow C + H_2O \quad (19)$$
$$CO_2 + 2H_2 \leftrightarrow C + 2H_2O \quad (20)$$
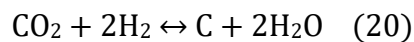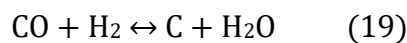
Hydrogen production varies significantly with different reaction pathways. To maximize hydrogen production, it is crucial to ensure sufficient supply of steam and to minimize ethanol dehydration and decomposition.

5.2.2. Calculation of equilibrium constants

In this sub-paragraph, through the calculation of the equilibrium constants as a function of the temperature, $T_{\Delta G_0 = 0}$ will be obtained for each reaction.

Hence, thermodynamic study of this path of reactions was carried out by calculating the equilibrium constant for each chemical reaction.

It can be expressed as follows:

$$K_{eq}(T) = \exp\left(-\frac{\Delta G_0}{RT}\right)$$

where:

- ΔG_0 is the Gibbs free energy;

- R is the universal gas constant;

- T is the temperature (in Kelvin).

The Gibbs free energy can be calculated as:

$$\Delta G_0 = \Delta H_r^0 - T\,\Delta S_r^0$$

where:

- ΔH_r^0 is the enthalpy of the reaction and it is equal to:

$$\Delta H_r^0 = \sum v_p \cdot H_{f,products}^0 - \sum v_r \cdot H_{f,reagents}^0$$

- ΔS_r^0 is the entropy of the reaction that is equal to:

$$\Delta S_r^0 = \sum v_p \cdot S_{f,products}^0 - \sum v_r \cdot S_{f,reagents}^0$$

The thermodynamic data used to calculate the enthalpies and the entropies of formation of the single chemical species (H_f^0, S_f^0) are taken from Perry's Chemical Engineers' handbook at the temperature of 298 K. Data not available in the manual is taken from National Institute of Standards and Technology (NIST) [204]. After calculating the previous thermodynamic quantities, the equilibrium constant was calculated for each reaction in the temperature range of 300÷1500 K, remembering that K_{eq} depends on temperature (both in the exponential and in the ΔG_0). In this way, the evolution of the equilibrium constants as function of the temperature has been plotted. Since the reading of the graph is made difficult by too many curves represented on the same graph, it was decided to plot five curves at a time. The results are shown in the Figure 5.1-5.4:
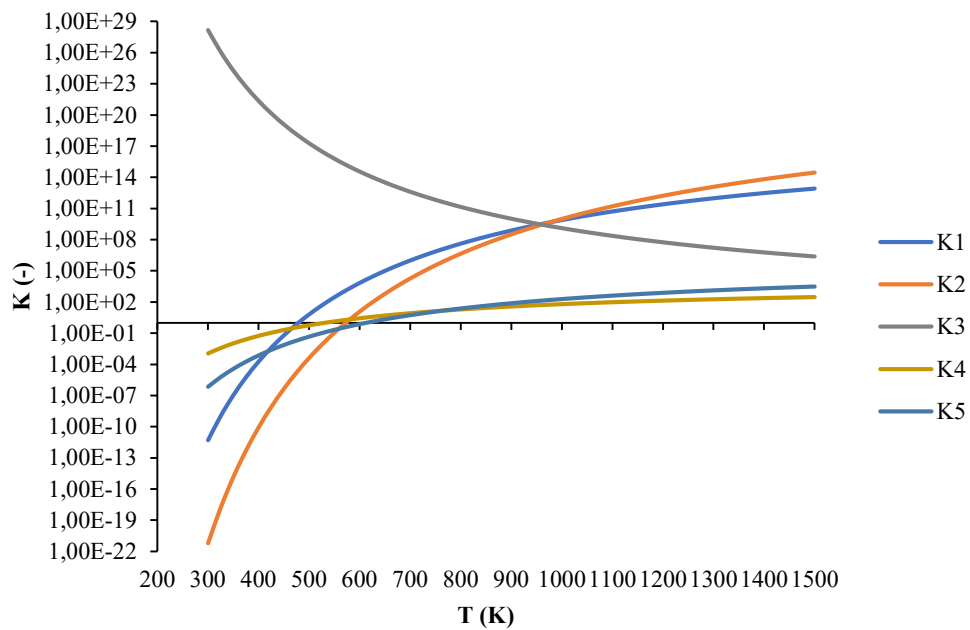
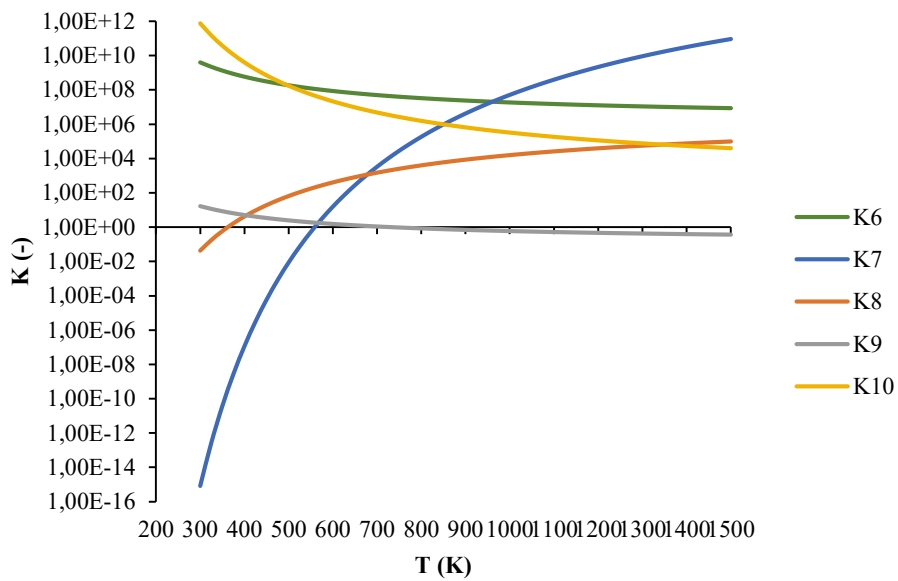*Figure 5.1 - The temperature dependent evolution of the equilibrium constants (R1-R5)*

Figure 5.2 - The temperature dependent evolution of the equilibrium constants (R6-R10)
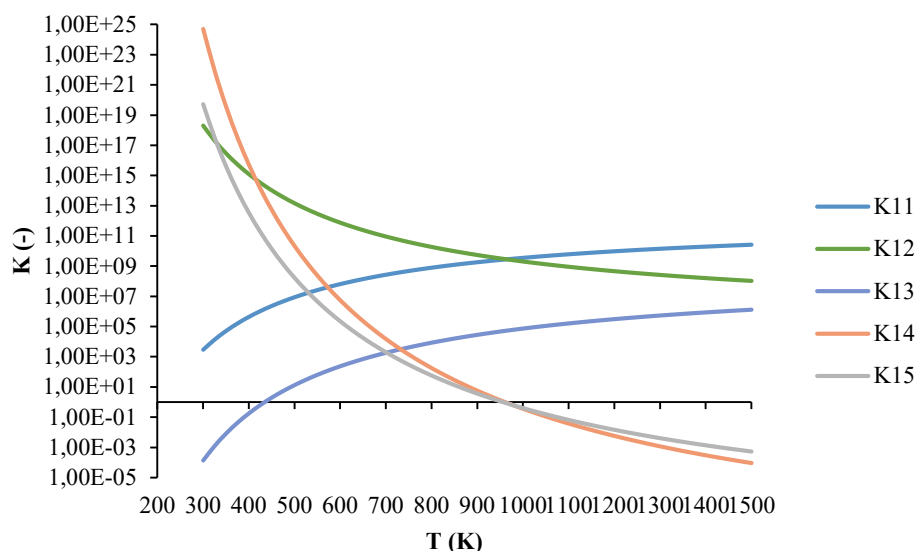
Figure 5.3 - The temperature dependent evolution of the equilibrium constants (R11-R15)
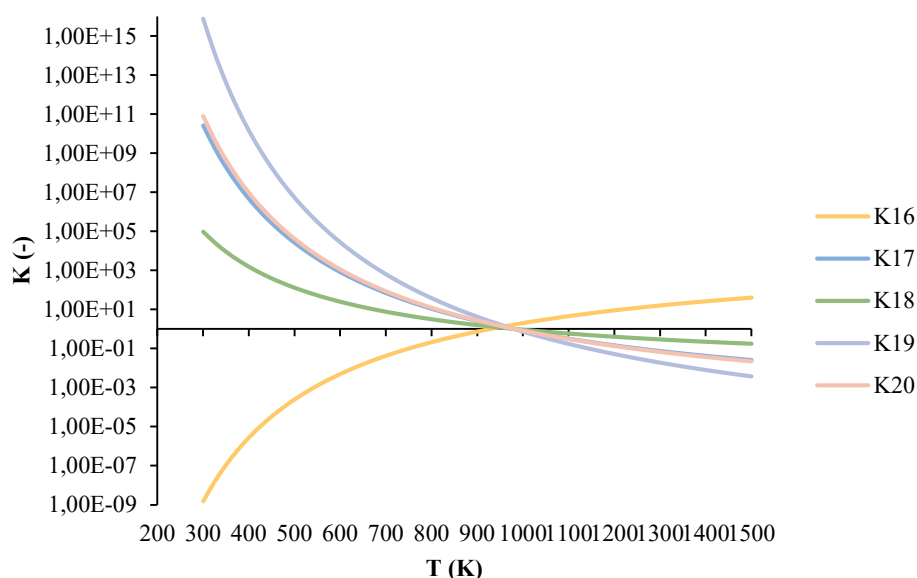

Figure 5.4 - The temperature dependent evolution of the equilibrium constants (R16-R20)

From these graphs, it is possible to identify the temperature corresponding to $\Delta G_0 = 0$ for each reaction, i.e., the temperature at which $K_{eq} = 1$. This temperature is represented in the Table 5.1, and it is very useful to individuate when a reaction is thermodynamically favoured or not. If the reaction is exothermic, it is favoured at temperature lower than $T_{\Delta G_0=0}$; while the endothermic reaction is favoured at temperature higher than $T_{\Delta G_0=0}$. So the reaction R1, R2, R4, R5, R7, R8, R11, R13, R16 are favoured at $T > T_{\Delta G_0=0}$ because are endothermic ($\Delta H_r^0 > 0$); instead the reaction R3, R6, R9, R10, R12, R14, R15, R17, R18, R19, R20, being exothermic ($\Delta H_r^0 < 0$), are favoured at $T < T_{\Delta G_0=0}$.

Reaction no.	ΔH_{298K} (kJ mol^{-1})	ΔS_{298K} (kJ mol^{-1} K^{-1})	$T_{\Delta G0=0}$ (K)
R1	173,7	0,36317	480
R2	256	0,44721	560
R3	-156,3	0,01797	very high
R4	38,9	0,07337	540
R5	69,1	0,11268	610
R6	-19,2	0,11991	very high
R7	186,9	0,33453	560
R8	45,7	0,12615	360
R9	-11,9	-0,01649	725
R10	-52,3	0,05324	very high
R11	49,9	0,23259	very low
R12	-73,8	0,10427	very high
R13	71,7	0,16494	440
R14	-206,1	-0,21462	960
R15	-165	-0,1726	960
R16	74,8	0,08071	930
R17	-86,2	-0,08797	980
R18	-41,2	-0,04202	990
R19	-131,3	-0,13391	980
R20	-90,1	-0,09189	980

Table 5.1 - ΔH_r^0 , ΔS_r^0 and $T_{\Delta G_0=0}$ for all the reaction examinated

In this way, $T_{\Delta G_0=0}$ was obtained for each reaction.

For the reactions R3, R6, R10, R11 and R12 it was not possible to derive it because it was either too high or too low with respect to the temperature ranges investigated. This means

that, in this temperature ranges, we can consider them as always favoured reactions from a thermodynamic point of view.

Since the operating conditions used in this thesis work are usually variable between 25 °C and 300 °C, the thermodynamic analysis is focused on this range of temperature to better see which reactions are favoured thermodynamically in those temperature ranges. The results are showed in the Table 5.2:

Temperature (K)	Favourite reactions
300	R3, R6, R9, R10, R11, R12, R14, R15, R17, R18, R19, R20
350	R3, R6, R9, R10, R11, R12, R14, R15, R17, R18, R19, R20
400	R3, R6, R8, R9, R10, R11, R12, R14, R15, R17, R18, R19, R20
450	R3, R6, R8, R9, R10, R11, R12, R13, R14, R15, R17, R18, R19, R20
500	R1, R3, R6, R8, R9, R10, R11, R12, R13, R14, R15, R17, R18, R19, R20
550	R1, R3, R4, R6, R8, R9, R10, R11, R12, R13, R14, R15, R17, R18, R19, R20
600	R1, R2, R3, R4, R6, R7, R8, R9, R10, R11, R12, R13, R14, R15, R17, R18, R19, R20

Table 5.2 - Thermodynamic analysis results: favourite reactions in the range 300K÷600 K

At this point, through the minimization of the Gibbs free energy, reactions are no longer taken into consideration but now the aim is to identify the species present at thermodynamic equilibrium in particular conditions of temperature and pressure, described in *Chapter 4*. Then it will be possible to calculate yield and selectivity of hydrogen for steam reforming of ethanol. All this was done with the help of the software Aspen Plus. Particularly, diagrams of hydrogen yield and molar fractions of the products in the output stream at equilibrium versus pressure as the feed ratio changes will be reported.

It was decided to represent the graphs at the temperature of 300 °C and with the pressure varying between 1 bar and 40 bar, since these are the operating conditions of our experiments. Therefore, it will be useful to make a comparison at the end.

As for the hydrogen yield, it decreases as the pressure increases (see Figure 5.5), in accordance with the endothermicity of the steam reforming reaction, which is favoured at low pressures and grows with increasing feed ratio $\left(n = \frac{H_2O}{fuel}\right)$ because the fuel becomes sub-stoichiometric compared to water and reacts completely.
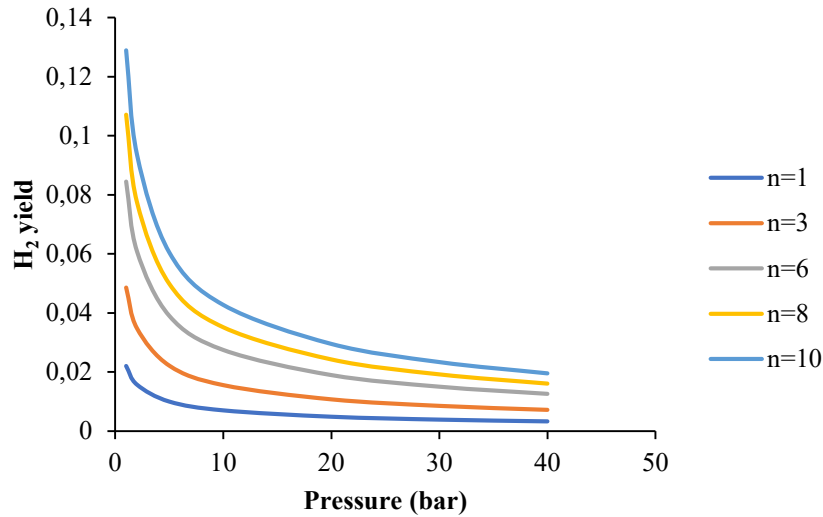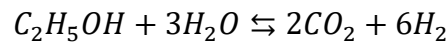

Figure 5.5 - Hydrogen yield vs pressure as function of feed ratio at 300 °C

Below, however, only the molar fractions of H_2, CO_2 and CH_4 in output stream versus pressure are shown because the molar fraction of all the other considered compounds at equilibrium was negligible. As shown in the graph, H_2 molar fraction decreases when the pressure increases because the reaction is shifted to the left (see the formula of K(T)):

$$C_2H_5OH + 3H_2O \leftrightarrows 2CO_2 + 6H_2$$

$$K(T) = \frac{nCO_2^2 * nH_2^6}{nC_2H_5OH * nH_2O^3} * \frac{P^4}{n_{tot}^4}$$

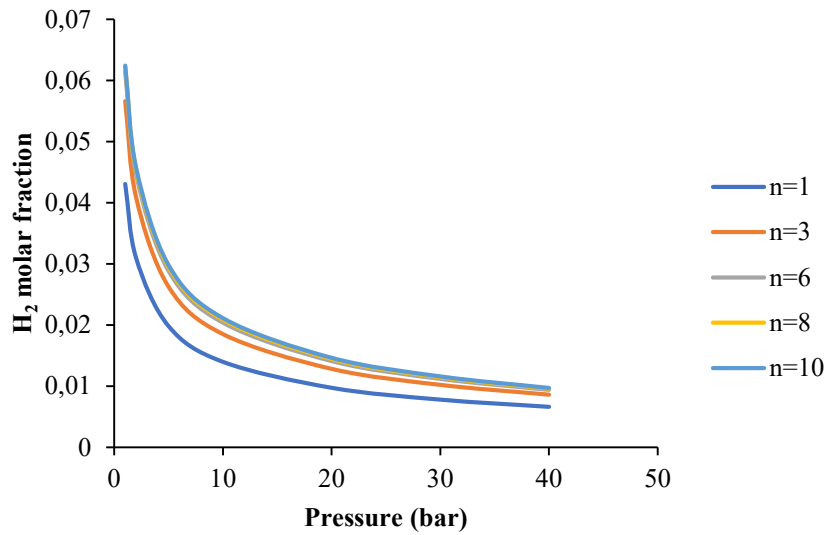Moreover, H_2 molar fraction grows when n increases because it is, precisely, H_2 yield that increases (Figure 5.6).

Figure 5.6 - Hydrogen molar fraction vs pressure as function of feed ratio at 300 °C

Regarding CO_2 and CH_4 molar fraction, they decrease with increasing of n, but they are not influenced by the variation of the pressure and remain almost constant (Figure 5.7÷5.8):
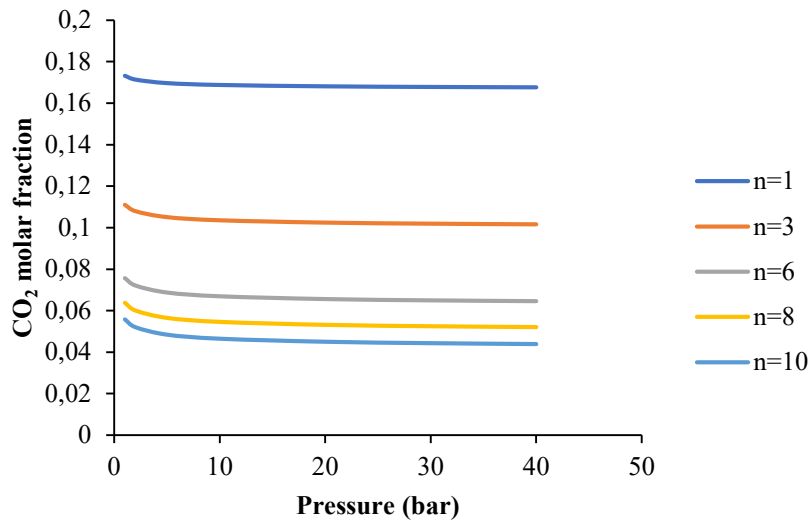

Figure 5.7 - CO_2 molar fraction vs pressure as function of feed ratio at 300 °C
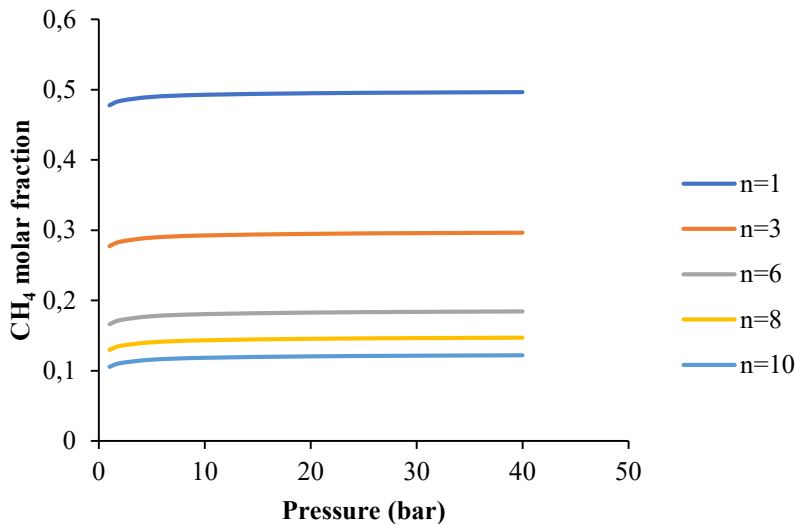
116

Figure 5.8 - CH$_4$ molar fraction vs pressure as function of feed ratio at 300 °C

Hence, in the operating conditions of our experiments (at 300 °C), according to thermodynamics, the maximum yield occurs for n = 10 and P = 1 bar and is approximately 13 % with: $yH_2 = 0,06$, $yCO_2 = 0,05$ and $yCH_4 = 0,1$. The remaining fraction is all water, being in excess of water.

5.3. Thermodynamic analysis of steam reforming of different fuels using Gibbs free energy minimization method

This paragraph shows the results obtained from the thermodynamic analysis using the software Aspen Plus V10 and the operating conditions described in the previous chapter.

In this work, it was decided to carry out a thermodynamic analysis of the following fuels: methane, biogas, propane, methanol, ethanol, glycerol.

In particular, only the comparisons, between the different fuels, of the hydrogen yield at fixed pressures, temperatures and / or feed ratios, appropriately chosen, will be shown in detail. In fact, it is believed that they are the most significant for a subsequent comparison with the experimental results carried out. For simplicity, from now on, the letter "n" will indicate the water-to-fuel feed ratio.

5.3.1. H$_2$ yield vs pressure at the same temperature (T=300, 500, 700 °C) and feed ratio (H$_2$O/fuel=1, 10, stoichiometric)

In this sub-paragraph, hydrogen yield as a function of the pressure at different temperatures and feed ratios, are plotted. At first, with a water-to-fuel feed ratio equal to

1, the three temperatures of 300 °C, 500°C and 700 °C were chosen. Then, in order to better visualize and understand the effect of excess or not of water compared to the fuel, the same diagrams were repeated also for a water-to-fuel feed ratio equal to 10 and after that again equal to the stoichiometric value, which is different for each reaction.

First of all, for all the temperatures and water-to-fuel feed ratio analysed in this subsection:

- hydrogen yield decreases with increasing pressure. This happens because the steam reforming reactions occur with an increase in the number of moles. Therefore, it is obvious that an increase in pressure disfavours the steam reforming reaction by moving it to the reagents.

  By way of example, to better understand what has just been said, the formula for the equilibrium constant of methane steam reforming is given below, together with the overall methane steam reforming reaction:

$$CH_4 + 2\,H_2O \leftrightarrows CO_2 + 4\,H_2$$
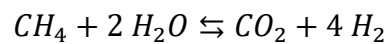
$$K(T) = \frac{nCO_2 * nH_2^4}{nCH_4 * nH_2O^2} * \frac{P^2}{n_{tot}^2}$$

  Therefore, an increase in pressure results in an increase in the numerator. To balance the equilibrium, hence, the denominator must increase. This means that the moles of methane and water have to increase. Thus, the reaction must inevitably shift to the left. The same can be said for all the other fuels too.

- at 300 °C hydrogen yield is very low for all the fuels: in fact, since steam reforming is an endothermic reaction, it is favoured at high temperatures (greater than $T_{\Delta G^0=0}$);

- by increasing the temperature, the yield increases significantly until reaching the highest values at 700 °C.

Analysing the diagrams with n = 1 (Figure 5.9÷5.11), it can be inferred that:

- propane is always the fuel with the worst yield: this happens because, at n = 1, the water is sub-stoichiometric compared to the propane fed (being n_{stoic} = 6). Therefore, water is the limiting reactant and a lot of unconverted propane remains;

- at 300 °C methane has the best yield (although under 10%), followed by methanol and biogas; while ethanol and glycerol, instead, are almost the same;

- at 500 °C there is an inversion between methane and methanol;
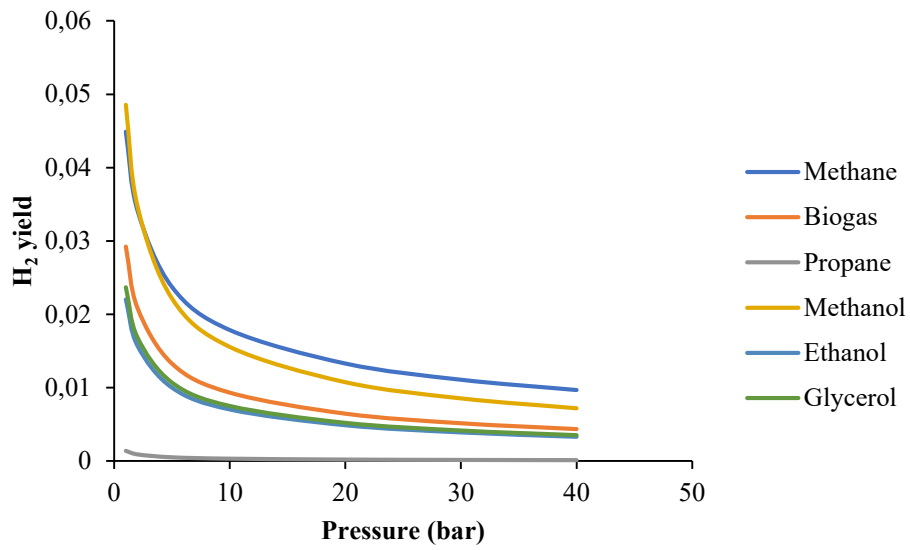- at 700 °C glycerol becomes better than ethanol.

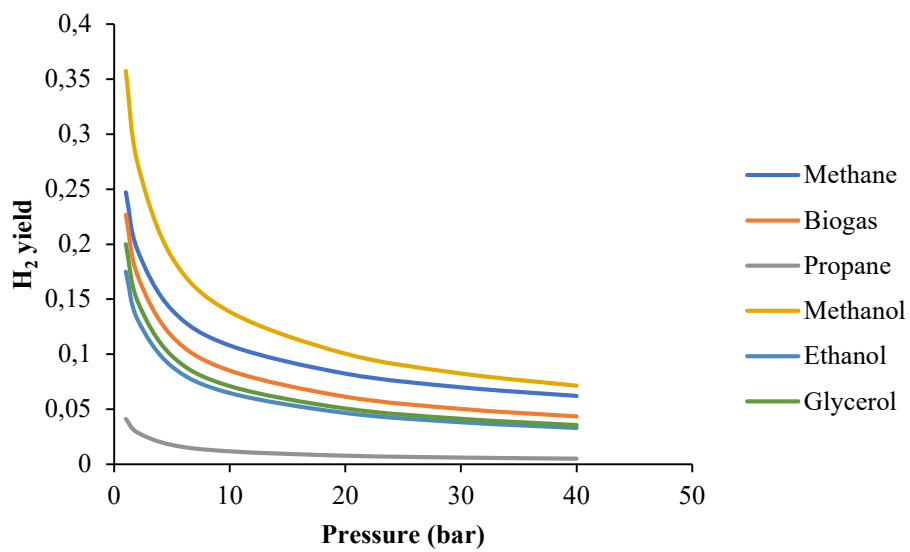*Figure 5.9 - Hydrogen yield vs pressure as function of fuel (T=300°C and n=1)*

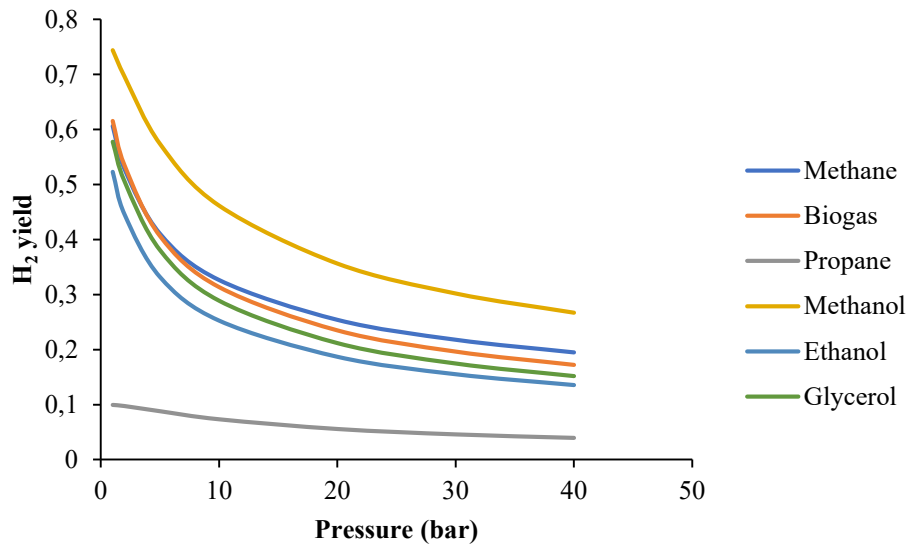*Figure 5.10 - Hydrogen yield vs pressure as function of fuel (T=500°C and n=1)*

Figure 5.11 - Hydrogen yield vs pressure as function of fuel (T=700°C and n=1)

Now, to analyse the influence of excess water in the feed stream, the diagrams with n=10 are examined (Figure 5.12÷5.14). It can be immediately noted that the yield is higher even already at 300 °C because the fuel is sub-stoichiometric in the case of n = 10. Hence, the fuel is completely consumed, being the limiting reactant, and so the yield increases. Moreover, as for n = 1, the propane is the worst fuel (even if it is very close to all the others unlike n = 1) and the same inversion between methane and methanol is noted, going from 300 °C to 500 °C. Another important aspect to consider is that, by increasing n, ethanol becomes better than glycerol, in terms of yield, exceeding it at any temperature.

Finally, the condition in which maximum yield is obtained for each fuel is approximately at temperatures around 700 ° C, low pressures (usually 1 bar) and with a very high water-to-fuel feed ratio (n=10). In this condition, hydrogen yield varies between 85% and 95% following this trend:
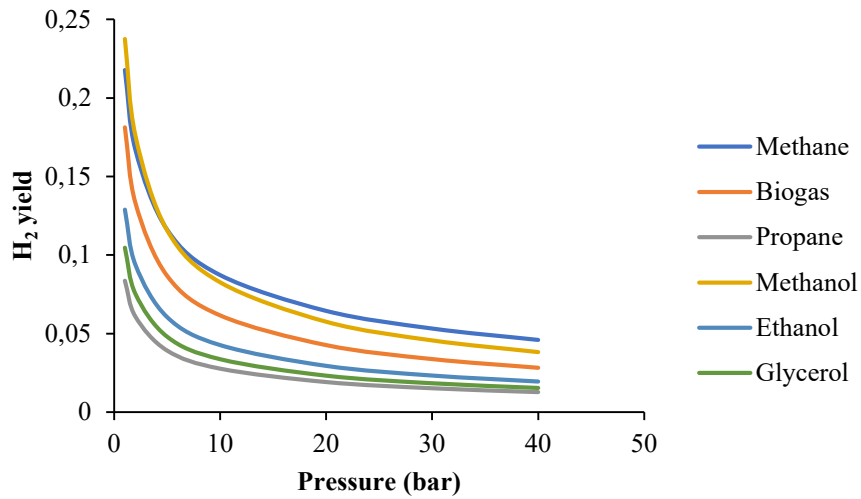
methanol > methane > biogas > ethanol > glycerol > propane

Figure 5.12 - Hydrogen yield vs pressure as function of fuel (T=300°C and n=10)

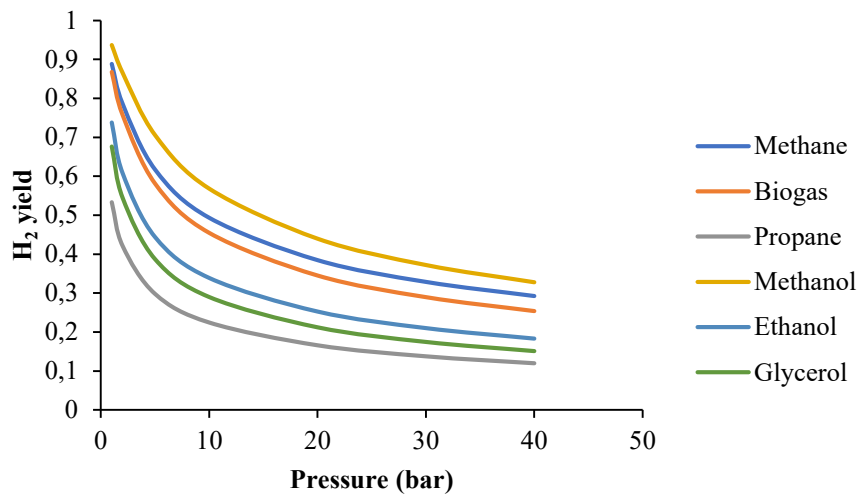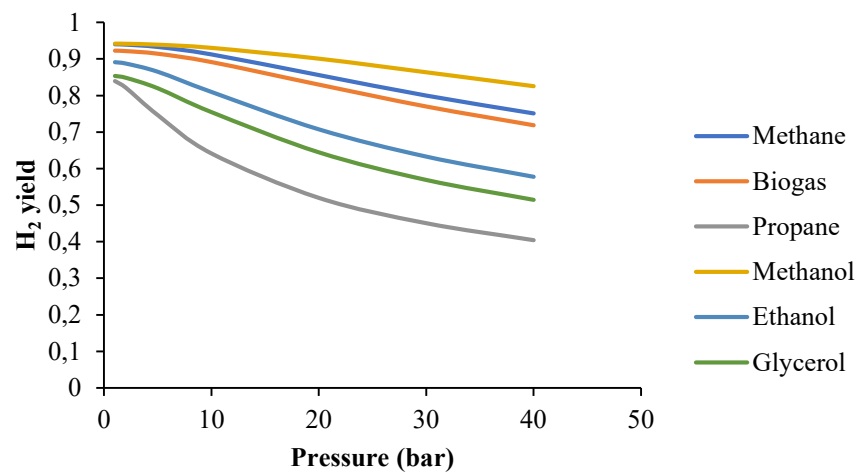*Figure 5.13 - Hydrogen yield vs pressure as function of fuel (T=500°C and n=10)*

Figure 5.14 - Hydrogen yield vs pressure as function of fuel (T=700°C and n=10)

121

For completeness, it has been decided to compare the various fuels at the stoichiometric value of n (n_{stoic}) which obviously differs according to the fuel. In the Table 5.3, it is represented the overall steam reforming reaction with the respective n_{stoich} for each fuel:

Fuel	Overall steam reforming reaction	n_{stoich}
Methane	$CH_4 + 2H_2O \leftrightarrows CO_2 + 4H_2$	2
Biogas	$CH_4 + 2H_2O \leftrightarrows CO_2 + 4H_2$	2
Propane	$C_3H_8 + 6H_2O \leftrightarrows 3CO_2 + 10H_2$	6
Methanol	$CH_3OH + H_2O \leftrightarrows CO_2 + 3H_2$	1
Ethanol	$C_2H_5OH + 3H_2O \leftrightarrows 2CO_2 + 6H_2$	3
Glycerol	$C_3H_8O_3 + 3H_2O \leftrightarrows 3CO_2 + 7H_2$	3

Table 5.3 - Overall steam reforming reactions

The graphs with a water-to-fuel feed ratio equal to the stoichiometric value of the overall steam reforming reaction (n = n_{stoich}) are shown in Figure 5.15÷5.17.

At 300 °C, except for methane, all the others have almost the same values. Increasing the temperature, methane also gets closer to the others and, in fact, at 700 °C, both the trend and the values are practically similar.

Moreover, using n_{stoic}, propane is inferior only to methane. This confirm the motivation given above on the bad yield of propane for n = 1 unlike all the other fuel, namely that it is a problem of water sub-stoichiometric.
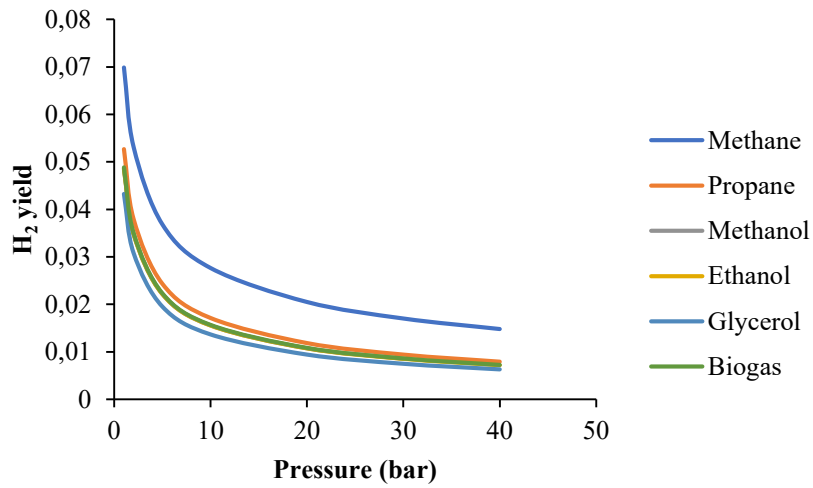
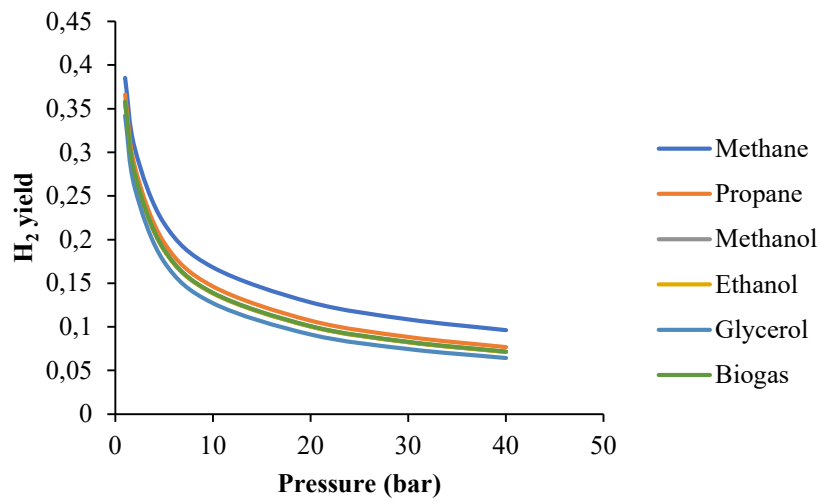*Figure 5.15 - Hydrogen yield vs pressure as function of fuel (T=300 °C and n=n$_{stoic}$)*

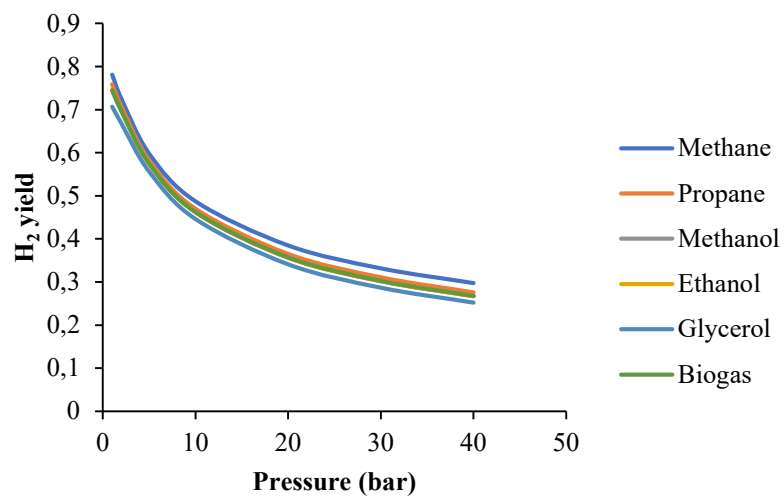*Figure 5.16 - Hydrogen yield vs pressure as function of fuel (T=500 °C and n=n$_{stoic}$)*

Figure 5.17 - Hydrogen yield vs pressure as function of fuel (T=700 °C and n=n$_{stoic}$)

5.3.2. H$_2$ yield vs temperature at the same pressure (P=1, 30 bar) and feed ratio (H$_2$O/fuel=1, 10, stoichiometric)

In this sub-paragraph, hydrogen yield as a function of the temperature at different pressures and feed ratios, are plotted. At first, with a water-to-fuel feed ratio equal to 1, the two pressures of 1 bar and 30 bar were chosen. Then, as previously done, the same diagrams were repeated also for a water-to-fuel feed ratio equal to 10 and equal to the stoichiometric value.

As regards the graph at n = 1 and P = 1 bar (Figure 5.18), all fuels have a yield trend that increases with increasing temperature up to a maximum value. This latter then, for methanol and glycerol, decreases slightly, settling at a stationary value. Clearly, depending on the fuel, the position of this peak changes (for methanol is placed at temperatures around 700 ° C, slightly lower than glycerol). The maximum yield value achieved, obviously at different temperatures for each fuel, is also different (75% for methanol at 700 ° C, followed by 74% for methane but at 1000 ° C and then by all the others up to 12% of propane, which appears to be, as already said several times, the worst). It should be noted that, exceeding 830 °C, ethanol outperforms glycerol in hydrogen yield.

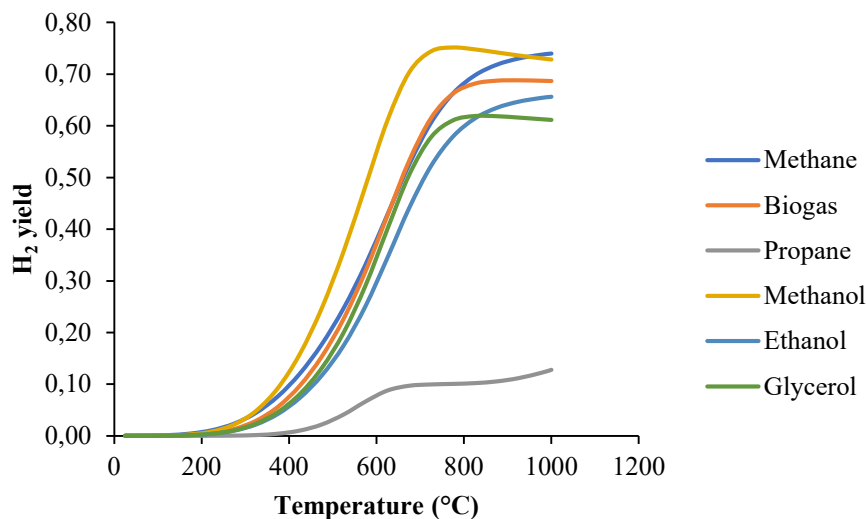*Figure 5.18 - Hydrogen yield vs temperature as function of fuel (P=1 bar and n=1)*

As was to be expected, by increasing the pressure (P=30 bar), the yield decreases significantly (Figure 5.19). The curves flatten and therefore it is necessary to move to much higher temperatures to obtain higher yields. This confirms the fact that steam reforming reactions are favoured at high temperatures and low pressures.
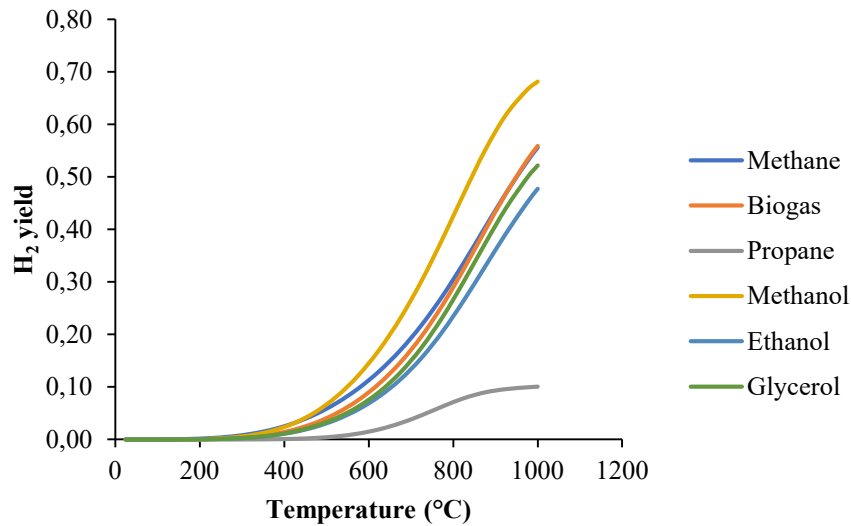
124

Figure 5.19 - Hydrogen yield vs temperature as function of fuel (P=30 bar and n=1)

By increasing the feed ratio to n = 10, as mentioned above, higher yields are obtained.

For n = 10 and P = 1 bar (Figure 5.20), all fuels show the same trend with a peak and then a slight decrease until reaching the stationary value. Unlike the same graph for n = 1, here the peaks, where the yield is maximum, are shifted to lower temperatures. This means that, increasing the water content in the feed, higher yields could be achieved at lower temperatures (96% at about 570 °C for methanol, 94% at 600 °C for methane and biogas, 90% for ethanol and 86% for glycerol at 630 °C, 84% for propane at 730 °C).

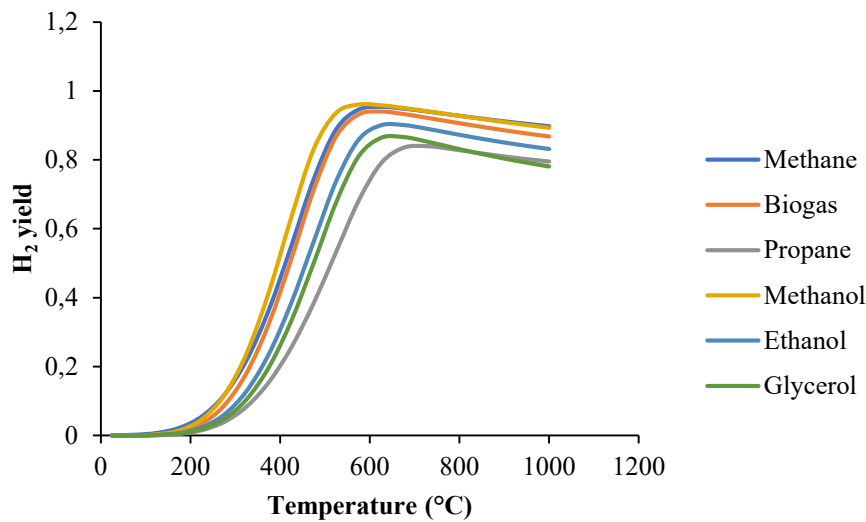
Figure 5.20 - Hydrogen yield vs temperature as function of fuel (P=1 bar and n=10)

By increasing the pressure, as already mentioned, the yields decrease, even if slightly, and the maximum value is reached for higher temperatures (Figure 5.21).
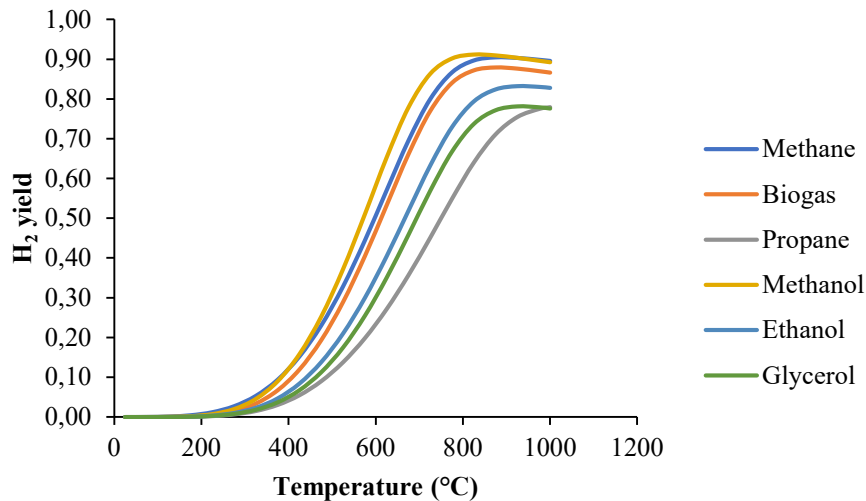
Figure 5.21 - Hydrogen yield vs temperature as function of fuel (P=30 bar and n=10)

Typically, ethanol steam reforming is carried out at 1 bar and has a good yield already at low temperatures (at temperatures below 600 °C it already has a yield of 80%); instead, methane steam reforming is typically carried out at higher pressures and, therefore, higher temperatures must be used. In fact, at 600 °C the methane has a yield of 50% and, for higher yields, it is necessary to reach 700÷800 °C.

At the value of n = n_{stoich}, the yield trend differs lightly between the various fuels only at 1 bar and for temperatures greater than 800 °C. In any case, at n = n_{stoic}, more than 80% cannot be obtained from thermodynamics and the hydrogen yield is always lower in the case of P=30 bar (Figure 5.22÷5.23).

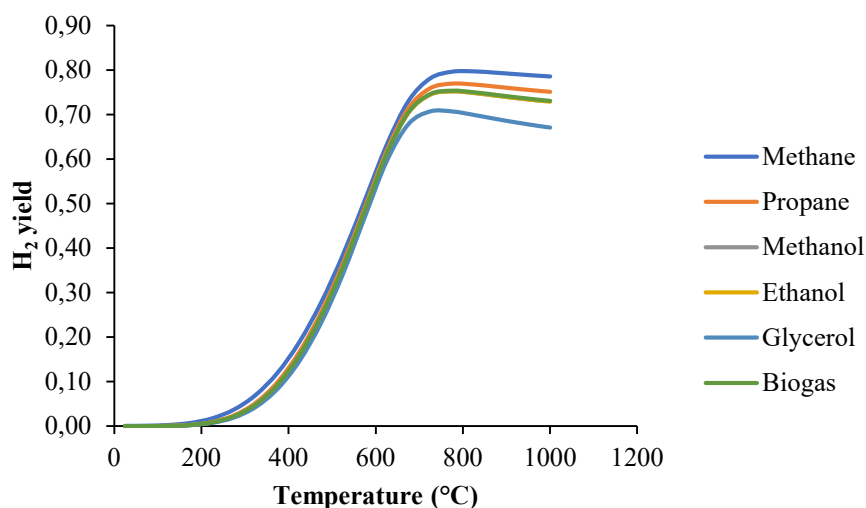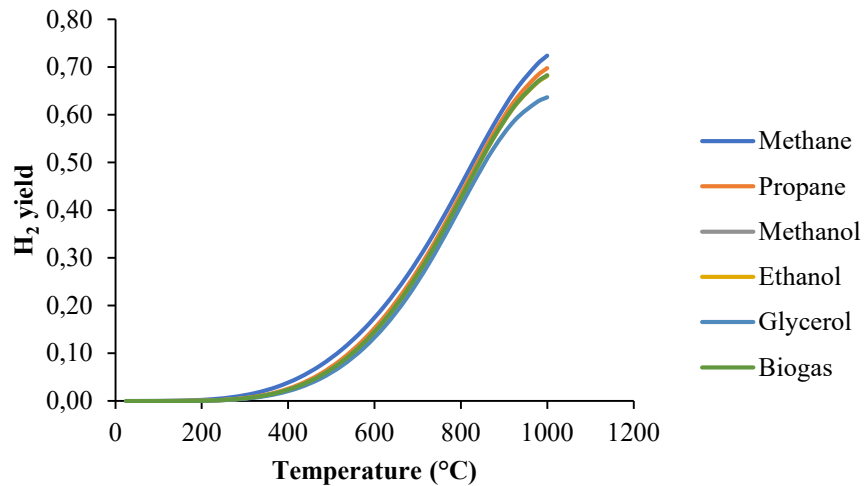*Figure 5.22 - Hydrogen yield vs temperature as function of fuel (P=1 bar and n=n_{stoic})*

126

Figure 5.23 - Hydrogen yield vs temperature as function of fuel (P=30 bar and n=n$_{stoic}$)

As seen in both paragraphs 5.3.1 and 5.3.2, biogas has hydrogen yields lower than methane or at the most similar to it. This is due to the non-negligible percentage of CO_2 in the feed. This CO_2, simultaneously, reacts with H_2 to form CO and H_2O. Thus, the water-gas-shift reaction is reversed because it is disadvantaged and so hydrogen yield decreases. In the operating conditions used to perform this thermodynamic analysis, the best parameters to have the highest yields (approximately 80% - 90%) for each fuel are the following:

-   pressure equal to 1 bar;
-   n = 10;
-   temperature between 570 °C and 730 °C, depending on the fuel.

In these conditions the scale of the fuels from the best to the worst in terms of hydrogen yield is reported:

methanol > methane > biogas > ethanol > glycerol > propane

Since our process takes place at 300 ° C, it is also necessary to report the comparison between the fuels relative to this temperature. For n=1 (Figure 5.9), the scale of the fuels from the best to the worst in terms of hydrogen yield is the following:

methane > methanol > biogas > glycerol > ethanol > propane

When n=10 (Figure 5.12), instead, there is only an inversion between ethanol and glycerol as seen below:

methane > methanol > biogas > ethanol > glycerol > propane

127

5.4. *Cyan* hydrogen production: process scheme

In this paragraph, the system tested for hydrogen production will be discussed in detail. It is based on double cycles of liquid alcohol and water, alternatively fed to the system and added to $NaBO_2 \cdot 4H_2O$, in order to exploit the co-catalytic effect of sodium metaborate to release hydrogen.

The test is schematized in Figure 5.24:
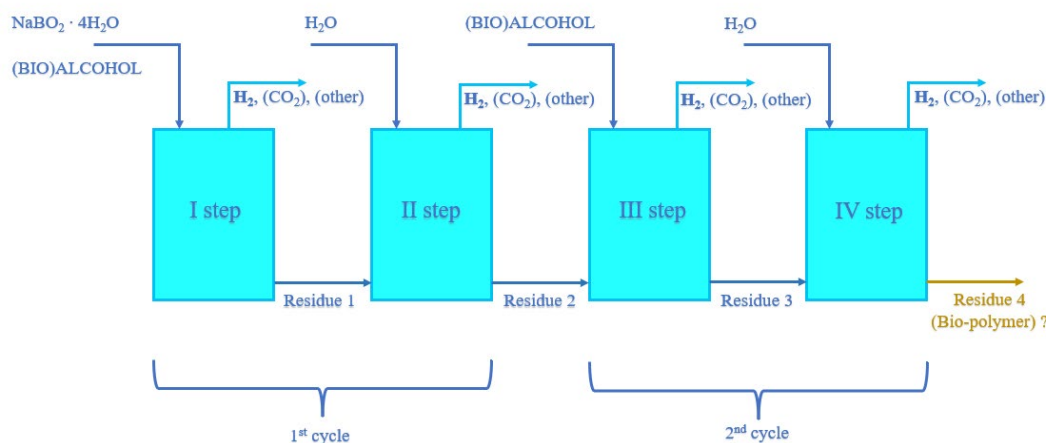
Figure 5.24 – Process Diagram

The tests are all performed in the PARR reactor, described in the *Chapter 4*. Being a closed system, the pressure increases indicating the formation of substances in the gaseous state. Therefore, the evolution of the reaction is investigated, using the increase in pressure over time as its indicative parameter. The pressure trend does not change. It is in all the tests increasing over time and reaches a different plateau value at each step. The reason why at some point the curve P-t reaches a plateau could be due to the achievement of the thermodynamic equilibrium of one of the reactions that evolve in the system.

In this work, the operating conditions that will always remain the same for each test and for each step are the following:

- Temperature: 300 °C;
- Stirring speed: 500 RPM;
- Mass of $NaBO_2 \cdot 4H_2O$ in the I step: 2 g;
- Reaction time: 6 h;

- Gas sampling temperature: 50 °C (in the test with methanol); 60 °C (for all the other tests).

In the following paragraphs, the other operating conditions - such as initial pressure, volume of the alcohol in the I and III step (depending on the alcohol chosen) and volume of water in the II and IV step - will be changed one at a time to verify their effect on the final results and to try to optimize the process in terms of hydrogen yield.

5.5. Standard double cycle ethanol-water

In this paragraph, the test carried out using ethanol as alcohol to be fed to the system is described. It is the test starting from which one operating condition will be changed at a time. Therefore, it will be used as the basis for all the following comparisons.

In this test, the operating conditions of each step are shown in Table 5.4:

Variables	*I step*	*II step*	*III step*	*IV step*
Temperature	300°C	300°C	300°C	300°C
Gas sampling temperature	60°C	60°C	60°C	60°C
Initial pressure (N_2)	0,3 barg	0,3 barg	0,3 barg	0,3 barg
Final pressure	12,9 barg	33,9 barg	39,4 barg	62,4 barg
Gas sampling pressure	0,5 barg	0,8 barg	0,8 barg	0,8 barg
Mass of $NaBO_2 \cdot 4H_2O$ (IN)	2 g	/	/	/
Volume of EtOH (IN)	5 mL	/	5 mL	/
Volume of H_2O (IN)	/	10 mL	/	10 mL
Stirring speed	500 RPM	500 RPM	500 RPM	500 RPM
Reaction time	6 h	6 h	6 h	6 h

Table 5.4 – Operating conditions of the standard double cycle EtOH-water

As shown in Figure 5.25, the pressure trend is always similar, i.e., it increases and then reaches a plateau value. This one is different in each step and increases going from step I

to step IV. The final pressures reached at the end of steps I, II, III and IV are respectively: 12,9 barg, 33,9 barg, 39,4 barg and 62,4 barg.

Each step has been interrupted after about six hours, as it was seen that it is a time necessary to reach a constant pressure value for an extended time, the so-called plateau, which is an indirect indication of gas production stop.
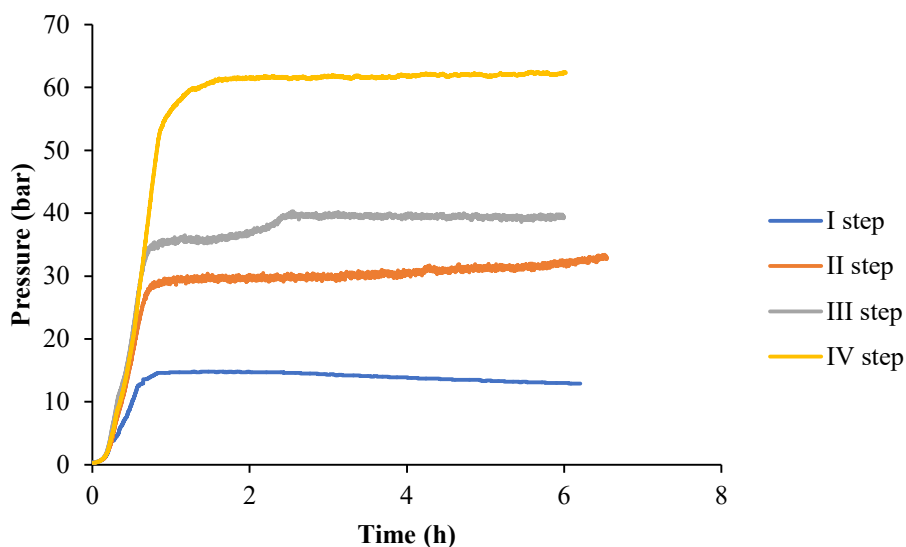
Figure 5.25 - Curve pressure-time for each step for standard double cycle EtOH-water

5.5.1. GC Analysis

The gases withdrawn at the end of each step were analysed in *microGC*. Only the volumetric compositions as a percentage of the compounds present in larger quantities (i.e., H_2, CO_2 and sometimes CH_4), normalized as explained below, are reported.

In the Table 5.5, normalized volumetric compositions (%) of the gas samples at each step are shown:

	H_2 *(%)*	CO_2 *(%)*	*Other (%)*
I step	**97,42**	2,41	0,18
II step	**98,17**	1,57	0,26
III step	**99,42**	0,31	0,27
IV step	**92,16**	1,52	6,32

Table 5.5 - Normalized volumetric compositions (%) of the gases leaving the reactor at each step

The compositions shown in the table do not include the inert, as mentioned above. The results show that there is a considerable production of hydrogen. Hydrogen obviously must always be purified, since the presence of impurities greatly reduces the application efficiency, but the gas stream produced already has a high degree of purity. This means that the ethanol exploits the co-catalytic effect of sodium metaborate in order to release hydrogen at a low temperature (300°C) compared to the multiple methods developed. Another relevant aspect lies in the fact that the reaction that evolves, under the operating conditions listed above, produces a minimum amount of CO_2. Some advantages of this process will be listed below. They justify the launch of an experimental campaign in order to investigate all aspects and optimize the operating conditions. The reactants are sodium metaborate tetrahydrate, which is a cheaper raw material and a waste by-product of some industrial operations and is also the by-product of $NaBH_4$ hydrolysis and the ethanol that can be produced from biomass. Another advantage concerns the fact that the operating temperature is relatively low compared to many hydrogen production methods. Moreover, a minimum amount of carbon dioxide is produced. Ethanol includes carbon atoms, for this reason if the composition of CO_2 is so low, due to a mass balance, the carbon atoms will be incorporated into the solid and/or liquid phase, or another possible explanation could be that carbon dioxide is consumed, participating in a reactive step. Therefore, it is very important to analyse the solid phase and the liquid phase taken at the end of the test.

5.5.2. Analysis of solid phase

At the end of IV step, the solid residue has been treated in accordance with the procedure explained in the *Chapter 4* and subjected to FTIR analysis.

The spectrum is reported in Figure 5.26:
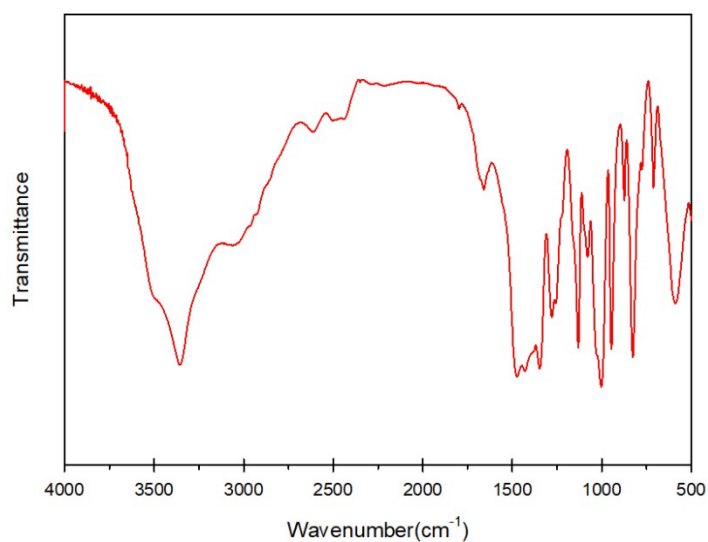
Figure 5.26 – FTIR spectrum of standard double cycle EtOH-H$_2$O

FTIR spectrum is quite similar to that of sodium tetraborate (Na$_2$B$_4$O$_7$ · H$_2$O) taken from NIST data (Figure 5.27).
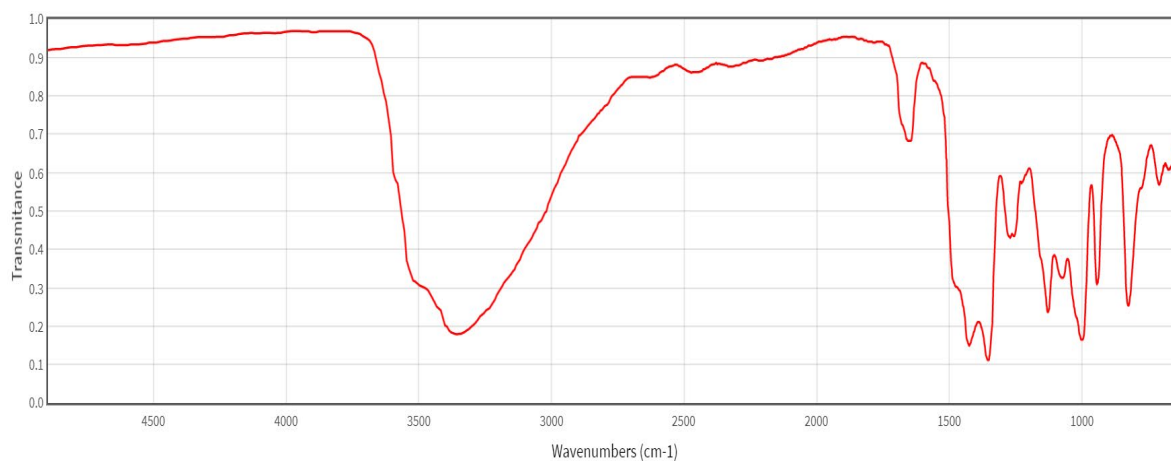

Figure 5.27 - FTIR of sodium tetraborate from NIST; Source: [205]

From literature data, a spectrum belonging to Na$_2$B$_4$O$_7$ · 10 H$_2$O was found that is similar to that of the solid residue. It is shown in Figure 5.28:
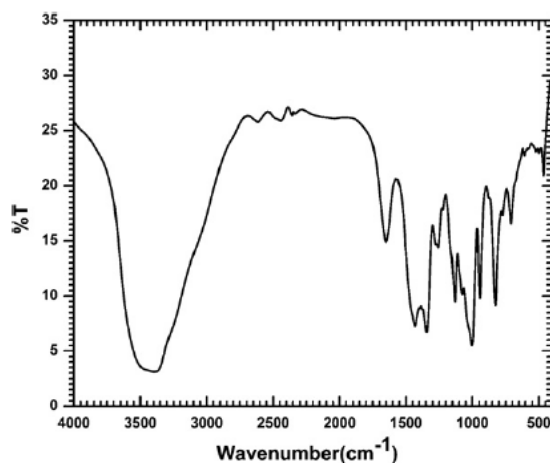
Figure 5.28 - FTIR spectrum of sodium tetraborate; Source: [206]

The assignment of the bands to the various functional groups is reported in the Table 5.6:

Band (cm⁻¹)	Assignment
3400	Stretching mode of OH
1650	Bending mode of H-O-H
1432	Asymmetric stretching of B–O bond in BO_3
1344	Asymmetric stretching of B–O bond in BO_3
1258	Asymmetric stretching of B–O bond in BO_3
1130	Asymmetric stretching of B–O bond in BO_4
1076	Asymmetric stretching of B–O bond in BO_4
944	Symmetric stretching of B–O in BO_3
826	Symmetric stretching of B–O in BO_4
710	Out-of plane bending of B–O in BO_3
500	O–B–O ring bending in the structure
454	O–B–O ring bending in the structure

Table 5.6 - Assignment of the absorption bands of the $Na_2B_4O_7 \cdot 10\,H_2O$; Source: [206]

133

The band at about 1650 cm^{-1} and the broad band at 3400 cm^{-1} shows that this compound contains water molecules. This could probably indicate that the solid residue would have needed more time to dry better.

So, the B-O bonds typical of borates, which are present in the low wavenumbers zone, would suggest the presence of this compound as main component in the solid residue. However, there is evidence of an organic phase in the residue. Organic peaks corresponding to C-H bonds in the range of 3000 cm^{-1}-2800 cm^{-1} are not clearly visible in the FTIR analysis because the bands are overlapping. However, the presence of the organic phase is evident in the solid residue through TG analysis, molecular weight analysis etc. but some organic phase is also present in the liquid residues (aromatic and aliphatic) [147].

Moreover, comparing the FTIR spectrum of the solid residue with that of sodium metaborate tetrahydrate (Figure 5.29), there do not seem to be any bands belonging to the metaborate, suggesting its complete conversion into $Na_2B_4O_7 \cdot 10\ H_2O$.

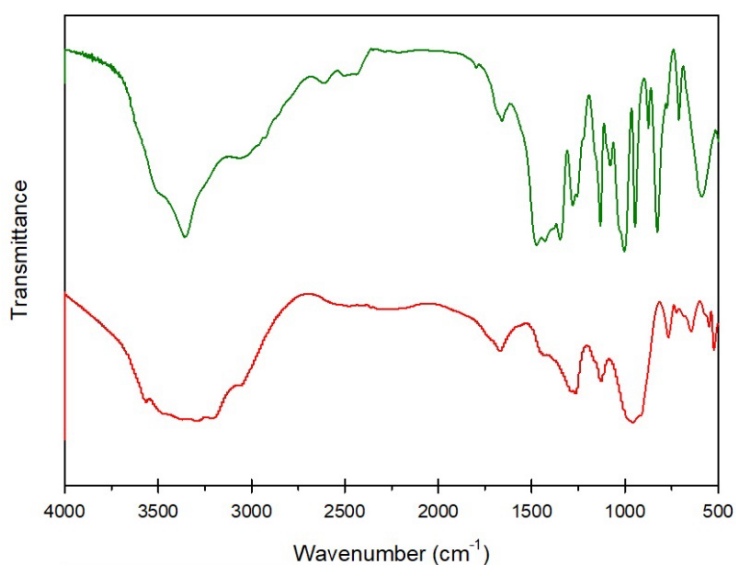*Figure 5.29 - FTIR spectrum of NaBO$_2$·4H$_2$O (red); FTIR spectrum of standard double cycle EtOH-H$_2$O (green)*

To investigate the thermal properties of the samples taken, a TG analysis in nitrogen flow was conducted. The results are reported in the Figure 5.30:
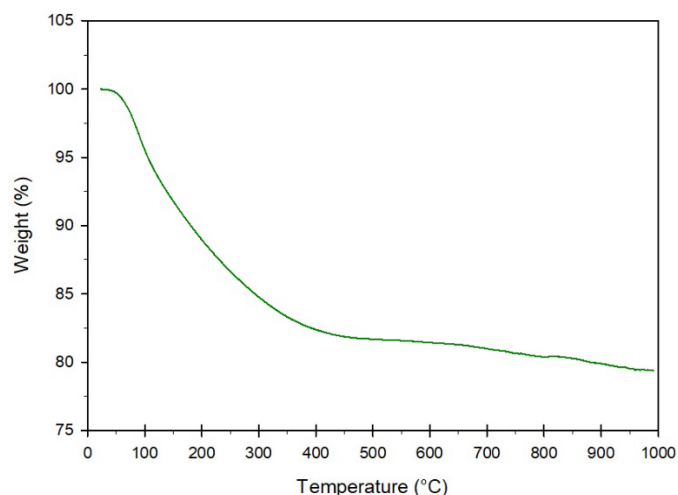
Figure 5.30 – TG (in N$_2$) analysis results (standard double cycle EtOH-H$_2$O)

As can be seen, the overall weight loss is 20% and occurs in a single step. The weight loss up to 200 °C corresponds to the desorption of water on the surface and the desorption of volatile compounds. Of major interest is the weight loss from 200 °C to 400 °C. In this range of temperature, the weight loss has been of about 10%. This degradation zone corresponds to full decomposition of the organic compounds, which are therefore estimated to be about 10% of the solid residue. Furthermore, the weight percentage change curve does not reach a plateau but continues to decrease slightly at the maximum temperature reached during the analysis, indicating possible decomposition at temperatures above 1000°C.

5.6. Double cycle ethanol-water: effect of the fed water

Here, it has been decided to change the quantity of water to be fed at the II and IV steps, in order to investigate the effect that water has in the success of the process. In particular, three double cycles were carried out, progressively decreasing the water content to avoid high dilution of the liquid residue. In the first of the three double cycle, 5 mL of water has been injected at the II step and IV step, in the second one 2,5 mL of water and in the last one 1,1 mL of water.

The operating conditions of each test are shown in the Table 5.7÷5.9:

Variables	I step	II step	III step	IV step
Temperature	300°C	300°C	300°C	300°C
Gas sampling temperature	60°C	60°C	60°C	60°C
Initial pressure (N_2)	0,3 barg	0,3 barg	0,3 barg	0,3 barg
Final pressure	11,7 barg	24,3 barg	22,4 barg	36,4 barg
Gas sampling pressure	0,9 barg	0,9 barg	0,9 barg	0,9 barg
Mass of $NaBO_2 \cdot 4H_2O$ (IN)	2 g	/	/	/
Volume of EtOH (IN)	5 mL	/	5 mL	/
Volume of H_2O (IN)	/	**5 mL**	/	**5 mL**
Stirring speed	500 RPM	500 RPM	500 RPM	500 RPM
Reaction time	6 h 19'	6 h 32'	7 h 15'	6 h 20'

Table 5.7 - Operating conditions of Double cycle EtOH-H_2O: 5 mL H_2O

Variables	I step	II step	III step	IV step
Temperature	300°C	300°C	300°C	300°C
Gas sampling temperature	60°C	60°C	60°C	60°C
Initial pressure (N_2)	0,3 barg	0,3 barg	0,3 barg	0,3 barg
Final pressure	12,7 barg	18,4 barg	23,3 barg	27,9 barg
Gas sampling pressure	0,8 barg	0,9 barg	1 barg	0,9 barg
Mass of $NaBO_2 \cdot 4H_2O$ (IN)	2 g	/	/	/
Volume of EtOH (IN)	5 mL	/	5 mL	/
Volume of H_2O (IN)	/	**2,5 mL**	/	**2,5 mL**
Stirring speed	500 RPM	500 RPM	500 RPM	500 RPM
Reaction time	6 h	6 h	6 h 22'	7 h 09'

Table 5.8 - Operating conditions of Double cycle EtOH-H_2O: 2,5 mL H_2O

Variables	I step	II step	III step	IV step
Temperature	300°C	300°C	300°C	300°C
Gas sampling temperature	60°C	60°C	60°C	60°C
Initial pressure (N_2)	0,3 barg	0,3 barg	0,3 barg	0,3 barg
Final pressure	14,4 barg	18,9 barg	18,6 barg	18,8 barg
Gas sampling pressure	0,7 barg	0,9 barg	0,8 barg	0,8 barg
Mass of $NaBO_2 \cdot 4H_2O$ (IN)	2 g	/	/	/
Volume of EtOH (IN)	5 mL	/	5 mL	/
Volume of H_2O (IN)	/	**1,1 mL**	/	**1,1 mL**
Stirring speed	500 RPM	500 RPM	500 RPM	500 RPM
Reaction time	6 h 2'	6 h 2'	6 h 1'	6 h 11'

Table 5.9 - Operating conditions of Double cycle EtOH-H_2O: 1,1 mL H_2O

The pressure trends over time, for each test, are reported in the Figure 5.31-5.33:

Figure 5.31 - Curve pressure-time for each step for double cycle EtOH-water with 5 mL H_2O (the trend of curve grey is not growing monotone due to some experimental fluctuations)
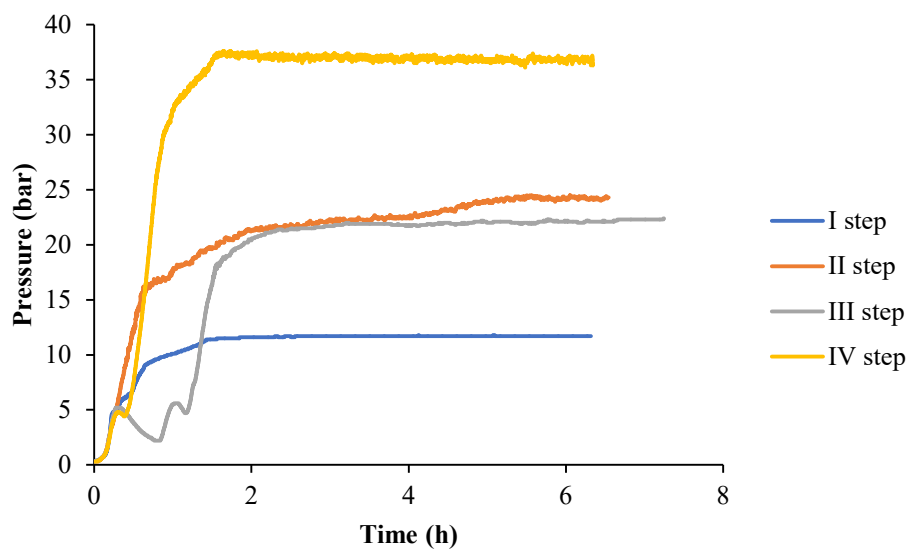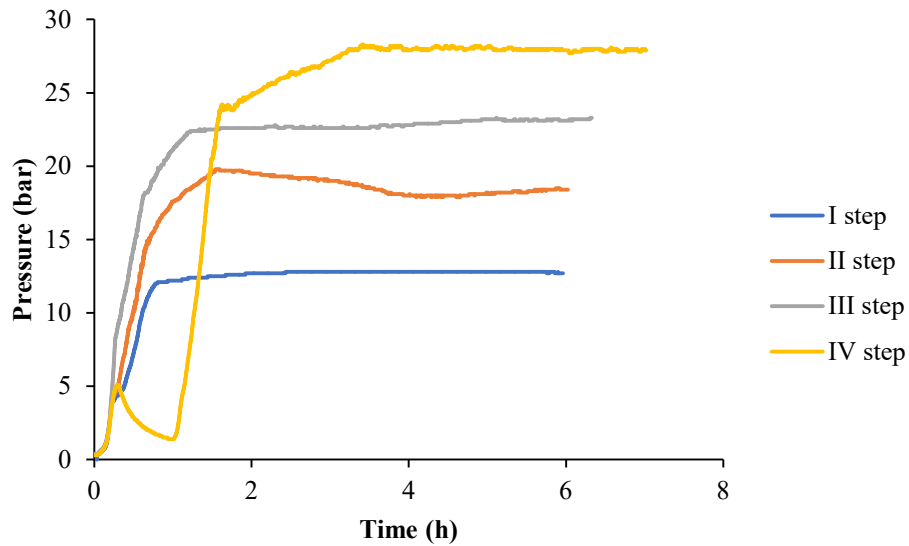
Figure 5.32 - Curve pressure-time for each step for double cycle EtOH-water with 2,5 mL H₂O (the trend of curve yellow is not growing monotone due to some experimental fluctuations)
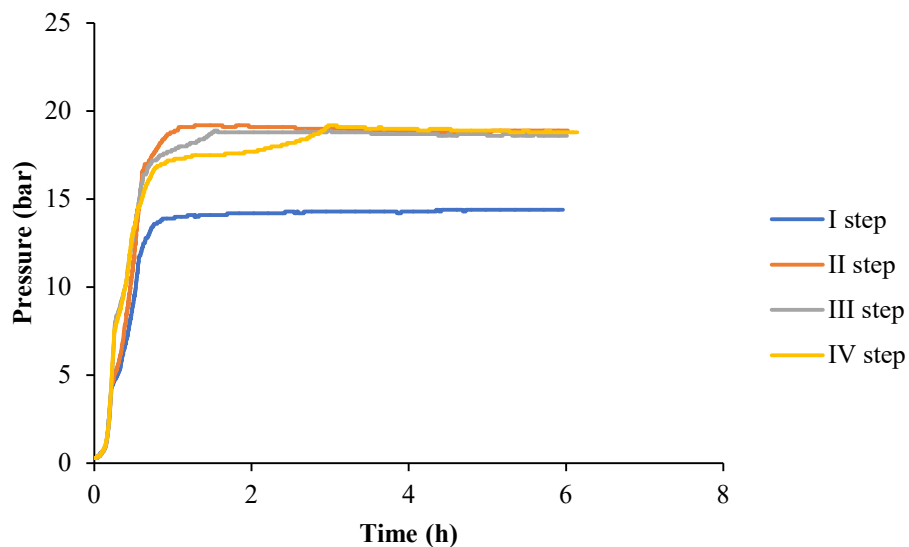
Figure 5.33 - Curve pressure-time for each step for double cycle EtOH-water with 1,1 mL H₂O

The P-t trends always have the same qualitative trend, except for the III step of the test with 5 mL of water and the IV step of the test with 2.5 mL of water for experimental fluctuations.

As can be seen from the graphs above, in the first step the final pressure reached is more or less always the same, demonstrating a good reproducibility of I step that is always the same in all three tests. In the test with 1.1 mL of water, the trend of the II, III and IV steps are almost identical. This could be attributed to the fact that the amount of water fed was very low.

138

5.6.1. GC Analysis

The gas samples at each step are subjected to GC analyses. In the Table 5.10÷5.12, normalized volumetric compositions (%) of the gases leaving the reactor at each step for the three tests are shown:

	H_2 (%)	CO_2 (%)	CH_4 (%)	Other (%)
I step	92,85	0,18	3,93	3,04
II step	88,03	0,14	4,22	7,62
III step	58,01	39,89	0,00	2,10
IV step	93,26	0,27	1,06	5,40

Table 5.10 - Normalized volumetric compositions (%) of the gases leaving the reactor at each step: test with 5 mL H_2O

	H_2 (%)	CO_2 (%)	CH_4 (%)	Other (%)
I step	94,88	0,20	0,00	4,91
II step	95,14	0,31	1,04	3,52
III step	94,46	0,24	0,74	4,56
IV step	25,79	71,66	0,00	2,54

Table 5.11 - Normalized volumetric compositions (%) of the gases leaving the reactor at each step: test with 2,5 mL H_2O

	H_2 (%)	CO_2 (%)	CH_4 (%)	Other (%)
I step	93,77%	0,81%	0,77%	4,65%
II step	91,39%	0,37%	0,72%	7,52%
III step	96,62%	1,15%	0,81%	1,41%
IV step	95,54%	0,30%	1,02%	3,14%

Table 5.12 - Normalized volumetric compositions (%) of the gases leaving the reactor at each step: test with 1,1 mL H_2O

The results show that changing the water content has minimal influence on the hydrogen production. In fact, it slightly decreases by a few percentage points compared to the standard double cycle with 10 mL of water, as does the volumetric composition of CO_2. Consequently, the volumetric composition of other species present rises slightly. Among others, in fact, the presence of methane is highlighted. It is not present in the double cycle with 10 mL, probably due to the excess of water with respect to the fed ethanol, which results sub-stoichiometric.

It should be noted that the lower percentage of hydrogen at step III of the test with 5 mL of water and at step IV of the test with 2,5 mL of water is most likely due to the experimental drawbacks discussed above.

5.6.2. Analysis of solid phase

The solid residues collected at the end of each test were dried as described in chapter 4 and subjected to FTIR analysis. In the Figure 5.34, the spectra of each test are shown compared with the spectrum of the reagent $NaBO_2 \cdot 4H_2O$:
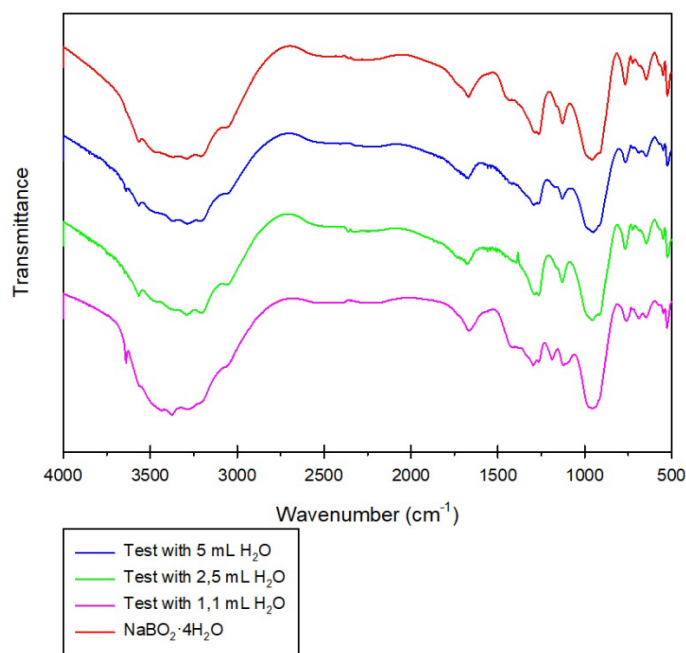

Figure 5.34 – FTIR spectrum of double cycle with 5 mL H_2O (blue), FTIR spectrum of double cycle with 2,5 mL H_2O (green); FTIR spectrum of double cycle with 1,1 mL H_2O (pink); FTIR spectrum of $NaBO_2$ $\cdot 4H_2O$ (red)

Even by decreasing the amount of water in the tests, in the range 3000 cm^{-1} - 2800 cm^{-1}, organic peaks are not easily appreciated.

As can be seen, the spectra appear to be identical in the position of the peaks but also in intensity. All three spectra are completely coincident with that of the metaborate, probably due to the high quantity of $NaBO_2 \cdot 4H_2O$ present in the solid residue. The interpretation of this result is not easy to understand. It was enough to halve the quantity of water to be fed to find some metaborate unconverted at the end of the process. Therefore, further investigations should be carried out, perhaps trying to carry out other tests using a quantity of water between 10 mL (where it was seen that the spectrum was different from the metaborate) and 5mL, to try to find the optimal condition between not having too much dilution in water and not having too much unconverted metaborate.

In order to investigate the thermal properties of the samples, a TG analysis was conducted. Nitrogen was fluxed as purge gas and the sample was heated at a rate of 10 °C min^{-1} to 1000°C. TG curves are shown in Figure 5.35÷5.37.

The TG curves of the tests with 5 mL, 2,5 mL and 1,1 mL exhibit an overall weight loss of 50 %, 40 % and 52 % respectively. For all samples, the weight loss up to 200 °C corresponds to the desorption of water on the surface and the desorption of volatile compounds. Of major interest is the weight loss from 200 °C to 400 °C. This degradation zone corresponds to full decomposition of the organic compounds.

In the tests with 5 mL and 2,5 mL, a weight loss of only a few percentage points is noted between 200 ° C and 400 ° C, while in the test with 1.1 mL the weight loss in that temperature range is much greater (about 13%). Furthermore, in the thermogram of the latter, three different changes in the slope of the curve can be seen in the temperature range 350÷450 °C, whereas for the residues of the tests with a higher water content, only two changes can be seen. Therefore, a percentage of 13% of the solid residue of the test with 1.1 mL is attributable to organic compounds.
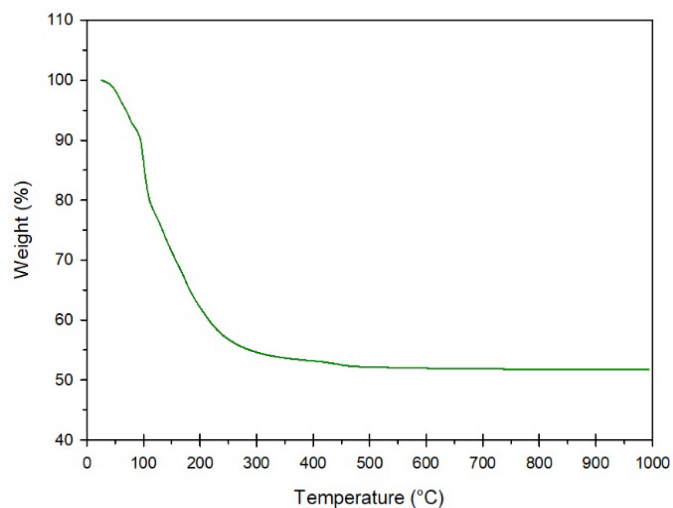
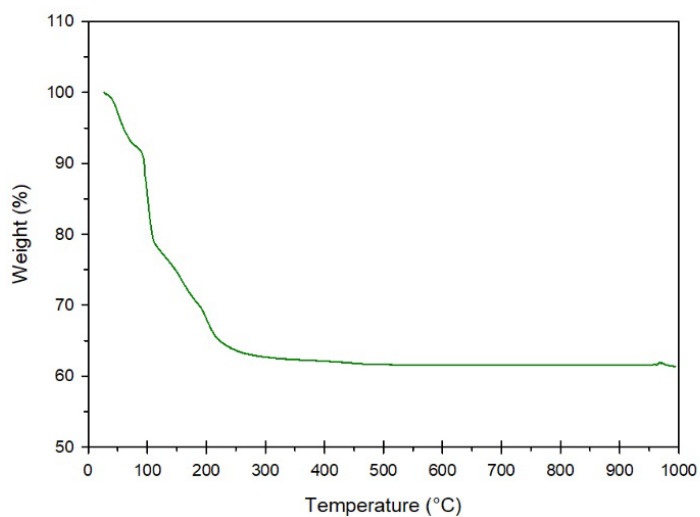*Figure 5.35 – TG (in N_2) analysis results (test with 5 mL H_2O)*

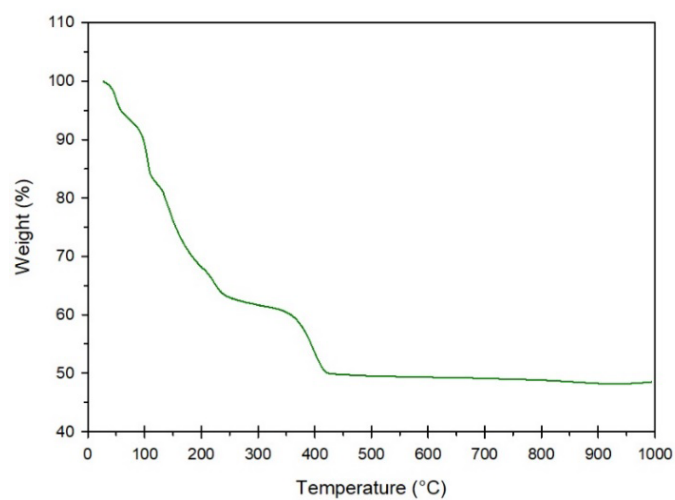*Figure 5.36 - TG (in N_2) analysis results (test with 2,5 mL H_2O)*

Figure 5.37 - TG (in N_2) analysis results (test with 1,1 mL H_2O)

To better visualize the differences, TG curves of the three tests are shown all on the same graph in Figure 5.38:
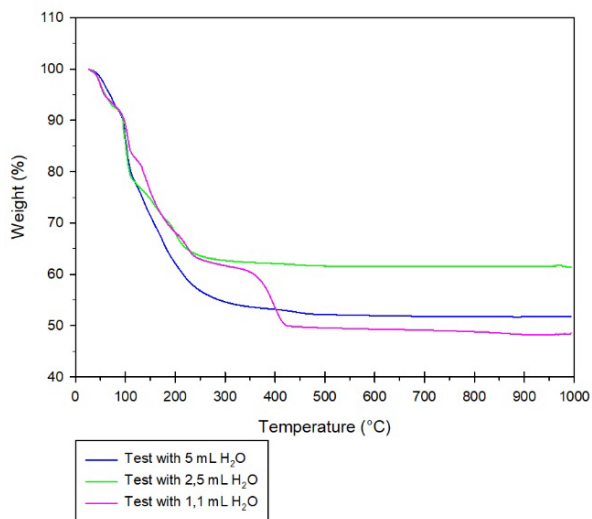

Figure 5.38 - TG (in N₂) analysis results (blue: test with 5 mL H₂O; green: test with 2,5 mL H₂O; pink: test with 1,1 mL H₂O)

As can be seen, when the water content in the feed stream varies, the curves have different slopes. In particular, in the test with 5 mL of water there is a unique slope that reaches the plateau; in the test with 2,5 mL of water a small difference in slope begins to be seen at intermediate temperatures; in the test with 1,1 mL there are two slopes totally separated. Having different slopes means that different species are decomposing with different rates of decomposition.

In the case of the test with 1,1 mL of water, the end decomposition temperature is shifted to 400 °C, indicating a more complex organic species. By increasing the water content in the feed stream, the decomposition ends at lower and lower temperatures. In fact, the end decomposition temperature decreases until it reaches about 250 ° C for the test with 5 mL of water.

5.7. Double cycle ethanol-water: effect of starting pressure

Subsequently, a test was also carried out by increasing the initial pressure of N_2 at the beginning of each step to see how an increase in pressure could influence the hydrogen yield but also the formation of a possible polymer in the final residue, knowing that the formation of polymers is favoured at high pressure. It was decided to use 5 barg of inert gas as the initial pressure. For safety reasons, it was decided not to increase the initial pressure too much due to the operating limits of the reactor used.

The operating conditions of the test are shown in the Table 5.13:

Variables	I step	II step	III step	IV step
Temperature	300°C	300°C	300°C	300°C
Gas sampling temperature	60°C	60°C	60°C	60°C
Initial pressure (N_2)	**5 barg**	**5 barg**	**5 barg**	**5 barg**
Final pressure	20,2 barg	44,6 barg	40,1 barg	66,1 barg
Gas sampling pressure	From 6,1 to 4,1 barg	From 6 to 4 barg	From 6,1 to 4,6 barg	From 6,1 to 4,4 barg
Mass of $NaBO_2 \cdot 4H_2O$ (IN)	2 g	/	/	/
Volume of EtOH (IN)	5 mL	/	5 mL	/
Volume of H_2O (IN)	/	10 mL	/	10 mL
Stirring speed	500 RPM	500 RPM	500 RPM	500 RPM
Reaction time	6 h 1'	6 h	5 h 57'	6 h

Table 5.13 - Operating conditions of Double cycle EtOH-H_2O: 5 barg

As shown in Table 5.13, the pressure was still high at the time of gas sampling (about 6 barg). Hence, it was decided to take only a certain amount in order not to break the gas sampling bag. The remaining gas was vented under the hood.

The trend of the P-t curve for each step is shown in Figure 5.39:
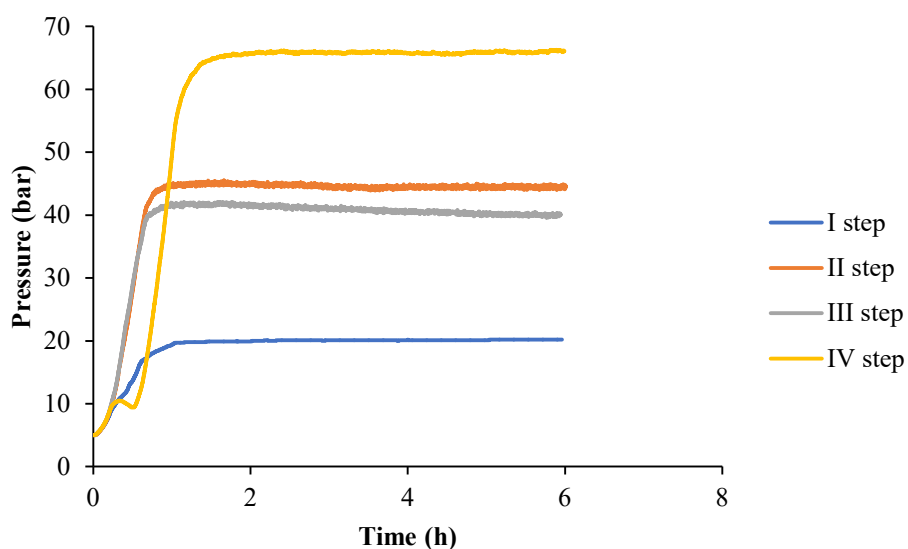
Figure 5.39 - Curve pressure-time for each step for double cycle EtOH-water at 5 barg

The final pressure value reached at each step is higher than that reached in the standard double cycle but not as much as we could have expected. Furthermore, a difference can be observed with respect to all the other tests, namely the fact that the final pressure reached in the III step is lower than that in the II step.

5.7.1. GC Analysis

The gas withdrawals at each step are subjected to GC analyses and the results are shown in Table 5.14:

	H_2 (%)	CO_2 (%)	Other (%)
I step	**90,84**	0,62	8,54
II step	**91,64**	1,25	7,12
III step	**95,33**	0,82	3,84
IV step	**90,10**	0,50	9,40

Table 5.14 - Normalized volumetric compositions (%) of the gases leaving the reactor at each step: test with starting pressure of 5 barg

Compared to the standard double cycle, the increase in pressure causes a lowering of the volumetric composition of hydrogen in favour of other species. This could suggest that

145

what happens in the reactor is very similar to the steam reforming reaction, which is also disadvantaged at high pressures. Obviously, it cannot be said with certainty that what happens is steam reforming or not. Further investigations should be made. However, already the fact that hydrogen is produced at significantly lower temperatures than steam reforming makes this process very promising also because it is possible to produce minimal quantities of CO_2.

5.7.2. Analysis of solid phase

The solid residue obtained at the end of the double cycle with an initial pressure of 5 barg was also subjected to FTIR analysis. The resulting spectrum is provided in the Figure 5.40:
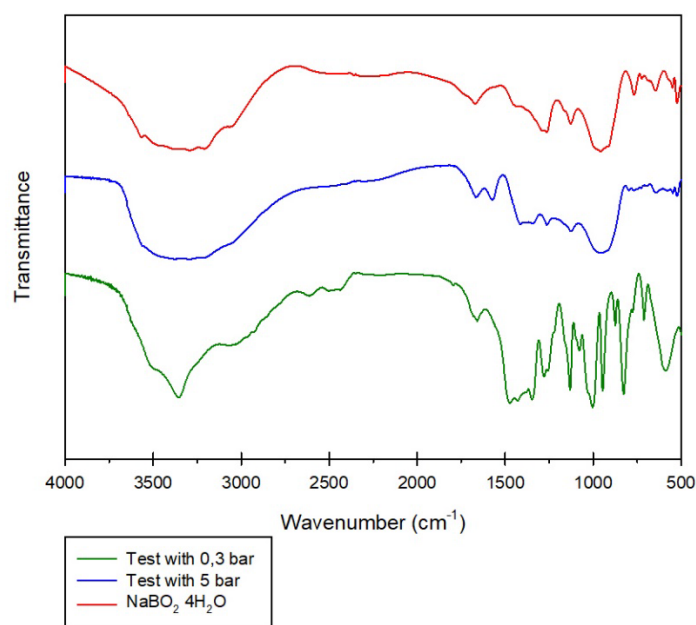
Figure 5.40 - FTIR spectrum of double cycle with 5 bar (blue), FTIR spectrum of standard double cycle with 0,3 bar (green); FTIR spectrum of NaBO₂ ·4H₂O (red)

From the comparison with the spectrum of $NaBO_2 \cdot 4H_2O$, some similarities of peaks in the range between 1750 cm^{-1} and 800 cm^{-1} can be seen, in particular at wavenumber of 1750 cm^{-1}, 1500 cm^{-1}, 1200 cm^{-1}, 1100cm^{-1} and 850 cm^{-1}. The range between 1300 cm^{-1} and 500 cm^{-1} is the so-called fingerprint zone, which is the area whose peaks are typical and characteristic signals of the molecule. It makes sure that it is not possible for different molecules to have the same infrared spectrum. Although in the test with an initial pressure of 5 bar in this area the peaks are not very evident (especially between 800cm^{-1} and 500cm^{-1}), they are in any case at the same wavenumbers. At higher wavenumbers it is not possible to give an evaluation because the peaks, if they exist, cannot be appreciated well.

146

Thus, it could be assumed that these higher-pressure conditions could disadvantage the process and leave some metaborate unconverted. However, further investigations should be made to confirm this hypothesis, perhaps even increasing the initial pressure a little more before each step.

To investigate the thermal properties of the sample, TG analysis was conducted. Nitrogen was fluxed as purge gas and the sample was heated at a rate of 10°C min^{-1} to 1000°C. The TG curve is shown in the Figure 5.41:
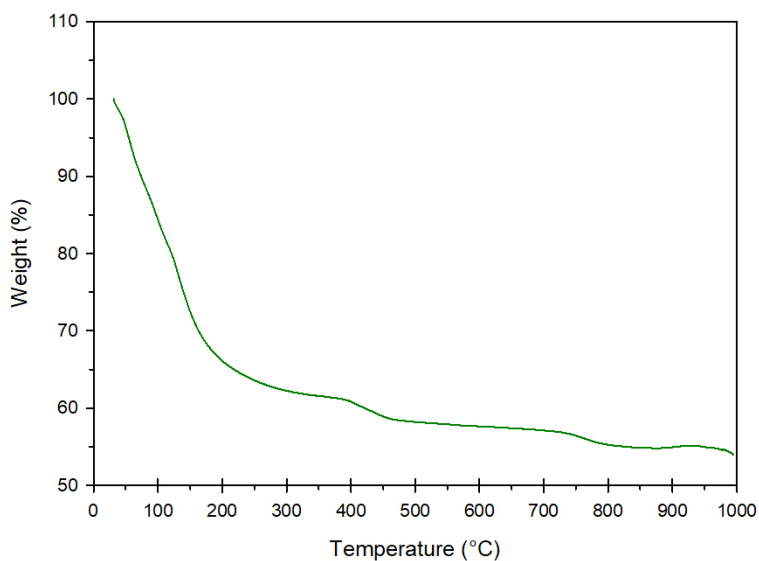
Figure 5.41 - TG (in N₂) analysis results (test with starting pressure of 5 bar)

The result indicates that the overall weight loss is 45 %. The weight loss of major interest is that from 200 °C and 400 °C and corresponds to 3 %, so a percentage of 3 % of the solid residue is ascribable to organic compounds. Being a very low percentage, it is normal that in the FTIR spectrum it is not possible to appreciate any organic peak.

5.8. Double cycle alcohol-water: effect of different (bio)alcohols

Finally, other tests were carried out by changing the alcohol fed to the I step and III step to see if and how this could affect the hydrogen yield. In particular, methanol and glycerol were chosen as two other alcohols to compare with ethanol.

Different volumes of alcohol have been fed compared to the double standard EtOH-water cycle, ensuring that the moles fed to the system are always the same. The calculation of the volumes to be fed is explained below.

Knowing the density and molecular weight of ethanol, the moles of ethanol injected with 5mL are calculated below:

$$n_{EtOH} = \frac{m_{EtOH}}{MW_{EtOH}} = \frac{\rho_{EtOH} \cdot V_{EtOH}}{MW_{EtOH}} = \frac{0,789 \frac{g}{mL} \cdot 5mL}{46,07 \frac{g}{mol}} = 0,085 \; mol$$

It was chosen to inject the same moles for each alcohol used, namely:

$$n_{EtOH} = n_{MetOH} = n_{Glycerol} = 0,085 \; mol$$

Then, it is necessary to calculate the volume to be injected respectively of methanol and glycerol so that this number of moles are injected for both:

$$V_{MetOH} = \frac{m_{MetOH}}{\rho_{MetOH}} = \frac{n_{MetOH} \cdot MW_{MetOH}}{\rho_{MetOH}} = \frac{0,085mol \cdot 32,04 \frac{g}{mol}}{0,792 \frac{g}{mL}} = 3,5 \; mL$$

$$V_{Glycerol} = \frac{m_{Glycerol}}{\rho_{Glycerol}} = \frac{n_{Glycerol} \cdot MW_{Glycerol}}{\rho_{Glycerol}} = \frac{0,085mol \cdot 92,09 \frac{g}{mol}}{1,26 \frac{g}{mL}} = 6,2 \; mL$$

The molecular weight and density of each alcohol used for these calculations are shown in the Table 5.15:

	Molecular Weight (g/mol)	*Density (g/mL)*
Ethanol	46,07	0,789
Methanol	32,04	0,792
Glycerol	92,09	1,26

Table 5.15 – Molecular weight and density of the alcohols

The operating conditions of each test are shown in the Table 5.16÷5.17:

Variables	I step	II step	III step	IV step
Temperature	300°C	300°C	300°C	300°C
Gas sampling temperature	50°C	50°C	50°C	50°C
Initial pressure (N_2)	0,3 barg	0,3 barg	0,3 barg	0,3 barg
Final pressure	13,6 barg	43,7 barg	33,3 barg	55,2 barg
Gas sampling pressure	0,8 barg	0,7 barg	0,8 barg	0,8 barg
Mass of $NaBO_2 \cdot 4H_2O$ (IN)	2 g	/	/	/
Volume of MetOH (IN)	**3,5 mL**	/	**3,5 mL**	/
Volume of H_2O (IN)	/	10 mL	/	10 mL
Stirring speed	500 RPM	500 RPM	500 RPM	500 RPM
Reaction time	5 h 47'	6 h 9'	6 h 10'	5 h 45'

Table 5.16 - Operating conditions of Double cycle MetOH-H_2O

Variables	I step	II step	III step	IV step
Temperature	300°C	300°C	300°C	300°C
Gas sampling temperature	60°C	60°C	60°C	60°C
Initial pressure (N_2)	0,3 barg	0,3 barg	0,3 barg	0,3 barg
Final pressure	13,2 barg	32,4 barg	30,8 barg	50,9 barg
Gas sampling pressure	1,9 barg	0,8 barg	0,9 barg	0,8 barg
Mass of $NaBO_2 \cdot 4H_2O$ (IN)	2 g	/	/	/
Volume of Glycerol (IN)	**6,2 mL**	/	**6,2 mL**	/
Volume of H_2O (IN)	/	10 mL	/	10 mL
Stirring speed	500 RPM	500 RPM	500 RPM	500 RPM
Reaction time	5 h 59'	6 h	6 h	6 h

Table 5.17 - Operating conditions of Double cycle Glycerol-H_2O

The pressure trends over time, for each test, are reported in the Figure 5.42÷5.43, which refer to methanol and glycerol double cycle respectively:
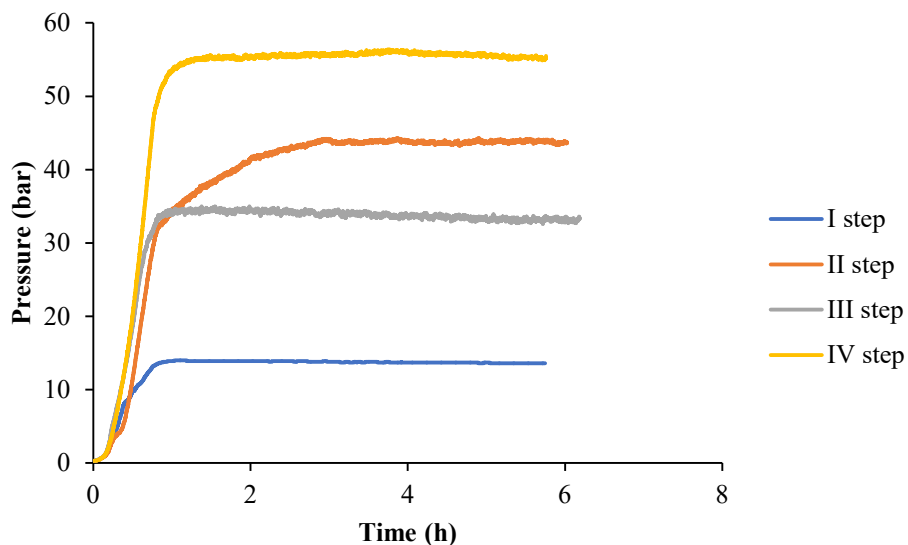
Figure 5.42 - Curve pressure-time for each step for methanol double cycle
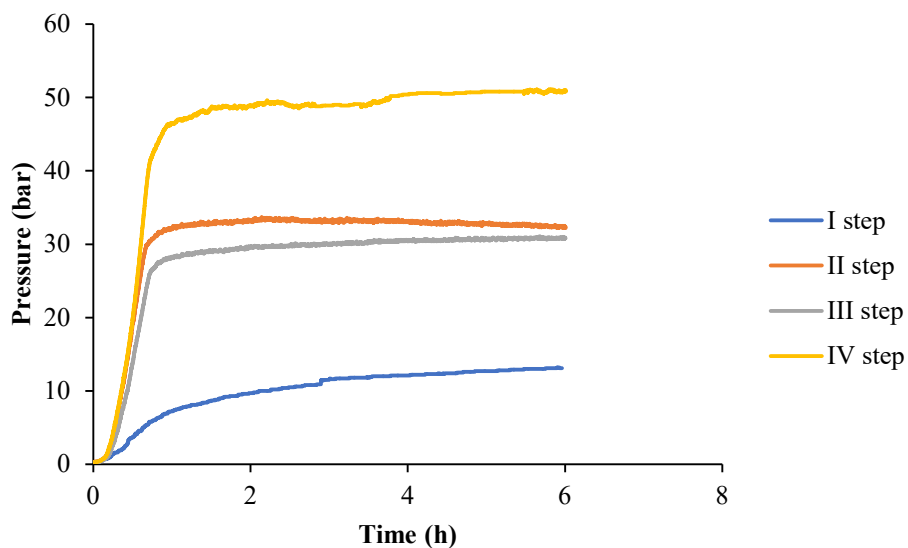
Figure 5.43 - Curve pressure-time for each step for glycerol double cycle

In the first step, the plateau value of the pressure is almost similar for all reagent tested. In step II, however, it is still similar for ethanol and glycerol, while it is about ten bars higher for methanol. Furthermore, the pressure-time curve referring to methanol reaches the plateau value in about three hours, while for the other reagents the plateau is reached after about 1 hour. In step III, the pressure plateau value is a bit higher for ethanol as well

as for step IV. It should be noted, however, that during the first step of the test with glycerol, the final plateau value was not well reached in the 6 hours of the test. On the graph, it is not possible to appreciate this well for a matter of scale. Most likely, more time would have taken because the boiling point of glycerol is 290 °C. Hence, as long as 290 ° C is not exceeded, the glycerol is still liquid.

5.8.1. GC Analysis

The gas withdrawals at each step are subjected to GC analyses and the results are shown in Table 5.18÷5.19:

	H_2 (%)	CO_2 (%)	CH_4 (%)	Other (%)
I step	27,87	69,59	0,00	2,54
II step	96,15	0,17	0,37	3,32
III step	98,30	0,11	0,71	0,88
IV step	97,86	0,30	0,21	1,63

Table 5.18 - Normalized volumetric compositions (%) of the gases leaving the reactor at each step: test with methanol

	H_2 (%)	CO_2 (%)	CH_4 (%)	Other (%)
I step	56,20	37,73	4,89	1,19
II step	49,28	47,07	2,77	0,88
III step	52,97	41,97	3,64	1,42
IV step	45,66	49,94	2,84	1,55

Table 5.19 - Normalized volumetric compositions (%) of the gases leaving the reactor at each step: test with glycerol

As regards methanol, a very low production of hydrogen (below 30%) is observed in the step I if compared with the step I of the test with ethanol and also an excessive production of CO_2. From the step II onwards, the yield to hydrogen assumes values that are entirely

151

similar to those of the test with ethanol. Even at the step IV, the hydrogen composition is even higher.

In the test with glycerol, the observed hydrogen yields are much lower. In fact, an excessive production of CO_2 and an appreciable presence of CH_4 is observed compared to methanol and ethanol. Therefore, only from the analysis of the gases, it would seem that the use of glycerol goes against the objectives of our process namely H_2 production while producing little CO_2. However, it is also necessary to analyse the solid and liquid residue to have further indications about its use. In fact, if it were possible to produce a high added value polymer using glycerol, which is a waste material, and in addition it was also able to produce hydrogen, it would still be a stimulating process even if the hydrogen yields were not really very high.

5.8.2. Analysis of solid phase

As regards the solid residue, it is appropriate to compare the spectra of the FTIR analysis of the various tests with different alcohols used. The FTIR spectra are shown in the Figure 5.44:
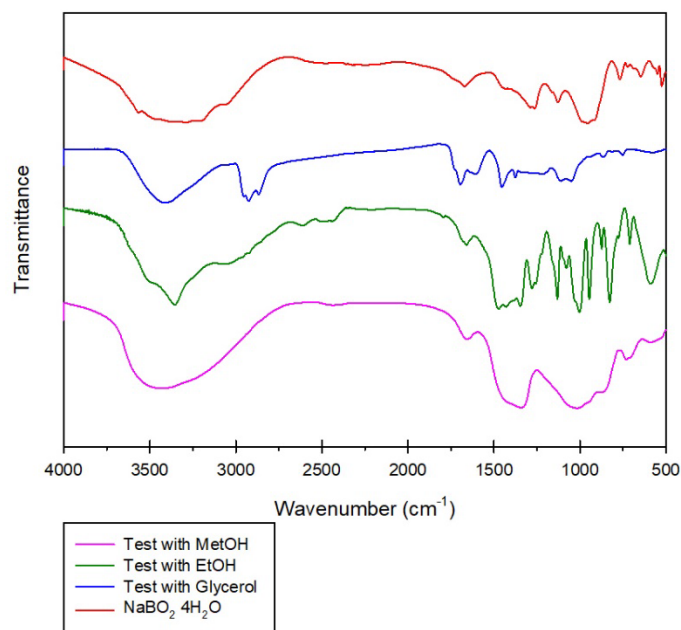
Figure 5.44 - FTIR spectrum of double cycle with glycerol (blue), FTIR spectrum of standard double cycle with ethanol (green); FTIR spectrum of double cycle with methanol (pink); FTIR spectrum of $NaBO_2 \cdot 4H_2O$ (red)

At first glance, it can be seen immediately that all three spectra differ almost entirely from the spectrum of sodium metaborate. This proves the fact that it reacted almost completely in the system. In the test with glycerol, it can be seen immediately that two weak bands

are present in the area between 2800 cm^{-1} and 3000 cm^{-1}. These bands are due to C-H stretching. This result is very promising as this could be indicative of the formation of a polymer. The broad band in the range (3500÷3000 cm^{-1}) is instead associated with the OH stretching.

A comparison between FTIR spectrum of test with glycerol with FTIR spectrum of different polymers is shown in Figure 5.45:
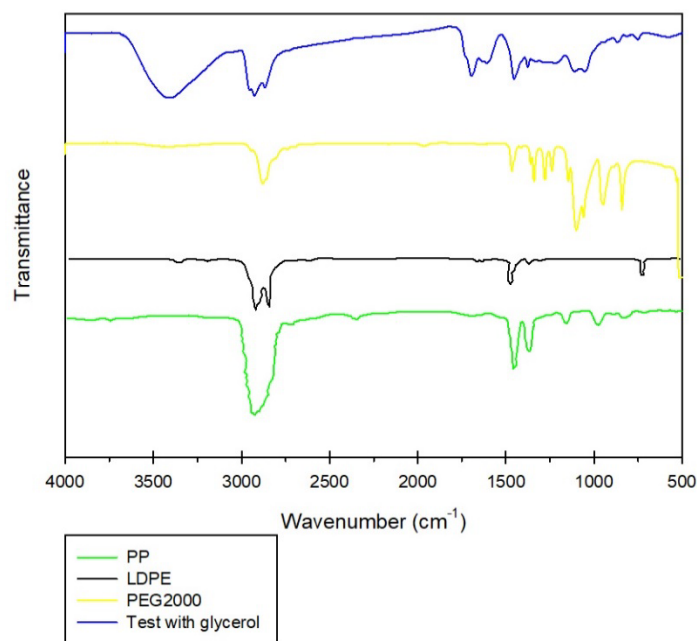

Figure 5.45 - FTIR spectrum of PP (green); FTIR spectrum of LDPE (black); FTIR spectrum of PEG2000 (yellow); FTIR spectrum of test with glycerol (blue)

In particular, the peaks in the range (2800 cm^{-1} ÷ 3000 cm^{-1}), typical of C-H stretching, are very similar to FTIR spectrum of PE. Another peak in common with the PE can be found at wavenumbers of about 1500 cm^{-1}. The band at around 1500 cm^{-1} it is also typical of the PEG and PP.

However, what has just been said are only suppositions. Anyway, other different analyses will have to be made to affirm with certainty the nature of polymer formed.

As for the FTIR spectrum of the test with methanol, its reading is difficult to understand as it appears with very wide and poorly defined peaks. Hence, it was not easy to give precise evaluations about the functional groups present in the solid residue. What is certain is that in both the test with methanol and the test with ethanol, the vibration peaks between 2800 cm^{-1} and 3000 cm^{-1} are not present. Therefore, these alcohols used in the process under examination may not favour the formation of the polymer. This result could

be attributed to the fact that they are species with a low number of carbon atoms and that perhaps, by using species with an increasing number of carbon atoms, the formation of the polymer could be even more favoured. However, further investigations should be made to ascertain this with greater certainty.

To investigate the thermal properties of the samples taken, a TG analysis in nitrogen flow was conducted exactly as performed for the tests described in the previous paragraphs. The results are reported in the Figure 5.46÷5.47:

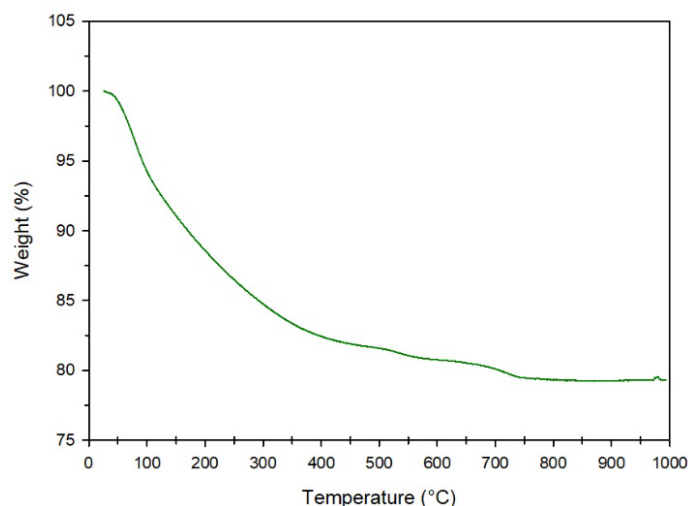*Figure 5.46 - TG (N₂) analysis results (test with methanol)*
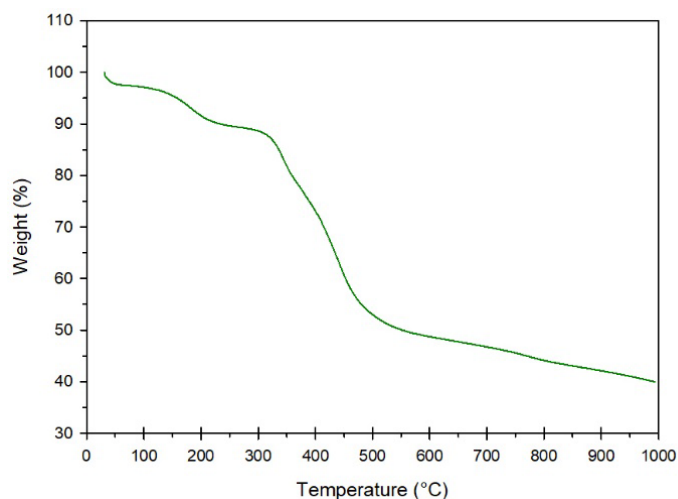

Figure 5.47 - TG (N₂) analysis results (test with glycerol)

In the test with methanol, the overall weight loss is 20% and occurs in a single step; in the test with glycerol, on the other hand, the overall weight loss is 60% but occurs in two steps and the loss between 200 ° C and 400 ° C is very high (about 25%). Therefore, this

is a further confirmation of the high presence of organic substance in the solid residue, i.e., about 25%.

To better visualize the differences, TG curves of the three tests of different fuels are all shown on the same graph in Figure 5.48:
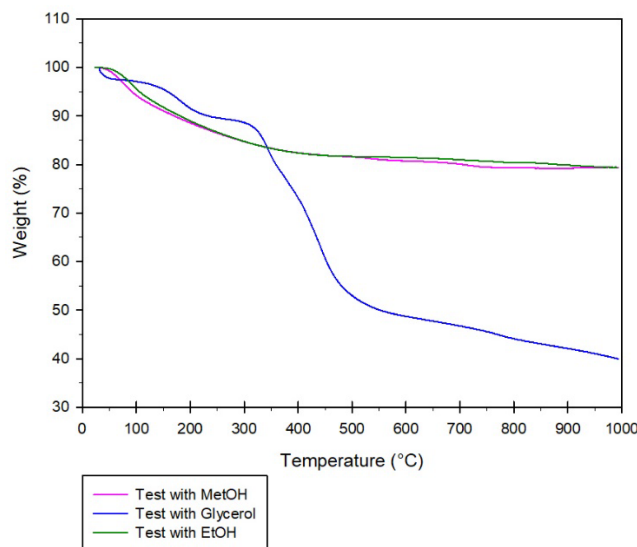

Figure 5.48 - TG (N₂) analysis results (pink: test with methanol; blue: test with glycerol; green: test with ethanol)

As can be seen, TG curves of the test with methanol and the test with ethanol are almost overlapping. This means that the organic content present in the residues of the two tests is approximately identical. Moreover, there is a unique slope that reaches the plateau.

On the other hand, the case of the test with glycerol the TG curve has two different slopes. In this case, the decomposition is shifted to higher temperature. In fact, rather than starting at 200 ° C, it starts at 450 ° C.

Since the decomposition temperature is higher, it can be deduced that the organic species that decomposes is more complex in the case of the test with glycerol than in those with other fuels. For this reason, being more complex, it decomposes at higher temperatures.

To confirm what has just been said about the formation of the polymer in the test with glycerol, the results of the XRD analysis of the three tests are provided in order to have information on both the nature of the solids recovered from the reactor and the size of the crystals. The diffraction profiles of the solid samples recovered at the end of each double cycle test are shown in Figure 5.49÷5.51:
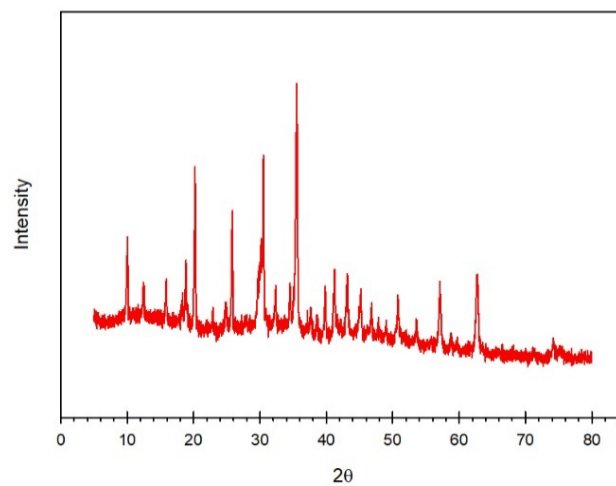
Figure 5.49 - XRD analysis (test with methanol)
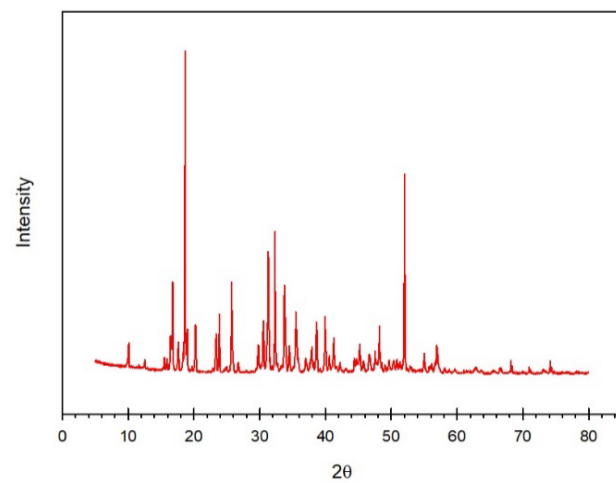

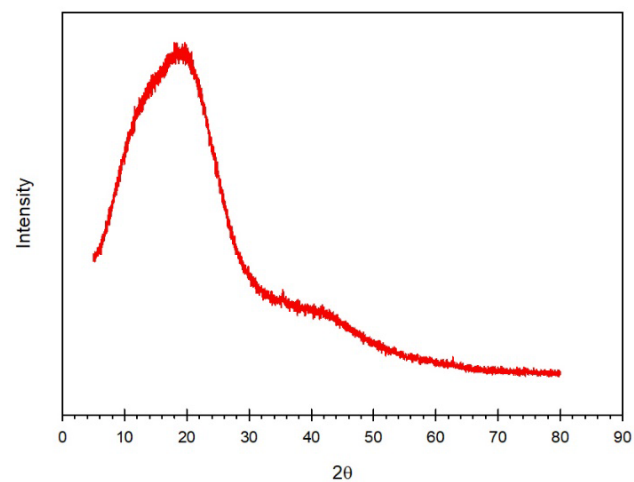*Figure 5.50 - XRD analysis (test with ethanol)*

Figure 5.51 - XRD analysis (test with glycerol)

By analysing the diffractograms, it is possible to verify the evolution of the sample as the kind of alcohol used varies. It is observed that in the diffractogram performed on the

sample of the test with glycerol, a wide band appears for 2θ values between 5 ° and 30 °. It is dominant with respect to the narrow reflections of the crystalline component. This suggests the formation of an amorphous phase. These signals are not noticed in the tests with methanol and ethanol. In particular, the XRD profile of the sample with ethanol has well-defined peaks on an almost flat bottom, indicating the quite high degree of crystallinity of the solid. The XRD analysis of the test with ethanol exhibits very narrow peaks and a very straight base similar to that of the sodium metaborate tetrahydrate shown in Figure 5.52:
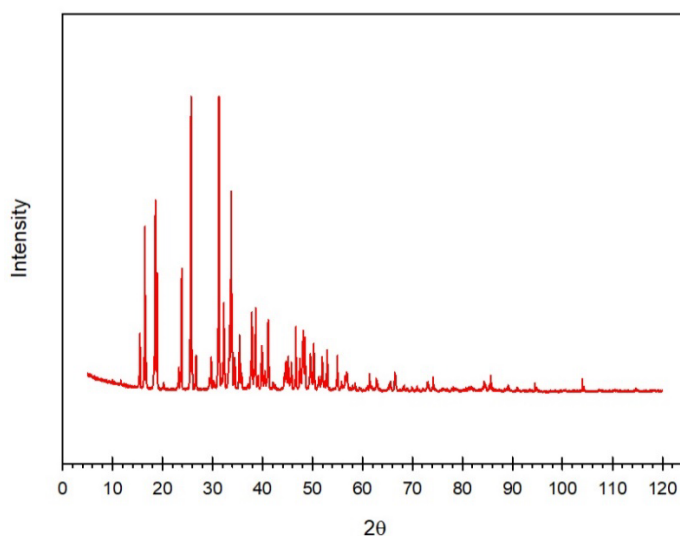
Figure 5.52 - XRD analysis of NaBO$_2$ ·4H$_2$O

Therefore, the amorphous band observed in the glycerol test confirms the formation of polymer chains with low crystallinity, already highlighted by the FTIR spectra.

However, for further confirmation of the nature of the polymer, subsequent investigations will be required in the future, together with the analysis of the liquids obtained after separation with the solid.

5.9. Comparison between simulation and experimental results

To get an idea of how much the process experimented in this work is placed above the steam reforming processes of the various fuels analysed in the thermodynamic study, it was decided to make a comparison.

It has been chosen to compare the count of hydrogen yield of the steam reforming process of the different fuels, made through thermodynamic analysis, with the calculation of the hydrogen yield obtained in our experiments.

In order for the comparison to be meaningful, the temperature was set at 300 ° C (as in all our experiments) and a water / fuel feed ratio (n) was chosen equal to the overall one of the standard double cycle with ethanol, i.e. equal to 6,83 (which is the same feed ratio that we also have in the double cycle with methanol and glycerol since the moles fed to the system are the same). The calculation of the feed ratio n is explained below:

$$n_{EtOH,feed} = n_{EtOH}^{I\ step} + n_{EtOH}^{III\ step} = 0,08563\ mol + 0,08563\ mol = 0,17126\ mol$$

$$n_{H_2O,feed} = n_{H_2O}^{I\ step} + n_{H_2O}^{II\ step} + n_{H_2O}^{IV\ step} = 0,05803\ mol + 0,55555\ mol + 0,55555\ mol$$
$$= 1,16913\ mol$$

$$n = feed\ ratio = \frac{n_{H_2O,feed}}{n_{EtOH,feed}} = \frac{1,16913\ mol}{0,17126\ mol} = 6,83$$

Therefore, the simulations were carried out on Aspen for the calculation of the hydrogen yield of the various fuels in these conditions (n = 6.83 and T = 300 ° C) and the graph of the hydrogen yield vs the pressure as the fuels varies is represented in Figure 5.53:
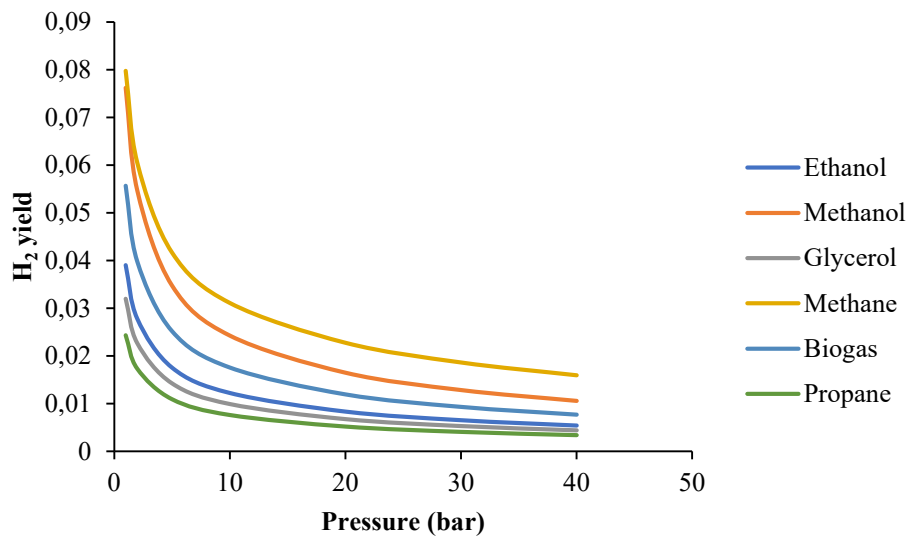
Figure 5.53 – H₂ yield vs pressure as fuel varies (n=6,83 and T=300°C)

The hydrogen yield considered in the simulations was defined in *Chapter 4*.

As regards the definition of the yield of our experiments, it was chosen to define it as the sum of the moles of hydrogen produced at the end of the four steps divided by the theoretical moles of hydrogen that could be formed at most from the respective alcohol (not considering the water), namely:

$$H_2 \ yield_{experimental} = \frac{\sum_{i=1}^{4} n_{H_2,out}^{step \ i}}{3 * \left(n_{EtOH,in}^{I \ step} + n_{EtOH,in}^{III \ step}\right)} \quad (double \ cycle \ standard \ with \ ethanol)$$

$$H_2 \ yield_{experimental} = \frac{\sum_{i=1}^{4} n_{H_2,out}^{step \ i}}{2 * \left(n_{MetOH,in}^{I \ step} + n_{MetOH,in}^{III \ step}\right)} \quad (double \ cycle \ with \ methanol)$$

$$H_2 \ yield_{experimental} = \frac{\sum_{i=1}^{4} n_{H_2,out}^{step \ i}}{4 * \left(n_{Glyc,in}^{I \ step} + n_{Glyc,in}^{III \ step}\right)} \quad (double \ cycle \ with \ glycerol)$$

The theoretical moles of hydrogen present in the denominator were chosen by simply considering the formula of the alcohol molecule. In fact, 2, 3 and 4 theoretical hydrogen molecules (H_2) can be obtained at most respectively from methanol, ethanol and glycerol in the feed.

Therefore, the calculation of the experimental hydrogen yield for the double cycles with ethanol, methanol and glycerol are shown below:

$$H_2 \ yield_{experimental} = \frac{n_{H_2,out}^{step \ I} + n_{H_2,out}^{step \ II} + n_{H_2,out}^{step \ III} + n_{H_2,out}^{step \ IV}}{3 * \left(n_{EtOH,in}^{I \ step} + n_{EtOH,in}^{III \ step}\right)}$$
$$= \frac{0,0079 + 0,0127 + 0,0129 + 0,0119}{3 * (0,08563 + 0,08563)} = 0,089$$

$$H_2 \ yield_{experimental} = \frac{n_{H_2,out}^{step \ I} + n_{H_2,out}^{step \ II} + n_{H_2,out}^{step \ III} + n_{H_2,out}^{step \ IV}}{2 * \left(n_{MetOH,in}^{I \ step} + n_{MetOH,in}^{III \ step}\right)}$$
$$= \frac{0,0037 + 0,0113 + 0,0132 + 0,0131}{2 * (0,08563 + 0,08563)} = 0,12$$

$$H_2 \ yield_{experimental} = \frac{n_{H_2,out}^{step \ I} + n_{H_2,out}^{step \ II} + n_{H_2,out}^{step \ III} + n_{H_2,out}^{step \ IV}}{4 * \left(n_{Glyc,in}^{I \ step} + n_{Glyc,in}^{III \ step}\right)}$$
$$= \frac{0,018 + 0,0066 + 0,008 + 0,006}{4 * (0,08563 + 0,08563)} = 0,056$$

The Figure 5.54 shows the comparison between the yields calculated through the simulation for the different fuels and the experimental yields obtained from the innovative process proposed in this work to better visualize where this process is positioned with respect to the steam reforming of the various fuels in the same operating conditions:
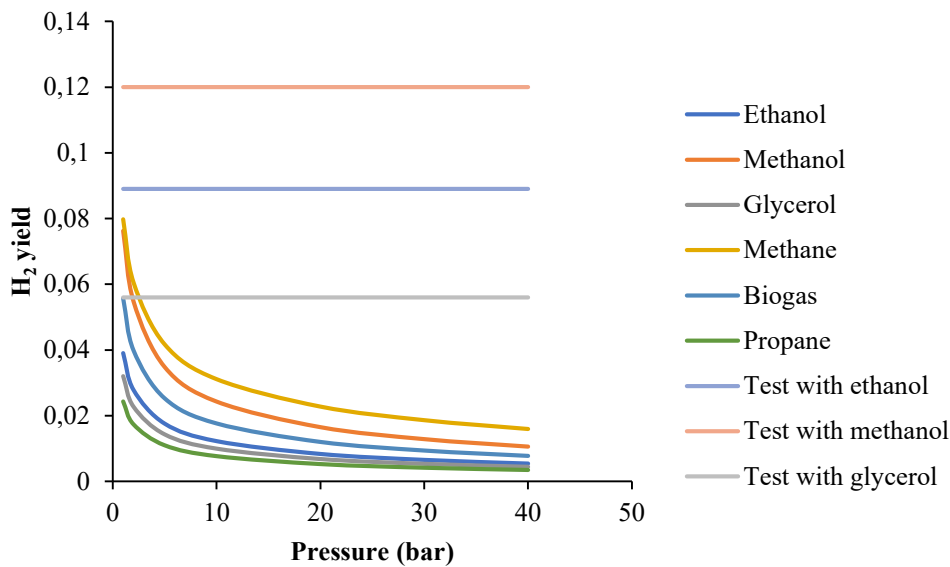
Figure 5.54 - H₂ yield vs pressure as fuel varies: comparison between simulation and experimental results

Wanting to think conservatively, since from the simulation data of steam reforming the yield increases as the pressure decreases, the experimental results can be compared with the simulation ones at the lowest possible pressures reached in our experimental system, so as to consider the highest possible yields in the simulations to compare. Considering the fact that, in our experimental process, the lowest plateau pressures are almost always found at step I and are never lower than 13 barg, we carry out the comparison considering the yields of the simulation data at 10 bar.

As can be seen in the comparison between simulation and experimental data, the yields obtained from the process proposed in this thesis are far above the yields obtained with the calculation of the steam reforming processes.

So, without a doubt, our process is very stimulating and promising and certainly requires further optimization processes in the future.

Chapter 6

CONCLUSION

In this thesis, a novel method for hydrogen production has been studied. The is based on double cycle and the raw materials of the process are metaborate, a low-value by-product, and bio-alcohols, typically obtained from biomass, thus no fossil-based raw material is used.

First of all, a thermodynamic study was carried out first only on the steam reforming of ethanol and then on the comparison of the steam reforming of different fuels.

As regards the steam reforming of ethanol, a reaction path has been found in the literature that considers twenty possible reactions that can occur. Their $T_{\Delta G_0=0}$ were calculated to identify the temperature ranges in which each is favoured. Subsequently, the hydrogen yield was calculated as a function of pressure at various feed ratios and at a temperature of 300 ° C (equal to that of experiments). It has been found that in these conditions the maximum possible yield achievable by thermodynamics is equal to about 0,12, obtained for the feed ratio n equal to 10 (the largest considered in the analysis) and for pressure equal to 1 bar.

As regards instead the comparison with other fuels, it has been seen that the highest possible yields are always obtained for n = 10 and P = 1 bar and at 300 °C the scale of the fuels from the best to the worst in terms of hydrogen yield is the following:

methane > methanol > biogas > ethanol > glycerol > propane

In the second place, experiments were carried out to improve a highly innovative process present in previous thesis works [146, 147] through which it is possible to obtain a very pure current in hydrogen and very low concentrations of CO_2 in the output stream.

In particular, some parameters were changed to try to find the optimal operating conditions of the process. The parameters involved in the process can be multiple. To optimize the process, it was decided to investigate the effect of the water fed at II and IV step, of the bio-alcohol fed and of the starting pressure.

By changing the quantity of water to be fed, a difference of mainly compared to the typical compositions obtainable with SRE only a few percentage points less were noted as regards the composition of hydrogen in the outlet stream. As regards, instead, the solid

residue, it has been noted that by lowering the water content in the feed stream, the organic content increases.

Even by increasing the pressure, a slight decrease in hydrogen production is noted, demonstrating how this hydrogen production process is disadvantaged at high pressures, as is the case for steam reforming processes.

On the other hand, by carrying out the tests with various fuels, a very similar production of hydrogen is noted between the test with ethanol and that with methanol, confirming the fact that, only considering the gas phase, the role of the fuel in this process is not attributable to a single compound but probably to its class (bio-alcohol). Also the composition of carbon dioxide does not present significant variations between the test with ethanol and with methanol.

As regards the case with glycerol, however, a significant decrease in hydrogen production was observed, compared to the previous two. In addition, a large amount of CO_2 was detected in the output stream. However, a considerable quantity of organic was present in the solid residue, which immediately led to think of the formation of a high-value-added polymer and whose nature is to be ascertained in future analyses. If the latter confirmed this, it would be an excellent result as it would be possible to produce hydrogen from waste material and biomass at low temperature and at the same time a polymer to be used in various applications. In future works, it could therefore be thought of continuing to carry out tests with glycerol, perhaps trying to optimize the conditions in order to have a good yield of hydrogen, capture as much CO_2 as possible and form a very useful polymer.

Finally, the simulation results were compared with the experimental ones. It has been seen that much higher hydrogen yields are obtained through the experimental process, object of this thesis, respect than the steam reforming of the various fuels in the same conditions of feed ratio (n = 6,83) and temperature (300 °C).

Therefore, a colour has been given to the hydrogen production process investigated in this thesis, namely cyan, as shown in Figure 6.1:
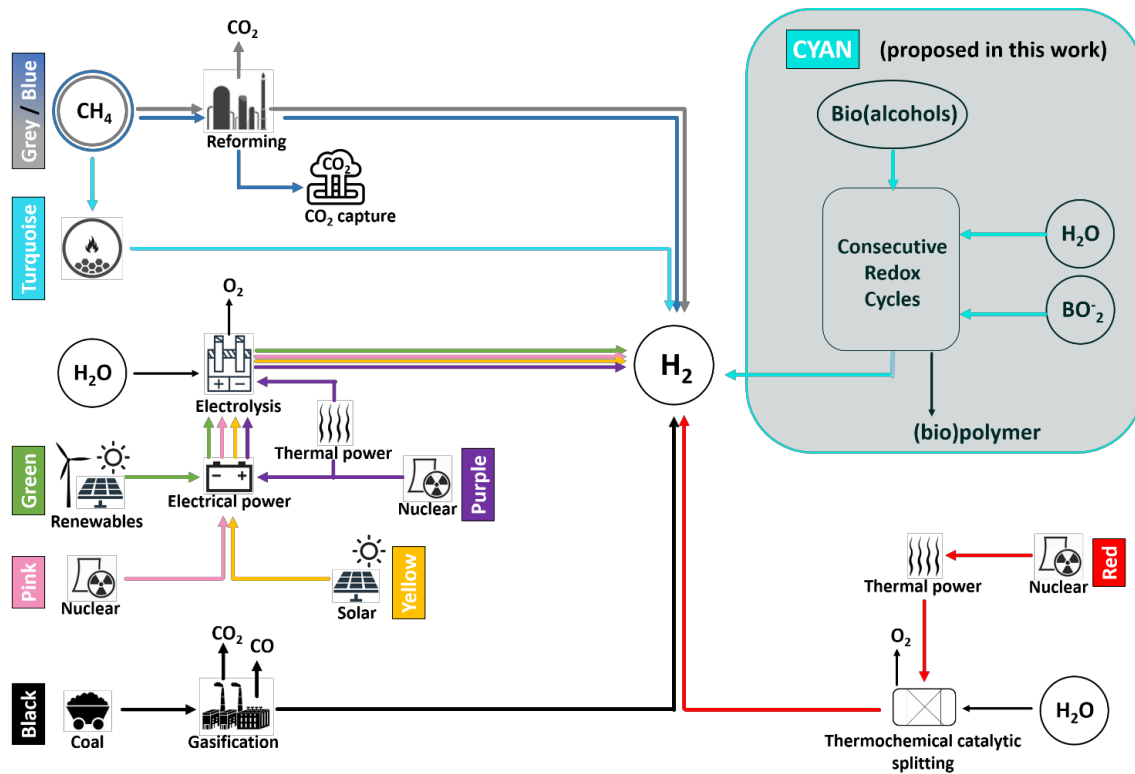
Figure 6.1- Cyan Hydrogen: a new colour of hydrogen

The cyan colour was chosen among the various shades of blue as the process aims to produce an almost pure hydrogen stream as "pseudo" steam reforming at very low temperatures (300°C) and starting from green raw materials and not from fossil fuels that are currently used in steam reforming.

In summary, the advantages of this innovative process are:

- production of an almost pure hydrogen stream at low temperature (as already mentioned) which results in the high competitiveness of the process and the low purification costs;
- use of waste raw materials and bio-based materials;
- production of a high-added value polymer capturing the carbon dioxide.

Future investigations will focus on the optimization of the other operating conditions of the process such as the quantity of bio-alcohol and/or diol fed, the increase in the number of cycles, the use of techniques for the analysis also of the liquid residue and the use of advanced techniques to identify with certainty the nature of the polymer.

163

Reference

[1] Midilli A, Olgun H, Rzayev P, Ayhan T. Solar hydrogen production from hazelnut shells. Int J Hydrogen Energy 1991; 25:723–32; http://dx.doi.org/10.1016/S0360-3199(99)00097-X

[2] Marbán G, Valdés-solís T.Towards the Hydrogen Economy? vol. 32. p. 1625–37. 2007; http://www.lib.ysu.am/articles_art/c361514596e86ba6c889386e2bd41896.pdf

[3] Momirlan M, Veziroglu TN. The Properties of Hydrogen as Fuel Tomorrow in Sustainable Energy System for a Cleaner Planet.vol.30.p.795–802. 2005; https://doi.org/10.1016/j.ijhydene.2004.10.011

[4] Pasman HJ, Rogers WJ. Safety challenges in view of the upcoming hydrogen economy: an overview.J Loss Prev Process Ind 2010; 23(6):697–704; https://doi.org/10.1016/j.jlp.2010.06.002

[5] Van Mierlo J, Maggetto G, Lataire P. Which Energy Source for Road Transport in the Future? A Comparison of Battery, Hybrid and Fuel Cell Vevehicles. Vol 47.p.2748–60. 2006; https://doi.org/10.1016/j.enconman.2006.02.004

[6] https://www.aria.developpement-durable.gouv.fr/wp-content/files_mf/SY_hydrogen_GB_2009.pdf

[7] A. Midilli, M. Ay, I. Dincer, M.A. Rosen, On hydrogen and hydrogen energy strategies: I: current status and needs, Renewable and Sustainable Energy Reviews, Volume 9, Issue 3, 2005, Pages 255 271, ISSN 1364-0321; https://doi.org/10.1016/j.rser.2004.05.003.

[8] https://www.airships.net/hydrogen-airship-accidents/.

[9] http://www.fchea.org/h2-day-2018.

[10] Furat Dawood, Martin Anda, G.M. Shafiullah, Hydrogen production for energy: An overview, International Journal of Hydrogen Energy, Volume 45, Issue 7, 2020, Pages 3847-3869, ISSN 0360 3199, https://doi.org/10.1016/j.ijhydene.2019.12.059.

[11] Ali Keçebaş, Muhammet Kayfeci, Chapter 1 - Hydrogen properties, Editor(s): Francesco Calise, Massimo Dentice D'Accadia, Massimo Santarelli, Andrea Lanzini, Domenico Ferrero, Solar Hydrogen Production, Academic Press, 2019, Pages 3-29, ISBN 9780128148532, https://doi.org/10.1016/B978-0-12-814853-2.00001-1.

[12] Vincent I, Bessarabov D. Low cost hydrogen production by anion exchange membrane electrolysis: a review. Renew Sustain Energy Rev 2018; https://doi.org/10.1016/j.rser.2017.05.258.

[13] Parra D, Zhang X, Bauer C, Patel MK. An integrated technoeconomic and life cycle environmental assessment of power-to-gas systems. Appl Energy 2017; https://doi.org/10.1016/j.apenergy.2017.02.063.

[14] He C, Yu R, Sun H, Chen Z. Lightweight multilayer composite structure for hydrogen storage tank. Int J Hydrogen Energy 2016; https://doi.org/10.1016/j.ijhydene.2016.04.184.

[15] Brandon NP, Kurban Z. Clean energy and the hydrogen economy. Philos Trans R Soc A Math Phys Eng Sci 2017; 375; https://doi.org/10.1098/rsta.2016.0400.

[16] Halm D, Fouillen F, Laine E, Gueguen M, Bertheau D, van Eekelen T. Composite pressure vessels for hydrogen storage in fire conditions: fire tests and burst simulation. Int J Hydrogen Energy 2017; https://doi.org/10.1016/j.ijhydene.2017.06.088.

[17]https://www.inail.it/cs/internet/docs/dinamica_dei_fenomeni_esplosivi_pdf_2443085454519.pdf?section=attivita.

[18] San Marchi C, Hecht ES, Ekoto IW, Groth KM, LaFleur C, Somerday BP, et al. Overview of the DOE hydrogen safety, codes and standards program, part 3: advances in research and development to enhance the scientific basis for hydrogen regulations, codes and standards. Int J Hydrogen Energy 2017/03/16/2017; 42: 7263-74; https://doi.org/10.1016/j.ijhydene.2016.07.014.

[19] Ayas C, Fleck NA, Deshpande VS. Hydrogen embrittlement of a bimaterial. Mech Mater 2015; 80:193-202. 2015/01/01/; https://doi.org/10.1016/j.mechmat.2014.06.002.

[20] Labs DN. Safe use of hydrogen. 30 May. 2019. Available, https://www.energy.gov/eere/fuelcells/safe-use-hydrogen.

[21] Melaina OAMW, Penev M. Blending hydrogen into natural gas pipeline networks: a review of key issues. USA: National Renewable Energy Laboratory (NREL); 2013. Technical ReportMarch 2013; https://www.h2knowledgecentre.com/content/researchpaper1511.

[22] Ultanir MO. Hidrojenin yakit olarak kullanimi ve ö zellikleri. Çevre-Enerji Kongresi, TMMOB Makine Mühendisleri Odasi. 1997, p. 295–315.

[23] Rosen MA, Scott DS. Comparative efficiency assessments for a range of hydrogen production processes. Int J Hydrogen Energy 1998; 23(8):653–9; https://doi.org/10.1016/S0360-3199(97)00080-3.

[24] Olgun H, Midilli A, Rzayev P, Ayhan T. Pyrolysis studies of nutshells. Proceedings of 10th International Conference on Thermal Engineering and Thermogrammetry (THERMO), Budapest, Hungary. 1997, p. 16–21.

[25] Midilli A, Rzayev P, Ayhan T. Gunes enerjili kapali c¸evrimli hidrojen ayristirma sistemi. Gunes Gunu Sempozyumu ve Fuari, Izmir, Turkiye, vol. 1. 1998, p. 34–8.

[26] Hart D, Freund P, Smith A. Hydrogen-today and tomorrow. IEA Greenhouse Gas R&D Programme. ISBN 1 898373 24 8.

[27] Sloop LJ. Liquid hydrogen as a propulsion fuel. The NASA History Series, Washington (DC); 1978; https://core.ac.uk/download/pdf/10339184.pdf.

[28] Veziroglu TN, Barbir F. Hydrogen energy technologies. Emerging technology series. Vienna, Austria: UNIDO; 1998; https://open.unido.org/api/documents/4808760/download/HYDROGEN%20ENERGY%20TECHNOLOGIES.%20EMERGING%20TECHNOLOGY%20SERIES%20(21974.en).

[29] M. Della Pietra, S. McPhail, L. Turchetti, G. Monteleone, I 'colori' dell'idrogeno nella transizione energetica, «Energia, ambiente e innovazione», 2020, pp. 92-95; https://www.eai.enea.it/archivio/energia-e-green-new-deal-sommario/i-colori-dell-idrogeno-nella-transizione-energetica.html.

[30] World Energy Council. National Hydrogen Strategies. 2021. Available online: https://www.worldenergy.org/assets/downloads/Working_Paper_-_National_Hydrogen_Strategies_-_September_2021.pdf.

[31] https://www.worldenergy.org/assets/downloads/Working_Paper_-_National_Hydrogen_Strategies_-_September_2021.pdf.

[32] https://feem-media.s3.eu-central-1.amazonaws.com/wp-content/uploads/NDL2020-013.pdf.

[33] S. Agnoli, Idrogeno, la nuova frontiera dell'economia «green»: che cos'è, a cosa serve, come si può impiegare", Corriere della Sera, 20/12/2020; https://www.corriere.it/economia/finanza/cards/idrogeno-nuova-frontiera-dell-

economia-green-che-cos-cosa-serve-come-si-puo-impiegare/che-cos-l-idrogeno_principale.shtml.

[34] Enidatalab elaboration on lea data 2018 by Statista.

[35] https://www.pembina.org/reports/hydrogen-climate-primer-2020.pdf.

[36] Snam e Mckinsey Report, "The hydrogen challenge: the potential of hydrogen in Italy", 2019; https://www.snam.it/it/hydrogen_challenge/repository_hy/file/The-H2-challenge-Position-Paper.pdf.

[37] BloombergNEF. Note: NCS-CEHP is NEO Climate Scenario: Clean Electricity and Hydrogen Pathway.

[38] Bing Zhang, Sui-Xin Zhang, Rui Yao, Yong-Hong Wu, Jie-Shan Qiu, Progress and prospects of hydrogen production: Opportunities and challenges, Journal of Electronic Science and Technology, Volume 19, Issue 2, 2021, 100080, ISSN 1674-862X; https://doi.org/10.1016/j.jnlest.2021.100080.

[39] J.D. Holladay, J. Hu, D.L. King, Y. Wang, An overview of hydrogen production technologies, Catalysis Today, Volume 139, Issue 4, 2009, Pages 244-260, ISSN 0920-5861; https://doi.org/10.1016/j.cattod.2008.08.039.

[40] R. Farrauto, S. Hwang, L. Shore, W. Ruettinger, J. Lampert, T. Giroux, Y. Liu, O. Ilinich, Annual Review of Materials Research 33 (2003) 1–27; https://www.annualreviews.org/doi/abs/10.1146/annurev.matsci.33.022802.091348?casa_token=dfsqmrDVYsAAAAAA:ViKOe3lBjT9zDbcxntxGZLwR6Ce7Es0P5ltA8r4vhIeRZLpIvQbp1MWn2zw1jf-CVNjRjhIXtQ-PMg.

[41] Trevor L. LeValley, Anthony R. Richard, Maohong Fan, The progress in water gas shift and steam reforming hydrogen production technologies – A review, Int. J. Hydrogen Energy 39 (30) (2014) 16983–17000; https://doi.org/10.1016/j.ijhydene.2014.08.041.

[42] L. Barelli, G. Bidini, F. Gallorini, S. Servili, Hydrogen production through sorption-enhanced steam methane reforming and membrane technology: a review, Energy 33 (2008) 554–570; https://doi.org/10.1016/j.energy.2007.10.018.

[43] Magnus Rydén, Mehdi Arjmand, Continuous hydrogen production via the steam–iron reaction by chemical looping in a circulating fluidized-bed reactor, Int. J. Hydrogen Energy 37 (6) (2012) 4843–4854; https://doi.org/10.1016/j.ijhydene.2011.12.037.

[44] M Steinberg, Modern and prospective technologies for hydrogen production from fossil fuels, Int. J. Hydrogen Energy 14 (11) (1989) 797–820; https://doi.org/10.1016/0360-3199(89)90018-9.

[45] M.H. Halabi, M.H.J.M. de Croon, J. van der Schaaf, P.D. Cobden, J.C. Schouten, Low temperature catalytic methane steam reforming over ceria–zirconia supported rhodium, Appl. Catal. A 389 (1-2) (2010) 68–79; https://doi.org/10.1016/j.apcata.2010.09.004.

[46] A.M. Adris, B.B. Pruden, Canadian Journal of Chemical Engineering 74 (1996) 177; https://doi.org/10.1002/cjce.5450740202.

[47] J. Rostrup-Nielsen, in: I.T. Horvath (Ed.), Encyclopedia of Catalysis, Wiley Interscience, 2003 4; https://www.wiley-vch.de/en/areas-interest/natural-sciences/chemistry-11ch/catalysis-11ch4/encyclopedia-of-catalysis-978-0-471-24183-6.

[48] J.R.H. Ross, in: M.W. Roberts, J.M. Thomas (Eds.), Surface and Defect Properties of Solids, Chemical Society, London (1974) 34; https://pubs.rsc.org/en/content/ebook/978-0-85186-270-5.

[49] K. McHugh, Hydrogen Production Methods, MPR Associates Inc., 2005,, p. 41.

[50] A.E. Lutz, R.W. Bradshaw, L. Bromberg, A. Rabinovich, Thermodynamic analysis of hydrogen production by partial oxidation reforming, Int. J. Hydrogen Energy 29 (2004) 809–816; https://doi.org/10.1016/j.ijhydene.2003.09.015.

[51] A Koh, L Chen, W Keeleong, B Johnson, T Khimyak, J Lin, Hydrogen or synthesis gas production via the partial oxidation of methane over supported nickel–cobalt catalysts, Int. J. Hydrogen Energy 32 (6) (2007) 725–730; https://doi.org/10.1016/j.ijhydene.2006.08.002.

[52] Renika Baruah, Marm Dixit, Pratik Basarkar, Dhrupad Parikh, Atul Bhargav, Advances in ethanol autothermal reforming, Renew. Sustain. Energy Rev. 51 (2015) 1345–1353; https://doi.org/10.1016/j.rser.2015.07.060.

[53] J. Castro, R. Rivera-Tinoco, C. Bouallou, Hydrogen production from natural gas: auto-thermal reforming and CO2 capture, Chem. Eng. 21 (2010).

[54] W. Wu, K. Yoshikawa, JSME International Journal Series B-Fluids and Thermal Engineering 45 (2002) 487–491; https://doi.org/10.1299/jsmeb.45.487.

[55] A. Demirbas, Energy Sources 25 (2003) 67–75; https://www.researchgate.net/publication/233213559_Hydrocarbons_from_Pyrolysis_and_Hydrolysis_Processes_of_Biomass.

[56] J. Yi Zheng, G. Chao, H. Wen Kuang, Z. Yanqiu, A. Huczko, M. Bystrzejewski, M. Roe, L. Chi Young, S. Acquah, H. Kroto, D.R.M. Walton, Carbon 43 (2005) 1944– 1953.

[57] A.P. Karaeva, V.Z. Mordkovich, V.F. Tretyakov, Solid Fuel Chemistry 39 (2005) 61–76.

[58] N. Muradov, Journal of Power Sources 118 (2003) 320–324; https://doi.org/10.1016/S0378-7753(03)00078-8.

[59] Y.-S. Guo, W.-J. Fang, R.-S. Lin, Zhejiang Daxue Xuebao (Gongxue Ban)/Journal of Zhejiang University (Engineering Science) 39 (2005) 538–541.

[60] https://chevetol.com/trading/petrochemical-products/methanol/.

[61] http://dept.harpercollege.edu/chemistry/msds/Methyl%20alcohol%20ScienceLab.pdf.

[62] S. Sá, H. Silva, L. Brandão, J. M. Sousa, and A. Mendes, "Catalysts for methanol steam reforming-A review," Appl. Catal. B Environ., vol. 99, no. 1–2, pp. 43–57, 2010; https://doi.org/10.1016/j.apcatb.2010.06.015

[63] Rod L. Borup, Michael A. Inbody, Troy A. Semelsberger, José I. Tafoya, Dennis R. Guidry, Fuel composition effects on transportation fuel cell reforming, Catalysis Today, Volume 99, Issues 3–4, 2005, Pages 263-270, ISSN 0920-5861; https://doi.org/10.1016/j.cattod.2004.10.014.

[64] B. A. Peppley, J. C. Amphlett, L. M. Kearns, and R. F. Mann, "Methanol–steam reforming on Cu/ZnO/Al2O3. Part 1: the reaction network," Appl. Catal. A Gen., vol. 179, no. 1–2, pp. 21–29, 1999; https://doi.org/10.1016/S0926-860X(98)00298-1.

[65] B. A. Peppley, J. C. Amphlett, L. M. Kearns, and R. F. Mann, "Methanol–steam reforming on Cu/ZnO/Al2O3 catalysts. Part 2. A comprehensive kinetic model," Appl. Catal. A Gen., vol. 179, no. 1–2, pp. 31–49, 1999; https://doi.org/10.1016/S0926-860X(98)00299-3.

[66] R. Thattarathody, M. Artoul, R. M. Digilov, and M. Sheintuch, "Pressure, Diffusion, and S/M Ratio Effects in Methanol Steam Reforming Kinetics," Ind. Eng. Chem. Res., vol. 57, no. 9, pp. 3175–3186, 2018; https://doi.org/10.1021/acs.iecr.7b05033.

[67] J. P. Breen and J. R. . Ross, "Methanol reforming for fuel-cell applications: development of zirconia-containing Cu–Zn–Al catalysts," Catal. Today, vol. 51, no. 3–4, pp. 521–533, 1999; https://doi.org/10.1016/S0920-5861(99)00038-3.

[68] .J. Jiang, D.L. Trimm, M.S. Wainwright, N.W. Cant, Kinetic study of steam reforming of methanol over copper-based catalysts, Applied Catalysis A: General, Volume 93, Issue 2, 1993, Pages 245-255, ISSN 0926-860X; https://doi.org/10.1016/0926-860X(93)85197-W.

[69] https://etd.lib.metu.edu.tr/upload/12623155/index.pdf.

[70] https://etd.lib.metu.edu.tr/upload/12619575/index.pdf.

[71] Díaz Alvarado F. and Gracia F., "Steam reforming of ethanol for hydrogen production: Thermodynamic analysis including different carbon deposits representation," Chem Eng J, 165 (2): 649–657, 2010; https://doi.org/10.1016/j.cej.2010.09.051.

[72] http://www.neuroscienzedipendenze.it/alcol.html.

[73] Ni M., Leung D. Y. C., and Leung M. K. H., "A review on reforming bio-ethanol for hydrogen production," Int J Hydrog. Energ, 32 (15): 3238–3247, 2007; https://doi.org/10.1016/j.ijhydene.2007.04.038.

[74] Wenju Wang,yand Y. Q. Wang, Thermodynamic analysis of steam reforming of ethanol for hydrogen generation, International Journal Of Energy Research Int. J. Energy Res.2008; 32: 1432–1443; https://doi.org/10.1002/er.1459.

[75] Nichele V., Signoretto M., Pinna F., Menegazzo F., Rossetti I., Cruciani G., Cerrato G., and Michele A. Di, "Ni/ZrO2 catalysts in ethanol steam reforming: Inhibition of coke formation by CaO-doping," *Appl Catal B-Environ*, 150–151: 12–20, 2014; https://doi.org/10.1016/j.apcatb.2013.11.037.

[76] Kumar P., Sun Y., and Idem R. O., "Nickel-Based Ceria, Zirconia, and Ceria–Zirconia Catalytic Systems for Low-Temperature Carbon Dioxide Reforming of Methane," Energ Fuel, 21 (6): 3113–3123, 2007; https://doi.org/10.1021/ef7002409;

[77] Rossetti I., Lasso J., Nichele V., Signoretto M., Finocchio E., Ramis G., and Michele A. Di, "Silica and zirconia supported catalysts for the low-temperature ethanol steam reforming," Appl Catal B Env., 150–151: 257–267, 2014; https://doi.org/10.1016/j.apcatb.2013.12.012.

[78] https://agronotizie.imagelinenetwork.com/bio-energie-rinnovabili/2016/02/02/la-glicerina-un-sottoprodotto-energetico-da-consumare-con-cautela/47323#:~:text=alto%20potere%20calorifico%20(comparabile%20con,bassa%20tossicit%C3%A0.

[79] https://www.sigmaaldrich.com/IT/it/product/sigma/49767.

[80] http://www.chm.bris.ac.uk/motm/glycerol/glycerolh.htm.

[81] https://www.frontiersin.org/articles/10.3389/fchem.2018.00573/full.

[82] Silva, J. M., Soria, M. A., & Madeira, L. M. (2015). Challenges and strategies for optimization of glycerol steam reforming process. Renewable and Sustainable Energy Reviews, (Vol. 42, pp. 1187–1213); https://doi.org/10.1016/j.rser.2014.10.084.

[83] Reddy, R., Patel, S., Nair, S., & Suvikram, Y. (2011). Preparation of Hydrogen from Glycerol via Steam Reforming Process. Institute of Technology, Nirma University, Ahmedabad – 382 481.

[84] Adeniyi, A. G., & Ighalo, J. O. (2019). A review of steam reforming of glycerol. Chemical Papers, 73(11), 2619–2635; https://doi.org/10.1007/s11696-019-00840-8.

[85] Adhikari, S., Fernando, S., & Haryanto, A. (2007). Production of hydrogen by steam reforming of glycerin over alumina-supported metal catalysts. Catalysis Today, 129(3–4), 355–364. https://doi.org/10.1016/j.cattod.2006.09.038.

[86] Fasolini, A., Cespi, D., Tabanelli, T., Cucciniello, R., & Cavani, F. (2019). Hydrogen from renewables: A case study of glycerol reforming. Catalysts, 9(9), 722; https://doi.org/10.3390/catal9090722.

[87] Schwengber, C. A., Alves, H. J., Schaffner, R. A., Da Silva, F. A., Sequinel, R., Bach, V. R., & Ferracin, R. J. (2016). Overview of glycerol reforming for hydrogen production. Renewable and Sustainable Energy Reviews, 58, 259–266; https://doi.org/10.1016/j.rser.2015.12.279.

[88] Adhikari, S., Fernando, S. D., & Haryanto, A. (2008). Hydrogen production from glycerin by steam reforming over nickel catalysts. Renewable Energy, 33(5), 1097–1100; https://doi.org/10.1016/j.renene.2007.09.005.

[89] Bagnato, G., Iulianelli, A., Sanna, A., & Basile, A. (2017). Glycerol Production and Transformation: A Critical Review with Particular Emphasis on Glycerol Reforming Reaction for Producing Hydrogen in Conventional and Membrane Reactors. Membranes, 7(2), 17; https://doi.org/10.3390/membranes7020017.

[90] Barker-Hemings, E., Cavallotti, C., Cuoci, A., Faravelli, T., & Ranzi, E. (2012). A Detailed Kinetic Study of Pyrolysis and Oxidation of Glycerol (Proane-1,2,3-triol). Combustion Science and Technology, 184(7-8), 1164–1178; https://doi.org/10.1080/00102202.2012.664006.

[91] Basile, A., Tong, J., & Millet, P. (2013). Inorganic membrane reactors for hydrogen production: An overview with particular emphasis on dense metallic membrane materials. In Handbook of Membrane Reactors (Vol. 1); https://doi.org/10.1533/9780857097330.1.42.

[92] Pal, D. B., Chand, R., Upadhyay, S. N., & Mishra, P. K. (2018). Performance of water gas shift reaction catalysts: A review. Renewable and Sustainable Energy Reviews, 93 (December 2017), 549–565; https://doi.org/10.1016/j.rser.2018.05.003.

[93] Stangeland, K., Kalai, D., Li, H., & Yu, Z. (2017). CO_2 Methanation: The Effect of Catalysts and Reaction Conditions. Energy Procedia, 105(1876), 2022–2027; https://doi.org/10.1016/j.egypro.2017.03.577.

[94] Idriss, H., Scott, M., & Subramani, V. (2015). Introduction to hydrogen and its properties. In Compendium of Hydrogen Energy (pp. 3–19); https://doi.org/10.1016/b978-1-78242-361-4.00001-7.

[95] Schaaf, T., Grünig, J., Schuster, M. R., Rothenfluh, T., & Orth, A. (2014). Methanation of CO_2 - storage of renewable energy in a gas distribution system. Energy, Sustainability and Society, 4(1), 1–14; https://doi.org/10.1186/s13705-014-0029-1.

[96] https://amslaurea.unibo.it/13900/1/Sanghez%20de%20Luna_Giancosimo_Tesi.pdf.

[97] L.B. Allegue, J. Hinge , Biogas and bio-syngas upgrading, http://www.teknologisk.dk/_root/media/52679_Report-Biogas and syngas upgrading.pdf, (2012)

[98] Devendra Pakhare, James Spivey, A review of dry (CO_2) reforming of methane over noble metal catalysts, Chem. Soc. Rev. 43 (2014) 7813-7837; https://doi.org/10.1039/C3CS60395D.

[99] G. C. de Arauj, S. M. de Lima, J. M. Assaf, M. A. Pena, J. L. Garcia Fierro, M. d. C. Rangel, Catalytic evaluation of perovskite-type oxide $LaNi_{1-x}Ru_xO_3$ in methane dry reforming, Catal. Today 133 (2008)129–135; https://doi.org/10.1016/j.cattod.2007.12.049.

[100] Shaobin Wang, G. Q. (Max) Lu, and Graeme J. Millar, Carbon Dioxide Reforming of Methane To Produce Synthesis Gas over Metal-Supported Catalysts: State of the Art, Energy & Fuels 1996 10 (4), 896-904; https://doi.org/10.1021/ef950227t.

[101] C. Carrara, J. Munera, E. A. Lombardo, L. M. Cornaglia, Kinetic and Stability Studies of Ru/La_2O_3 Used in the Dry Reforming of Methane, Top. Catal. 51 (2008) 98–106; https://link.springer.com/article/10.1007/s11244-008-9131-y.

[102] J.T. Richardson, S.A., Paripatyadar, Carbon dioxide reforming of methane with supported rhodium; Appl. Catal. 61 (1990) 293-309; https://doi.org/10.1016/S0166-9834(00)82152-1.

[103] J. Zhang, H. Wang, A. K. Dalai, Development of stable bimetallic catalysts for carbon dioxide reforming of methane; J. Catal. 249 (2007) 300–310; https://doi.org/10.1016/j.jcat.2007.05.004.

[104] A. Brush, E. J. Evans Jr., G. M. Mullen, K. Jarvis, C. B. Mullins, Tunable Syn-gas ratio via bireforming over coke-resistant Ni/Mo_2C catalyst, Fuel Process. Technol., 153 (2016) 111–120; https://doi.org/10.1016/j.fuproc.2016.07.012.

[105] A. Czernichowski, P. Czernichowski, K. Wesolowska, Fuel Cell Science, Engineering and Technology—2004, Plasma-Catalytical Partial Oxidation of Various Carbonaceous Feeds into Synthesis Gas, American Society of Mechanical Engineers, New York, United States/Rochester, NY, United States, 2004, pp. 669–676; https://doi.org/10.1115/FUELCELL2004-2537.

[106] https://it.wikipedia.org/wiki/Propano.

[107] https://www.chimica-online.it/composti-organici/propano.htm.

[108] Mohammad A. Rakib, John R. Grace, C. Jim Lim, Said S.E.H. Elnashaie, Bahman Ghiasi, Steam reforming of propane in a fluidized bed membrane reactor for hydrogen

production, International Journal of Hydrogen Energy, Volume 35, Issue 12, 2010, Pages 6276-6290, ISSN 0360 3199; https://doi.org/10.1016/j.ijhydene.2010.03.136.

[109] Jensen MB, Raberg LB, Sjastad AO, Olsbye U. Mechanistic study of the dry reforming of propane to synthesis gas over a Ni/Mg(Al)O catalyst. Catalysis Today 2009; 145:114-20; https://doi.org/10.1016/j.cattod.2008.05.025.

[110] Whittington BI, Jiang CJ, Trimm DL. Vehicle exhaust catalysis.1. The relative importance of catalytic-oxidation, steam reforming and water-gas shift reactions. Catalysis Today 1995; 26:41-5; https://doi.org/10.1016/0920-5861(95)00093-U.

[111] Minutillo M. On-board fuel processor modelling for hydrogen-enriched gasoline fuelled engine. International Journal of Hydrogen Energy 2005; 30:1483-90; https://doi.org/10.1016/j.ijhydene.2004.12.006.

[112] Rostrup-Nielsen JR. Activity of nickel catalysts for steam reforming of hydrocarbons. Journal of Catalysis 1973; 31: 173-99; https://doi.org/10.1016/0021-9517(73)90326-6.

[113] J. R. Rostrup-Nielsen, Steam Reforming Catalyst, Teknisk Forlag, Denmark, 1975.

[114] M.V. Twigg, Catalyst Handbook, 2nd ed., Manson, London, 1994.

[115] Trimm DL. Coke formation and minimisation during steam reforming reactions. Catalysis Today 1997; 37: 233-8; https://doi.org/10.1016/S0920-5861(97)00014-X.

[116] Ayhan Demirbaş, Biomass resource facilities and biomass conversion processing for fuels and chemicals, Energy Conversion and Management, Volume 42, Issue 11, 2001, Pages 1357-1378, ISSN 0196-8904; https://doi.org/10.1016/S0196-8904(00)00137-0.

[117] Diego Iribarren, Ana Susmozas, Fontina Petrakopoulou, Javier Dufour, Environmental and exergetic evaluation of hydrogen production via lignocellulosic biomass gasification, Journal of Cleaner Production, Volume 69, 2014, Pages 165-175, ISSN 0959-6526; https://doi.org/10.1016/j.jclepro.2014.01.068.

[118] Ni M, Leung DYC, Leung MKH, Sumathy K. An overview of hydrogen production from biomass. Fuel Process Technol 2006; 87(5): 461–72; https://doi.org/10.1016/j.fuproc.2005.11.003.

[119] Debabrata Das, T.Nejat Veziroğlu, Hydrogen production by biological processes: a survey of literature, International Journal of Hydrogen Energy, Volume 26, Issue 1, 2001, Pages 13-28, ISSN 0360-3199; https://doi.org/10.1016/S0360-3199(00)00058-6.

[120] Pavlos Nikolaidis, Andreas Poullikkas, A comparative overview of hydrogen production processes, Renewable and Sustainable Energy Reviews, Volume 67, 2017, Pages 597-611, ISSN 1364-0321, https://doi.org/10.1016/j.rser.2016.09.044.

[121] De Falco, Marcello, Marrelli Luigi, Iaquaniello Gaetano. Membrane reactors for hydrogen production processes, 264. London, England: Springer; 2011.

[122] T.A.H. Ratlamwala, I. Dincer, Comparative energy and exergy analyses of two solar-based integrated hydrogen production systems, International Journal of Hydrogen Energy, Volume 40, Issue 24, 2015, Pages 7568-7578, ISSN 0360-3199; https://doi.org/10.1016/j.ijhydene.2014.10.123

[123] Ramin Moradi, Katrina M. Groth, Hydrogen storage and delivery: Review of the state of the art technologies and risk and reliability analysis, International Journal of Hydrogen Energy, Volume 44, Issue 23, 2019, Pages 12254-12269, ISSN 0360-3199; https://doi.org/10.1016/j.ijhydene.2019.03.041.

[124] White C, Steeper R, Lutz A. The hydrogen-fueled internal combustion engine: a technical review. Int J Hydrogen Energy 2006; 31(10):1292-305; https://doi.org/10.1016/j.ijhydene.2005.12.001.

[125] Niaz S, Manzoor T, Pandith AH. Hydrogen storage: materials, methods and perspectives. Renew Sustain Energy Rev 2015; 50:457-69; https://doi.org/10.1016/j.rser.2015.05.011.

[126] Barthelemy H, Weber M, Barbier F. Hydrogen storage: recent improvements and industrial perspectives. Int J Hydrogen Energy 2017; 42(11):7254-62; https://doi.org/10.1016/j.ijhydene.2016.03.178.

[127] Stolten D, Samsun RC, Garland N. Fuel cells: data, facts, and figures. John Wiley & Sons; 2016; https://books.google.com/books?hl=it&lr=&id=602cCwAAQBAJ&oi=fnd&pg=PR5&ots=Llm2NZldif&sig=WYezW7yU1QB7hY0krxiQrVFHRSA.

[128] Xia Y, Yang Z, Zhu Y. Porous carbon-based materials for hydrogen storage: advancement and challenges. J Mater Chem 2013;1(33):936-81; https://pubs.rsc.org/en/content/articlelanding/2013/TA/c3ta10583k.

[129] Zhu Q-L, Xu Q. Metaleorganic framework composites. Chem Soc Rev 2014;43(16):5468-512; https://www.scopus.com/record/display.uri?eid=2-s2.0-84899894614&origin=inward.

[130] Zhang F, Zhao P, Niu M, Maddy J. The survey of key technologies in hydrogen energy storage. Int J Hydrogen Energy 2016; 41(33):14535-52; https://doi.org/10.1016/j.ijhydene.2016.05.293.

[131] Ren J, Musyoka NM, Langmi HW, Mathe M, Liao S. Current research trends and perspectives on materials-based hydrogen storage solutions: a critical review. Int J Hydrogen Energy 2017; 42(1):289-311; https://doi.org/10.1016/j.ijhydene.2016.11.195.

[132] Hani Nasser Abdelhamid, A review on hydrogen generation from the hydrolysis of sodium borohydride, International Journal of Hydrogen Energy, Volume 46, Issue 1, 2021, Pages 726-765, ISSN 0360-3199; https://doi.org/10.1016/j.ijhydene.2020.09.186.

[133] W. Chen, L.Z. Ouyang, J.W. Liu, X.D. Yao, H. Wang, Z.W. Liu, M. Zhu, Hydrolysis and regeneration of sodium borohydride (NaBH4) – A combination of hydrogen production and storage, Journal of Power Sources, Volume 359, 2017, Pages 400-407, ISSN 0378-7753; https://doi.org/10.1016/j.jpowsour.2017.05.075.

[134] J. Andrieux, L. Laversenne, O. Krol, R. Chiriac, Z. Bouajila, R. Tenu, J. J. Counioux and C. Goutaudier, "Revision of the $NaBO_2$-H_2O Phase Diagram for Optimized Yield in the H2 Generation through NaBH4 Hydrolysis," Int. J. Hydrogen Energy, vol. 37, pp. 5798-5810, 2012; https://doi.org/10.1016/j.ijhydene.2011.12.106.

[135] E. Y. Marrero-Alfonso, J. R. Gray, T. A. Davis and M. A. Matthews, "Minimizing Water Utilization in Hydrolysis of Sodium Borohydride: The Role of Sodium Metaborate Hydrates," Int. J. Hydrogen Energy, vol. 32, pp. 4723-4730, 2007; https://doi.org/10.1016/j.ijhydene.2007.08.014.

[136] W. G. Woods, "An Introduction to Boron: History, Sources, Uses, and Chemistry," Environ. Health Perspect., vol. 102, pp. 5-11, 1994; https://www.jstor.org/stable/3431956.

[137] M. Marezio, H. A. Plettinger and W. H. Zachariasen, "The Bond Lengths in the Sodium Metaborate Structure," Acta Cryst., vol. 16, pp. 594-595, 1963; https://scripts.iucr.org/cgi-bin/paper?a03866.

[138] https://core.ac.uk/download/pdf/268939392.pdf.

[139] https://it.funcmater.com/Metaborato-di-sodio-tetraidrato-%28NaBO2%E2%80%A24H2O%29-Crystaline-pd49368375.html.

[140] A. Kanturk, M. Sari, S. Piskin, Synthesis, crystal structure and dehydration kinetics of NaB(OH)$_4$•2H$_2$O, Korean Journal of Chemical Engineering 25 (6) (2008) 1331–1337; https://link.springer.com/article/10.1007/s11814-008-0218-8.

[141] S. Piskin, PhD Thesis, Istanbul Technical University, Faculty of Mining, Istanbul, Turkey (1983).

[142] Garrett, D.E., 1998. Borates. Academic Press, California, 483 p.

[143] Chengguang Lang, Yi Jia, Jiangwen Liu, Hui Wang, Liuzhang Ouyang, Min Zhu, Xiangdong Yao, NaBH4 regeneration from NaBO$_2$ by high-energy ball milling and its plausible mechanism, International Journal of Hydrogen Energy, Volume 42, Issue 18, 2017, Pages 13127-13135, ISSN 0360-3199; https://doi.org/10.1016/j.ijhydene.2017.04.014.

[144] Eun Hee Park, Seong Uk Jeong, Un Ho Jung, Sung Hyun Kim, Jaeyoung Lee, Suk Woo Nam, Tae Hoon Lim, Young Jun Park, Yong Ho Yu, Recycling of sodium metaborate to borax, International Journal of Hydrogen Energy, Volume 32, Issue 14, 2007, Pages 2982-2987, ISSN 0360-3199; https://doi.org/10.1016/j.ijhydene.2007.03.029.

[145] T. Kemmitt, G.J. Gainsford, Regeneration of sodium borohydride from sodium metaborate, and isolation of intermediate compounds, International Journal of Hydrogen Energy, Volume 34, Issue 14, 2009, Pages 5726-5731, ISSN 0360-3199; https://doi.org/10.1016/j.ijhydene.2009.05.108.

[146] Chierchia Antonia, Studio dell'utilizzo di NaBH$_4$ per la produzione di H$_2$, tesi di laurea, Università degli Studi di Napoli "Federico II", Anno Accademico 2019/2020

[147] Staiano Giulia, Simultaneous cyan H$_2$ production and CO$_2$ valorization from NaBO$_2$ and reducing agent, tesi di laurea, Università degli Studi di Napoli "Federico II", Anno Accademico 2020/2021

[148] https://webthesis.biblio.polito.it/7388/.

[149] Z.-Z. Yang, Q.-W. Song, L.-N. He, Introduction, in: Capture Util. Carbon Dioxide with Polyethyl. Glycol, Springer Berlin Heidelberg, Berlin, Heidelberg, 2012, pp. 1-5; https://www.amazon.it/Capture-Utilization-Polyethylene-SpringerBriefs-Molecular-ebook/dp/B00A9YGY84.

[150] Rajendran Muthuraj, Tizazu Mekonnen, Recent progress in carbon dioxide (CO_2) as feedstock for sustainable materials development: Co-polymers and polymer blends, Polymer, Volume 145, 2018, Pages 348-373, ISSN 0032-3861; https://doi.org/10.1016/j.polymer.2018.04.078.

[151] https://sustainability-lab.net/2022/04/03/produrre-polimeri-dalla-co%E2%82%82/.

[152] Nova-Institut2021

[153] https://renewable-carbon.eu/news/carbon-dioxide-co2-as-chemical-feedstock-for-polymers-already-nearly-1-million-tonnes-production-capacity-installed/.

[154] Laura Pires da Mata Costa, Débora Micheline Vaz de Miranda, Ana Carolina Couto de Oliveira, Luiz Falcon, Marina Stella Silva Pimenta, Ivan Guilherme Bessa, Sílvio Juarez Wouters, Márcio Henrique S. Andrade, José Carlos Pinto, Capture and Reuse of Carbon Dioxide (CO2) for a Plastics Circular Economy: A Review: Processes 2021, 9(5), 759; https://doi.org/10.3390/pr9050759.

[155] Bruno Grignard, Sandro Gennen, Christine Jerome, Arjan W. Kleij and Christophe Detrembleur, Advances in the use of CO_2 as a renewable feedstock for the synthesis of polymers; Chem Soc Rev; https://doi.org/10.1039/C9CS00047J.

[156] S. Inoue, H. Koinuma, T. Tsuruta, Copolymerization of carbon dioxide and epoxide with organometallic compounds, Die Makromol. Chem. 130 (1969) 210-220; https://doi.org/10.1002/macp.1969.021300112.

[157] Shunjie Liu, Xianhong Wang, Polymers from carbon dioxide: Polycarbonates, polyurethanes, Current Opinion in Green and Sustainable Chemistry, Volume 3, 2017, Pages 61-66, ISSN 2452-2236; https://doi.org/10.1016/j.cogsc.2016.08.003.

[158] J. Langanke, A. Wolf, J. Hofmann, K. Böhm, M. A. Subhani, T. E. Müller, W. Leitner and C. Gürtler; Carbon dioxide (CO_2) as sustainable feedstock for polyurethane production; https://doi.org/10.1039/C3GC41788C.

[159] https://www.jaci.or.jp/english/gscn/pdf/IntoductionToGSC_02.pdf.

[160] V. N. Gama, A. Ferreira and A. Barros-Timmons, Polyurethane Foams: Past, Present, and Future, Materials, 2018, 11; https://doi.org/10.3390/ma11101841.

[161] J. Joseph, R.M.. Patel, A. Wenham, J.R. Smith, Biomedical applications of polyurethane materials and coatings, Trans. IMF, 2018, 96, 121–129; https://doi.org/10.1080/00202967.2018.1450209.

[162] N. von der Assen, A. Bardow, Life cycle assessment of polyols for polyurethane production using CO_2 as feedstock: insights from an industrial case study, Green Chem. 16 (2014) 3272-3280

[163] S. Lee, S.T. Baek, K. Anas, C.S. Ha, D.W. Park, J.W. Lee, I. Kim, Tuning of activity, induction period and polymer properties of double metal cyanide catalyzed ring-opening polymerizations of propylene oxide by using quaternary ammonium salts, Polymer 48 (2007) 4361-4367; https://doi.org/10.1016/j.polymer.2007.05.072.

[164] Y.G. Gao, Y.S. Qin, X.J. Zhao, F.S. Wang, X.H. Wang, Selective synthesis of oligo(carbonate-ether) diols from copolymerization of CO_2 and propylene oxide under zinc-cobalt double metal cyanide complex, J. Polym. Res. 19 (2012) 9; https://link.springer.com/article/10.1007/s10965-012-9878-5.

[165] https://it.wikipedia.org/wiki/Glicole_polietilenico.

[166] Jay Soni, Nusrat Sahiba, Ayushi Sethiya, Shikha Agarwal, Polyethylene glycol: A promising approach for sustainable organic synthesis, Journal of Molecular Liquids, Volume 315, 2020, 113766, ISSN 0167-7322; https://doi.org/10.1016/j.molliq.2020.113766.

[167] E. Canada, H. Canada, Canadian Environmental Protection Act (2000).

[168] M.W. Forkner, J.H. Robson, W.M. Snelling, A.E. Martin, F.H. Murphy, T.E. Parsons, Glycols–Ethylene Glycols, 2004.

[169] Jr. Bailey, E. Frederick, J.V. Koleske, Dekker, 2017 27–28 (ISBN 9780824783846).

[170] F. E. Bailey, Jr. and 1. V Koleske, Poly(Ethylene Oxide), Academic Press, New York (1976).

[171] F. E. Bailey, Jr. and 1. V Koleske, Alkylene Oxides and Their Polymers, Marcel Dekker, New York (1991); https://fdocuments.net/document/alkylene-oxides-polymers.html?page=6.

[172] J. Milton Harris, Introduction to Biotechnical and Biomedical Applications of Poly(Ethylene Glycol), Poly(Ethylene Glycol) Chemistry pp 1–14; https://doi.org/10.1007/978-1-4899-0703-5_1.

[173] Denise Fan, Der-Jong Dai and Ho-Shing Wu, Ethylene Formation by Catalytic Dehydration of Ethanol with Industrial Considerations; https://doi.org/10.3390/ma6010101.

[174] Minhua Zhang and Yingzhe Yu, Dehydration of Ethanol to Ethylene Industrial & Engineering Chemistry Research 2013 52 (28), 9505-9514; https://pubs.acs.org/doi/abs/10.1021/ie401157c?casa_token=qXGr88hJgZAAAAAA:ef xdWfH-Dz6nEl3CDg3USwCmTwR5zNscyunkbr4sajLBItszzjCiBY_4hXzzkIsf5o6vJqJju89XS Q.

[175] Robert T. Mathers, How well can renewable resources mimic commodity monomers and polymers?; https://doi.org/10.1002/pola.24939.

[176] Paul D. Mobley, Jonathan E. Peters, Nandita Akunuri, Joshua Hlebak, Vijay Gupta, Qinghe Zheng, S. James Zhou, Marty Lail, Utilization of CO2 for Ethylene Oxide, Energy Procedia, Volume 114, 2017, Pages 7154-7161, ISSN 1876-6102; https://doi.org/10.1016/j.egypro.2017.03.1878.

[177] Liguo Wang, Huiquan Li, Shumin Xin, Peng He, Yan Cao, Fengjiao Li, Xinjuan Hou, Highly efficient synthesis of diethyl carbonate via one-pot reaction from carbon dioxide, epoxides and ethanol over KI-based binary catalyst system, Applied Catalysis A: General, Volume 471, 2014, Pages 19-27, ISSN 0926-860X; https://doi.org/10.1016/j.apcata.2013.11.031.

[178] https://www.chempep.com/ChemPep-Polyethylene_glycol_PEG.htm.

[179] Veronese FM, Pasut G. 2005. PEGylation, successful approach to drug delivery. Drug Discovery Today. 10 (21):1451-1458; https://doi.org/10.1016/s1359-6446(05)03575-0.

[180] https://readitaliano.com/wiki/it/Miralax.

[181] Hyun-Jun Jang, Chan Young Shin, Kyu-Bong Kim, Safety Evaluation of Polyethylene Glycol (PEG) Compounds for Cosmetic Use, Toxicol. Res. Vol. 31, No. 2, pp. 105-136 (2015); http://dx.doi.org/10.5487/TR.2015.31.2.105.

[182] Abas Mohsenzadeh,Akram Zamani,Mohammad J. Taherzadeh, Bioethylene Production from Ethanol: A Review and Techno-economical Evaluation; ChemBioEng Rev 2017, 4, No. 2, 75–91; https://doi.org/10.1002/cben.201600025.

[183] Antonio Morschbacker, Bio-Ethanol Based Ethylene; Polym. Rev. 2009, 49 (2), 79–84; https://doi.org/10.1080/15583720902834791.

[184] S. Matar, L. F. Hatch, Chemistry of Petrochemical Processes, Gulf Professional Publishing, Houston, TX 2001; https://www.elsevier.com/books/chemistry-of-petrochemical-processes/matar-ph-d/978-0-88415-315-3.

[185] H. Zimmermann, R. Walzl, Ethylene, in Ullmann's Encyclopedia of Industrial Chemistry, Wiley-VCH Verlag, Weinheim 2000; https://doi.org/10.1002/14356007.a10_045.pub3.

[186] https://www.chimica.unifi.it/upload/sub/LAUREA/PUB/2015-2016/ELABORATI/romi_sebastiano-e.pdf.

[187] https://www.chimicaindustrialeessenziale.org/polimeri/polietilene/.

[188] https://it.wikipedia.org/wiki/Propanolo.

[189] https://it.wikipedia.org/wiki/1-propanolo.

[190] https://it.wikipedia.org/wiki/2-propanolo.

[191] https://it.wikipedia.org/wiki/Propilene.

[192] https://www.chimica-online.it/composti-organici/propilene.htm.

[193] https://it.wikipedia.org/wiki/Polipropilene.

[194]https://www.chimicaindustrialeessenziale.org/polimeri/polipropilene/#:~:text=La%20polimerizzazione%20avviene%20in%20propilene,liquido%2C%20che%20viene%20quindi%20riciclato.

[195] E. Nicolo, "Fatto il polipropilene": a tribute to Giulio Natta; https://link.springer.com/article/10.1007/s10029-007-0237-0.

[196] Jean-Luc Dubois, Georgeta Postole, Lishil Silvester, Aline Auroux, Catalytic Dehydration of Isopropanol to Propylene; http://dx.doi.org/10.3390/catal12101097.

[197] Zhang H, Grinstaff MW, Recent Advances in Glycerol Polymers: Chemistry and Biomedical Applications, Macromol Rapid Commun 35:1906–1924 (2014); https://doi.org/10.1002/marc.201400389.

[198] Holger Frey, Rainer Haag, Dendritic polyglycerol: a new versatile biocompatible material, Reviews in Molecular Biotechnology, Volume 90, Issues 3–4, 2002, Pages 257-267, ISSN 1389-0352; https://doi.org/10.1016/S1389-0352(01)00063-0.

[199] Steven C. Zimmerman Prof.,Jordan R. Quinn,Ewelina Burakowska,Rainer Haag Prof. Dr., Cross-Linked Glycerol Dendrimers and Hyperbranched Polymers as Ionophoric, Organic Nanoparticles Soluble in Water and Organic Solvents; Volume 46, Issue43 November 5, 2007 Pages 8164-8167; https://doi.org/10.1002/anie.200702580.

[200] Shailja Goyal, Nacú B Hernández, Eric W Cochran, An update on the future prospects of glycerol polymers ; https://doi.org/10.1002/pi.6209.

[201] Ioannides T. Thermodynamic analysis of ethanol processes for fuel cell applications. Journal of Power Sources 2001; 92:17–25; https://doi.org/10.1016/S0378-7753(00)00498-5.

[202] Freni S, Maggio G, Cavallaro S. Ethanol steam reforming in a molten carbonate fuel cell: a thermodynamic approach. Journal of Power Sources 1996; 62:67–73; https://doi.org/10.1016/S0378-7753(96)02403-2.

[203] Benito M, Sanz JL, Isabel R, Padilla R, Arjona R, Daza L. Bio-ethanol steam reforming: insights on the mechanism for hydrogen production. Journal of Power Sources 2005; 151:11–17; https://doi.org/10.1016/j.jpowsour.2005.02.046.

[204] https://www.nist.gov/.

[205] https://webbook.nist.gov/cgi/cbook.cgi?ID=B6000455&Units=SI&Mask=80#IR-Spec.

[206] Neeti Goel, Nidhi Sinha, Binay Kumar, Growth and properties of sodium tetraborate decahydrate single crystals, Materials Research Bulletin, Volume 48, Issue 4, 2013, Pages 1632-1636, ISSN 0025-5408; https://doi.org/10.1016/j.materresbull.2013.01.007.

Acknowledgments

Ad ogni inizio c'è una fine ma per ogni fine c'è sempre un nuovo inizio.

Tuttavia, prima di iniziare un nuovo percorso, credo sia giusto e anche necessario tirare le somme e ringraziare tutti coloro che mi hanno aiutato e incoraggiato in questi cinque anni.

Vorrei iniziare col ringraziare la professoressa Almerinda Di Benedetto, mia relatrice, che mi ha seguito durante tutti questi mesi. Grazie per la sua totale disponibilità, per la professionalità che ha dimostrato e per i confronti costruttivi che hanno contribuito alla stesura del presente lavoro di tesi.

Allo stesso modo vorrei ringraziare la professoressa Giuseppina Luciani per aver contribuito con i suoi preziosi commenti e spunti di riflessione al raggiungimento dei risultati ottenuti.

Grazie ad Alessandra per avermi seguito sempre da vicino in laboratorio non facendomi mai mancare il suo appoggio in ogni momento.

Grazie a Maria per la sua disponibilità e per il suo aiuto durante la scrittura della tesi.

Grazie a Danilo per i suoi consigli e suggerimenti durante le riunioni.

Ringrazio poi tutti i miei amici e colleghi che hanno condiviso con me questo percorso tra chiacchierate, pause caffè, momenti di gioia e di sconforto.

Ringrazio mia mamma e mio papà per avermi permesso di studiare supportando ogni mia scelta, sopportando i miei malumori e non facendomi mancare mai nulla. È grazie a voi e a tutti i vostri sacrifici e rinunce se oggi ho potuto raggiungere questo traguardo. Ve ne sarò sempre grato per questo.

Grazie a mia sorella Ida che è sempre stata fiera di me, mi ha sempre ascoltato quando ne avevo bisogno e ha gioito sempre per i miei risultati. È stato importante averti avuta al mio fianco in questi anni.

Ringrazio la mia fidanzata Ilaria, la persona che più di tutte è stata capace di capirmi e sostenermi nei momenti più difficili. So che non è stato facile starmi accanto. Hai dovuto subire tutte le mie ansie e delusioni, hai dovuto asciugare le mie lacrime ma non c'è stata mai una volta in cui non abbia sentito il tuo appoggio. Sei stata la mia motivazione più

grande senza la quale non so se sarei arrivato fin qui. Grazie per esserci sempre stata. Grazie per il tuo amore incondizionato.

Spero vivamente che questo sia solo l'inizio di una carriera ricca di soddisfazioni.

<div align="right">*Vincenzo*</div>